UNIVERSITY OF SOUTHAMPTON

FACULTY OF NATURAL AND ENVIRONMENTAL SCIENCES

Biological Sciences

Development of methods to study oriented membrane proteins using synchrotron radiation circular dichroism spectroscopy

by

Luke Sean Evans

Thesis for the degree of Doctor of Philosophy

September 2017

UNIVERSITY OF SOUTHAMPTON

ABSTRACT

FACULTY OF NATURAL AND ENVIRONMENTAL SCIENCES

Biological Sciences

Thesis for the degree of Doctor of Philosophy

DEVELOPMENT OF METHODS TO STUDY ORIENTED MEMBRANE PROTEINS USING SYNCHROTRON RADIATION CIRCULAR DICHROISM SPECTROSCOPY

Luke Sean Evans

Membrane proteins are important targets for structural biology. They account for a disproportionately large percentage of pharmacological targets, but only a minority of available protein structures. The intractability of membrane proteins to recombinant expression and purification has been a limiting factor in their structural characterisation. Of those structures available the majority rely on detergent solubilisation of the protein. This removes the native lipid environment which is established to have structural and functional implications.

A number of techniques allow the investigation of membrane proteins in lipid bilayers which mimic the cellular membranes. In this thesis, two of these approaches, oriented synchrotron radiation circular dichroism (OSRCD) and solid-state nuclear magnetic resonance (NMR) spectroscopies have been used to investigate the orientation and structure of the transmembrane domain of a putative glycosyltransferase fukutin. We have developed a method for OSRCD based on the conventional means of sample preparation, where aligned bilayers are prepared on a support substrate. This allowed the orientation of the fukutin transmembrane domain to be determined in bilayers of different thickness which model membranes of different cellular compartments. Both OSRCD and NMR results indicate that the protein adapts by changing its tilt angle and forming large oligomers in thicker membranes, potentially providing a model for retention of fukutin in the thinner Golgi apparatus membranes, which appears to be essential for its function.

As the preparation of well oriented samples can be challenging, a novel method of OSRCD using magnetic alignment of lipid phases has also been developed. The goal of this work was to align lipid phases in a magnetic SRCD instrument. Extensive characterisation of lipid mixtures using NMR, electron paramagnetic resonance and conventional CD enabled identification of conditions to allow alignment at low magnetic fields such as those found in magnetic SRCD instruments. Although OSRCD measurements on magnetically aligned samples were not successful, a number of further modifications are suggested which may allow sample alignment under different conditions.

With a view to expansion of the oriented techniques to a more complex protein, attempts were made to express and purify the pore region of the voltage-gated potassium channel expressed by the human *Ether-á-go-go* related gene (hERG). hERG is a particularly important target for structural characterisation as it has proclivity for non-specific drug binding, which can block the channel and result in drug induced long-QT syndrome, a phenomenon affecting a large number of newly developed pharmaceuticals.

Table of Contents

List of Tables

List of Figures

DECLARATION OF AUTHORSHIP

I, LUKE SEAN EVANS

declare that this thesis and the work presented in it are my own and has been generated by me as the result of my own original research.

Development of methods to study oriented membrane proteins using synchrotron radiation circular dichroism spectroscopy

I confirm that:

1. This work was done wholly or mainly while in candidature for a research degree at this University;
2. Where any part of this thesis has previously been submitted for a degree or any other qualification at this University or any other institution, this has been clearly stated;
3. Where I have consulted the published work of others, this is always clearly attributed;
4. Where I have quoted from the work of others, the source is always given. With the exception of such quotations, this thesis is entirely my own work;
5. I have acknowledged all main sources of help;
6. Where the thesis is based on work done by myself jointly with others, I have made clear exactly what was done by others and what I have contributed myself.

Signed: .....

Date: .....

Acknowledgements

I would like to thank my supervisor Phil Williamson for all of his guidance, support and constant belief in my ability to succeed. Phil has spent a lot of the past four years helping me patiently with the spectrometer, sparing his time to answer questions and even transporting me when I was incapacitated, and I can't thank him enough. I also thank Giuliano Siligardi and Rohanah Hussain, who have been constantly encouraging and enthusiastic throughout this project. I have learned a huge amount about the practical aspects of CD from them.

Many people have helped me along the way during this PhD. I must thank the various members of the Williamson group who have come and gone over the years who have been great company and help in the lab. Thanks go to Neville Wright for his enlightening anecdotes, experimental advice, and most importantly, wine recommendations. I thank Marilyn Jenkins for her words of encouragement and helping me find my way around the lab. I'd also like to gratefully acknowledge the fantastic B23 team at Diamond, who have been incredibly helpful throughout my beam time sessions.

There have been many people with whom I have been fortunate to share the lab (and occasionally a drink) during my time at Southampton, especially Mary Beton, Andy Hutchin, Ben Yarnall and Monika Kudelska. Rafael Gomes deserves a special thanks for his friendship over the past four years. I cannot thank Mike Jolly enough, without his company and humour I would not have made it through this PhD. Megha Rai has been a fantastic travelling companion, and I will really miss our office chats. I thank Charlotte Hill for her humour and provision of cake and cookies that have got me through the last few weeks of writing.

I would like to acknowledge Biological Sciences at Southampton and Diamond Light Source for funding my studentship, and Diamond Light Source for the B23 beam line access which enabled much of this work.

Finally I thank all of my family for all of their encouragement, words of advice and wisdom. I especially need to thank my parents, who had faith in my ability to finish the PhD even during the times when I did not. I could not have done this without them.

Definitions and Abbreviations

AP	action potential
CD	circular dichroism
CMC	critical micelle concentration
CP	cross polarisation
cryo-EM	cryo-electron microscopy
CSA	chemical shielding anisotropy
CSL	cholestane spin label
DDM	n-dodecyl-β-D-maltoside
DEER	double electron-electron resonance
DHPC	1,2-dihexanoyl-sn-glycero-3-phosphocholine
diLQTS	drug-induced long QT syndrome
DHPC	1,2-dihexanoyl-sn-glycero-3-phosphocholine
DLPC	1,2-dilauroyl-sn-glycero-3-phosphocholine
DMPC	1,2-dimyristoyl-sn-glycero-3-phosphocholine
DMPE	1,2-dimyristoyl-sn-glycero-3-phosphoethanolamine
DOPC	1,2-dioleoyl-sn-glycero-3-phosphocholine
DPhPC	1,2-diphytanoyl-sn-glycero-3-phosphocholine
DPPC	1,2-dipalmitoyl-sn-glycero-3-phosphocholine
DRM	detergent resistant membranes
DSS	disuccinimidyl suberate
DTPA	diethylenetriaminepentaacetic acid
ECG	electrocardiogram
EPR	electron paramagnetic resonance

ER	endoplasmic reticulum
ESI	electrospray ionisation
FCMD	Fukuyama congenital muscular dystrophy
fid	free induction decay
FRP	fukutin related protein
GPI	glycophosphatidylinositol
HEK	human embryonic kidney
hERG	human *Ether-à-go-go* related gene
IPTG	isopropyl β-D-1-thiogalactopyranoside
ISDU	isopotenital spin-dry ultracentrifugation
L/P	lipid to protein ratio
LB	linear birefringence
LCP	lipidic cubic phase
LD	linear dichroism
LDAO	lauryldimethylamine oxide
LPS	lipopolysaccharide
LQTS	long QT syndrome
MAS	magic angle spinning
MD	molecular dynamics
MCE	magnetic circularly polarised emission
MLV	multilamellar vesicle
MscL	mechanosensitive channel of large conductance
NMR	nuclear magnetic resonance
OG	octyl glucoside

PA	phosphatidic acid
PC	phosphatidylcholine
PDB	protein data bank
PE	phosphatidylethanolamine
PG	phosphatidylglycerol
PLA_2	phospholipase A_2
PI	phosphatidylinositol
PISA	polar index slant angles
PISEMA	polarisation inversion spin exchange at the magic angle
POMGnT1	protein O-linked-mannose β-1,2-N-acetylglucosaminyltransferase 1
POMT1/2	protein O-mannosyltransferases 1/2
POPC	1-palmitoyl-2-oleoyl-sn-glycero-3-phosphocholine
rf	radio frequency
$S_{bicelle}$	bicelle order parameter
S_{nN}	deuterium spectra order parameter (NMR)
S_{mol}	cholestane order parameter (EPR)
S/N	signal to noise ratio
SDS	sodium dodecyl sulphate
SMA	styrene maleic acid
SRCD	synchrotron radiation circular dichroism
SUV	small unilamellar vesicle
TMD	transmembrane domain
ToF	time of flight

Chapter 1. Introduction

1.1. Cellular membranes

Cellular membranes are composed of three biomolecules of life: proteins, lipids and carbohydrates. They form the protective outer layer of cells, compartmentalise functional regions within cells and mediate the interactions and communication of cells with the external environment. There is great complexity within the membrane and carefully controlled interactions between the lipids and proteins allow them to sustain cellular functioning.

Our current understanding of the organisation, architecture and dynamics of membranes formed of lipids, protein and sterols was first described by the fluid mosaic model. This model was developed by Singer and Nicolson in 1972[1] (Figure 1.1) and describes the formation of a bilayer from lipids in an aqueous environment, and membrane proteins embedded within it.

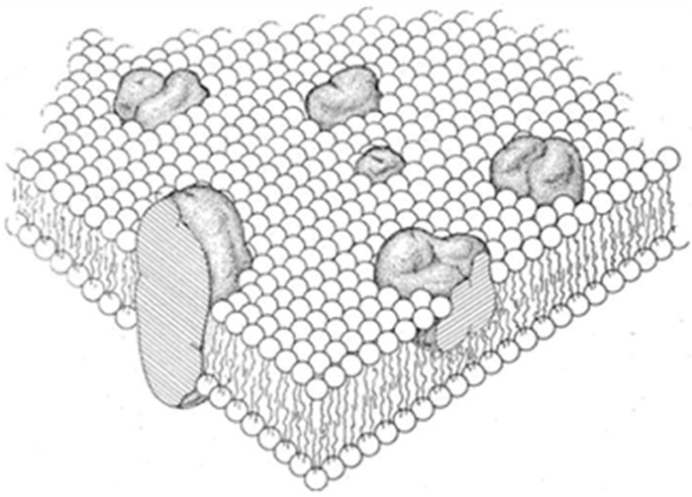

Figure 1.1: ***Original 1972 Singer and Nicolson fluid mosaic model of cellular membranes.*** *The lipid bilayer acts as a matrix to support the embedded integral membrane proteins. From Singer and Nicolson, 1972[1]. Reprinted with permission from American Academy for the Advancement of Science.*

Membrane proteins are vital to regulate the flow of molecules and information into and out of the cell. They are implicated in many disease processes, and their significance is illustrated by the fact that they account for around 50 % of all pharmaceutical targets[2]. The ability to understand their structure, function and activity is therefore paramount for rational drug design, but very few membrane proteins have been structurally characterised relative to their soluble counterparts. Of approximately 52000 unique entries in the protein

data bank (pdb) only 712 are unique membrane protein structures. The paucity of membrane protein structures is a result of the onerous nature of their study, which presents a series of challenges. There is a clear necessity for highly sensitive tools which enable the investigation of membrane protein structure.

The work in this thesis aims to combine the use of two structural techniques to develop an understanding of membrane protein structure in lipid environments which mimic the cellular membranes. The techniques, circular dichroism (CD) and nuclear magnetic resonance (NMR) spectroscopies, are highly complementary, and have been applied here to study physiologically significant proteins.

1.1.1. Lipids in cell membranes

Lipids are amphiphilic molecules with a hydrophilic headgroup and hydrophobic tails. In aqueous environments bilayers form due to the favourable interactions of the polar headgroups with the surrounding water, whilst apolar hydrophobic acyl chains cluster to exclude water and minimise the energetic cost. Within the membrane, lipids and other constituents undergo rapid lateral diffusion which make the membranes highly fluid. This fluidity is however dependant on factors including the membrane composition and temperature, and below its 'phase transition' or melting temperature (T_m) the membrane adopts a gel (crystalline) phase.

In excess of 20000 unique lipids have been identified in nature (LIPID MAPS Lipidomics Gateway, www.lipidmaps.org), with the majority in eukaryotic cell membranes categorised as either phospholipids, sphingolipids or sterols. Within these categories are hundreds of further species with different physical properties which modulate membrane properties including charge, curvature and phase[3]. As well as forming membranes they additionally have roles as second messengers in cell signalling pathways[4]. Phospholipids account for a large proportion of lipids in mammalian cell membranes. They are synthesised by the ester linkage of acyl chains, two in most cases, to glycerol-3-phosphate, yielding phosphatidic acid (PA). Further esterification of alcohols to the PA produces phosphatidylcholine (PC), phosphatidylserine (PS), phosphatidylinositol (PI) phosphatidylethanolamine (PE) and phosphatidylglycerol (PG) headgroups. Examples of the structure of a number of these types of lipid are given in Figure 1.2. PE and PC are zwitterionic whilst PS, PG and PI are anionic. The different headgroups also have different sizes and shapes, which affects the bilayer structure and phase behaviour[3]. PC lipids, which are most populous in eukaryotic cell membranes, are generally cylindrically shaped and are therefore can pack to form

bilayers, whilst PE lipids have a much smaller headgroup and so cannot form bilayers alone, but do have valuable roles in inducing membrane curvature during vesicular budding[4].

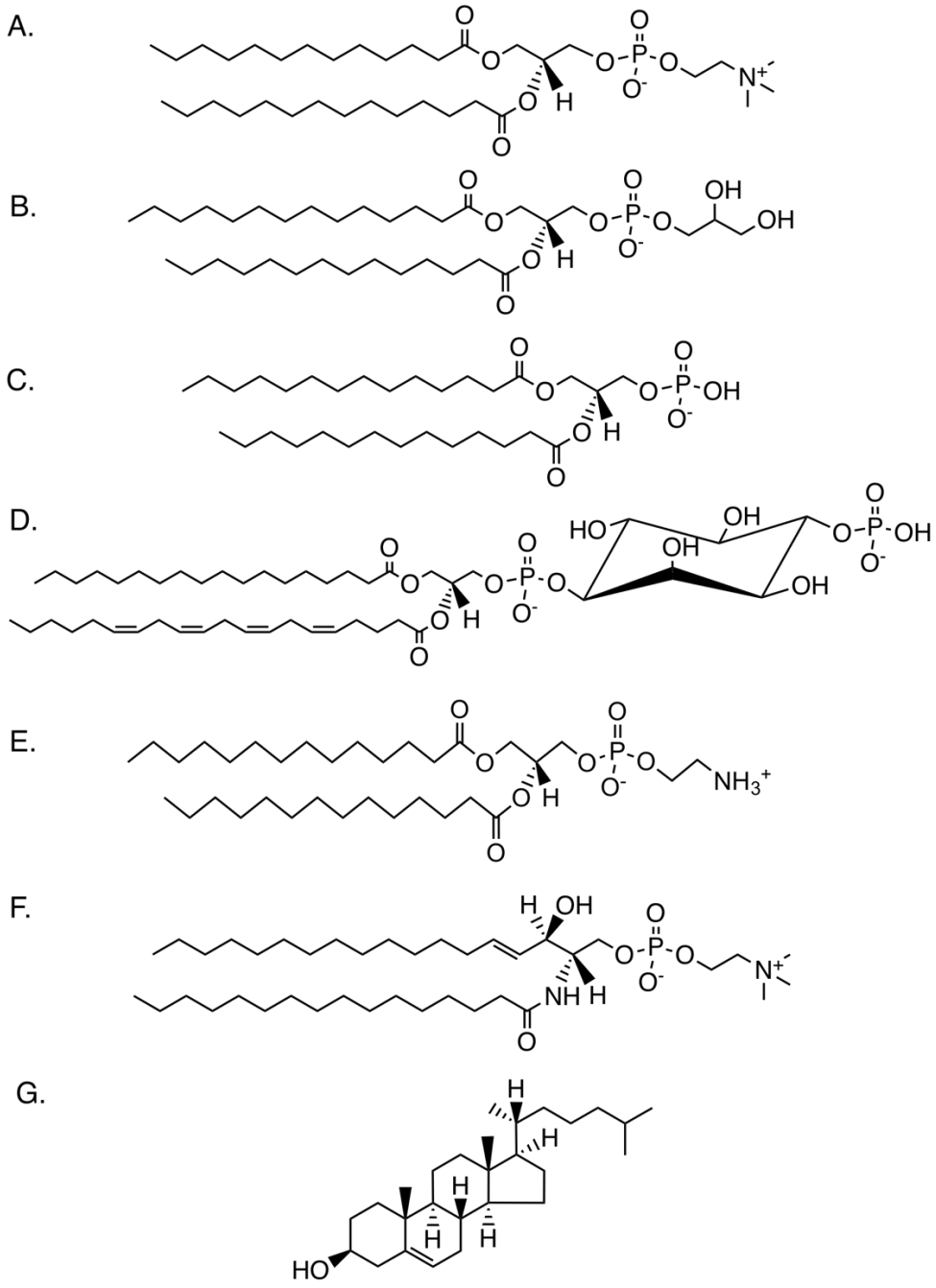

Figure 1.2: ***Molecular structure of various lipids.*** *A. 1,2-dimyristoyl-sn-glycero-3-phosphocholine (DMPC). B. 1,2-dimyristoyl-sn-glycero-3-phospho-(1'-rac-glycerol) (DMPG). C. 1,2-dilauroyl-sn-glycero-3-phosphate (DLPA). D. L-α-phosphatidylinositol-4-phosphate (PI4P). E. 1,2-dimyristoyl-sn-glycero-3-phosphoethanolamine (DMPE). F. Sphingomyelin. G. Cholesterol.*

Sphingolipids differ from phospholipids in that they have a sphingosine rather than glycerol backbone. Subsequently one acyl chain is attached via an ester linkage whilst the second attaches via an amide bond. The headgroups of sphingolipids are most commonly either PE or PC, although cerebrosides and gangliosides, other classes of sphingolipid, have carbohydrate headgroups and are involved in cell-cell recognition processes. Sphingolipids are generally enriched in cells of the nervous system, where they can provide insulation to neuronal axons as a component of the myelin sheath. They can act as potent second messengers, including the hydrolysis of sphingomyelin by sphingomyelinase to produce ceramide, which can illicit downstream effects including cell differentiation, senescence, necrosis and apoptosis[5].

The acyl chains of both sphingolipids and phospholipids, as well as the headgroups, give rise to the lipid phase behaviour[6]. Lipids in natural membranes have between 10 and 24 carbons in their acyl chains, with longer chains predominating in sphingolipids. Longer acyl chains give rise to greater T_m. It is common for phospholipids in the bilayer to have at least one, if not more, carbon-carbon double bonds which contributes to the conformation of the acyl chains by creating kinks. When these double bonds are present the T_m is reduced. Below the T_m, the acyl chains are in the gel phase, where they are ordered, fully extended and tilted (Figure 1.3). Above the T_m, in the fluid or liquid disordered phase, the chains are highly mobile and rapidly fluctuating. The T_m is dependent on the non-covalent interactions, especially van de Waals interactions, between neighbouring acyl chains, so longer, extended acyl chains require greater thermal energy to disrupt than shorter, kinked acyl chains. The hydrophobic thickness of bilayers is also determined by the acyl chain length and saturation[7].

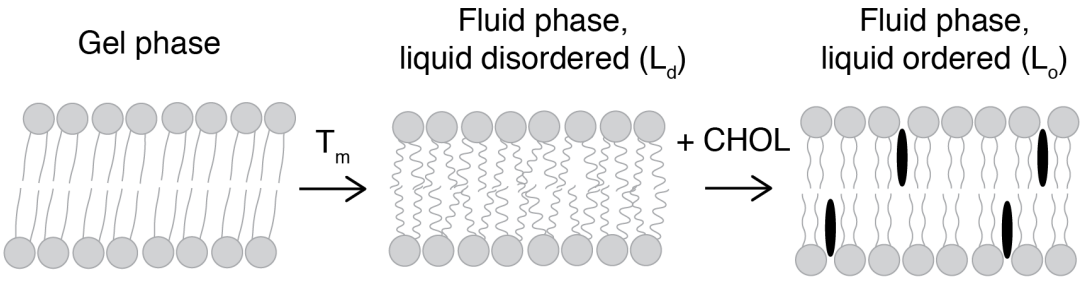

Figure 1.3: ***Phase behaviour of bilayer lipids****. Below the transition temperature T_m the acyl chains are tilted and extended, which then become mobile to form the liquid disordered phase above the T_m. When cholesterol is added the liquid disordered phase becomes ordered due to interactions of the cholesterol with the acyl chains.*

In addition to the formation and stabilisation of the bilayer mediated by acyl chain interactions, it is thought there are also extensive interactions of the lipid headgroups and the hydrating water[8]. Electrostatic interactions result in attractive and repulsive forces between charged headgroups, whilst hydrogen bonding can occur between either charged or neutral lipids[8]. These can be mediated by water and through interactions of amines in PE and PS lipids and oxygens of the phosphate and carbonyl groups[8].

An additional component of the bilayer are sterols with a characteristic four hydrocarbon ring structure (Figure 1.2 F.). The predominant sterol in mammalian cells is cholesterol, which is most concentrated in the plasma membrane at approximately 20–40 mol %[9]. Cholesterol aligns parallel with lipid acyl chains and has a small hydrophilic headgroup, which interacts with the headgroups of other lipids[10]. The inflexibility of cholesterol means that it preferentially interacts with extended, saturated acyl chains which are relatively straight. The membrane phase behaviour is also significantly affected by the presence of cholesterol, which by fitting between acyl chains is able to promote ordering of the acyl chains in the bilayer, and gives rise to a liquid ordered phase[4] (Figure 1.3). It also reduces cooperativity in the phase transitions (i.e. the sharpness of the transition), and at sufficient concentrations can abolish detectable transitions altogether[11].

1.1.2. Distribution and composition of lipid bilayers

Lipid membranes are present across almost all organisms, from the one or two membranes in prokaryotes (Gram positive and negative respectively) to the numerous membranes in eukaryotes. The composition of membranes is diverse and variable, both between organisms and between organelles in eukaryotes. Prokaryotic membranes are often thought to be less complex than those of eukaryotes, and this is especially true of *Escherichia coli* (*E. coli*) whose membranes are composed of three predominant components, PE (~75 %), PG (~20 %) and cardiolipin (~5 %) (a lipid with two PG headgroups and four acyl chains)[12]. The outer leaflet of prokaryotic membranes is commonly enriched in anionic lipids such as PG[13], which has provided a basis for targeting by cationic antimicrobial peptides. The majority of prokaryotic membranes are devoid of sterols, although bacterial membranes commonly contain hopanoids, which similar to cholesterol can modulate the bilayer fluidity[14]. One importnt lipid component of Gram negative organisms is lipid A, a phosphorylated glucosamine disaccharide typically having six acyl chains, which anchors the potent toxin lipopolysaccharide (LPS) into the outer membrane[14].

Within eukaryotes different organellar membranes are enriched with different types of lipid. Whilst the endoplasmic reticulum (ER) forms the primary site of cholesterol synthesis, its membrane has very low concentrations of cholesterol relative to the plasma membrane since it is transported intracellularly to other membranes[15]. The resulting bilayer is therefore more flexible and less ordered, and is presumed to help in the insertion of newly synthesised membrane proteins and lipids into the membranes[4]. The Golgi membranes are also thinner than those of the plasma membranes, due to their lower cholesterol content and hydrophobic thickness of the Golgi proteins[16], a property which is thought to be implicated in protein sorting and trafficking[17]. The plasma membranes contain much greater levels of cholesterol and sphingolipids, which provide more ordered and robust membranes[4]. Within the mitochondrial membranes a number of lipids are present which are not found elsewhere in the cell, and reflect their bacterial origins, such as lysophosphatidic acid and cardiolipin[18].

Even within a membrane the distribution of lipids between leaflets can be far from homogeneous, and this is closely related to membrane functionality. Whilst the ER membrane is symmetric, the remaining eukaryotic membranes are not[4]. In the plasma membranes for example, the outer cytosolic leaflet is enriched with sphingolipids, whilst the inner leaflet has a greater content of PI, PS and PE lipids. This is highly important, for example PI molecules involved in signalling can cluster in specific regions of the cytoplasmic but not the outer leaflet[19]. Since PI lipids are implicated in signalling pathways their clustering stimulates greater downstream effects. The distribution of lipids in the leaflets is maintained through a number of mechanisms. Transverse diffusion of lipids passively from one leaflet to another occurs at a very slow rate, since there is a high energy barrier to overcome for a hydrophilic headgroup to pass though the hydrophobic interior. Membrane asymmetry can be regulated by active mechanisms including P-type ATPases, particularly ‘flippases’ (type IV P-type ATPases), which can translocate PC, PS and PE phospholipids across the plasma membrane[20]. Bidirectional non-specific translocation of lipids is achieved through scramblase proteins[21].

Although the fluid mosaic model has formed the basis of our understanding of membrane structure for many decades, the model did not take into account localised changes in lipid composition. Within single leaflets, regions of the membrane can be enriched with specific types of lipid which are proposed to give rise to so called lipid rafts or lateral domains. These presumed rafts were first observed by Simons and van Meer in 1988[22], who made use of fluorescence probes to identify bilayer heterogeneity. Aggregation of certain types

of lipid (generally sphingolipids) may occur as a result of recruitment by membrane proteins binding specific lipids, or through the inherent physical properties of the lipids, such as the clustering of lipids with similar acyl chain lengths. Lateral domains identified in plasma and Golgi membranes are proposed to have an active role in signal transduction, vesicle formation, and transport and trafficking, potentially by selecting membrane proteins from the Golgi for targeting to the plasma membrane[23]. Rafts are also enriched with lipid-anchored proteins as part of their role in protein sorting[24] as well as cholesterol. Whilst it appears that sphingolipids are essential in raft formation, it is likely that cholesterol is locally concentrated in these domains since it has affinity for the sphingolipid saturated acyl chains rather than having any specific role in their formation. It does however promote an ordered state as would be expected[25] and also restricts lateral motility of the rafts[26]. The methodology which revealed the presence of microdomains has been questioned since it uses harsh detergents to strip away the non-domain forming lipids, a process which has been suggested to result in formation of laterally segregated detergent-resistant regions of membrane (detergent resistant membranes, DRMs) rather than domains occurring naturally in native membranes[27]. This was illustrated by Casadei et al.[28] who visualised the formation of lipid rafts using phase contrast and fluorescence microscopy when erythrocyte membranes are exposed to the detergent Triton X-100.

However, there is mounting evidence for the formation of nanoscale lateral domains in physiological cellular membranes. From molecular dynamics simulations it appears that these domains are relatively small, formed from up to 25 lipid molecules with cholesterol at the outer edges[29], which do not cluster to form larger domains. Förster resonance energy transfer (FRET) studies of model membranes have similarly identified liquid ordered (L_o) phase domains of approximately 10 nm[30]. A recent study has identified the formation of lateral domains in live cells for the first time using synthetic fluorescent labelled gangliosides, which were thought to be localised to these domains[31]. Using single-molecule fluorescence microscopy the authors determined that transient rafts form around the GPI-anchored protein CD59 which recruit gangliosides into the highly dynamic lateral domains, giving clear evidence for the physiological presence of lipid rafts for the first time.

1.1.3. Properties of membrane proteins

Membrane proteins are the basis for the ‘mosaic’ part of the fluid mosaic model of lipid bilayers. They are classed as either integral or peripheral membrane proteins, with integral proteins fully embedded into the bilayer and peripheral attached to the surface of the

membrane. The peripheral proteins bind to the membrane through a number of mechanisms. There may be electrostatic interactions between charged lipids and residues, lipids may be attached to proteins (such as glycophosphatidylinositol (GPI) anchoring and palmitoylation) or through interaction of amphiphilic helices or loop regions. Many peripheral proteins are enzymes requiring them to be localised close to the membrane for their function. One such example is phospholipase A_2 (PLA_2) which is responsible for the hydrolysis of bilayer lipids, releasing *sn*-2 fatty acids which undergo downstream processing to yield one of a number of inflammation mediating eicosanoids[32]. The group IVA PLA_2 has been shown to interact with the membrane surface through a combination of hydrophobic interactions between specific loop regions of the protein and electrostatic interactions between anionic lipids and charged residues, all of which are proximal to the hydrophobic active site[32, 33].

Integral membrane proteins have domains which are fully embedded within the lipid bilayer, with the majority completely spanning the membrane (Figure 1.4). There are a small number of examples of monotopic membrane proteins with hydrophobic domains which partially penetrate the bilayer, perhaps the most commonly studied example of this being the cytochrome P450 family[34]. Bitopic proteins which span the full hydrophobic thickness of the bilayer are either type I or type II, with their N termini on the extra- or intra-cellular side of the membrane respectively (Figure 1.4). Type III membrane proteins are formed from multiple, usually antiparallel, domains, containing upward of two helices. These proteins will often form oligomers through interactions between subunits.

With the exception of mitochondrial membrane proteins, which are inserted into the mitochondrial membranes by specific translocons[35], newly synthesised membrane proteins in eukaryotes are initially inserted into the ER membranes irrespective of their final destination. During translation membrane proteins emerge from the ribosome and are then targeted to ER membranes by the signal recognition particle which recognises membrane proteins through either specific N-terminal signal sequences or due to the protein's hydrophobicity[36]. The signal sequence, which can be later cleaved, is usually around 20 residues, and is formed from between one and five basic or polar residues followed by between seven and 15 apolar residues, and finally a polar cleavage site[37]. These sequences are generally too short to form a transmembrane domain, and are often cleaved. Alternatively signal anchor sequences which form a transmembrane domain to tether proteins in the membrane, and can be located anywhere in the protein sequence, are recognised by the signal recognition particle due to their hydrophobicity[37]. Once a signal

sequence has been recognised translation is paused (to prevent aggregation) until the entire complex is localised to the membrane, where the protein is then inserted into the bilayer by the translocon, a complex including the Sec61 protein at its core (in eukaryotes)[36]. Having matured through the ER, membrane proteins are then advanced to the Golgi apparatus in coat protein complex II (COPII) coated trafficking vesicles[38]. This process is mediated by the presence of sequence motifs in the cytosolic domain of the proteins, including di-acidic, di-hydrophobic, and tyrosine-based motifs[38]. From the Golgi the membrane protein can then be trafficked to other cellular membranes as necessary, through distinct trafficking pathways for different destinations[39]. These processes are also driven by signal motifs, which vary depending on the pathway and protein, such as the Kir2 subfamily of voltage-gated potassium channels, whose N-termini contain a series of positively charged residues which appear to be responsible for targeting the protein to the plasma membrane[40, 41].

The structural characteristics of integral membrane protein are much less diverse than those of their soluble counterparts. They are either α-helical or β-barrel structures, with β-barrel proteins limited to mitochondria, chloroplasts and prokaryotic outer membranes. This relative structural homogeneity occurs due to their amino acid composition and the physiochemical properties of the lipid bilayer. Due to the polar nature of the transmembrane domains, a hydrophobic solvent is essential to prevent aggregation of the proteins, and is provided by the acyl chains. The structures result from extensive hydrogen bonding between residues to prevent the high energetic cost associated with the insertion of a polar protein into the apolar hydrophobic region of the bilayer. Despite the relative homogeneity of membrane protein structures they have diverse functions, often arising from their amino acid composition. In order to span the hydrophobic length of the bilayer typically ~25 residues are required, with an average of 27±5 residues per transmembrane helix[42]. The membrane facing regions of integral membrane proteins are highly hydrophobic, allowing them to interact with acyl chains, and are also enriched with nonpolar residues. Residues with small side chains have been identified as important for helix packing either between helices in monomers or subunits in oligomerisation, and are often found spaced along the helix to facilitate tight packing, such has the GXXXG motif from glycophorin A[43, 44]. In such oligomers the small glycines form a “hole” into which branched side chains can penetrate. Aromatic residues are usually present at either end of the hydrophobic part of the domains, where their side chains extend into the bilayer’s interfacial region to interact with both head groups and chains[45]. Similarly lysines in

TMDs can “snorkel”, where the long, flexible side chain is able to position the charged amino group within the polar interfacial region[46]. These interactions stabilise the protein in the bilayer. Helices may also contain residues which break the helix to form a kink, particularly proline which introduces a hinge region to helices that are important in dynamics[37].

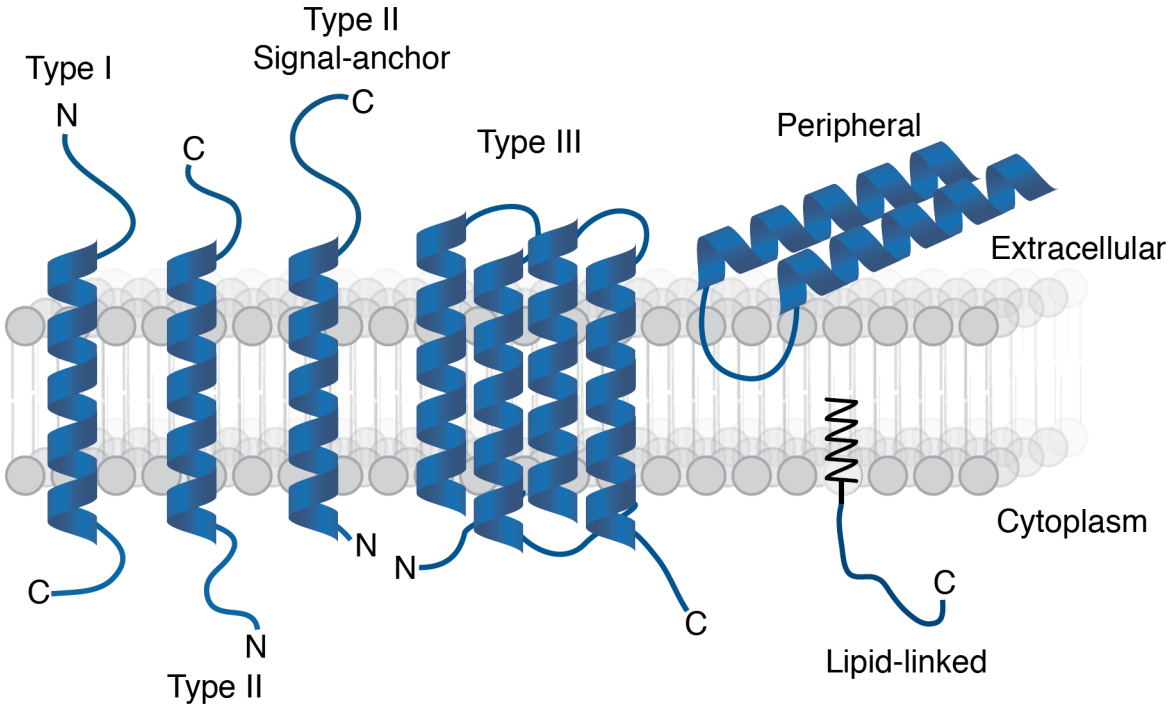

Figure 1.4: ***Topology of membrane protein types.*** *Single pass type I and II have extracellular or intracellular N termini respectively. Signal-anchor type II protein have an extracellular C terminus and no soluble N terminus. Type III proteins have multiple membrane spanning domains, while lipid-linked proteins such as GPI enable a protein without specific membrane binding domains to be localised proximal to the membrane. An example of a peripheral membrane protein associated with the bilayer through a hydrophobic loop.*

Somewhere between integral and peripheral membrane proteins are membrane active peptides such as antimicrobial peptides and toxins. These can associate with the membrane either through interactions with headgroups or the acyl chains, leading to changes in their orientation in the bilayer and the bilayer integrity. These interactions can occur according to three proposed mechanisms: the carpet model, barrel stave model or the toroidal pore model[47]. The carpet model describes the disruption of the membrane when a sufficiently high concentration of peptide binds exclusively to the surface. The barrel stave model involves the insertion of the peptide into the bilayer to form a pore with a hydrophilic

interior, whilst toroidal pores result from the inserted peptide remodelling the bilayer to line the pore with a monolayer of lipids.

1.1.4. Lipid-protein interactions

The membrane proteins and lipids in the bilayer are not discrete components. The lipids do not merely provide a hydrophobic solvent for the hydrophobic regions of membrane proteins; both lipid and protein can have profound effects on each other and proteins are known to be functionally and structurally modulated by changes in the bilayer composition[48]. This occurs as a result of lipid-protein interactions where both the lipid headgroup and acyl chains have significant effects on the protein. In context of such lipid-protein interactions the lipids in the bilayer can be described as either bulk, annular or non-annular. The bulk lipids form the majority of the bilayer and the annular lipids form a single layer surrounding the exposed regions of the protein. The bulk and annular lipids rapidly exchange, although around 5-10 x more slowly than the diffusion of bulk lipids[49, 50], and on binding the individual lipids distort to fit around the protein, with their acyl chains interacting with the protein's hydrophobic surface. Non-annular lipids bind with high affinity to specific residues or clusters of residues, generally at the site of protein-protein interactions.

The interactions of membrane proteins with annular lipids have been well characterised using a number of approaches, but electron paramagnetic resonance (EPR) spectroscopy has been one of the most informative methods, primarily due to the its favourable timescales[51]. The EPR spectra of spin labelled lipids in the presence of membrane proteins can be deconvoluted to determine the contribution of mobile and immobile components on the EPR timescale, i.e. the annular and bulk lipids[49]. This has allowed the determination of lipid binding specificity of membrane proteins, such as the preferential binding of cardiolipin and stearic acid over PC lipid by the Na^+K^+-ATPase[52], and the stoichiometry of lipid binding, such as cytochrome oxidase where 56 PC lipids were determined to form the annulus[53]. Another method used to study lipid-protein interactions is fluorescence quenching[54], where tryptophan residues are introduced to a protein in regions where annular lipids are thought to bind. Lipids with a bromine in their acyl chain quench the tryptophan fluorescence signal when bound. This has been applied to study of a number of membrane proteins including the mechanosensitive channel of large conductance (MscL) and revealed that in contrast to expectations, the binding constant of lipids with different acyl chain lengths is relatively unchanged, indicating that it is likely that the protein rather than the bilayer distorts to compensate for hydrophobic mismatch[55]. A number of other

methods have also been applied to the study of lipid-protein interactions including single molecule fluorescence microscopy[56] and NMR[57, 58].

It is important that the hydrophobic thickness of the bilayer is close to the hydrophobic span of the membrane proteins, as any mismatch would be energetically unfavourable. Any differences in these hydrophobic distances result in distortion of the structure of either the lipid or the protein, with the lipid acyl chains either extending or compressing to alter the local thickness of the bilayer, the protein changing its tilt angle, losing structure, or reorienting residues close to the aqueous interface[54] (Figure 1.5). These effects are very specific to the protein and membrane in question, but in general it appears that tilting of the protein is a less energetically demanding response than deformation of the bilayer[54], and has been observed using solid-state nuclear magnetic resonance (NMR)[59], oriented circular dichroism (CD)[60, 61] and molecular dynamics[62] amongst other techniques.

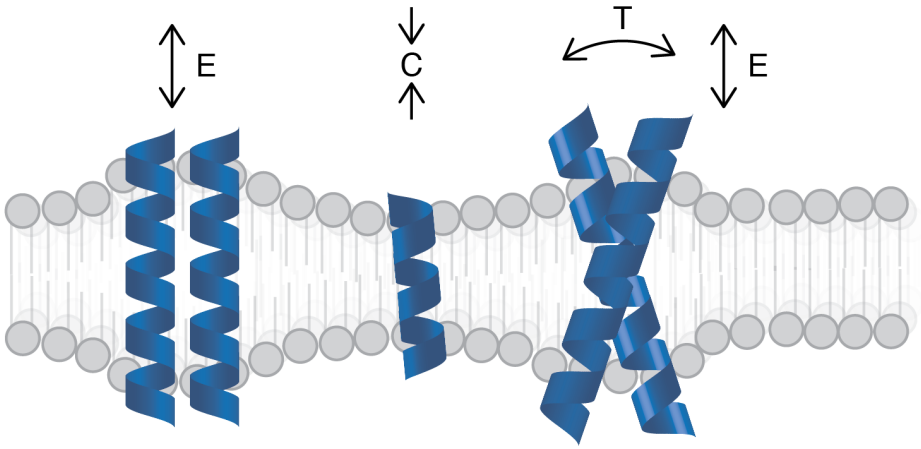

Figure 1.5: ***Consequences of hydrophobic mismatch in lipid bilayer.*** *Membrane proteins and the bilayer are able to respond to differences in hydrophobic thickness through extension of the acyl chains (E), compression of the chains (C) or changing the tilt angle of the protein (T). Figure redrawn from Mitra et al.*[16].

Non-annular lipids can be considered co-factors due to their high affinity binding in regions of protein-protein interactions, unlike the association of the annular lipids with the hydrophobic surface[54]. They have significant roles in protein activity which have been studied for a number of proteins, but none as extensively as the eukaryotic protein KcsA, which has become the archetypical potassium channel for biophysical and physiological studies. A crystal structure of KcsA reveals a bound lipid molecule between each subunit interface, which has been identified as possessing an anionic headgroup[63]. Fluorescence quenching and NMR studies have revealed the significance of R64 and R89[64, 65], which mediate electrostatic interactions with the anionic moiety. Without at least three bound

lipids the channel fails to open[66], and functional studies where the arginines are mutated to leucine also reduce the channel opening probability[64].

Annular lipids can have an important role in determining the activity of proteins, as has been illustrated by work on the Ca^{2+}-ATPase[48], whose ATPase activity was measured as a function of acyl chain length. It was found that C18 acyl chains result in the optimum activity, which have the greatest similarity in terms of thickness to the native membrane. It is postulated that this occurs due to emergence of structural confirmations not usually observed as a response to hydrophobic mismatch, which alters helix packing and obscures Ca^{2+} binding sites[48]. The *E. coli* ammonium transporter AmtB has been studied using ion mobility mass spectroscopy, which has revealed that PG lipids stabilise the trimeric state of the transporter to a much greater extent than phospholipids with other headgroups[67]. Crystallisation of the protein in the presence of PG generates a structure with resolved bound lipid molecules (Figure 1.6), which in general is very similar to structures obtained from crystallisation in detergent, but there is a loop region which undergoes significant reorientation such that the W80 side chain moves by 4 Å to protrude into the headgroup region of the bilayer[67].

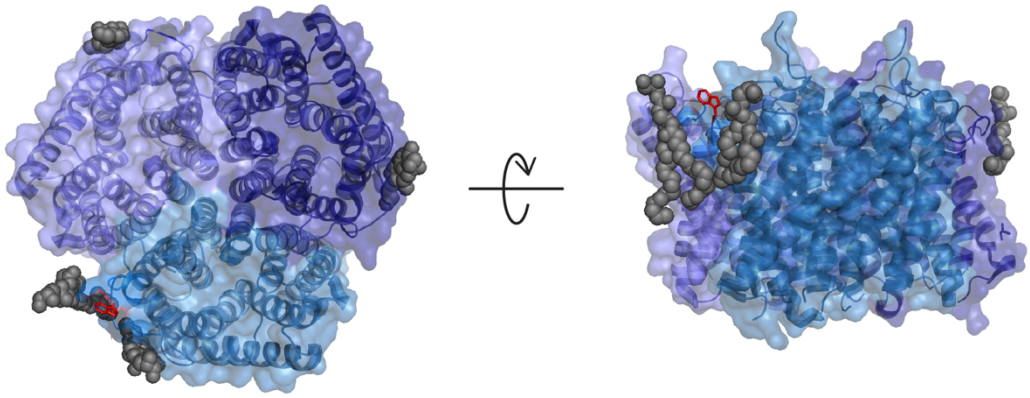

Figure 1.6: ***Crystal structure of the* E. coli *ammonium transporter AmtB showing bound PG lipid.*** *The W80 (red) reorients significantly on PG binding to interact with the bilayer. Figure produced using pdb code 4NH2 from Laganowsky et al.*[67].

Bulk lipids in the bilayer are similarly important in the structure and oligomerisation of proteins. Rather than interacting directly with the protein they provide lateral pressure through their acyl chains and headgroups, which can stabilise protein assemblies. In the case of KcsA, its tetrameric quaternary structure is destabilised when the membrane packing density is reduced using TFE[68], and correct folding of bacteriorhodopsin has been

demonstrated to be highly dependent on lateral pressure by measuring the folded yield in model membranes with different mixtures of bilayer and non-bilayer forming lipids (PC and PE respectively)[69].

1.2. Challenges of membrane protein structural biology

There is a great discrepancy in the number of membrane protein structures available relative to their soluble counterparts, in spite of their physiological significance. This is a result of challenges associated with all stages of their expression, purification and characterisation. In the following section each of these stages will be considered.

1.2.1. Systems for membrane protein expression

In all techniques the initial bottleneck is the expression and purification of membrane proteins, which is notoriously challenging, so it is desirable to be able to obtain maximal structural information using the smallest feasible quantity of material. In order to express membrane proteins, a number of *in vivo* and *ex vivo* systems have been employed. *E. coli* systems in particular have been used extensively due to their relative technical ease and speed, although eukaryotic membrane proteins have a tendency to be toxic to these cells. The prokaryotic folding machinery is quite different to that in eukaryotes, and can be easily overwhelmed during induced overexpression[70]. If the rate of expression exceeds the cell's ability to properly fold and insert the membrane protein in the bilayer, the protein can aggregate and form inclusion bodies, which require alternative extraction methods. This is particularly challenging for helical membrane proteins[71]. Finally, *E. coli* are not able to post-translationally modify expressed recombinant proteins, which can have significant functional implications, and can also direct the protein structure and folding[72]. In order to address this, yeast based systems (e.g. *Saccharomyces* and *Pichia*) have been popular for membrane protein expression, and are scarcely more complex than the *E. coli* approach, but have the advantage of eukaryotic folding and post-translational modification machinery[73]. A small number of membrane proteins have been successfully expressed in cultured insect and mammalian cell lines with good yields[74], and they are becoming increasing popular, although the costs associated with them are significantly greater than in bacterial expression systems[75].

1.2.2. Purification of recombinant membrane proteins

Once a protein is successfully expressed, its extraction from the cellular lipid membranes requires careful choice of a suitable detergent. There are a number of criteria to consider;

ideally the detergent would fully solubilise the protein, retain its structure and function and be amenable to any downstream assays or studies desired. In reality there is need to compromise between these requirements. Detergents can be categorised based on charge as zwitterionic, non-ionic or ionic, which broadly corresponds to the 'harshness' of the detergent. Ionic detergents such as sodium docedyl sulphate (SDS) are highly denaturing and in most instances disrupt any native protein-protein interactions. Non-ionic detergents like Brij and n-dodecyl-β-D-maltoside (DDM) are mild, non-denaturing and may be less effective solubilisers whilst maintaining protein function. Finally, zwitterionic detergents such as lauryldimethylamide oxide (LDAO) fall between the ionic and non-ionic detergents and can offer compromise between successful protein delipidation and maintenance of protein integrity. Of course, with any detergent the removal of the bilayer is likely to have profound effects on the stability and structure of the proteins, and it is not unusual for membrane proteins solubilised in detergent precipitate shortly after purification. It is also the case that the length of acyl chains in detergents can affect protein stability, with shorter chain non-ionic detergents being implicated in the inactivation of some proteins, such as the short chain octyl glucoside (OG) when solubilising the Ca^{2+}-ATPase from sarcoplasmic reticulum[76]. Further, it has been suggested that the aggregation number of the detergent can have a potent effect on protein stability. In the case of glycophorin A, solubilisation in detergents with increasing aggregation numbers results in a reduction in dimerisation of the protein to a greater extent than the acyl chain length[77].

The influence of the solubilising environment on protein structure has been elegantly illustrated by the influenza virus A M2 protein, for which structures in both detergent (solution NMR and crystallography) and lipid bilayers (solid-state NMR) are available[78] (Figure 1.7). These structures reveal significant differences in the helical tilt angle which dramatically alter the pore size, and it also appears that detergent molecules are able to bind within the pore, reducing its functionality. This clearly underlines the need for caution when interpreting structural and functional data from proteins solubilised in detergent environments.

Alternative approaches to membrane protein solubilisation have been developed using amphipols[79], polymers with a main chain interspersed with both hydrophobic and hydrophilic groups. Amphipols can be more stabilising that detergents, which appears to be because of the tendency of detergents to disrupt protein-lipid and protein-protein interactions[80]. More recently, the use of styrene maleic acid (SMA) has provided a novel

method to extract the membrane proteins in the presence of an annulus of native lipids[81], which not only allows lipid-protein interactions but also provides lateral pressure. SMA is a long chain polymer in which the hydrophobic styrene groups interact with the lipid acyl chains whilst the external facing maleic acid groups interact with the solvent. The method has been demonstrated on at least 30 membrane proteins, and it appears that activity is either maintained or enhanced relative to detergent solubilised membrane proteins[81]. Their ability to maintain membrane protein structural integrity has been demonstrated using spin-labelled bacteriorhodopsin in SMA lipid particles (SMALPs) compared to native purple membranes and OG detergent[82].

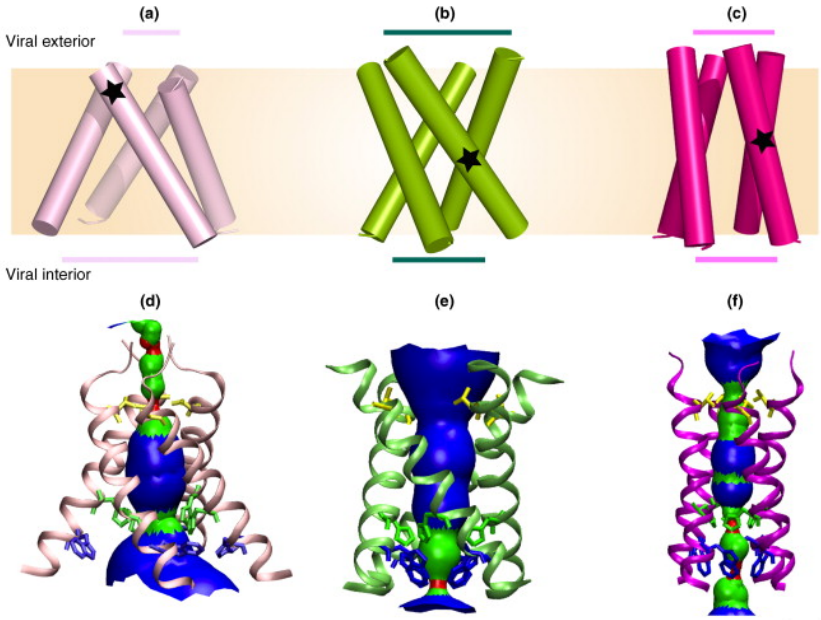

Figure 1.7: ***Structures of the influenza M2 channel solved in different environments.*** *A. Crystal structure in OG. B. Solid-state NMR structure in lipid bilayers. C. Solution-state NMR structure in DHPC micelles. Stars indicate the helix crossing point. D.-F. show the pore size of the channel for the structures above. Red > 1.2 Å, green < 3 Å and blue > 3 Å. Figure reproduced with permission from Cross et al.[78].*

1.2.3. Techniques to characterise membrane protein structure

To obtain high resolution protein structures studies are limited to X-ray crystallography, NMR and cryo-electron microscopy (cryo-EM). By far the most successful methodology in terms of number of structures obtained is crystallography, although in the majority of cases solubilisation is achieved without the presence of lipid in the crystallisation conditions. More recently methods to form crystals in the presence of a lipidic phase have shown potential to address this issue. This is also true of solution-state NMR spectroscopy, whereas solid-state NMR and cryo-EM allow a membrane protein in a lipidic environment

to be studied. EPR spectroscopy is being used increasingly to probe membrane protein structures, and can provide atomic resolution information regarding structural organisation, dynamics and interactions. In addition to these higher resolution methods, lower resolution techniques such as far-UV circular dichroism (CD; and oriented circular dichroism, OCD), and Fourier transform infrared (FTIR) spectroscopy can provide detail about the overall protein structure, but not site-specific information without combination with other methodologies. Further structural information can be gained using indirect approaches, such as electrophysiology, hydrogen-deuterium exchange or cross-linking studies, but those will not be considered here. The techniques used in this thesis, solid-state NMR and CD, are discussed in more detail later in this chapter.

1.2.3.1. Membrane protein crystallography

The majority of membrane protein structures have been solved using macromolecular crystallography, which typically produces structures at high resolution (< 4 Å). Broadly, two types of membrane proteins crystals can be produced, either type I or type II. Type I crystals are formed from membrane proteins in lipidic environments. The presence of lipid bilayers in the crystallisation conditions allows protein-protein contacts between hydrophobic regions. Crystallisation is carried out using lipids in aqueous solutions which form bicontinuous lipidic cubic phases (LCP) with carefully controlled hydration and temperature[83]. These provide a more native-like environment and allow tighter packing of the proteins, producing more ordered crystals. It must be noted that the membrane proteins added to the LCP in detergent micelles, meaning the environment is not purely lipidic[84]. A commonly used example is the monoolein and water system which forms the Pn3m phase, a bicontinuous cubic phase with a double-diamond morphology[85, 86]. Although LCP can be challenging to prepare and handle, the addition of additives such as detergent or polyethyleneglycol can create a “sponge” phase which has reduced viscosity and can be more amenable for certain proteins. An alternative approach has involved using lipid bicelles, which are simple to prepare and incorporate protein into, and in preparation of crystal trials can be treated essentially the same as detergent solubilised proteins[87].

Type II crystals use detergent solubilised proteins and mostly the same methodology as crystallography of soluble proteins, including vapour diffusion and microdialysis[86]. The relative simplicity of this type of crystallography has meant that the majority of membrane proteins crystals have been produced in this manner. The protein-protein contacts generally occur between the hydrophilic regions of the proteins which are not solvated by detergent. The detergent choice is extremely important; for example whilst OG is fairly poor in terms

of its ability to solubilise membrane proteins it is one of the most successful detergents for crystallography[88]. As type II crystals are formed through interactions of the hydrophilic regions they can be fragile and poorly ordered, which often results in low resolution structures. In many cases successful the formation of well diffracting crystals has relied on the presence of antibodies bound to the protein of interest[89], the removal of flexible loops and domains[90], and the introduction of mutations to stabilise the protein[91], all of which are likely to alter the structure in some manner, making it less representative of the physiological conformation. A number of experimental developments including the use of microfocussed beams have aided in the collection of high resolution data, and the increasing number of membrane protein structures available improves the chance of success in attempts at molecular replacement[86].

1.2.3.2. Cryo-electron microscopy

Two of the most common applications of cryo-EM to membrane proteins involve electron diffraction and or single particle cryo-EM. Electron diffraction uses membrane proteins embedded in two dimensional (2D) crystals in either a sheet-like or tubular form[92]. The use of 2D crystals is advantageous to solving the structure since it precludes the need to average over multiple orientations. One limitation however is the need to tilt the crystal around the beam to collect a 3D dataset, which is difficult at larger angles and is worsened by any flexibility in the crystal[93]. This can blur densities parallel to the bilayer normal. The first membrane protein structure was revealed using electron diffraction in this manner, where the purple membranes of *Halobacterium halobium* were studied and the structure of bacteriorhodopsin revealed[94]. Since then it has been applied to a small number of proteins, including solving the structure of the nicotinic acetylcholine receptor at a resolution of 4.6 Å, which was made possible through the use of tubular arrays[95].

The most rapidly developing structural methodology is single particle cryo-EM which has seen large technical advances in recent years. Through the introduction of detectors with vastly improved quantum efficiency and the development of new processing algorithms, membrane protein structures with resolution becoming comparable to crystallography (currently ~4 Å) have been achieved[96-98]. A particularly attractive feature of cryo-EM is the requirement for only μg quantities of protein, and glycosylated and flexible regions, which are not observed in crystal structures, are readily visualised in cryo-EM. In many cases flexible loop regions form functionally significant features such as enzyme active sites[99] and glycosylation has an important role in protein folding and structure[72]. In contrast to crystallography which reports only one conformation of the protein, it is possible to

observe multiple conformational states in cryo-EM. Although this may be troublesome since these different states need to be segregated to allow structures to be deciphered, it may also be highly valuable to allow insights into molecular mechanisms[100]. At present the resolution of cryo-EM still lags behind that attainable using crystallography, and a particular limitation of single particle cryo-EM is the size requirement; currently only larger proteins greater than approximately 150 kDa are amenable to the technique.

Samples are prepared from solutions of solubilised membrane protein which are deposited onto a perforated carbon grid and frozen, resulting in an array of protein orientations embedded in vitreous ice[101]. Two dimensional images of the proteins can then be taken and combined using algorithms to yield a 3D model of the protein. It may be necessary to acquire data over a number of weeks to ensure sufficient orientations are sampled to build a model, and heterogeneity of the proteins within the sample (e.g. open and closed states) can provide further challenges. Larger proteins have conventionally been a target for cryo-EM but it is being increasingly applied with success to smaller proteins, such as the transient receptor potential vanilloid 1 (TRP V1) which has been solved with some regions of the structure exhibiting resolution of 3.4 Å[102]. This protein is relatively small compared to typical targets for cryo-EM, at around 60 kDa per monomer. Park et al.[98] have recently solved the structure of the bovine CLC chloride channel and improved resolution through the use of monoclonal antibodies complexed to the channel to increase the molecular weight. Other methodological and technological developments will likely make feasible the application of cryo-EM to much smaller proteins.

1.2.3.3. Nuclear magnetic resonance

Both solution- and solid-state NMR have been successfully applied to membrane proteins in order to characterise their structure, but also dynamics and interactions – information not readily accessible using crystallographic approaches. Solution-state NMR has been significantly more successful in terms of structure determination than solid-state NMR, with just 109 structures in the protein data bank (PBD) solved exclusively using solid-state NMR compared to 12933 entries for solution-state NMR (non-unique entries; as of July 2017). This arises from poorer spectral resolution in solid-state and limited methodology to provide adequate distance restraints between nuclei. Solid-state NMR does however allow the examination of residue specific interactions, and allows proteins to be studied in a bilayer environment mimicking the cellular membranes. A pre-requisite for high-resolution NMR studies of proteins, in both solid and solution, is the ability to isotopically label the protein, conventionally using ^{15}N and/or ^{13}C, which are NMR active nuclei (i.e. spin $\neq 0$).

Proteins can be expressed in *E. coli* grown in isotopically-enriched media to achieve this labelling, although this can be challenging and expensive both financially and temporally. Particularly in the case of membrane proteins where there is paucity in their expression, adaptation of the expression protocols to isotopically enriched media is challenging. Expression of isotopically labelled mammalian proteins has been somewhat limited[103] although recently an interesting approach using *Caenorhabditis elegans* to express ^{15}N, ^{13}C bovine rhodopsin has been described[104]. When working with small proteins and peptides (< 100 amino acids) solid-phase synthesis can be used and isotopically labelled amino acids can be incorporated in a site specific manner.

Solution-state NMR has been used to mostly study small soluble proteins (< 30 kDa) which give sharp lines due to their rapid tumbling and averaging of anisotropic interactions. Larger proteins tumble more slowly, which broadens lines, and additional resonances crowd the spectra, making residue assignment a greater challenge. The use of fully deuterated proteins can increase this size limit to ~70 kDa, although production of these proteins is extremely expensive and time consuming. Membrane proteins studied by solution-state NMR are usually solubilised in detergent micelles or isotropic bicelles which contribute to the overall size, so the size limitation for membrane proteins is much smaller than soluble proteins. The micelle size is often considerable relative to the protein, for example in the case of the commonly used detergent 1,2-dihexanoyl-sn-glycero-3-phosphocholine (DHPC) the micelle size is ~20 000 kDa[105]. The majority of membrane proteins characterised have therefore been peptides and small proteins, although there are a small number of examples of larger proteins, including the structure of the 19 kDa β-barrel OmpA protein which has been solved using solution-state NMR in dodecylphosphocholine micelles[106]. Solution-state NMR structures involve the measurement of distance and orientation between nuclei, using measurements of residual dipolar couplings and the nuclear Overhauser effect.

In contrast to solution-state, since solid-state NMR does not rely on averaging of anisotropic interactions by Brownian motion, there is no inherent size limitation, although with larger proteins methods to address spectral crowding are not fully developed. The types of protein samples commonly studied by solid-state NMR are amyloid fibrils, crystalline proteins and membrane proteins in pure lipid environments, which cannot be studied using solution-state NMR due to their size. Solid-state NMR can be broadly categorised into oriented solid-state NMR or magic angle spinning (MAS) solid-state NMR. In solids, anisotropic interactions (chemical shift anisotropy, quadrupolar

interactions and dipolar couplings) dominate the spectra. Using MAS it is possible to average many of these interactions to produce a solution-like spectra with narrow lines. This is achieved by spinning the sample at high speeds (up to 110 kHz or more) in a rotor oriented at 54.7° with respect to the magnetic field[107]. MAS NMR has been successfully used to solve the structures of a number of membrane proteins in lipidic environments, including the *Anabaena* sensory rhodopsin, a 81 kDa homotrimer of seven helical bundles (Figure 1.8)[108]. This structure differs from the crystal structure of the same protein[109] (grown under LCP conditions), in which dimers were found, and a loop region which was disordered in the crystal structure is shown to form a hairpin. There are also significant changes in the tilt angle of helices A and E of up to 10°.

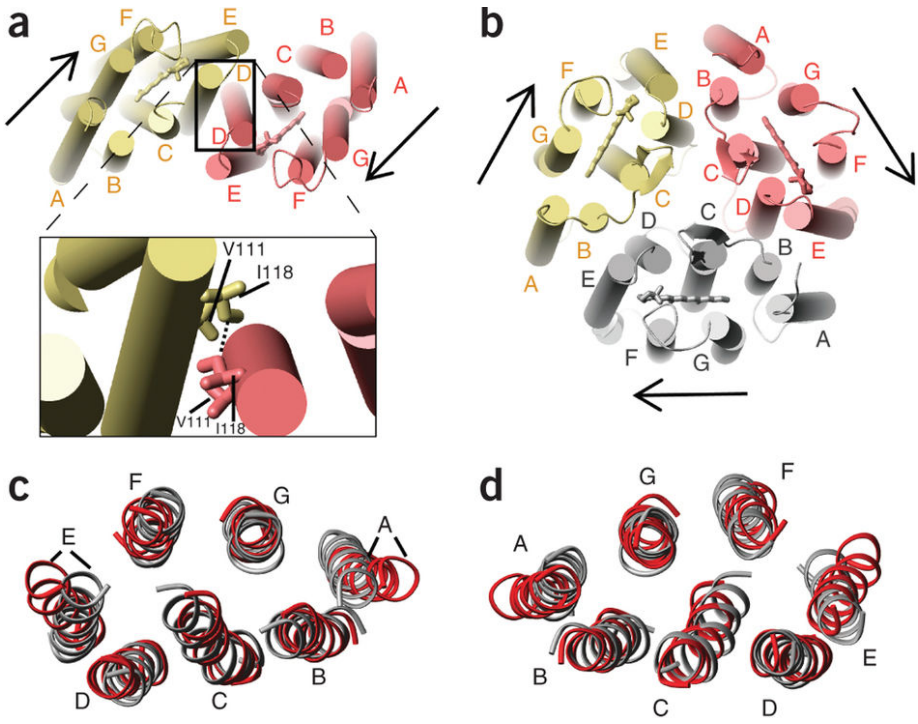

Figure 1.8: ***Structures of* Anabaena *sensory rhodopsin from crystallography (A.) and solid-state NMR (B.).*** *Arrows indicate the retinal orientation. Enlarged region of A. shows the interfacial region between monomers. C. and D. overlay the crystal (grey) and NMR (red) structures from the cytoplasmic and periplasmic sides respectively. Reprinted by permission from Macmillan Publishers Ltd, Wang et al.[108], copyright 2013.*

In contrast to MAS, oriented NMR exploits anisotropic interactions to characterise molecular orientation in a crystalline sample, such as the tilt angle of a helix in an oriented lipid bilayer. In such cases, bilayers are aligned either mechanically with lipids deposited on a support substrate, or magnetically using bicellar phases which spontaneously align in a magnetic field. Sensitivity is gained in oriented samples when there is a high degree of

alignment, since tensors oriented along the same axis are additive, and well aligned samples yield sharp spectral lines.

One dimensional solid-state NMR experiments measuring chemical shifts can reveal the orientation of proteins in oriented bilayers and additional information can be gleaned through the use of two dimensional experiments, such as PISEMA (polarisation inversion with spin exchange at the magic angle)[110]. PISEMA correlates chemical shifts and ^{15}N-^{1}H dipole-dipole couplings, two interactions in NMR which have a dependency on the molecular orientation. As the tensors for these interactions are not linearly aligned in the spectra their peaks give rise to 'PISA wheel' (polar index slant angle) patterns which allow assignment of resonances and the peptide tilt and pitch angle (Figure 1.9).

Although PISEMA has been most successfully applied to single pass membrane active peptides such as antimicrobial peptides, a number of more complex proteins have been characterised using the approach including the G protein coupled receptor CXCR1[111]. The influenza M2 proton channel has been studied extensively using PISEMA experiments[112-115], and its proton conductance and acid activation mechanism has been delineated based on structures produced. Constructs for residues 22 – 62 were reconstituted into oriented DOPC/DOPE (4:1) bilayers, with proteins labelled using both site specific and uniform ^{15}N labelling schemes[115]. The two-helical monomers were found, as expected, to assemble into a tetramer with one helix protruding through the bilayer as part of the proton conductance pathway, forming a kinked helix oriented between 22° and 32° to the bilayer, and with the second amphiphilic helix packed against the bilayer surface oriented at 105° to the bilayer. The amphiphilic helix was found to be essential for structural integrity, and significantly there are large differences in the structure and position of this helix when comparing the PISEMA structure to one obtained using solution-state NMR for a similar construct (for residues 18 – 60)[78]. This presumably occurs since in solution-state NMR the protein was solubilised in detergent micelles (DHPC) so interactions between the amphiphilic helix and lipid headgroups are not present to stabilise the structure, again highlighting the need for careful interpretation of structural data of membrane proteins obtained in a detergent environment.

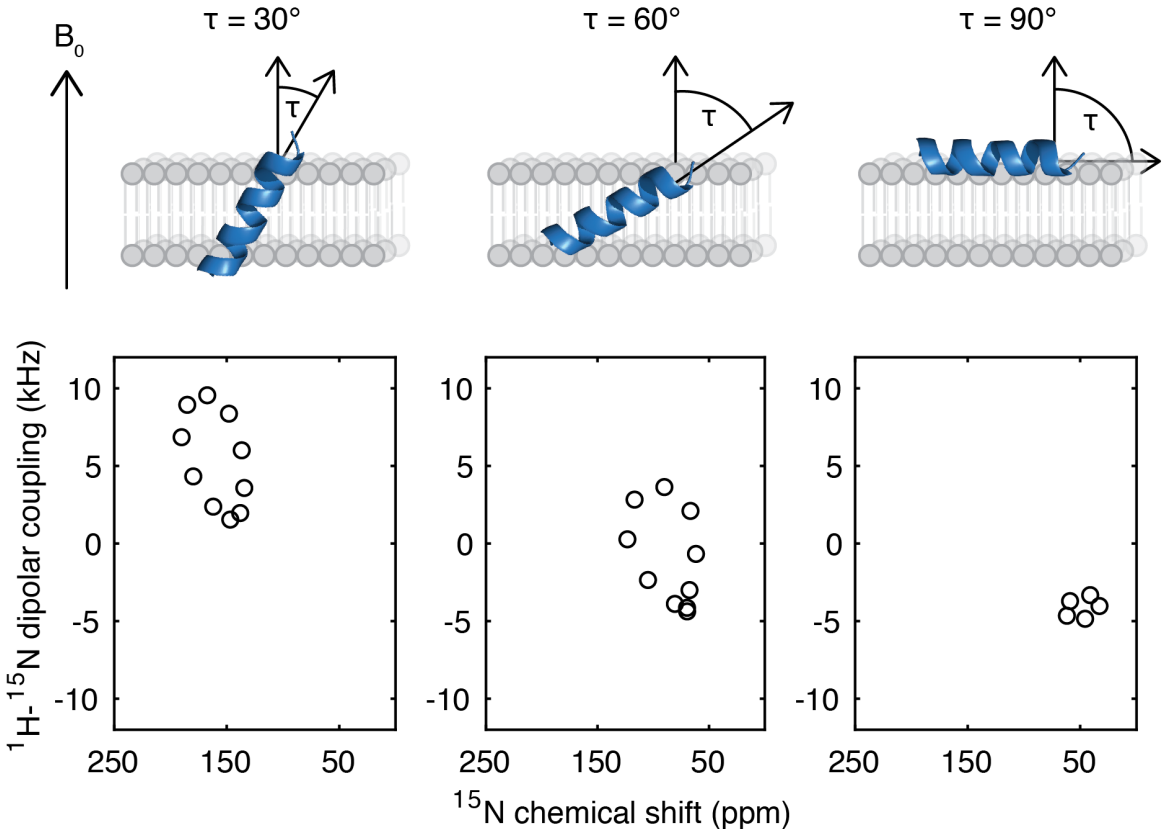

Figure 1.9: ***Simulated PISEMA spectra for an idealised α-helix (ϕ = -65°, ψ = -40°) in an oriented bilayer at different tilt angles .*** *PISEMA correlates the ^{15}N chemical shift and ^{1}H-^{15}N dipolar couplings and produces PISA wheels which trace out the helical tilt angle and pitch. The bilayer normal is oriented parallel to the B_0 field with the angle between the normal and the helix axis τ. Spectra were simulated using a custom written MATLAB script based on the method described by Wang et al.*[112].

1.2.3.4. Electron paramagnetic resonance

Electron paramagnetic resonance (EPR) spectroscopy has been applied to the study of membrane protein structure and dynamics. It has no protein size limitation and can readily be applied to membrane proteins in either detergent or lipidic environments. (A theoretical background to EPR is described in Chapter 3.)

An inherent requirement of the technique is the presence of a free radical, which are not present physiologically in the majority of membrane proteins. To introduce free radicals, site directed spin labelling is used, where either the spin label is present in amino acids used during solid-phase peptide synthesis, or where it is attached to cysteine residues via disulphide bonding in a recombinantly expressed protein. An advantage over NMR approaches is that there is no need to isotopically label the proteins, and less material is needed due EPR's high sensitivity.

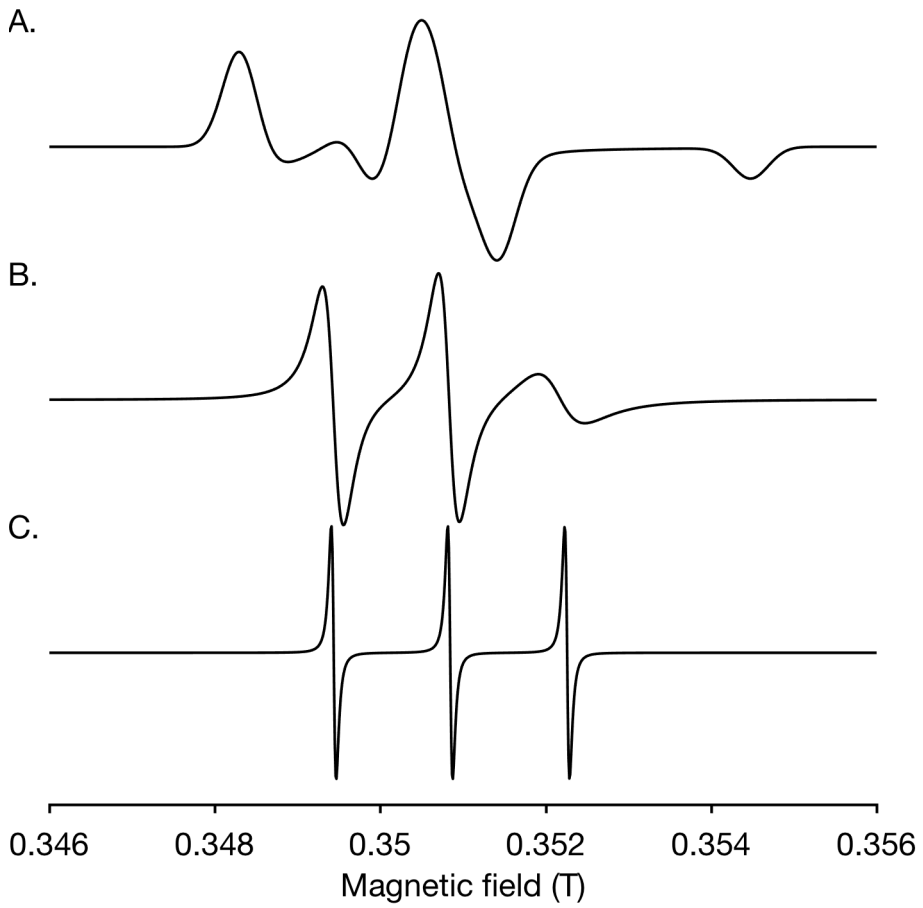

Figure 1.10: ***Simulated CW-EPR spectra for nitroxide spin labels with different rotational correlation times (τ_c) from powder (A.), motionally restricted (τ_c = 0.2 μs; B.) and isotropic (τ_c = 10 ns; C.).*** *Spectra were simul,ated using EasySpin, and the script used to generate the figure can be found in appendix A. Adapted from Sahu and Lorigan*[116].

EPR experiments can be either continuous wave (CW) or pulsed, with the two approaches providing different information. CW-EPR allows the motility of the spin label to be probed, which is reflected by changes in the spectra linewidths (Figure 1.10). This can allow estimations of secondary structure and investigation of membrane protein topology[117]. To study intramolecular distances between two spin labels, CW-EPR is useful for distances of 8-30 Å, whilst pulsed EPR experiments can investigate intramolecular distances up to 80 Å[116]. Double electron-electron resonance (DEER) experiments are commonly used for pulsed measurements and probe the distance dependent dipole-dipole couplings of two free radicals. DEER has been applied to the voltage-gated potassium channel KvAP to develop a model for its gating[118]. It was found that the S4 helix of the voltage sensing domain, which is positively charged and reorients in response to changes in voltage to link the pore structure to the transmembrane voltage, undergoes a ~3 Å shift to a resting state when the lipid composition is changed, leaving the channel unresponsive to changes in transmembrane voltage.

1.2.3.5. Circular dichroism spectroscopy

Circular dichroism (CD) spectroscopy has been widely used in the basic characterisation of soluble proteins and membrane proteins to determine their secondary structure. This information is provided in the far-UV region (180 - 260 nm). Information on the tertiary structure and interactions can be gleaned by studying aromatic residues in the near-UV region (250 – 350 nm). In the far-UV CD cannot provide the type of site specific resolution accessible using crystallography or NMR, but its relative simplicity, requirement for only small quantities of material (10s of μg) and acquisition times of minutes have made it a widely used and valuable tool for researchers investigating isolated proteins. It is possible to estimate the secondary structure content of proteins from CD spectra with relative ease through the use of algorithms which fit experimental data against datasets of CD spectra from proteins of known structure. To account for the diverse structural features of different classes a number of datasets have been made available, including those for soluble proteins[119], membrane proteins[120], and crystalline proteins[121], with a dataset for disordered proteins soon to be published.

A major limitation of the technique is the stringent buffer requirements for data acquisition in the far-UV region. Many of Good's buffers absorb in the far-UV region and thus must be avoided or used at minimal concentration. Additionally, chloride ions exhibit high absorbance at 180 nm meaning in samples with NaCl concentrations above approximately 10 mM measurements below ~195 nm are not feasible. Whilst problematic, these issues can often be addressed using buffers such as phosphate buffers, and chloride salts can be replaced with fluoride counterparts. It may be more challenging when wanting to study interactions with ligands which either strongly absorb unpolarised light or contain chiral groups.

1.2.3.6. Fourier transform infrared (FTIR) spectroscopy

FTIR is a spectroscopic technique which probes the vibrational frequencies of chemical bonds. Although FTIR spectra have a number of amide bands from proteins, unlike other structural techniques FTIR probes any chemical bonds and is not protein specific. It is therefore possible to investigate not just protein structure, but any ligands or other molecules present in the sample. Although there is no requirement for special isotope labelling, due to the strong water signal near to the amide bands, samples are usually dissolved in D_2O. The amide I band arises due to stretching of the C=O bond, with additional contributions from C-N, C-C-N, and N-H bending vibrations, whilst the amide

II band arises from N-H stretching and C-N bending vibrations[122]. Since hydrogen bonding to stabilise secondary structures involves the C=O and N-H groups the amide bands are highly sensitive to protein secondary structure. Bands can be deconvoluted into individual peaks which correspond to secondary structural features to estimate protein structure content. As well as determination of protein secondary structure in solution, it is possible to use polarised attenuated total reflectance FTIR (ATR-FTIR) to determine protein orientation in oriented lipid bilayers[122]. By application of light at s and p polarisation (where electric field vector is perpendicular and parallel to the plane of incidence respectively) the linear dichroic ratio of the two can determine the protein orientation relative to the electric field vector. Since the surrounding lipid molecules in the bilayer can also be observed by FTIR, it is possible to simultaneously determine a number of characteristics of the lipids, including the acyl chain order parameter, lipid phase and hydration, and the binding affinity of the lipid and proteins. An example of the potential of the method to simultaneously probe protein orientation, structure and the properties of lipid bilayer is given by Ding et al.[123], who have studied the *Saccharomyces cerevisiae* G-protein coupled α-factor pheromone receptor. Seven protein fragments corresponding to each of the transmembrane domains were reconstituted into oriented multilayers, which allowed determination of the tilt and secondary structure of each. Further, they were able to use hydrogen/deuterium exchange FTIR to estimate the number of residues embedded in the bilayer. It was also possible to determine the acyl chain order parameter and angle, which corresponded to values expected for a pure lipid bilayer, indicating the protein does not disrupt the bilayer integrity.

1.3. Theoretical basis of circular dichroism and nuclear magnetic resonance

The majority of the work in this thesis involves the methods circular dichroism (CD) and solid-state nuclear magnetic resonance (NMR) spectroscopies. The theoretical basis of these methods given below provides a background to the interpretation of the data. For more extensive discussion of these approaches, readers are referred to the excellent texts by Fasman et al.[124] or Levitt[125] for CD and NMR respectively.

1.3.1. Circular dichroism theory

Circular dichroism (CD) spectroscopy is a widely used biophysical technique which has a number of applications. The basis of the technique is the wavelength dependent differential

absorption of left and right circularly polarised light by a chiral molecule. For a given wavelength the molar CD (Δε) is given by:

$$\Delta\varepsilon = \varepsilon_L - \varepsilon_R \qquad (1.1)$$

where ε_L and ε_R are the molar extinction coefficients for left and right circularly polarised light respectively. The interaction of circularly polarised light and the chiral molecule results in a helical displacement of an electron to a higher orbital, induced by a combination of linear and circular displacement from electric and magnetic components of the light respectively.

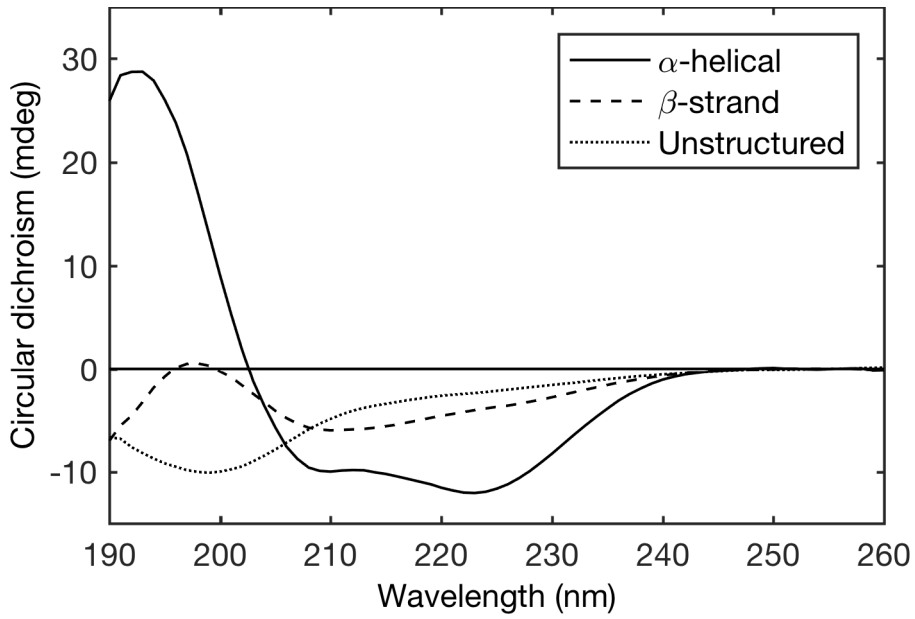

Figure 1.11: ***Example CD spectra of α-helical (solid line), β-strand (dashed line) and unstructured (dotted line) proteins.***

In a biological context CD spectroscopy has been applied to a number of systems, but it has been used most extensively in the characterisation of protein secondary structure. Secondary structure information can be extracted from spectra acquired in the far-UV region (< 260 nm) and is a popular way to confirm the structural integrity of proteins thanks to the relatively low concentration required (10-100 μg compared to mg quantities for NMR/crystallographic studies) and the ease and speed of data collection and analysis. Example CD spectra of proteins with majority α-helical, β-strand or disordered structure are given in Figure 1.11, each of which have a distinct spectral signature. Each band in the spectra is associated with an electronic transition of the peptide bond. In the following description α-helical proteins are considered. A typical α-helical spectra can be

deconvoluted into three characteristic features: a positively intense band centred around 190 nm, and two bands of negative intensity centred around 208 and 222 nm.

These bands in the CD spectra occur as a result of electronic transitions of the peptide bond and have their dipole moments polarised with respect to the helical axis, as predicted by Moffitt's exciton theory (Figure 1.12)[126, 127]. The n-π* transition has negative rotational strength and has its dipole moment polarised along the carbonyl bond. It gives rise to a band around 222 nm. The π-π* transition is split into three components, the first of which has negative rotational strength and is polarised along the helical long axis with its resulting band centred at 208 nm. The two remaining components produce a degenerate band around 190 nm, with one positive peak at 190 nm and a second, the so called 'helix band', around 188 nm. The exact intensity and position of the helix band has proved controversial with disagreement between experimental and calculated values[124], but it is clear that it contributes significantly to the spectra, as will be seen in the later in this chapter.

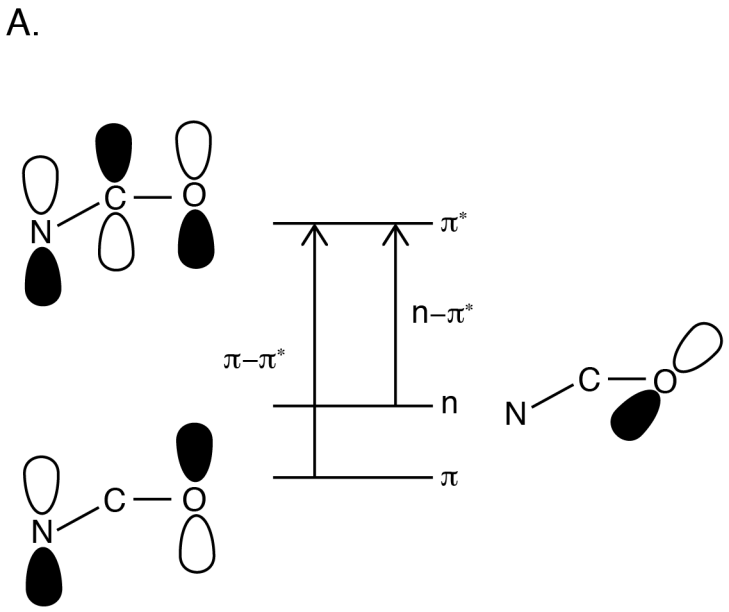

Transition	Wavelength
$\pi-\pi^*_{\perp}$	190 nm
$\pi-\pi^*_{\parallel}$	208 nm
n–π*	222 nm

Figure 1.12: ***Summary of electronic transitions of the peptide bond contributing to the far-UV CD spectra.*** *A. Representation of the change in polarisation of the orbitals between peptide bond transitions (adapted from Bulheller et al[128]). B. Alignment of transitions with respect to the helical axis. C. Table summarising peak positions resulting from the three transitions.*

If a protein in solution sample is measured, there is an isotropic average of the transition polarisations across the sample. For an α-helix this manifests peak intensity ratios of approximately 0.8 for 222:208 nm and 2 for 190:208 nm in soluble proteins. (Although it should be noted that a range of other factors can affect the peak intensities, such as solvent polarity, and a reduction in the 222:208 nm ratio has been observed in in coiled-coil type interactions[129].)

1.3.2. Application of CD to membrane proteins

The resolution of CD data does not allow for the assignment of topology to specific regions of a protein. It does however allow identification of structural changes as a result of mutations, ligand binding and environmental conditions, for example. The speed of data acquisition makes CD a convenient method to study such structural changes.

As membrane proteins are notoriously challenging to express and purify, techniques like CD which require relatively small quantities can be extremely valuable to characterise the protein structure. A further attractive quality is the ability to study membrane proteins in lipidic environments, which is challenging using other structural techniques such as crystallography and solution-state NMR. Lipid vesicle structures including small unilamellar vesicles[62], large unilamellar vesicles[130] and bicelles[131] have been used successfully for CD studies. Although these mimetics do not replicate the complexity of the native cellular membranes, the presence of a bilayer lipids confers properties such as charge[67] and lateral pressure[68] which have implications for protein structure and stability. However, the use of lipids presents a number of challenges for optical techniques. One of the most problematic artefacts in these measurements is differential light scattering, which occurs in particulate samples where the particle size is greater than approximately 1/10 of the wavelength[132] (in accordance with Rayleigh scattering). Avoidance of these effects when studying membrane proteins in lipidic environments can be achieved through the use of small unilamellar vesicles (SUVs) which are sufficiently small to preclude scattering effects (< 25 nm). However, such small vesicles have a much greater degree of membrane curvature than the majority of cellular membranes. An additional issue that can present in CD of SUVs is absorption flattening, which occurs due to the uneven distribution of chromophores in the sample and thus the invalidation of the Beer-Lambert law. This occurs in vesicle samples because multiple proteins can be embedded in each vesicle so there are localised changes in the protein concentration. This phenomenon supresses the signal in a wavelength dependant manner and is only completely addressed by either using

an isotropic solution (i.e. detergent micelles) or ensuring that only one protein is present in each vesicle, but this is experimentally challenging and requires high concentrations of lipid[132], whose carbonyl bonds absorb strongly around 220 nm. Therefore flattening effects cannot be completely avoided and must be considered when studying membrane proteins in lipid environments. An excellent review of the artefacts encountered in membrane protein CD and preventative measures has been provided by Miles and Wallace[132].

1.3.3. Oriented circular dichroism (OCD)

Whilst the majority of membrane protein CD studies use solution samples, a further application, OCD, can be used to report the orientation of membrane active peptides and proteins in a lipid bilayer. In a system where there is a driving force for alignment of the chromophores, such as helices in a lipid bilayer, the orientation of the chromophore with respect to the vector of the incident light beam can be evaluated. This method exploits the polarisation of transition dipole moments with respect to the helical axis (Figure 1.12 B). When transitions have their dipole moment polarised collinear to the electric vector of the light propagation there is no excitation and no band associated with that transition. Conversely, when the transition dipole and electric vector are perpendicular the band has maximal intensity.

In an OCD experiment the direction of propagation of the incident light *k* is usually parallel to the bilayer normal *n*. In this case, the angle α between the *k* and the helical long axis *a* determines the OCD signal θ. The OCD signal for a particular α angle is related to the OCD signal at α = 0° and α = 90° according to[133]:

$$\theta(\alpha) = \theta(0°) \cos^2 \alpha + \theta(90°) \sin^2 \alpha \qquad (1.2)$$

When *a* and *k* are parallel the molecular CD can be denoted by $G_{//}$ and when perpendicular by $G_{\perp}$. Since the intensity of the perpendicular component is twice as large as the parallel component in isotropic samples, experimentally the spectrum of a membrane protein in isotropic vesicles (θ_v) is related to the parallel and perpendicular OCD spectra by[133]:

$$\theta_v = \frac{1}{3} G_{||} + \frac{2}{3} G_{\perp} \qquad (1.3)$$

The CD spectra for $G_{||}$ and $G_{\perp}$ are a summation of bands arising from the CD of each transition. For the n-π* transition the signal at 222 nm is a Gaussian band of negative intensity which contributes to both parallel and perpendicular spectra. For the π-π*

transition there are three components to consider. The first is a negative intensity Gaussian band at 205 nm whose dipole moment is polarised parallel to the helical axis, whilst the remaining two have dipole moments polarised perpendicular to the helical axis and have amplitudes and lineshapes which vary depending on the angle α. When α is 0° the two components produce the Gaussian 'couplet' helix band centred at ~190 nm whilst at 90° the two produce a positive Gaussian also centred around 190 nm.

The Gaussian bands (g) take the form[133]:

$$g = A \exp\left(-(\lambda-\lambda_0)^2/\Delta^2\right) \qquad (1.4)$$

whilst the helix band (g_H) takes the form[134]:

$$g_H = A \left(2\,(\lambda-\lambda_0)\,(\lambda_0/\Delta^2) + 1\right) \exp\left(-(\lambda-\lambda_0)^2/\Delta^2\right) \qquad (1.5)$$

where A is the band amplitude, λ_0 is the peak position and Δ is the band width.

The molecular CD where the helix is either parallel or perpendicular to the light can therefore be given as[133]:

$$G_{/\!/} = \theta_{\pi\text{-}\pi^*}\left(g_H,\ 190\ \text{nm},\ /\!/\right) + \theta_{n\text{-}\pi^*}(-g,\ 224\ \text{nm},\ /\!/) \qquad (1.6)$$

$$G_{\perp} = \theta_{\pi\text{-}\pi^*}(+g,\ 190\ \text{nm},\ \perp) + \theta_{\pi\text{-}\pi^*}(-g,\ 205\ \text{nm},\ \perp) + \theta_{n\text{-}\pi^*}\left(-g,\ 224\ \text{nm},\ \perp\right) \qquad (1.7)$$

where the bracketed terms describe the shape and sign of the band, the band position and the orientation of the transition dipole moment and the incident light.

It is easy to see that the 205 nm band is most indicative of orientation as it is only present when the helical long axis is perpendicular to k. Calculated OCD spectra using values from an α-helical reference set by de Jongh, Goormaghtigh and Killian[135] are shown in Figure 1.13 which clearly demonstrate the spectral difference when a peptide is perpendicular (on the bilayer surface, A.) or parallel (inserted fully in the bilayer, B.). The resulting vesicle spectra according to equation 1.3 is shown in Figure 1.13 C. When the helix is aligned parallel to the incident light the band at 205 nm is nearly absent since the parallel component of the π-π* transition is not excited. In contrast when perpendicular the transition interacts maximally with the probing light and a strong negative intensity at 205 nm is observed.

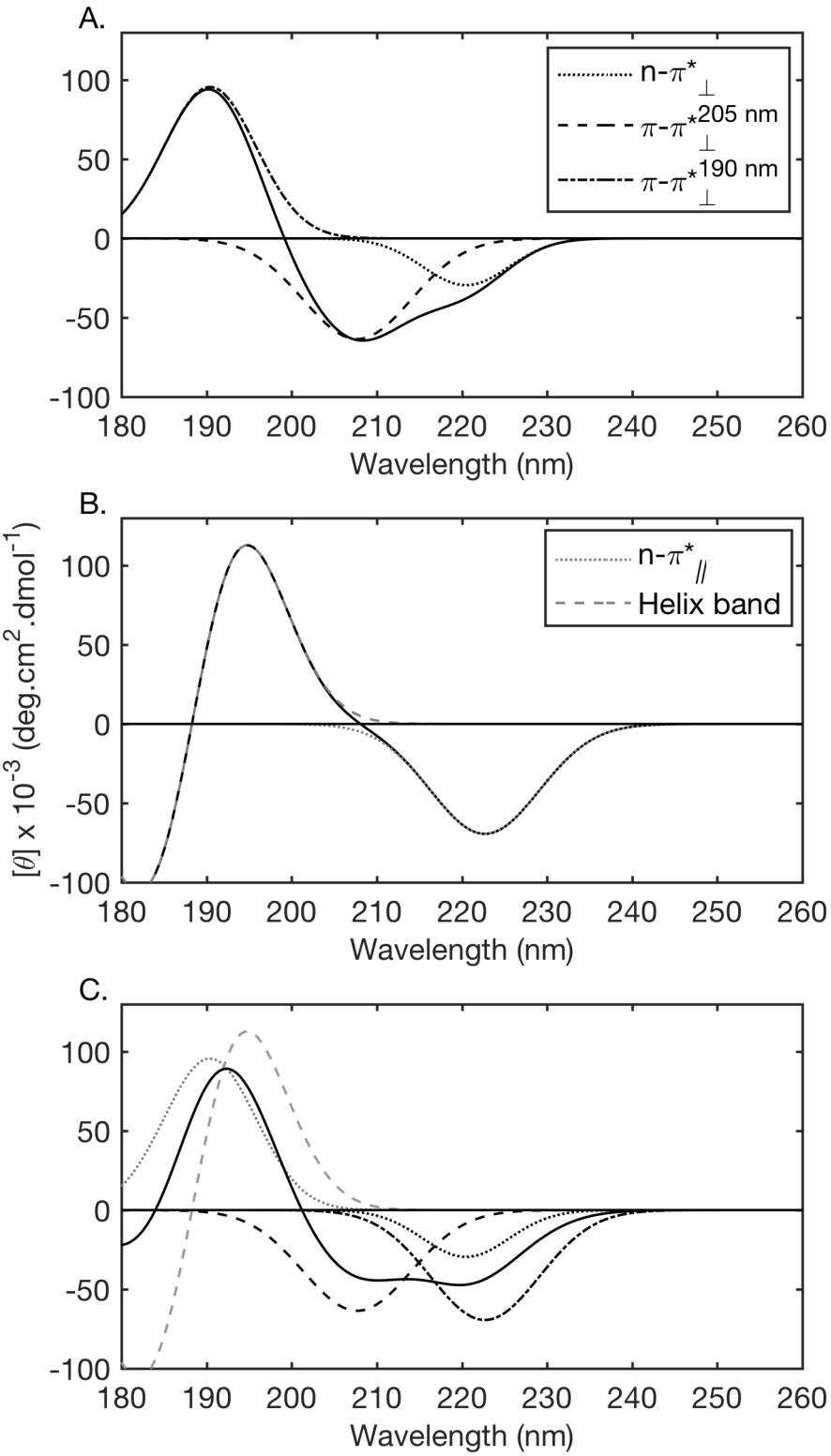

Figure 1.13: ***Computed OCD spectra of a helical peptide in an oriented lipid bilayer.*** *The bands for each transition were calculated according to the equations in the text, using band parameters given in de Jongh et al.*[135] *and summed. A. and B. show the OCD spectra for a helix aligned with its long axis parallel or perpendicular to the propagating light respectively (black solid lines). C. shows the spectra of the helix in isotropic vesicles (black solid line) overlaid with the bands associated with each transition.*

The measurement of OCD spectra assumes the availability of samples with a very high degree of alignment. To prepare oriented samples for OCD two approaches have been used to date. There is some variation in method between publications, but the basic methods are the same. The first and most commonly used method deposits lipid and peptide co-dissolved in organic solvent onto a fused silica substrate. The second method, which is typically used for hydrophilic and amphiphilic peptides, involves the preparation of lipid vesicles reconstituted with the peptide in aqueous solution[136]. This solution can then be spread onto a substrate and dried. In both cases the samples are hydrated by exposure to an environment with controlled humidity, usually achieved using a saturated salt solution, where hydration of the sample results spontaneous formation of aligned bilayers. The hydration of the samples is significant, since the optical properties of the sample, structure of the bilayer and orientation of peptides can be affected by changes in the degree of hydration. The antimicrobial peptide alamethicin has been shown to undergo reorientation as a result of changes in the relative humidity[133], and in studies of model PC membranes there is a distinct structural change in bilayers above 94% relative humidity, where the bilayer reaches its full thickness and headgroups protrude outwards into the aqueous environment between bilayers[137].

Similar to samples of membrane proteins in lipid vesicles, a number of artefacts can distort OCD spectra. In addition to scattering and flattening, oriented samples also present challenges due to linear dichroism (LD) and birefringence (LB) effects, both of which have a magnitude of $\sim 10^{-1}$ compared to the $\sim 10^{-4}$ CD signal. These occur as the light generated by the photoelastic modulator is not purely circularly polarised. LD results from the interaction of light with a tilted dielectric substrate, such as the fused silica used for OCD studies not being perpendicular to the incident light source. It is reported in the literature that the LD signal appears to arise in poorly prepared samples with an inhomogeneous distribution of lipids[136], but when the lipid long axis and the electric field vector are parallel, as should be the case in a well prepared sample, the LD is 0[136, 138]. It is possible to observe LD effects in oriented samples by measuring the CD spectra at fixed angles about the light director, and small contributions, if present, can be eliminated by averaging the spectra acquired at each rotation. The second contribution to consider, LB, occurs due to the changing refractive indices as light passes through the uniaxial sample. The LB can be calculated from the birefringence Δn of the sample at wavelength λ, the sample thickness D at angle α between the light and bilayer normal as[133]:

$$LB = 2\pi D \Delta n \frac{\sin^2 \alpha}{\lambda \cos \alpha} \qquad (1.8)$$

Since LB occurs due to sample uniaxiality there is no change in its intensity as the sample is rotated around the beam, as is the case with LD. It cannot be easily avoided through careful measurement or sample preparation, but Wu et al.[133] were able to quantify the contribution at a maximum of 3 % of their CD baseline signal, and thus could neglect the contribution.

Although there were previous CD measurements of membrane proteins in oriented bilayers[139, 140], the first experimental proof of Moffitt theory was given by Huang and Wu[141, 142] by studying alamethicin in oriented bilayers. Measurement of the sample at different angles between the bilayer normal and direction of light propagation demonstrated the polarisation of the band at 208 nm, confirming Moffitt theory. A comprehensive method for measurement and analysis of peptides in fully hydrated lipid films was published by Wu et al.[133], who first coined the name oriented circular dichroism, where the changes in orientation of alamethicin was studied as a function of hydration state of the bilayer. By modulation of the sample hydration it was possible to orient alamethicin both parallel and perpendicular to the bilayer normal which produced reference spectra for helices at either of these extremes, allowing deduction of the intermediate states since there is a relationship between the vesicle spectra (θ_v) and oriented spectra according to equation 1.3.

An alternative method of analysis has been put forward by de Jongh et al.[135] which rather than relying on orienting the protein of interest in both parallel and perpendicular orientations uses a dataset of proteins of known structure to determine band position and intensity for α-helical, β-strand and random coil proteins. These band parameters can then be fit to experimental data to deduce an orientation parameter for proteins which are not purely α-helical.

OCD has been particularly attractive in the study of antimicrobial peptides, where it has allowed the investigation of their mechanism of action. Alamethicin is one of the most widely studied antimicrobial peptides, which forms an ion conducting pore in cellular membranes. Using OCD, Huang and Wu[143] were able to demonstrate that the transition between the surface bound state ("S state") to its membrane inserted active state ("I state") is dependent on bilayer hydration and peptide concentration. At a critical concentration (140 L/P in DPhPC) the peptide reorients from the S state to the I state, providing

confirmation that in the non-conducting state the protein is associated with the surface of the membrane rather than inserted in the bilayer.

Not all peptides are fixed in either an I or S state, and an intermediate state, termed the "T state", in which the protein is between parallel and perpendicular orientations, has been observed for a number of peptides. A problem occurs in that it is impossible to distinguish this spectral shape from the spectra arising when there is a mixture of I and S state peptides in the sample, or alternatively when there is fast motion of the peptide between the I and S states. This is illustrated by the antimicrobial peptide PGLa first obtained from *Xenopus laevis* which does not fully adopt the I state at any protein-to-lipid ratio in the fluid phase[144]. Confirmation of the T state, where the peptide is tilted at approximately 30° from its S state orientation, was provided by solid-state NMR studies on the protein in oriented bilayers using ^{19}F labelled peptide[144, 145]. Whilst OCD is a valuable technique, its combination with other approaches, particularly solid-state NMR, which allows measurement of oriented samples in very similar conditions, is especially powerful.

It is important for OCD studies that samples are prepared with a very high degree of orientation throughout the sample. This contrasts with surface based methods such as ATR-FTIR which only require the initial layers to be well oriented. The majority of OCD studies have investigated small peptides, and to date the only published example of a multipass membrane measured by OCD is bacteriorhodopsin in oriented native purple membranes. This was first achieved by Muccio et al.[140] in dry multilayers, then secondly by de Jongh et al.[135] using fully hydrated bilayers. In these cases the spectra indicate that the helices are, on average, oriented parallel to the bilayer normal, as would be expected. It is not possible to discern changes in orientation of specific helices but the overall change in architecture can be ascertained. These studies could be highly revealing to study reorientation of helices in ligand-gated ion channels following ligand binding for example, or changes in the structure as a result of bilayer composition. The ability to combine this data with high resolution structure data could provide a basis for understanding mechanisms of action. A limiting factor in OCD studies on large, complex proteins has been the difficulty in preparation of oriented samples containing these proteins. In the case of the small peptides used in the majority of OCD studies, they can be readily dissolved in organic solvent and dried to a film. In contrast, large proteins may not be sufficiently robust to undergo solubilisation in organic solvents and drying. Even when reconstituted into lipid vesicles and deposited onto a fused silica support, drying may result in changes to the protein structure or stability. Attempts to orient membrane proteins using pressure

annealing have generally been unsuccessful since they also rely on the use of organic solvents and temperatures which may denature the protein[146]. A small number of larger proteins have been oriented successfully using isopotenital spin-dry ultracentrifugation (ISDU) in both native[147] and model membranes[146]. This involves the sedimentation of membrane fragments or vesicles onto a support substrate under vacuum by ultracentrifugation. Whilst this approach has been demonstrated as broadly applicable it is laborious and requires specialist apparatus. A method to orient proteins for NMR studies, the use of magnetically alignable lipid phases, is discussed in more detail in Chapter 3.

1.3.4. Synchrotron radiation circular dichroism spectroscopy

One limiting factor in conventional CD studies is the far-UV absorbance of a number of common biological buffers and salts, including the Good buffers and chloride salts. These may be necessary for protein stabilisation, but are intractable to CD in typical concentrations. It is also difficult to acquire data in the vacuum UV (< 190 nm) since the xenon arc lamps employed in CD instruments have reduced photon flux at lower ends of the spectrum, which means additional bands relating to further transitions cannot be observed.

It is possible to overcome these challenges through the use of synchrotron radiation CD (SRCD), which is theoretically identical to conventional CD but experimentally uses a synchrotron light source in place of a xenon arc lamp. SRCD in the far-UV region was pioneered by Sutherland et al. in 1980, who developed an SRCD beamline at the NSLS (Brookhaven National Laboratory)[148]. Since then a number of SRCD beamlines have been constructed, and at present eight are operational at the following synchrotrons: ANKA (Germany), ASTRID2 (Denmark), ANKA (Germany), BSRF (China), Diamond Light Source (UK), HiSOR (Japan), NSRRC (Taiwan) and SOLEIL (France), with plans for an additional beamline at the Brazilian LNSN synchrotron.

In accordance with the Maxwell equations, electromagnetic synchrotron radiation is produced when electrons pass through a magnetic field. This radiation ranges from X-ray to < 1 nm at high photon flux, allowing the measurement of protein CD spectra to ~160 nm in solution, at which point the absorption of water becomes a limiting factor. It is possible to measure to ~130 nm using protein films[149]. Previously the analysis of this data was challenging since the datasets used to deconvolute CD data only included data to 185 nm but a dataset published in 2007 provides a series of spectra acquired to 178 nm to allow researchers to capitalise on the additional information obtained using SRCD studies[119].

Another advantage of SRCD is its improved sensitivity. The high photon flux results in a gain in signal to noise (S/N), which means data can be acquired more rapidly and samples can be less concentrated than those measured in conventional instruments, and in some cases subtle changes in protein structure can be identified which are not observable using conventional instruments[150]. The higher intensity of the light beam means that even samples with absorbing components such as chloride can be tolerated to a degree as some light is able to reach the detector, which may help in the case of proteins which require specific salts for structure or stability. Similarly, samples which may cause light scattering in benchtop instruments are more readily measured using SRCD, particularly lipid vesicles and fibrillar proteins.

The SRCD beamline used for studies in this thesis, B23 at Diamond Light Source, is one of the most recently constructed beamlines and benefits from a number of advantages over beamlines available at other synchrotrons. One of the most significant advantages is the highly collimated beam, which at the sample has dimensions of 500 x 470 μm[151], in contrast to the 10s mm^2 area in bench top instruments. Foremost, this means that much smaller volumes of sample are required for CD measurements, illustrated by an application using a capillary tube with a pathlength of just 18 μm[151]. This also means that when studying non-solution samples such as liquid crystals or films it is possible to 'map' the area of the sample and detect any location specific features or homogeneity. This is possible by virtue of the module A end station which allows samples to be mounted horizontally rather than the conventional vertical setup and moved relative to the beam using a motorised stage. Recently a high throughput system has been developed which enables the automated measurement of samples in 96 well plates, allowing rapid data collection in a vast number of conditions[152]. A drawback of SRCD is that although the high intensity beam results in improved sensitivity the radiation flux is sufficient to result in protein denaturation[153]. Although it is possible to address this apparent problem through modulation of the beam optics and by defocussing of the beam[151], there are also efforts to exploit this deleterious effect in photostability assays as an alternative to thermal stability and chemical denaturation experiments[154].

1.3.5. Nuclear magnetic resonance (NMR) theory

NMR is a form of spectroscopy which has been used extensively to probe the structure, interactions, chemical environment and dynamics of molecules. The application of NMR spectroscopy to biological materials, particularly proteins, has enabled an understanding of

dynamics and interactions which are unattainable by other structural methodologies, such as macromolecular X-ray crystallography.

The phenomenon of NMR occurs in nuclei possessing spin angular momentum in the presence of a magnetic field. When a nucleus with spin ≠ 0 is exposed to a magnetic field, the Zeeman effect results in the splitting of the spin's degenerate ground state into 2I+1 energy levels (where I is the spin quantum number). Spins can be promoted to a higher energy state by applying electromagnetic radiation of a frequency which is equal to the separation of the energy levels. The energy separation ΔE between two levels is given by:

$$\Delta E = \hbar \gamma B_0 \qquad (1.9)$$

where $\hbar$ is the reduced Planck constant, γ is the nuclear gyromagnetic ratio and B_0 is the magnetic field strength. The Hamiltonian operator for the Zeeman interaction $\hat{H}_Z$ represents the complete energy of the interaction between a spin j and longitudinal field[125]:

$$\hat{H}_Z = - \gamma_j B_0 \hat{I}_j \qquad (1.10)$$

where $\hat{I}_j$ is the spin operator and B_0 is the magnetic field strength. $-\gamma_j B_0$ gives the Larmor frequency, or the frequency of precession of the nuclear magnetic moment around the field.

In addition to the Zeeman interaction, a number interactions of smaller magnitude contribute to the spin Hamiltonian, which can be viewed as perturbations to the Zeeman interaction:

$$\hat{H} = \hat{H}_Z + \hat{H}_{CS} + \hat{H}_Q + \hat{H}_J + \hat{H}_{DD} \qquad (1.11)$$

where J, CS, Q and DD represent the J-coupling, chemical shift, quadrupolar and dipole-dipole interactions respectively. The Zeeman interaction has the greatest magnitude (100s MHz) whilst the J-coupling has the smallest (10s Hz). For the oriented solid-state NMR measurements in this thesis, the interactions of most interest are chemical shifts and quadrupolar interactions.

The chemical shift is one of the most commonly studied interactions in NMR. Electrons circulating a nucleus create a local magnetic field, which opposes the external magnetic field. This has the effect of shielding the nucleus to the external field and therefore changes

the field that the nucleus experiences. This also means that the chemical shift is sensitive to the local electronic environment. There is usually an uneven distribution of electrons around a nucleus, but due to the rapid molecular tumbling in solution samples, the chemical shift is isotropic (δ_{iso}). In liquid crystals and solids however the uneven distribution of electrons in the nucleus means the chemical shielding is anisotropic (chemical shielding anisotropy, CSA), having an orientational dependence, and can be described by a second rank tensor diagonalised to its principle components in the molecular axis δ_{xx}, δ_{yy} and δ_{zz}, which are defined according to their magnitude[155]:

$$| \delta_{zz} - \delta_{iso} | \geq | \delta_{xx} - \delta_{iso} | \geq | \delta_{yy} - \delta_{iso} | \qquad (1.12)$$

where the isotropic chemical shift δ_{iso} is defined as:

$$\delta_{iso} = \frac{1}{3} (\delta_{xx} + \delta_{yy} + \delta_{zz}) \qquad (1.13)$$

Additionally, the CSA δ and asymmetry parameter η can be defined as:

$$\delta = \delta_{zz} - \delta_{iso} \qquad (1.14)$$

$$\eta = \frac{\delta_{yy} - \delta_{xx}}{\delta_{zz} - \delta_{iso}} \qquad (1.15)$$

In the case of uniaxially symmetric nuclei $\delta_{xx} = \delta_{yy}$ which can be assigned as the perpendicular axis $\delta_{\perp}$ whilst δ_{zz} can be assigned as the parallel axis $\delta_{\parallel}$.

The full chemical shift Hamiltonian (H_{CS}) can be given as[155]:

$$H_{CS} = -\gamma B_0 I_z \left(\delta_{iso} + \delta \left(\frac{3\cos^2\theta - 1}{2} + \frac{1}{2}\eta \sin^2\theta \cos 2\phi \right) \right) \qquad (1.16)$$

where θ and ϕ are Euler angles between the molecular principle axis system and the laboratory frame (i.e. B_0 field). In the case of an axially symmetric CSA (i.e. $\delta_{xx} = \delta_{yy} \neq \delta_{zz}$) $\eta = 0$ such that the Hamiltonian can be given as:

$$H_{CS} = -\gamma B_0 I_z \left(\delta_{iso} + \delta \frac{3\cos^2\theta - 1}{2} \right) \qquad (1.17)$$

Quadrupolar interactions occur in nuclei with spin > 1/2 as a result of an uneven distribution of charge in the nucleus, which interacts with external electric field gradients (EFG). The quadrupolar interactions are generally large, usually second in magnitude only to the Zeeman interaction, and are also anisotropic. The Hamiltonian of the quadrupolar interaction (H_Q) for a spin j in the principle axis system can be given as[125]:

$$H_Q = \omega_Q \times \frac{1}{6}(3\,\hat{I}_z^{\,2} - I(I+1)\,\hat{1}) \qquad (1.18)$$

where $\hat{1}$ is the unity operator and ω_Q is the quadrupolar coupling, given for an uniaxial electric field gradient tensor[125]:

$$\omega_Q = \frac{3\pi\, e^2 qQ}{I\,(2I-1)\,h}\left(\frac{3\cos^2\theta - 1}{2}\right) \qquad (1.19)$$

where $\frac{e^2qQ}{h}$ is the quadrupole coupling constant and θ is the angle between the molecular principle axis system and the laboratory frame.

Through space interactions can occur between magnetic moments of adjacent dipoles, dipole-dipole interactions, and similarly to quadrupolar and CSA interactions are orientationally dependant. Unlike the chemical shift tensor, the dipolar coupling tensor in isotropic liquids is averaged to zero. Since the interactions occur through space they can be either homonuclear or heteronuclear. The magnitude of the interaction between two spins i and j is given by the dipole-dipole coupling constant b_{ij}[125]:

$$b_{ij} = -\frac{\mu_0}{4\pi}\frac{\gamma_i\gamma_j\hbar}{r^3} \qquad (1.20)$$

where μ_0 is the permittivity constant and r is the distance between the two nuclei. In the case of the homonuclear dipole-dipole interaction between spins i and j, the dipolar Hamiltonian (H_{DD}) is given as[125]:

$$H_{DD} = b_{ij}\frac{1}{2}(3\cos^2\theta - 1)\,(3\,\hat{I}_{iz}\hat{I}_{jz} - \hat{\mathbf{I}}_i\cdot\hat{\mathbf{I}}_j) \qquad (1.21)$$

and for heteronuclear interactions:

$$H_{DD} = b_{ij}\frac{1}{2}(3\cos^2\theta - 1)\,(2\,\hat{I}_{iz}\hat{I}_{jz}) \qquad (1.22)$$

where $\hat{I}_{iz}$ and $\hat{I}_{jz}$ is the z component of the spin operator and $\hat{\mathbf{I}}_i$ and $\hat{\mathbf{I}}_j$ are the spin operators.

Interactions occurring between chemically bonded nuclei, J couplings, occur due to hyperfine coupling of the nuclei and the electrons. Although the J coupling tensor is a 3x3 matrix, since it is independent of molecular orientations it can be considered a scalar. The Hamiltonian for J coupling interactions between spins *i* and *j* can be given by[125]:

$$H_J = 2\pi\, \hat{\mathbf{I}}_i \cdot J_{ij} \cdot \hat{\mathbf{I}}_j \qquad (1.23)$$

where J_{ij} is the J coupling tensor for the two spins. As the J-coupling is scalar and has a small magnitude (~10 Hz) relative to the other interactions it is not commonly measured in solid-state NMR.

1.3.5.1. Common experimental approaches in solid-state nuclear magnetic resonance

The most basic NMR experiment involves the application of a π/2 pulse to a sample in a magnetic field. This tips the bulk magnetisation vector from the z-axis into the xy plane, where the relaxation of the magnetisation back to the z-axis can be measured as a free induction decay (fid). A number of additional experimental techniques can be applied to develop this basic concept and have been used extensively in this thesis, and are described below.

Heteronuclear decoupling

Interactions between protons and the nuclei of interest can result in significant line broadening in solid-state NMR spectra. In the case of heteronuclear couplings between protons and the nuclei of interest, high power continuous wave radio frequency (rf) radiation can be applied during acquisition at the proton Larmor frequency, which suppresses the couplings and thus results in improved spectral resolution.

Hahn echo

When applying an rf pulse in an NMR experiment to 'flip' the bulk magnetisation out of the z-axis, acquisition of the fid cannot occur immediately due to the dead time of the receiver. A Hahn echo experiment[156] is a widely used pulse sequence that addresses this issue by generating an 'echo' signal, which occurs following a time delay. The experiment consists of two pulses, first a π/2 pulse to 'flip' the bulk magnetisation from the z-axis into the xy plane, which then precesses about the z axis, followed by a π pulse which allows the

magnetisation to refocus in the xy plane. Continuous wave decoupling is applied throughout the echo. This is illustrated schematically in Figure 1.14.

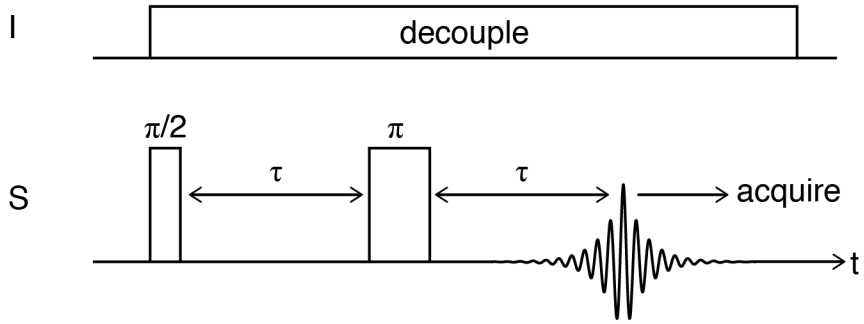

Figure 1.14 ***Pulse sequence for a Hahn echo experiment.*** *A π/2 pulse is followed by a π pulse in order to 'flip' then refocus the magnetisation in the xy plane. The fid is acquired after time delay τ. Continuous wave decoupling is applied throughout the echo.*

Quadrupolar echo

Whilst the Hahn echo can be used to measure chemical shifts, in quadrupolar nuclei an alternative echo sequence is required to account for the additional transitions between spin states. The use of a Hahn echo on quadrupolar nuclei results in incomplete refocussing of the magnetisation, introducing additional interactions[157]. This can be addressed using a quadrupolar echo, which is the same as a Hahn echo except with the π pulse replaced with a π/2 pulse.

Cross polarisation

Although isotopes such as ^{15}N and ^{13}C are NMR active and regularly incorporated into proteins for NMR studies, they have relatively low γ which means measurements of these nuclei are somewhat insensitive. In the case of ^{15}N the γ is 10 % of proton, which corresponds to sensitivity of detection 10 % of that for proton. To address the low sensitivity of nuclei such as these, cross polarisation can be used which enhances the sensitivity by the transfer of magnetisation from a nuclei with greater γ to a lower γ[158]. Protons are used mostly as the high energy spin due to their high γ and 99.98 % natural abundance. They also have much shorter T_1 than the lower γ nuclei, allowing a much shorter repetition delay. Cross polarisation can be viewed as a thermodynamic process in which there is a coupling between a high and low temperature reservoir. Thermal contact between the two reservoirs allows the transfer of energy, and between two spins occurs via dipolar interactions. Experimentally, the transfer of magnetisation polarisation can be

donee by satisfying the Hartmann-Hahn condition, achieved by matching the precession frequency of magnetisation between two spins *I* and *S*:

$$\gamma_I B_{1I} = \gamma_S B_{1S} \qquad (1.24)$$

A pulse sequence for a cross polarisation program is outlined in Figure 1.15. First, the bulk magnetisation is flipped into the xy axis using a π/2 pulse. A spin lock pulse is then applied to induce precession of the magnetisation about the x axis. The frequency of precession is matched between the two spins ($\omega_I = \omega_S$) to facilitate transfer of magnetisation by modulation of the B_1 field. For acquisition, the spin lock pulse is stopped and fid acquired whilst continuous proton decoupling is applied. In the scheme outlined in Figure 1.15 the amplitude of the spin lock pulse on spin *I* is ramped. This ramping allows for inhomogeneity in the B_1 field and ensures that the maximal number of spins match the Hartmann-Hahn condition.

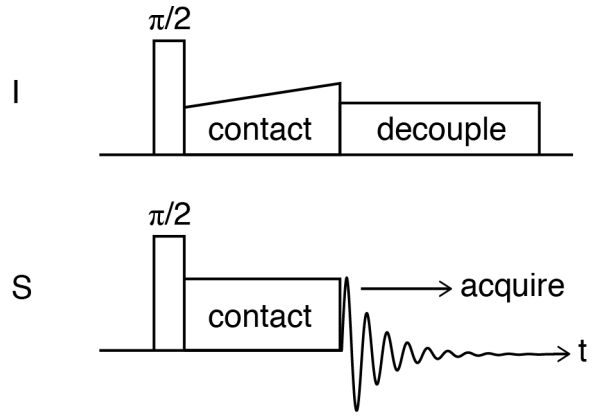

Figure 1.15: ***Pulse sequence for cross polarisation experiment.*** *A π/2 pulse is followed by spin lock contact pulse on both channels such that the Hartmann Hahn condition is satisfied. The fid is then acquired with continuous wave decoupling on the proton channel.*

1.4. Probing the effect of lipids on protein localisation

In this thesis two proteins are investigated, the first is the transmembrane domain of the protein fukutin, which is studied by CD and NMR in Chapters 2 and 3, and is introduced below. Second is the potassium channel hERG, which will be introduced in Chapter 4.

The localisation of certain proteins to specific cellular compartments may be mediated by the lipid composition of the bilayer in which the protein resides. This is particularly true of the glycosyltransferases which are localised to either ER or Golgi apparatus and are

functionally dependant on their correct localisation[17]. Glycosyltransferases are one of a number of different classes of enzyme which post-translationally modify synthesised proteins, and are usually found in the ER and Golgi apparatus. Post-translational modifications occur in almost all proteins, and in many cases have significant functional implications. The work in this thesis utilises fukutin as a model glycosyltransferase to probe the response of its TMD to changes in bilayer thickness, which may have a role in the retention of the protein in the cis-Golgi cisternae since such membranes are known to be thinner than those found later in the exocytic pathway[16]. This work complements a battery of existing biophysical studies on the fukutin TMD which have investigated its oligomeric state, structure and stability in a number of lipid environments[62, 159, 160].

Fukutin has been implicated in the physiopathology of a number of autosomal recessive congenital disorders, most significantly Fukuyama congenital muscle dystrophy (FCMD), which is the second most common type of muscular dystrophy in Japan with an incidence of 3 in 100000 individuals[161]. Symptomatically FCMD presents in early childhood with the classical muscle weakness and hypotonia associated with muscular dystrophy, but it is also characterised by mental retardation, impaired ocular development and various neurological defects. Patients rarely survive past 20 years of age[162].

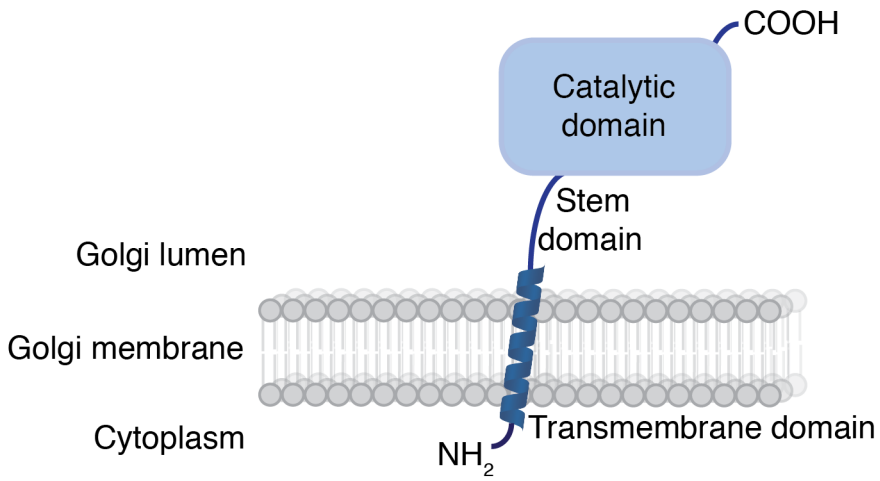

Figure 1.16: ***Predicted domain topology of fukutin.*** *The TMD is formed of a single transmembrane helix which links to the functional catalytic domain by a 'stem'.*

It has been suggested that fukutin functions as a glycosyltransferase of α-dystroglycan. Similarly to other glycosyltransferases, including the fukutin homologue fukutin-related protein, the domain topology of fukutin is likely to include a single helical transmembrane domain and a catalytic functional domain, linked by a stem domain[163] (Figure 1.16). Its putative function has been evidenced by sequence analysis indicating it is a type II

membrane protein possessing a DXD motif within its catalytic domain, common features amongst glycosyltransferases, and experimental data showing expression but not glycosylation of α-dystroglycan in FCMD mutant cells[164, 165]. In cultured muscle cells transiently expressing fukutin it is localised exclusively to the cis-Golgi apparatus (Figure 1.17)[166], again characteristic of glycosyltransferases. When properly glycosylated α-dystroglycan is responsible for muscle integrity by linking β-dystroglycan in the cellular membranes to proteins of the extracellular matrix (ECM) such as laminin and agrin[167]. Studies using antibodies targeting the glycan decorated region of α-dystroglycan indicate that in FCMD patients the protein is hypoglycosylated, which corresponds to a loss in binding activity to the ECM[164]. This hypoglycosylation has been attributed to the loss of fukutin activity. In FCMD patients mutations in the fukutin encoding gene *FKTN* have been identified, with the primary mutation responsible for the majority of cases being a 3 kb retrotransposal insertion in the 3' untranslated region (UTR), which occurs in as many as one in 90 of the Japanese population[167]. Patients with this mutation have demonstrably less *FKTN* mRNA transcript than healthy counterparts[168]. A number of smaller, additional mutations in *FKTN* have also been identified in both Japanese and non-Japanese FCMD patients[169, 170].

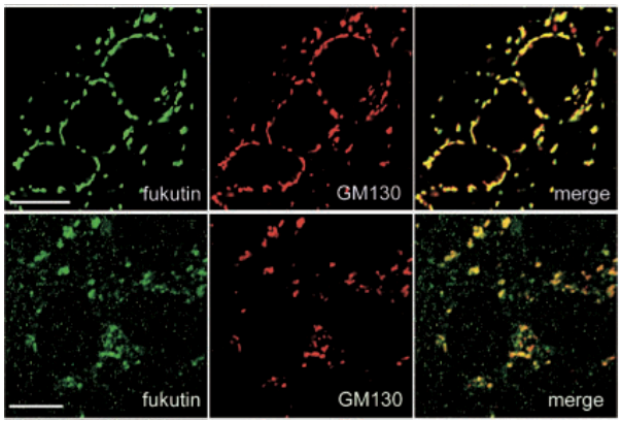

Figure 1.17: ***Subcellular localisation of WT fukutin in differentiated*** **mus musculus** ***C1C12 muscle cells.*** *Fukutin expression was induced by transfection with* FKTN *cDNA. Cells were stained using anti-fukutin antibody (green) or anti-GM130 (red), a protein found exclusively in the Golgi apparatus. Merged images demonstrate the co-localisation of the two proteins. In the bottom row cells were treated with brefeldin A to disrupt the Golgi which disperses the previously localised proteins. Scale bars represent 10 μm. Reproduced from Matsumoto et al.[166] with permission of Oxford University Press.*

In addition to fukutin there are a number of other putative glycosyltransferases thought to be responsible for glycosylation of α-dystroglycan, including fukutin related protein (FRP), LARGE1, protein O-linked-mannose β-1,2-N-acetylglucosaminyltransferase 1 (POMGnT1) and protein O-mannosyltransferases 1 and 2 (POMT1 and 2), which similarly to fukutin are implicated in a number of diseases, particularly congenital α-dystroglycanopathies[167]. Glycosyltransferases in general are heterologously distributed throughout the ER and Golgi cisternae, which is essential since proteins maturing through the Golgi/ER network must encounter the glycosyltransferases in a specific sequence to be correctly modified. This has been demonstrated for a number of glycosyltransferases involved in α-dystroglycan maturation. In C2C12 cells, FRP is localised to the ER[166] whilst LARGE1[171] and fukutin[166] are localised to the Golgi apparatus. In the case of LARGE1 it was demonstrated that the removal of the TMD results in the protein mislocalisation to the ER and consequent loss of activity[171], and POMGnT1 mislocalisation from the Golgi to the ER results in a reduction in its activity[172]. These examples illustrate both the significance of localisation to the correct compartments and the importance of the TMD. Wild-type fukutin is localised to the cis-Golgi apparatus, but through the introduction of missense mutations, which have been identified in patients, can become localised to ER independently of the 3' UTR insertion (Figure 1.18)[173]. It is clearly important that glycosyltransferases are retained within the correct region of the ER/Golgi to preserve functional activity, despite constant trafficking of proteins and molecules into and out of the Golgi.

A number of models have been proposed which enable the retention of glycosyltransferases within the ER/Golgi, which include oligomerisation, TMD lipid specificity and recognition motifs[17]. Oligomerisation of glycosyltransferases (both hetero- and homo-oligomerisation) is believed to create large complexes which are excluded from trafficking vesicles due to their size[174]. These large complexes are also speculated to have functional advantages, by making the sequential glycosylation reactions more efficient[175]. Oligomerisation also facilitates interactions between proteins which may exert effects on each other, for example it has been suggested that fukutin can interact with and regulate POMGnT1 activity[176]. As well as interactions between the soluble domains, the TMD is also likely to have a role in oligomerisation, with free cysteine and uncharged polar residues mediating inter-helix interactions[17]. It is also clear that the lipid composition in different cellular compartments is varied, with Golgi membranes being considerably thinner than plasma membranes[4]. This is significant because TMD of Golgi localised proteins are typically three or four residues shorter than TMD of proteins resident in the

plasma membrane, potentially excluding them from thicker membranes. The protein complex COPI mediates retrograde transport, and commonly proteins have a recognition motif in their C terminus to enable their transport by this mechanism[177]. Glycosyltransferases however lack these motifs, but it has been demonstrated that indirect interactions between the proteins and COPI can be facilitated, at least in yeast systems, by arginine based motifs and vps74 recognition motifs[17]. There are homologues which perform similar functions in mammalian cells, such as the Golgi phosphoprotein 3 which appears to interact with the POMGnT1 stem domain and mediate its localisation in the Golgi[172]. There is evidence for all of these pathways to retention, and it seems likely that these, as well as additional mechanisms must work cooperatively to ensure the correct localisation of glycosyltransferases.

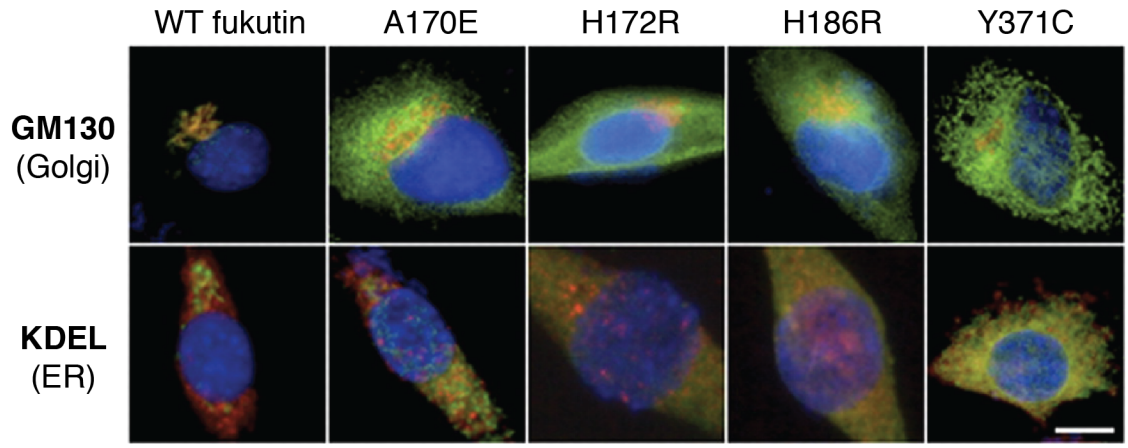

Figure 1.18: ***Effect of pathogenic mutations on the localisation of fukutin.*** *FLAG-tagged fukutin transitently expressed in C1C12 cells was visuallised using anti-FLAG antibody (green), with the Golgi marker GM130 (top row, red) or ER marker KDEL (bottom row, red). Nuclei are stained blue with DAPI. In the four mutants A170E, H172R, H186R and Y371C the fukutin is dispersed throughout the cell, whereas the wild type is localised to the Golgi apparatus. Scale bar is 10 μm. Figure adapted from Tachikawa et al.[173] (copyright the American Society for Biochemistry and Molecular Biology).*

The fukutin TMD is the first 36 residues of the N terminus of the complete 461 residue protein, and serves to anchor the protein into the Golgi membranes. Circular dichroism (CD) studies confirm as expected that the TMD is almost entirely helical in both lipid and detergent environments. Molecular dynamics (MD) revealed that fukutin TMD compensates for changes in the bilayer thickness through changes in its tilt angle in order to minimise the disruption to the bilayer or exposure of hydrophobic regions[62]. Its

dimerisation in 1,2-dilauroyl-sn-glycero-3-phosphocholine (DLPC) bilayers was observed in both FRET and crosslinking studies[160].

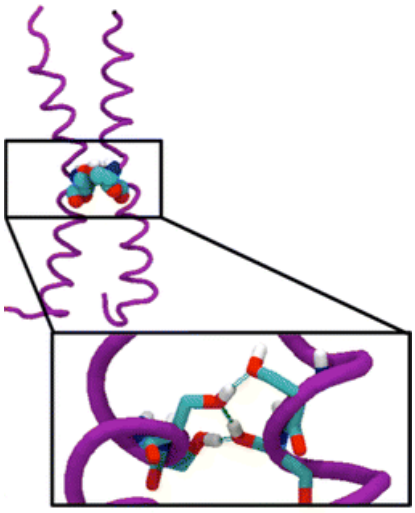

Figure 1.19: ***Dimerisation of fukutin TMD monomers in DLPC bilayer identified by molecular dynamics.*** *Dimerisation is mediated by the interaction of S17 and S18 residues (shown in space-filling format and expanded region showing hydrogen bonding). Reproduced from Marius et al.[160] with the permission of Springer.*

Further studies into the dimerisation using molecular dynamics have revealed that the closest contacts between monomers were located at S17 and S18, which are proposed to form the dimerisation domain as part of a TXXSS motif[160]. The monomers are arranged in an almost parallel orientation (Figure 1.19). Predominant interactions between S17-S18 and S18-S18 were observed, with hydrogen bonding between the carbonyl oxygens, leading to a slight kink of the helices around these residues. Similar interactions have been identified between helices in bovine cytochrome C oxidase, where a series of hydrogen bonds between serines on adjacent helices form a "zipper" along the length of the helices[178]. This parallel dimer structure is quite different to the interhelix interactions commonly observed in membrane proteins through GXXXG-type motifs, such as glycophorin A, which results in a crossing of the helices as a coiled-coil structure with minimal interhelical distance[179]. In a number of proteins such dimerisation is necessary for its functional activation, as has been proposed for the ErbB4 growth factor receptor tyrosine kinase[180]. It is also noteworthy that interactions between the soluble domains of other glycosyltransferases have been identified, including disulphide bridges between cysteine residues in the cytosolic N-terminus of FRP[181], and disulphide bridges between the stem regions of *N*-acetylglucosaminyltransferase V monomers[182], suggesting that the transmembrane domain is unlikely to exclusively responsible for oligomerisation. The

oligomerisation of fukutin, and potential formation of hetero-oligomers with other putative glycosyltransferases, is likely to have implications for the function of the protein, particularly as it has been suggested that fukutin is able to regulate POMGnT1 activity[176]. Indeed, it may be the case that parallel orientation of the monomers has implications for the confirmation of the stem and catalytic domains and its interaction with other proteins. Interestingly, in the MD studies the tilt angle of the monomers after dimerisation reduces from 38.8 ± 8° to 18.0 ± 10°, which has been attributed to the protein-protein interactions reducing the number of residues available to interact with the bilayer. The interaction of the protein with the lipid bilayer was studied, and five residues at either terminus were found to engage in both hydrogen bonding and charge-charge interactions with the lipid headgroup. These five residues, R3, K6, N26, K29, and R35, act to anchor the TMD in the bilayer[62].

1.5. Aims

The overall objective of this thesis was to implement and develop methods to study membrane protein orientation in lipid environments which mimic the cellular membrane using oriented SRCD (OSRCD). OSRCD is one of a small number of methods that allows the determination of membrane protein orientation and has been widely used to characterise the tilt angles of peptides and small proteins in lipid bilayers. The specific aims of this thesis were:

- To develop and implement a conventional method of OSRCD with mechanically aligned samples at the B23 beamline and to validate the findings using solid-state NMR;
- To address some of the challenges associated with mechanically aligned samples though the characterisation and development of a novel system, using solid-state NMR and X-band EPR, to orient membrane proteins for OSRCD using magnetically aligned lipid phases;
- To apply these methods to the putative glycosyltransferase fukutin to understand the response of the protein to changes in the lipid bilayer thickness and its implications for protein trafficking;
- To express and purify a human potassium channel, hERG, with a view to exploring the possibility of orienting larger, multidomain membrane proteins for analysis by OSRCD.

Chapter 2. Characterisation of the fukutin transmembrane domain in mechanically oriented samples using circular dichroism and solid-state NMR spectroscopy

2.1. Introduction

Methods used for studying molecular orientation provide a valuable tool to probe the structural and conformational response of protein to their environment and interactions. Since the advent of OCD (and oriented SRCD (OSRCD)) some 30 year ago a number of groups have used it to discern the orientation of membrane proteins, particularly antimicrobial and membrane active peptides, contributing significantly to the understanding of their mechanisms of action. In a similar fashion, oriented NMR has been applied to study the orientation and structure of membrane proteins in lipidic environments, albeit at atomic resolution. This has provided insights into the significance of the bilayer milieu, which are inaccessible using other approaches such as crystallography and solution-state NMR.

In this chapter strategies for the production of high quality oriented samples are outlined. Especially in the case of OCD this can be highly challenging, since samples must be prepared which do not induce optical artefacts. This has been aided by the use of the microfocused beam at the Diamond Light Source B23 beamline, which allows specific areas of the sample to be scanned, rather than measuring areas which potentially contribute artefacts to the spectra.

Interpretation of OSRCD data can be challenging, particularly in cases where the peptide is oriented at an intermediate state between parallel and perpendicular. In such cases the use of solid-state NMR can be highly valuable to provide complementary data to more clearly the understand the tilt of the protein in the bilayer. At present there are no *de novo* methods for analysis of OSRCD data. It would be very useful therefore to produce a dataset of membrane proteins characterised in different lipid bilayers from which general algorithms for the interpretation of such OSRCD data could be developed. Although this chapter does not address this aim directly, it lays foundations for development of such a dataset to interpret OSRCD data through its comparison with solid-state NMR data.

These oriented methods have been applied to the fukutin TMD, which appears to be responsible for retention of the soluble region of the protein to the Golgi apparatus, a

process important for its function. In addition to this biological significance, there is also the availability of previous biophysical data. Through the joint use of oriented NMR and OSRCD the implication of the bilayer thickness on the protein and its ability to avoid hydrophobic mismatch have been studied. A prerequisite for these oriented studies is the ability to prepare high quality oriented samples, and in the case of OSRCD these samples must have suitable optical properties. Strategies for the production of such samples are outlined in this chapter.

2.1.1. Theoretical background

2.1.1.1. ^{31}P NMR

Phosphorous-31 NMR is a powerful tool to assess the overall degree of orientation of a lipid bilayer. This is due to ^{31}P being the naturally occurring isotope of phosphorous meaning no isotopic labelling is required, its high gyromagnetic ratio (40.5 % of proton) allowing sensitive detection, and relatively simple interpretation of spectra as it is a spin-1/2 nucleus. The interactions which contribute to the NMR spectra of a nucleus can be described by its spin Hamiltonian, which for ^{31}P in an anisotropic sample is given by:

$$H = H_{CSA} + H_{DD} \qquad (2.1)$$

where H_{CSA} is the chemical shielding anisotropy and H_{DD} is the proton-phosphorous dipolar interaction. Since the dipolar interaction is usually suppressed in ^{31}P measurements using decoupling, the spectra is dominated by the CSA. In liquid crystalline (L_α) phase, there is fast rotational averaging of the lipids with respect to the bilayer normal, producing an axially symmetric chemical shift tensor (i.e. $\eta = 0$). In an axially symmetric powder pattern, $\delta_{xx} = \delta_{yy}$, yielding two 'edges' (Figure 2.1 A.), denoted as 0° and 90° edges ($\delta_{//}$ and $\delta_{\perp}$ respectively). Experimentally, the CSA (Δ) for ^{31}P spectra can be given conveniently as the difference between the 0° and 90° edges:

$$\Delta = \delta_{\perp} - \delta_{//} \qquad (2.2)$$

where Δ is related to δ by $\Delta = 3/2\ \delta$.

The CSA is dependent on a range of factors, including the structure of the lipid headgroup, bilayer hydration, lipid phase and the interaction of components (such as cholesterol, proteins, small molecules) with the lipid headgroups.

In oriented samples the resonance frequency is dependent upon the orientation of the bilayer normal with respect to the magnetic field, with bilayers oriented parallel to the magnetic field resonant at $\delta_{//}$ and bilayers oriented perpendicular resonant at $\delta_{\perp}$ (Figure 2.1). This orientation dependence of the chemical shift is defined as[183]:

$$\nu(\theta)\,[\text{ppm}] = \delta_{iso} + \delta\left(\frac{3\cos^2\theta - 1}{2}\right) \qquad (2.3)$$

In these spectra the peak width is representative of the lipid mosaic spread, i.e. the distribution of angles around the bilayer normal or degree of misorientation.

Whilst the ^{31}P spectra of oriented samples are predominated by a single peak whose position is dependent on the bilayer orientation, the spectra of a vesicular sample represents the summation of peaks for each possible orientation and yields a powder spectrum with a large intensity $\delta_{\perp}$ and a lower intensity $\delta_{//}$ (Figure 2.1).

2.1.1.2. ^{15}N NMR

Many of the above principles for ^{31}P NMR are the same as those for ^{15}N NMR. It is similarly a spin-1/2 nuclei, and instead of reporting the orientation of the lipid bilayer with respect to the magnetic field it can be used to report the orientation of amide groups in the protein backbone. They differ in that ^{15}N has a low natural abundance (< 0.4 %) and so proteins must be isotopically enriched by either expression in labelled media or incorporation of labelled amino acids during peptide synthesis. The low gyromagnetic ratio of ^{15}N means it has poor sensitivity, and requires alternative experiments to maximise the signal. Cross polarisation (CP) is a widely used pulse sequence in solid-state NMR to improve sensitivity by transfer of magnetisation from proton to ^{15}N (as described in more detail in Chapter 1).

As for ^{31}P, during acquisition proton decoupling is applied to supress the dipolar coupling to the surrounding protons which would otherwise lead to broadening of the spectral lines. It should be noted however that it is also possible to exploit the orientation dependant proton-nitrogen dipolar couplings to provide additional information on helix orientation. Primarily this has involved the use of PISEMA and related experiments, the application of which is outlined in Chapter 1.

A further consideration with ^{15}N is that the chemical shielding tensor, unlike ^{31}P, is not axially symmetric ($\eta > 0$). In this case the CSA is determined according to equation 1.14.

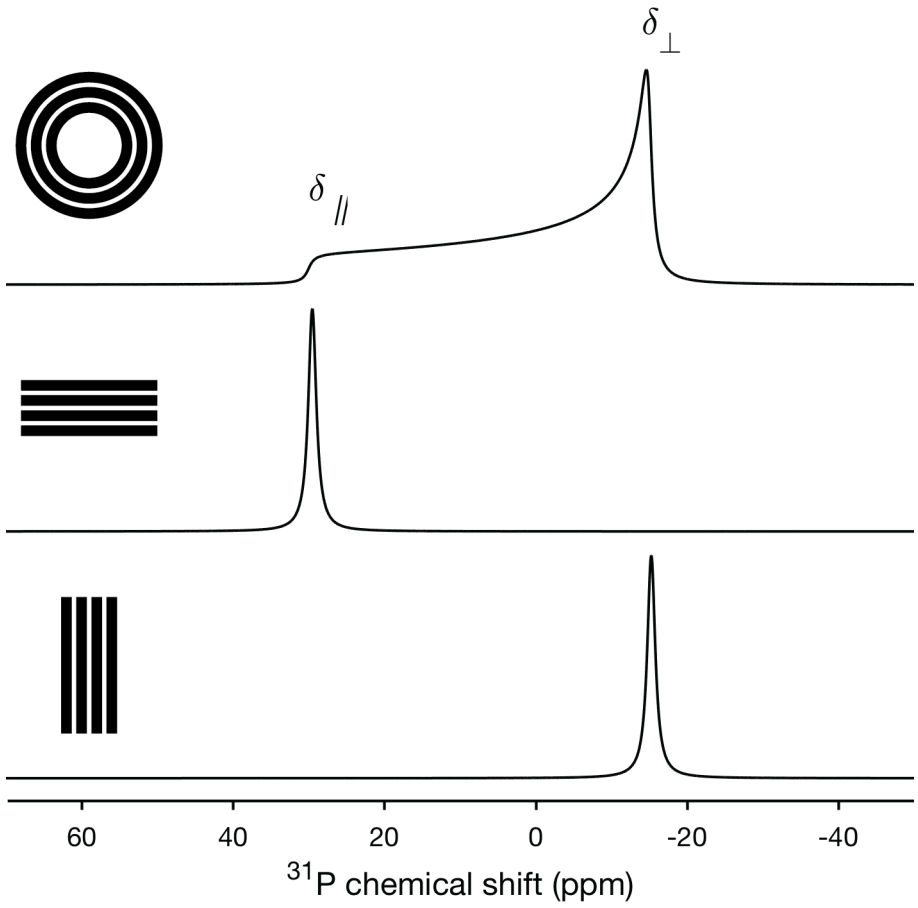

Figure 2.1: ***Simulated ^{31}P spectra of lipid bilayers****. Top: Powder spectrum of multilamellar vesicles with no orientational preference. Edges arising from ^{31}P nuclei oriented either 0° or 90° to the B_0 field. Middle: spectrum of lipid bilayers oriented with bilayer normal parallel (0°) to B_0 field. Bottom: spectrum of lipid bilayers oriented with bilayer normal perpendicular (90°) to B_0 field.*

2.1.1.3. ^{2}H NMR

^{2}H is a spin-1 nuclei, and therefore its Hamiltonian is dominated by a large quadrupolar interaction. The natural abundance of ^{2}H is too low (0.015 %) to perform measurements on unlabelled lipids, meaning that lipids can be selectively deuterated to probe different regions of the lipid (either the acyl chains or headgroup). In this thesis acyl chain deuterated lipids are used, such as POPC-d31, which in isotropic samples produce a narrow, single line. In anisotropic samples however each CD group in the lipid gives rise to a well resolved doublet, characterised by the quadrupolar splitting ($\Delta\nu_Q$) [184]:

$$\Delta\nu_Q = \frac{3}{2}\frac{e^2qQ}{\hbar} S_{CD} \cdot \left(\frac{3\cos^2\theta - 1}{2}\right) \qquad (2.4)$$

where θ is the angle between the CD group and the magnetic field and S_{CD} is the order parameter for acyl chain deuterons. Whilst there may be a symmetry parameter for CD bonds it is usually sufficiently small that it can be neglected[184]. S_{CD} can be viewed as the deviation of the CD group from the bilayer director, where completely mobile groups have $S_{CD} = 0$ and the most ordered have $S_{CD} = 1$. It follows that the most mobile CD groups, such as at the terminal end of the acyl chain, produce the smallest splitting. The motionally restricted groups at the ester-linked end of the lipid produce the greatest splitting and give rise to the "edges" of the powder pattern in vesicle samples. Similar to ^{31}P we can use the position of these edges to determine the degree of orientation of the sample.

In simulated ^{2}H spectra of a single CD group this orientational dependence is easily observed (Figure 2.2) In the oriented spectra, the change in angle between the CD group and the B_0 field results in a change in the $\Delta\nu_Q$ between the two resonances (Figure 2.2, middle and bottom spectra). In a powder spectrum representing lipid vesicles (Figure 2.2, top spectra) where all possible orientations are present, the shoulders are derived from the perpendicular orientation of the CD group (0° edges) to the magnetic field, whilst the well resolved resonances inside the shoulder indicate CD groups that are aligned parallel (90° edges) to the magnetic field.

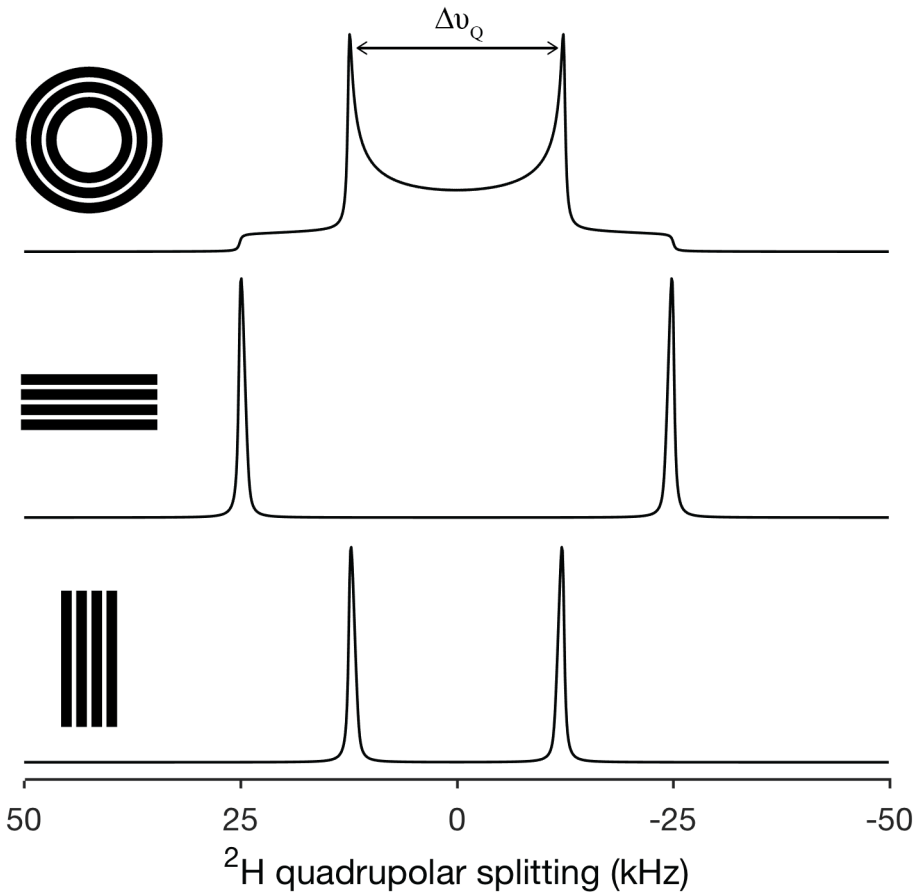

Figure 2.2: ***Simulated ^{2}H spectra of a single CD group in a lipid acyl chain.*** *Top: Powder spectrum of multilamellar vesicles with no orientational preference. Edges arising from CD group oriented either 0° or 90° to the B_0 field. The splitting for the 90° edges is illustrated. Middle: spectrum of lipid bilayers oriented with bilayer normal parallel (0°) to B_0 field. Bottom: spectrum of lipid bilayers oriented with bilayer normal perpendicular (90°) to B_0 field.*

2.1.2. Simulations of NMR spectra

To aid in the interpretation of ^{31}P and ^{15}N NMR data, spectra were simulated according to the theoretical principles. The methods used to simulate these spectra are outlined below.

2.1.2.1. ^{31}P simulations

Oriented spectra were analysed using custom written scripts in MATLAB (MathWorks, Inc.). For ^{31}P spectra, where the chemical shielding anisotropy is axially symmetric (i.e. $\delta_{xx} = \delta_{yy} \neq \delta_{zz}$), the resonance frequency ν for each molecular orientation was calculated according to:

$$\nu(\theta) = \delta_{iso} + \delta\left(\frac{3\cos^2\theta - 1}{2}\right) \qquad (2.5)$$

where θ is the angle between the principle axis of the chemical shield anisotropy and the B_0 field. The signal from a particular orientation (crystallite), *S(θ)*, can therefore be calculated as:

$$S(\theta,t) = e^{-i(\nu(\theta)-\lambda)t} \qquad (2.6)$$

where λ represents the decay of the signal. The spectra were calculated in the time domain, with the appropriate phenomenological relaxation rate (T_2; λ) employed to mimic the experimental observed linewidth. For powder samples the signal was integrated across all possible angles of θ and weighted according to the distribution of crystallites in a powder:

$$S(t) = \int_0^{\pi/2} e^{-i(\nu(\theta)-\lambda)t} \cdot \sin\theta \cdot d\theta \qquad (2.7)$$

Numerically this was achieved using Cheng powder averaging[185]. Typically, simulations converged with 1154 powder points. For oriented samples, the signal intensity around a given director was weighted assuming a Gaussian distribution around the director normal to account for mosaic spread. The resulting signal function is therefore given as:

$$S(t) = \int_0^{\pi/2} e^{-i(\nu(\theta)-\lambda)t} \cdot \sin\theta \cdot \frac{1}{\Delta\theta\sqrt{2\pi}} e^{-\frac{1}{2}\left(\frac{\theta-\Delta\theta}{\Delta\theta}\right)^2} d\theta \qquad (2.8)$$

where $\Delta\theta$ is the variance about the director normal, representative of the mosaic spread.

By arraying the relative contributions of oriented and powder to the simulated spectra it was possible to estimate the degree of orientation from experimental data. The disordered component was varied from 0 to 100 % in 1 % steps, and the resulting spectra were subtracted from the experimental data. The difference was squared to yield the root mean squared deviation (rmsd), and the lowest rsmd was taken as the best fit.

2.1.2.2. ^{15}N simulations

For ^{15}N simulated spectra custom written MATLAB (MathWorks, Inc.) scripts were again used. These used the equations to calculate ^{15}N chemical shifts and ^{15}N-^{1}H dipolar couplings for PISEMA spectra given by Wang et al.[112]. An idealised helix is assumed and the chemical shift for each residue is calculated by rotating the helix axis by the angle ρ, with a tilt angle τ. The signal function for the chemical shift can be given as:

$$S(\rho,\tau) = \delta_{xx}\left(-0.828\cos\rho\sin\tau + 0.558\sin\rho\sin\tau - 0.047\cos\tau\right)^2 + \delta_{yy}\left(0.554\cos\rho\sin\tau + 0.803\sin\rho\sin\tau - 0.22\cos\tau\right)^2 + \delta_{zz}\left(-0.088\cos\rho\sin\tau - 0.206\sin\rho\sin\tau - 0.975\cos\tau\right)^2 \quad (2.9)$$

The fukutin TMD used in the ^{15}N experiments in this thesis is labelled with ^{15}N-leucine in seven of the eight leucine positions. To simulate these spectra we increased the ρ to rotate around the helix axis and calculated the spectra when that rotation coincided with a labelled residue then summed the result for the entire helix.

To fit the simulated spectra with the experimental data, both the τ (tilt angle) and ρ (rotation angle) were arrayed since neither are known experimentally. Simulated spectra were subtracted from the experimental data to yield the difference spectra which was then squared to give the rmsd. The lowest rsmd value was taken as the best fit.

For powder spectra, the method used for ^{31}P was applied here. In order to account for the asymmetry of the ^{15}N CSA an additional term from the chemical shift Hamiltonian for axially asymmetry was added to equation 2.5:

$$\nu(\theta) = \delta_{iso} + \frac{\delta}{2}\left((3\cos^2\theta - 1) + \frac{\eta}{2}\sin^2\theta\cos 2\varphi\right) \quad (2.10)$$

where θ and φ are the angles between the principle axis of the chemical shield anisotropy and the B_0 field. Powder averaging was against achieved using the Cheng method[185], this time with 50000 powder points to reach convergence.

2.2. Methods and materials

2.2.1. Materials

All reagents were sourced from Fisher Scientific (Loughborough, UK) unless otherwise stated. Sol-grade detergents (DDM and OG) were purchased from Anatrace (Ohio, USA). Lipids were purchased as lyophilised powders from Avanti Polar Lipids (Alabama, USA) and prepared as 10 mg mL^{-1} stocks in methanol and stored at -20 °C unless otherwise stated.

Unlabelled murine fukutin TMD (Uniprot accession number Q8R507, residues 1- 36) was synthesised commercially by Peptide Protein Research Ltd (Fareham, UK) as a TFA salt at > 90 % purity with amino acid sequence:

MSRINKNVVLALLTLTSSAFLLFQLYYYKHYLSARN (36)

(Polar residues are coloured red, apolar residues blue and charged residues black.)

Purity was confirmed by HLPC and mass spectrometric analysis performed by the manufacturer. For NMR studies, ^{15}N-leucine labelled fukutin TMD was produced by Chinese Peptides (Hangzhou, China) as TFA salt supplied at greater than 98 % purity, confirmed by HPLC and mass spectrometry. The sequence was identical except for the removal of the N-terminal methionine (position 1). ^{15}N-leucine was incorporated for all leucines with the exception of position 15. Stocks of peptide in methanol were prepared at 1 mg mL^{-1} and stored at -20 °C.

Suprasil fused silica and calcium fluoride cuvettes used for CD measurements were manufactured by Hellma (Essex, UK). Fused silica (Spectrosil 2000) coverslips for oriented CD measurements were custom made by UQG Optics Ltd (Cambridge, UK) in a range of dimensions with 1 mm thickness. Glass coverslips for oriented NMR studies were custom made by Paul Marienfeld GmbH (Lauda-Königshofen, Germany) with dimensions either 25x4 mm or 25x8 mm. Both fused silica and glass coverslips were cleaned by soaking in 70 % nitric acid (Sigma-Aldrich, UK) for at least 1 hour, followed by repeated washing with H_2O and 70 % ethanol before drying at room temperature. Calcium fluoride demountable cells were cleaned extensively with methanol to solubilise lipids, and where necessary in 2 % Hellmanex solution (Hellma Analytics, Essex, UK), before being extensively washed in ethanol and H_2O.

2.2.2. Methods

2.2.2.1. Expression, purification and characterisation of fukutin TMD

Expression in E. coli

The protocol for expression and purification of the fukutin TMD was based on previously published work from the group[159].

A synthetic gene encoding the transmembrane domain of murine fukutin (residues 3 – 36 of UniProt accession no. Q8R507) was previously cloned into a pQE32 vector with an N-terminal 6x histidine tag (for affinity chromatography) and enterokinase cleavage sequence (to facilitate removal of the histidine tag)[159]. The full amino acid sequence, annotated for histidine tag (underlined) and enterokinase cleavage site (bold), is as follows:

MRGS<u>HHHHHH</u>**DDDD**KRINKNVVLALLTLTSSAFLLFQLYYYKHYLSARN (49)

For protein expression, the resulting pFk plasmid was transformed into chemically competent M15 cells carrying the pREP4 plasmid which expresses the lac repressor protein (Qiagen) according to manufacturer's protocols and spread onto LB agar plates with 100 μg mL^{-1} ampicillin and 25 μg mL^{-1} kanamycin. A single colony was used to inoculate 10 mL of LB media (1 % w/v tryptone, 0.5 % w/v yeast extract, 1 % w/v NaCl) supplemented with ampicillin and kanamycin and grown shaking for 16 hours at 37 °C. 5 mL of this starter culture was used to inoculate 0.5 L of LB, again with ampicillin and kanamycin. The culture was grown at 37 °C, shaking at 180 rpm to an optical density at 600 nm (OD_{600}) of 0.7. To induce protein expression, isopropyl β-D-1-thiogalactopyranoside (IPTG) was added to a final concentration of 1 mM and the culture was incubated for a further 16 hours at 18 °C. Cells were harvested by centrifugation at 5000 *g* for 20 minutes at 4 °C.

Fukutin TMD purification

The cell pellet from 1 L of culture was fully resuspended in 50 mL buffer A (50 mM Tris-Cl pH 7.4, 150 mM KCl, 150 mM NaCl) and lysed by sonication on ice using a program of 10 s on, 30 s off for 5 minutes total on time at power level 7 (Misonix XL). The membrane fraction was extracted from the lysate by ultracentrifugation at 142 000 *g* for 40 minutes at 4 °C. The pelleted membrane fraction was then resuspended in 50 mL solubilisation buffer (50 mM Tris-Cl pH 7.4, 150 mM KCl, 150 mM NaCl, 10 mM DDM, 50 mM imidazole) and gently stirred at room temperature for 2 hours. Insoluble material was pelleted by centrifugation at 20 000 *g* for 30 minutes at 4 °C. The resulting clarified solubilised membrane fraction was filtered through a 0.4 μm syringe filter and incubated for 1 hour at 4 °C with 1 mL Ni Sepharose resin (GE Healthcare, UK) pre-equilibrated with wash buffer (50 mM Tris-Cl pH 7.4, 150 mM KCl, 150 mM NaCl, 200 mM imidazole). The resin was applied to a gravity flow column and washed with 15 bed volumes of wash buffer. A relatively high concentration of imidazole (200 mM) could be used in the wash buffer due to the high affinity binding of fukutin TMD, which improved the purity of the eluate. The protein was then eluted from the resin in 6x 1 mL fractions using elution buffer (50 mM Tris-Cl pH 7.4, 150 mM KCl, 150 mM NaCl, 600 mM imidazole, 1 mM DDM).

SDS-PAGE

Tricine SDS-PAGE was used to assess the degree of protein expression and purity. Gels were prepared with 4 % stacking and 15 % resolving layers according to the recipe in Table 2.1.

Table 2.1: ***Recipe for tricine SDS-PAGE gels.***

	Stacking gel	Resolving gel
Acrylamide (30 %; 37.5:1 acrylamide:bisacrylamide)	0.66 mL	5 mL
3 M Tris-Cl pH 8.45, 0.3 % SDS	1.24 mL	3.33 mL
H_2O	2.9 mL	1.67 mL
Tetramethylethylenediamine (TEMED)	10 µL	10 µL
Ammonium persulphate (10 mg mL^{-1})	25 µL	50 µL

Samples were prepared in 4x gel loading buffer (250 mM Tris-Cl pH 7.4, 8 % w/v SDS, 4 mg mL^{-1} bromophenol blue, 20 % v/v glycerol, 12 mM β-mercaptoethanol) to 1x final concentration. Gels were run at 120 V constant voltage for approximately 75 minutes with buffers:

Anode buffer: 200 mM Tris-Cl pH 8.9.

Cathode buffer: 100 mM Tris-Cl pH 8.2, 0.1 % SDS.

Gels were then stained using InstantBlue Coomassie protein stain (Expedeon, Cambridgeshire, UK) and imaged.

Mass spectrometry analysis

For confirmation of the protein molecular weight mass spectrometry analysis was performed. To extract detergent and salt from membrane protein samples for mass spectrometry analysis, protein was first precipitated using methanol-chloroform. Briefly, 1 volume of sample was mixed with 4 volumes of methanol, 1 volume of chloroform and 3 volumes of water, all on ice. After vortexing the solution was centrifuged to separate the aqueous and organic phases. The aqueous upper layer was aspirated and discarded and 3 volumes methanol added. The sample was then vortexed and the centrifuged to pellet the precipitated protein. Following aspiration of the methanol, the precipitant was washed once with water before resuspension in 50:50 methanol-formic acid. Mass spectrometry was

performed by Mr J. Neville Wright (Biophysical laboratory, University of Southampton) using a LCT Micromass electrospray ionisation (ESI) time-of-flight instrument (Waters Ltd., Elstree, UK) in positive ion mode. Mass-to-charge (*m/z*) spectra were deconvoluted using MaxEnt software (Waters Ltd., Elstree, UK) to yield the relative molecular mass with a resolution of 1 Da.

Conventional CD spectroscopy measurements

To ensure purified fukutin TMD adopted the expected helical structure conventional CD spectroscopy was performed using a nitrogen purged J-720 spectropolarimeter (Jasco, Tokyo, Japan). To remove imidazole and salts which absorb in the far-UV region the eluted protein was dialysed (Pur-A-Lyzer dialysis kit, 3500 MWCO, Sigma-Aldrich) into 10 mM Tris-Cl pH 7.4, 1 mM DDM for 16 hours and diluted to 0.1 mg mL^{-1}. Spectra were acquired at room temperature using a 1 mm pathlength fused silica cuvette (Hellma Analytics, Essex, UK) from 260 to 190 nm with 1 nm step resolution, 2 nm bandwidth and 1 s response time. The presented spectra represent an average of eight scans which were baseline corrected against the sample buffer. Data was truncated when the high tension (HT) voltage exceeded 600 V.

2.2.2.2. Preparation of oriented samples for solid-state NMR

Oriented samples were prepared by the co-dissolving lipid and peptide (where appropriate) in organic solvent. Organic solvents with different dielectric constants were selected for each lipid based on experience and suggested solvents in the literature[186]. In most cases pure methanol was sufficient. In the case of DLPC a 1:1:1 chloroform:methanol: trifluroethanol (TFE) mixture was used, and when fukutin TMD was added this mixture was changed to 4:1 methanol:TFE.

To increase the surface tension and prevent the solvent running onto the underlying support, coverslips were mounted on small pieces of modelling clay. The dissolved lipids (and protein as necessary) were deposited in a single aliquot, preventing the need for repeated deposition and drying, which produced poor quality samples based on visual inspection. After aliquot was applied to the coverslips, the samples were gently rocked to ensure even distribution of the lipid across the surface during drying. Solvent was allowed to fully evaporate on the bench at room temperature, or in the case of DPPC (which proved to dry very slowly at room temperature) in an incubator at 37 °C. Air dried samples were transferred to a lyophiliser and dried under vacuum for a minimum of 4 hours to remove residual traces of solvent.

Hydration of sample was achieved by either direct hydration or partial hydration.

Direction hydration

A small quantity (~5 μL) of water was applied directly to the surface of each coverslip. Hydrated samples were stacked and placed into a 5 mm diameter NMR tube of approximately 30 mm length. A small drop of water was added to the end of the tube to promote a humid environment before sealing.

Partial hydration using vapour method

A small volume of ddH_2O was applied to the surface of each coverslip (~5 μL). The coverslips were then placed into an airtight container with a beaker of a saturated K_2SO_4 solution. This 'hydration chamber' was then placed into an incubator at 37 °C to achieve a relative humidity of 97 %[187] for a minimum for between 16 hours and 3 days. Hydrated samples were removed from the chamber, stacked, hydrated further with an addition few μL ddH_2O to the edges the sample, wrapped in parafilm and sealed in polythene bags. Sealed samples were stored at 4 °C until measurement.

2.2.2.3. Preparation of 'powder' samples for NMR

Powder samples of non-oriented lipid multilamellar vesicles were prepared in order to determine the CSA of the lipid. Typically 10 mg of lipid was dissolved in methanol and then dried to a film under vacuum. The film was resuspended in ddH_2O to yield a 30 % w/v solution and subject to 5 - 8 rounds of freezing in liquid nitrogen and thawing at 40 °C. It was then transferred to a polythene bag and sealed.

2.2.2.4. Preparation of samples for SRCD

Vesicle samples

Appropriate volumes of fukutin TMD and lipids were mixed in glass vials then dried to a film for at least 4 hours under high vacuum. 10 mM potassium phosphate buffer was added to the film to achieve a fukutin concentration of 0.125 mg mL^{-1} and left to hydrate for 30 minutes. The solution was then sonicated extensively to clarity using an ultrasonic water bath at 25 °C to yield SUVs. Samples were centrifuged for 5 minutes at 12000 *g* to remove large vesicles and unincorporated material. Vesicles of lipid without protein were prepared by identical means for use as a baseline.

Oriented samples

Samples were prepared in a similar manner to those outlined for oriented NMR samples (*c.f.* 2.2.2.2). Appropriate volumes of lipid and fukutin TMD stocks in methanol were combined to achieve desired concentrations of lipid and protein. These were then applied to the surface of either demountable cuvettes (calcium fluoride or fused silica) or custom made fused silica coverslips. The substrate material is described in the figure legends as appropriate. The samples were dried to a film under nitrogen gas then subject to 4 hours under high vacuum.

Modifications and more detailed descriptions of the sample preparation method are outlined in the results section.

2.2.2.5. Solid-state NMR measurements

All oriented NMR measurements were acquired using a 400 MHz Chemagnetics/Varian CMX spectrometer equipped with a commercial double resonance static probe. Free standing solenoidal coils were wound with suitable geometries for samples as necessary. Samples were aligned in the coil with the normal of the coverslip parallel to the B_0 field.

Deuterium

The orientation of samples containing acyl-chain deuterated lipid was probed using ^2H NMR. All spectra were acquired at 61.53 MHz using a quadrupolar echo pulse program, with a 4 μs 90° pulse, 4 μs dwell time, 45 μs echo delay, 1024 points and 0.5 s recycle delay. Spectra presented represent accumulation of 1024 acquisitions. Sample temperature was maintained at 25 °C. Samples were measured at 0° and 90° with respect to the normal of the coverslips and B_0 field. Data was processed in matNMR[188], where the fid was left-shifted to the top of the echo and exponential line broadening of 50 Hz applied prior to Fourier transformation.

Phosphorous-31

Oriented samples were characterised using ^{31}P to assess degree of bilayer orientation. Spectra were acquired at 161.84 MHz using a Hanh echo pulse program[156] with typical acquisition parameters of 4.5 μs 90° pulse, 2 μs dwell time, 50 μs echo delay, 2048 points and 2.5 s recycle delay. Continuous wave proton decoupling (typically with a field of 35 kHz) was applied during acquisition. Between 64 and 16 384 scans were accumulated for each spectrum depending on the quantity of lipid. Spectra were referenced externally to H_3PO_4 at 0 ppm. Data was processed in matNMR[188], where the fid was left-shifted to the

top of the echo, zero filled to 16384 points and exponential line broadening of 100 Hz applied prior to Fourier transformation.

Nitrogen-15

^{15}N spectra of ^{15}N-leucine fukutin TMD were acquired to determine the orientation of the protein in oriented lipid bilayers. Spectra were acquired using a variable-amplitude cross polarisation (^{1}H to ^{15}N) pulse program[158] to excite the ^{15}N, followed by a spin echo prior to acquisition at a ^{15}N frequency of 40.51 MHz. Typical parameters for acquisition included 4 μs 90° pulse, 1 ms contact time, 10 μs dwell time, 50 μs echo delay, 1024 points and 2.5 s recycle delay. Low-power proton decoupling (field strength for each given in the text) was applied throughout acquisition, since probe limitations and concerns regarding sample heating prevented high power decoupling. The number of scans is given in figure legends. Spectra were referenced externally to NH_4Cl at 41.5 ppm[189]. Data was processed in matNMR[188], where the fid was left-shifted to the top of the echo and exponential line broadening of 300 Hz applied prior to Fourier transformation.

2.2.2.6. Synchrotron radiation circular dichroism measurements

SRCD measurements were recorded at B23, Diamond Light Source, UK, during beamtime allocations including SM9452, SM11722 and SM14147. Measurements were recorded using either the module A or B end station, both of which are equipped with a highly modified DSM 20 spectropolarimeter (Olis Inc, Georgia, USA)[190]. Far-UV measurements were carried out with slit width of 1 nm, 1 nm step increment and 1 s integration time. Prior to each set of measurements the signal calibration was checked using a standard solution of 0.6 mg mL^{-1} camphor sulphonic acid, which is expected to yield a ratio of 2:1 for the absolute peak intensity at 290.5 and 192.5 nm[191]. At least four repeat scans were measured and averaged and spectra were baseline corrected as appropriate. SRCD data was processed in CDApps[192] and MATLAB (Mathworks, Inc.). Generally spectra were not smoothed but in those cases where smoothing was applied the details are given in the accompanying figure legend.

Vesicle samples

A 1 mm path fused silica cuvette was used for all measurements. A Peltier temperature controlled cell holder was used to maintain sample temperature (Quantum Northwest, Washington, USA). Secondary structure analysis was performed using the Dichroweb server[193] with the CONTIN LL algorithm[194, 195] and basis set 10 which comprises a mixture

of soluble and membrane proteins. Data is given as molar circular dichroism, Δε, calculated according to the following[196]:

$$[\theta] = \frac{\theta \ MRW}{10 \ l \ c} \qquad (2.11)$$

$$\Delta\varepsilon = \frac{[\theta]}{3298} \qquad (2.12)$$

where [θ] is the ellipticity, θ is the CD in millidegrees (mdeg; machine units), *MRW* is the mean residue weight (protein molar mass/number of residues – 1), *l* is the pathlength in mm and *c* is the protein concentration in mg mL^{-1}.

Oriented samples

The type of sample holder varied depending on the nature of the sample. For oriented samples prepared on calcium fluoride substrate, a micro cell assembly was used[197]. Similarly, samples were prepared on one half of a fused silica demountable cuvette. Oriented samples on fused silica coverslips were placed either directly onto a temperature controlled stage (Linkam, UK) of module A such that there were oriented horizontally.

In some instances it is difficult to baseline correct lipid-protein samples with pure lipid samples since the sample preparation can be different. Since the quantity of lipids used should have a relatively small absorption signal it is not inappropriate to baseline correct against the clean substrate[132]. The baseline used for each sample is described in the figure legend.

2.4. Results and discussion

2.4.1. Expression and purification of fukutin TMD

We were able to successfully reproduce the published protocol for purification of the histidine-tagged fukutin TMD in *E. coli*[159]. Typical yields, determined by absorption at 280 nm, were in the region of 1 mg per L media, and densitometry analysis of SDS-PAGE indicated an approximate purity of 80 % (Figure 2.3). To ensure the protein was correctly folded a CD spectrum was obtained (Figure 2.3) which features two minima centred around 222 nm and 212 nm, indicating qualitatively a significant helical content of the protein as expected [198]. It was not possible to perform secondary structure deconvolution as accurate analysis requires data points from 190 nm, whereas the data here was cleaved at 197 nm due to exceedance of the acceptable HT voltage.

There is a discrepancy in the band position on SDS-PAGE (Figure 2.3) where the fukutin TMD appears at a higher molecular weight than predicted by ProtParam analysis[199] (approximately 8 kDa in contrast to predicted 5.88 kDa). It has been extensively reported in the literature that membrane proteins often do not run true to size[200]. Presumably in the case of fukutin TMD this inconsistency arises because it is stable in SDS, and SDS-PAGE relies on the assumption that proteins are fully denatured. In order to confirm the molecular weight of the predominant species in eluate, ESI mass spectrometry was employed. Proteins in the eluate were precipitated using methanol-chloroform extraction (*cf*. section 2.2.2.1) and washed to remove detergent and salt before analysis. Deconvolution of the mass-to-charge ratio spectrum reveals a predominant peak corresponding to a molecular weight of 5877 Da, and a second peak at 5893 Da. These peaks represent the fukutin TMD and the fukutin TMD with oxidation of the methionine at position one respectively.

Whilst the expression and purification of fukutin TMD was successful, the purity of the protein is inadequate in current form for more complex CD studies and would require further purification. Additionally, cleavage of the histidine-tag is necessary, protocols to reconstitute the protein into lipids should be developed and expression in nitrogen-15 labelled media for NMR studies are desirable. Considering these factors, alongside the modest yield, we made the decision to source commercially synthesised fukutin TMD, which was used in all further experiments.

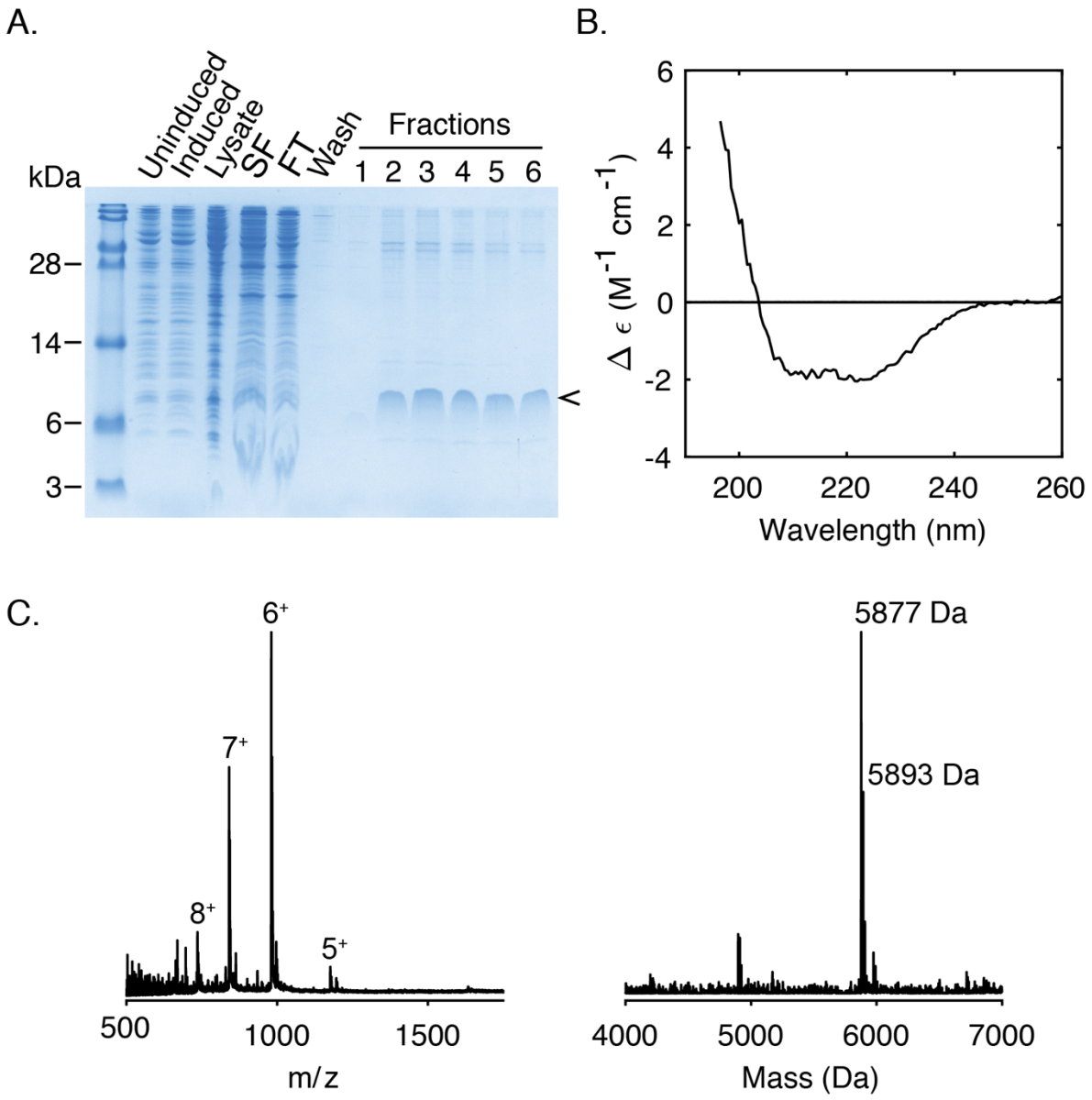

Figure 2.3: ***Purification and characterisation of histidine-tagged fukutin TMD****. A. SDS-PAGE analysis of fukutin TMD expression in* E. coli *and purification. Uninduced and induced samples show total cellular protein before and after induction of expression with IPTG, lysate is sonicated cells, SF is the solubilised membranes, FT is the flow through. Arrowhead indicates the position of fukutin TMD band. B. Conventional CD spectra of fukutin TMD in 10 mM Tris-Cl pH 7.4, 1 mM DDM. C. ESI mass spectra of fukutin TMD. (Left) ESI-ToF mass-to-charge spectrum of fukutin TMD annotated with envelope of fukutin TMD multiply charged states indicated; (right) deconvoluted mass spectrum annotated with molecular mass of predominant species.*

2.4.2. Oriented nuclear magnetic resonance measurements

To probe the tilt angle of fukutin TMD in lipid bilayers of different thickness we acquired NMR spectra of ^{15}N-leucine labelled peptide in DLPC, DMPC and DPPC. These measurements will validate the results from the OCD spectra. The lipids were chosen since they produce bilayers of increasing thickness (Table 2.2), representing the change in bilayer thickness between different cellular compartments. DLPC has a total bilayer thickness of ~38.9 Å[201] which is comparable to the thickness of native Golgi membranes where fukutin is resident (thickness of cellular membranes is summarised in Table 2.3). The use of lipids with a greater thickness may provide an indication of the mechanisms which prevent the exclusion of fukutin TMD in thicker cellular membranes.

Table 2.2: ***Bilayer thickness (D_B) of saturated PC lipid bilayers in fluid phase determined by X-ray scattering.*** *DLPC and DMPC values from Kučerka et al.[201], DPPC value from Nagle and Weiner[202].*

Lipid	Bilayer thickness (Å)
DLPC	38.9
DMPC	43.3
DPPC	47.2

Table 2.3: ***Bilayer thickness of cell compartment membranes in rat hepatocytes determined by solution X-ray scattering.*** *Values from Mitra et al[16].*

Membrane	Bilayer thickness (Å)
Endoplasmic reticulum	37.5 ± 0.4
Golgi apparatus	39.5 ± 0.4
Basolateral plasma	35.6 ± 0.6
Apical plasma	42.5 ± 0.3

The use of three lipids with the same phosphatidylcholine (PC) headgroup but different acyl chain lengths allows the specific effect of the bilayer thickness on the fukutin TMD tilt angle to be investigated. Although using a single lipid in these samples fails to replicate the complexity of the natural membranes, which contain vastly diverse phospholipid and sphingolipid species, cholesterol, and other membrane proteins amongst additional constituents, we opted to establish methods for a simplified system which can give way to the introduction of further components at a later stage. This was also a good starting point

since molecular dynamics studies on fukutin TMD have been previously published in DLPC and DPPC[62, 160], indicating that the protein alters its tilt angle to respond to the change in bilayer thickness.

2.4.2.1. Optimising preparation of oriented bilayer samples

The first step was to ensure lipid bilayers on glass coverslips could be prepared with a high degree of alignment, as measured by ^{31}P NMR. Initially the lipid per area was varied to determine the maximal amount that could be deposited without perturbing the quality of alignment. For later studies using $^{15}N_{leu}$ labelled fukutin TMD to measure the protein orientation in bilayers, is it desirable to incorporate as much peptide as possible to achieve good S/N, which is dependent on the amount of lipid used. There is therefore a degree of compromise between the need for sufficient mass of lipid and quality of alignment. The quantities of lipid were based around values given for similar studies in the literature[203]. The spectra were then fitted with simulated spectra for oriented samples containing an increasing disordered component to estimate the percentage of the sample which was not aligned. A value of around 70 % for the oriented component was considered sufficiently aligned, where there is only a small powder contribution to the spectra. Simulations were calculated with a CSA from the powder spectrum and isotropic chemical shift of -0.9 ppm (from Lindström et al.[204]). Small adjustment of the CSA and isotropic shift values were needed to account for slight variations in peak positions between samples, owing to subtle changes in hydration and/or slight offsets from parallel sample alignment in the coil.

The first lipid considered was DLPC which has C12:0 acyl chains. Samples were prepared with masses of lipid from 0.5 mg/coverslip (2.5 µg mm^{-2}) to 2 mg/coverslip (10 µg mm^{-2}) (Figure 2.4 B.-E.). A powder spectrum was also recorded from 30 % w/v DLPC vesicles (Figure 2.4 A.) which shows a typical axially symmetric powder lineshape, with its 90° edge at 31 ppm and 0° edge at -14.2 ppm, yielding a CSA of 45.2 ppm. Visual inspection of the spectra indicates that generally the orientation is good, and the preparation of well aligned samples was consistent and reproducible, somewhat in contrast with the literature which suggests achieving such alignment of DLPC is challenging[186]. It was particularly important during the preparation of DLPC samples to rock the coverslips as the solvent was drying in order to prevent the ‘pulling’ of the lipid into a small spot of solvent. The high quality of orientation is indicated by the presence of a predominant peak centred around 34 ppm, which is close to the 0° edge of the DLPC powder spectrum (Figure 2.4A.). There is an increasing powder component as the quantity of lipid is increased, indicated by the peak at -13 ppm and low intensity between the two edges, but this is a

small contribution to the spectra in all cases. The powder or disordered component in these spectra arises from lipids which are not in the planar bilayer, and are associated with the uneven edges of sample or vesicles forming in areas of the sample with a high degree of hydration. Indeed, fits of simulations of the ^{31}P spectra indicate that the disordered component of the spectra for 0.5, 1.0, 1.5 and 2.0 mg/coverslip are 15 %, 17 %, 17 % and 20 % respectively, with a mosaic spread of 1° up to 1.5 mg and 3° for 2 mg, indicating very well ordered bilayers. The trend clearly increases with the quantity of lipid deposited, and it was notable during preparation that lower lipid per area produced samples which appeared to be more homogenous. The disordered component in oriented samples such as these typically arises from the edges of the lipid film, which tend to be uneven and crusted, even with careful preparation. Although there is a decrease in the oriented component of the samples with increased lipid per area, the oriented component is still a large majority of the 2 mg/coverslip spectrum. As such we decided to prepare samples with $^{15}N_{leu}$ fukutin TMD using 2 mg DLPC/coverslip in order to maximise the amount of protein in the sample.

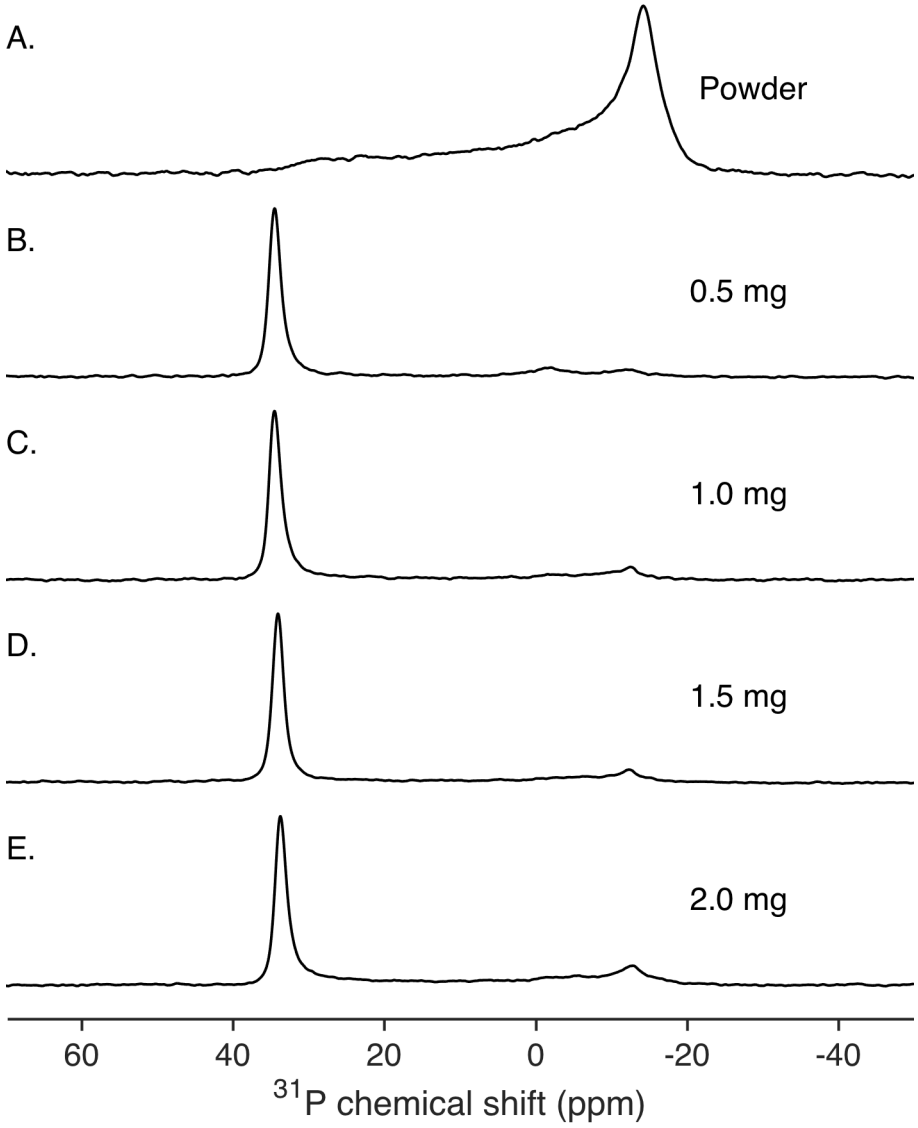

Figure 2.4: ***^{31}P NMR spectra of pure DLPC bilayers across various masses of lipid per 8x25 mm glass coverslip.*** *All spectra were acquired at 25 °C. A reference 'powder' spectrum of multilamellar vesicles at 30 % hydration was recorded (A). For oriented samples, the normal of the coverslips was oriented parallel to the B_0 field. The quantity of lipid per coverslip is indicated on the figure (equal to lipid per area of 2.5, 5.0, 7.5 and 10.0 μg mm^{-2} for B. to E. respectively). Typical samples comprised 5 coverslips.*

In an identical manner to DLPC, ^{31}P spectra were acquired of DMPC (C14:0) bilayer samples prepared with an array of lipid per areas (Figure 2.5). The 90° edge gives rise to a peak at approximately -11.5 ppm, and the 0° edge a peak around 35 ppm, yielding typical CSA values of 46.5 ppm, which are consistent with values for similar samples in the literature at 46.6 ppm for DMPC multilamellar vesicles[205]. Whilst there are subtle changes in 0° edge position between spectra, they are sufficiently small to be considered within experimental error, most likely due to a combination of changes in the degree of hydration and slight deviation of the sample from the 0° orientation with respect to the B_0 field. The degree of hydration modulates the lipid motility though interaction with the lipid headgroup. It follows that the motionally averaged CSA is broadened if the hydration, and therefore motility is reduced. It is also clear that attempting to perfectly align the sample in the coil is very challenging, but we were confident that the sample was ±5° with respect to the probehead by visually confirming the correct alignment of the coverslips prior to insertion of the probe into the magnet. Similar to DLPC the intensity of the 90° peak is low, indicating a high degree of alignment. This is confirmed by fitting simulated spectra, which give the disordered contributions of 13 %, 12 %, 18 % and 15 % for 0.5, 1.0, 1.5 and 2.0 mg DMPC/coverslip respectively, with a mosaic spread of 5-6° throughout. As there was little difference in the quality of alignment the 2.0 mg regime was selected for preparation of samples with $^{15}N_{leu}$ peptide.

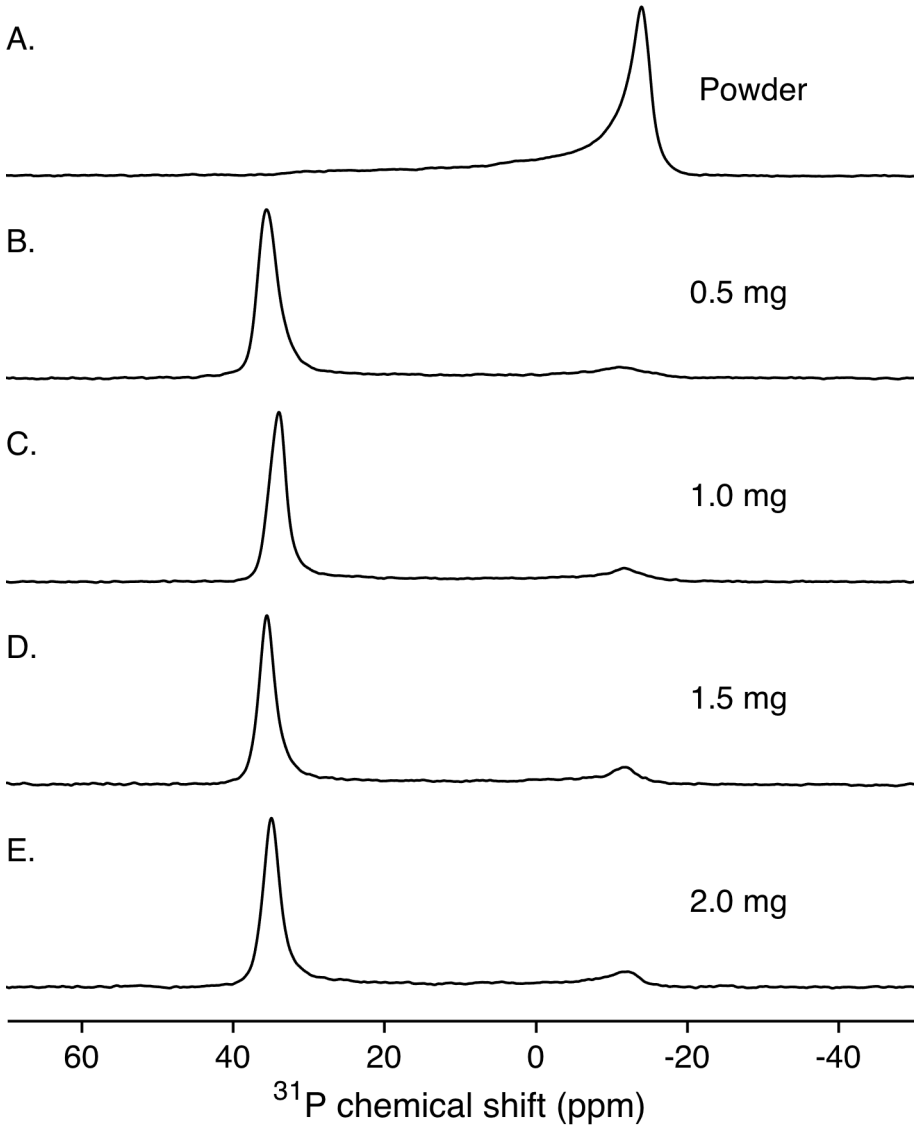

Figure 2.5: ***^{31}P NMR spectra of pure DMPC bilayers across various masses of lipid per 8x25 mm glass coverslip.*** *All spectra were acquired at 35 °C. A reference 'powder' spectrum of multilamellar vesicles at 30 % hydration was recorded (A). For oriented samples the normal of the coverslips was oriented parallel to the B_0 field. The quantity of lipid per coverslip is indicated on the figure (equal to lipid per area of 2.5, 5.0, 7.5 and 10.0 μg mm^{-2} for B. to E. respectively). Typical samples comprised 5 coverslips.*

The final lipid considered was DPPC (C16:0) (Figure 2.6). This was somewhat more challenging to work with, mainly due to its relatively high T_m of 41 °C. Although the lipid distributed evenly across the surface fairly spontaneously, it was necessary to dry the samples above room temperature, usually at 37 °C to ensure the bulk of the solvent was removed before being placed under vacuum. In the case of 0.5 and 1.0 mg (Figure 2.6 B. and C.) there is no 90° edge and a single peak from the 0° edge at 31.2 and 33.2 ppm respectively, indicating a high degree of alignment. In the 1.5 and 2 mg spectra a small 90° edge is present, indicating a small disordered component (Figure 2.6 D. and E.). The CSA

of the ^{31}P spectra increases from -44.6 ppm for powder to ~ -46.0 ppm in the oriented samples, which is very close to the value in literature of approximately 47 ppm[206]. The greater level of hydration in the power sample results in increased motility of the lipids and explains the reduced CSA. A second component is observed in the 1.5 mg spectra which may be present to a lesser extent in the other spectra, manifesting as a shoulder at the upfield side of the resonance. This is likely to represent a different confirmation of the PC headgroup, resulting from different degrees of hydration between populations of lipid. Similar observations have been observed in ^{31}P spectra by Marassi and Crowell[207], occurring when there is variation in the degree of hydration below 10 water molecules per lipid. Similar observations have been observed using deuterium NMR, where the lipid headgroup confirmation was highly sensitive up to 14 waters per lipid[208]. It is also the case that the phase of the lipid can be disrupted in low hydration conditions (relative humidity below 45%), and the thickness is dependent on the number of hydrating waters[137], signifying the need to ensure that samples are appropriately hydrated. The disordered contribution to the spectra was calculated as 5 %, 10 %, 20 % and 30 %, again indicating that the amount of lipid has an impact on the quality of sample alignment, although similar to DMPC the mosaic spread is constant at 6°. For the following $^{15}N_{leu}$ fukutin TMD samples, initially 1.5 mg lipid was selected for sample preparation with DPPC.

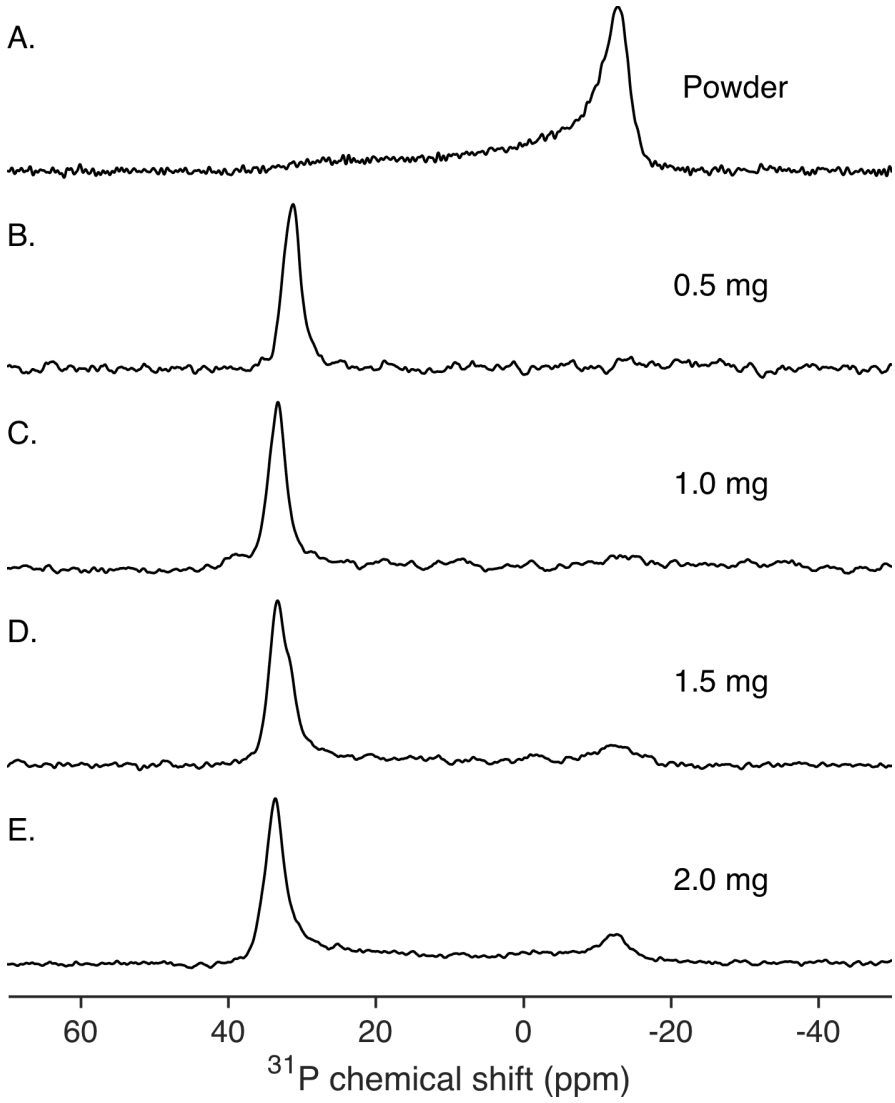

Figure 2.6: ***^{31}P NMR spectra of pure DPPC bilayers across various masses of lipid per 8x25 mm glass coverslip.*** *Spectra were acquired above 45 °C, with oriented samples (B. to E.) measured with the normal of the coverslips parallel to the B_0 field (0°). The quantity of lipid per coverslip is indicated on the figure (equal to lipid per area of 2.5, 5.0, 7.5 and 10.0 μg mm^{-2} for B. to E. respectively). Typical samples comprised five coverslips.*

2.4.3. Estimating the tilt angle by 1D ^{15}N NMR

2.4.3.1. ^{31}P NMR measurements

To ensure a good degree of alignment was still achieved when fukutin TMD was added, ^{31}P spectra were acquired of the samples prepared with $^{15}N_{leu}$ fukutin TMD (Figure 2.8). These spectra are overlaid with the equivalent spectra of pure lipid samples (reproduced from figures in the previous section). Initially lipid/protein ratios (L/P) of 50 were tested. This ratio was selected to maximise the quantity of protein to achieve good signal to noise, provide a similar environment to the cellular membranes, which have a lipid-to-protein ratio between 50 and 100 (depending on the organelle)[209] and match similar oriented

studies[61]. The final L/P ratio for DLPC was 50, whilst for DMPC and DPPC it was increased to 100. This was based on preliminary experiments which revealed a poor degree of alignment at L/P of 50 for DMPC and DPPC. In the example of DPPC with fukutin TMD at L/P of 50 (Figure 2.7) it is clear that there is a large powder component in the spectra, estimated at 40 % with a high mosaic spread of 13° from fitting, suggesting a disordered bilayer.

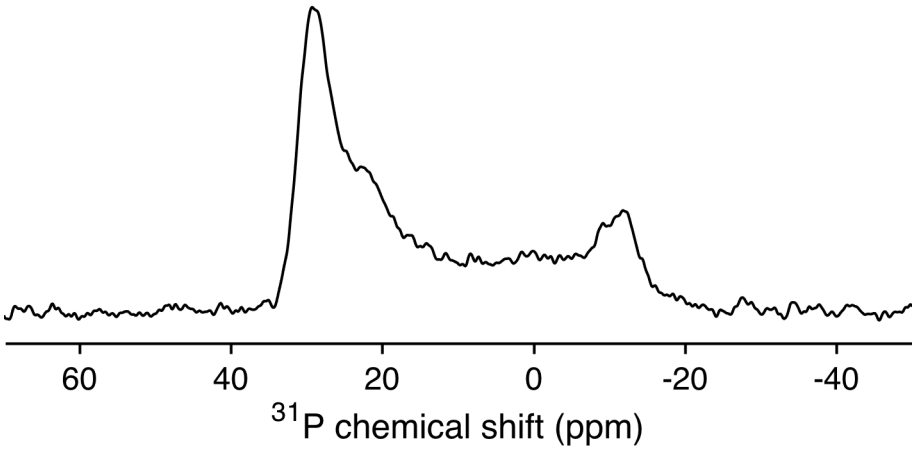

Figure 2.7: ***^{31}P spectra of DPPC with fukutin TMD at 50 L/P.*** *Sample were prepared with 1.5 mg lipid per 25x8 mm and acquired at 60 °C.*

The percentages of the disordered component from the ^{31}P spectra of the final samples are summarised in Table 2.4. For all of the lipids there are subtle changes in the position of the 0° edge relative to the pure lipid samples, which is likely to result from slight changes in the humidity or alignment of the coverslips. It is also possible that the interaction of fukutin TMD with the headgroups could result in these observations, although further experiments using vesicles are necessary to rule out hydration or orientation dependant effects.

When fukutin TMD is added to the DLPC bilayers the degree of alignment improves, from 24 to 12 % disordered contribution, although the mosaic spread of the sample decreases from 1° to 6°, explaining the broadened 0° peak. There is low intensity in the 90° edge at around -13 ppm and low intensity across the entire CSA (Figure 2.8 A.). The quality of alignment was not entirely unsurprising since DLPC produced the most reliable and consistently oriented samples.

Table 2.4: ***Percentage of disordered component in oriented samples prepared with and without fukutin TMD.*** *In DLPC with L/P was 50:1 and 100:1 in DMPC and DPPC.*

	Without fukutin TMD	With fukutin TMD
DLPC	20 %	11 %
DMPC	15 %	36 %
DPPC	30 %	25 %

In the DMPC bilayers there is a significant increase in the disorder of the sample, although there is little change in the mosaic spread (from 6° to 7° with fukutin TMD). Similar values for mosaic spread have been reported in the literature for DMPC bilayers containing gramicidin[210]. Whilst there may be an effect of fukutin TMD which results in disruption of the bilayer, it is also important to consider that DMPC samples were more challenging to prepare than either DLPC or DPPC. In particular, homogeneous distribution of lipid on the coverslips was difficult to achieve, as assessed by visual inspection of the dried samples. This was made more difficult with the fukutin TMD, which is much less soluble in organic solvent than the lipids, meaning it was necessary to dissolve the lipid and peptide in a large volume and repeatedly apply then dry the sample onto the coverslip. It was clear visually that this resulted in poorer samples, with the edges often crusted and inhomogeneous. Even using careful selection of coverslips which appeared to be homogeneous there is still a significant disordered contribution to the spectrum (36 %).

For DPPC, although the initial screening without peptide demonstrated that 1.5 mg/coverslip was most effective, we were able to increase the amount of lipid to 2 mg/coverslip by increasing the L/P to 100. Indeed, this resulted in a more ordered sample than those without fukutin TMD, with 25 % disorder, and there is small increase in mosaic spread to 7°. From our experience, it is not usual to see significant changes in orientation between ostensibly identical samples so it is likely that rather than being an effect of the protein on the bilayer that it is simply variation in the sample preparation. However, it should be noted that similar to the DLPC sample there is an increase in peak width, this time more significantly from 1 to 4 ppm, possibly reflecting reduced motion due to interactions of the headgroups with the protein.

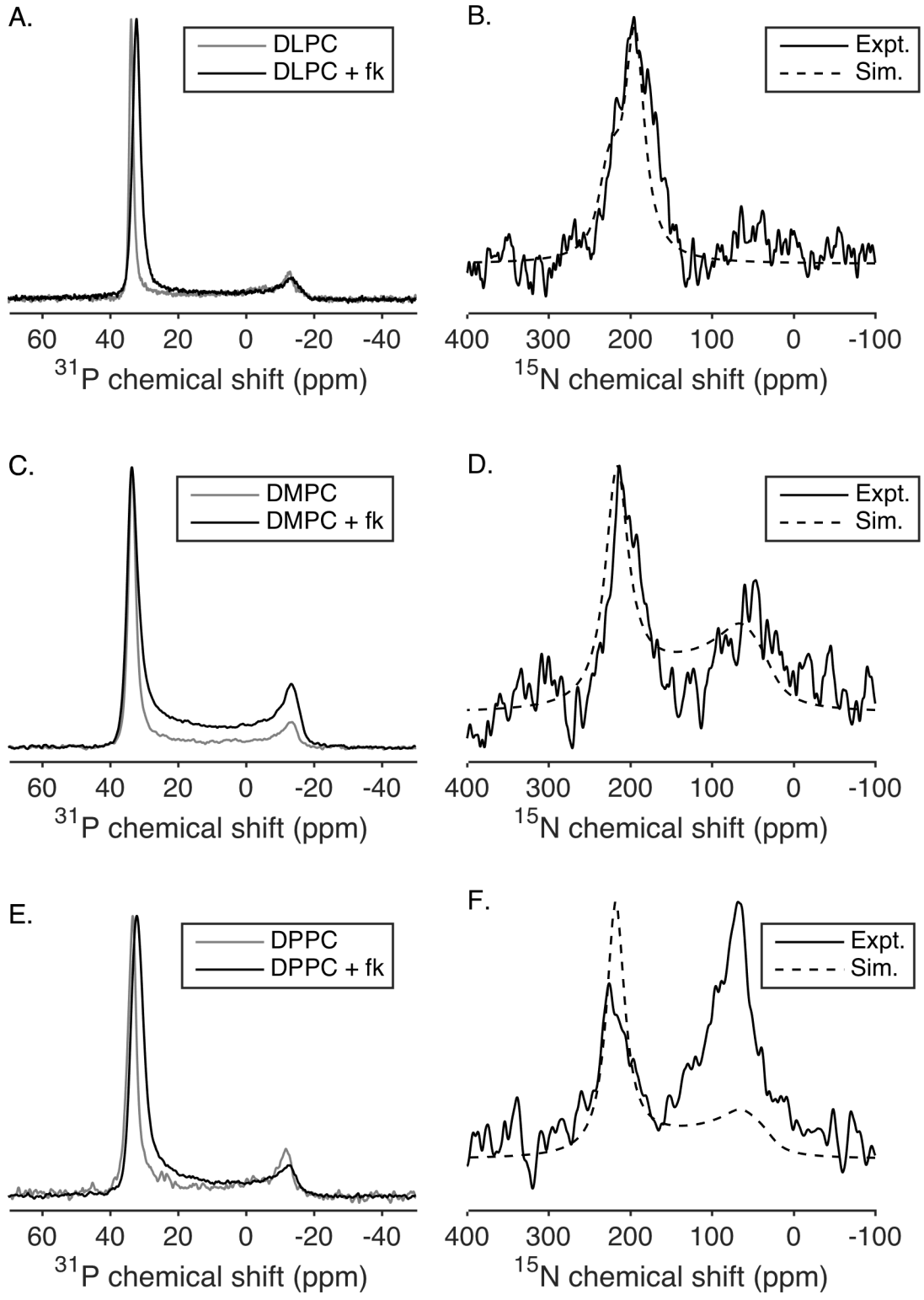

Figure 2.8: ***Oriented ^{31}P (left) and ^{15}N (right) spectra of fukutin TMD in lipid bilayers.*** *In ^{31}P spectra the black line is for samples with fukutin TMD (fk) and grey for pure lipid samples, in ^{15}N spectra the black line is the experimental data and the dashed lines are the fitted simulated spectra. In all cases there was 2 mg lipid per coverslip with L/P ratios of 50 for DLPC (A. and B.) and 100 for DMPC (C. and D.) and DPPC (E. and F.). For ^{15}N typically 200 000 scans were acquired. Simulated ^{15}N spectra were computed as described in the text. Spectra were acquired above the lipid phase transition temperature.*

2.4.3.2. ^{15}N NMR measurements

The tilt angle of proteins in the bilayer can be estimated based on the peak position in the ^{15}N spectra. In general, helices in bilayers with the normal parallel to the field give rise to resonances < 75 ppm when the helical long axis is perpendicular to the normal and resonances at > 200 ppm are found when the peptide is parallel to the normal. To estimate the tilt angle of the peptide it is possible to fit simulated spectra with different tilt angles, which requires the knowledge of the protein's isotropic chemical shift tensors, which were found to be 25.2, 61.7 and 222.4 ppm for δ_{xx}, δ_{yy} and δ_{zz}. based on the powder spectrum of the lyophilised peptide (Figure 2.9). This gives an isotropic chemical shift of 103 ppm and a CSA (δ_{zz} - δ_{iso}) of 119.3 ppm. These values are not dissimilar to values for ^{15}N amide chemical shifts in the literature (107 ppm and 110±5 ppm for isotropic chemical shift and CSA respectively)[211]. A powder spectrum calculated using these values is plotted over the experimental spectra (Figure 2.9), indicating good agreement between the edges of the experimental and powder spectra.

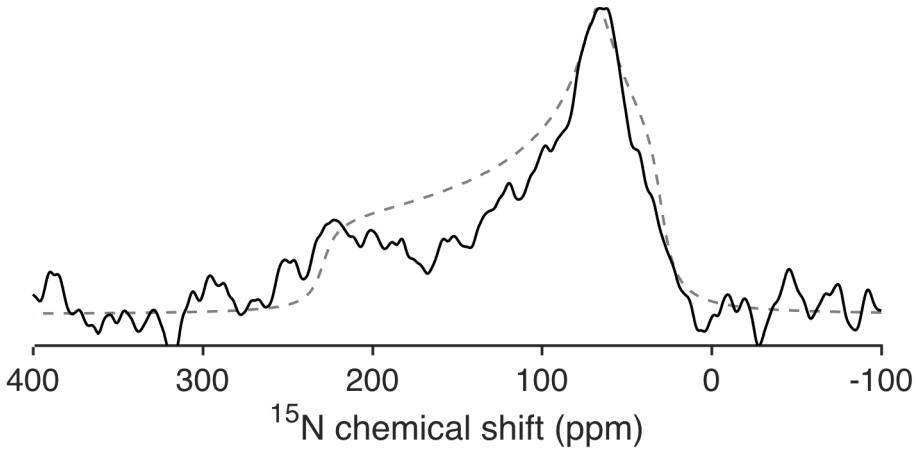

Figure 2.9: ***Spectrum of $^{15}N_{leu}$ fukutin TMD lyophilised powder****. Spectrum was acquired using a cross polarisation pulse sequence with 262 000 scans and processed with 300 Hz exponential line broadening. The simulated powder spectrum was calculated assuming an asymmetric tensor with the principle components 25.2, 61.7 and 222.4 ppm with 50000 powder points.*

^{15}N spectra of fukutin TMD were acquired in the three different lipids (Figure 2.8). The in the DLPC spectra there is one predominant peak, centred around 194 ppm, whilst there are two peaks in the DMPC and DPPC spectra. For DMPC there is a downfield peak at 213 ppm and an upfield peak at approximately 60 ppm (around the powder pattern 0° edge), and for DPPC the peaks are centred around 226 and 68 ppm respectively. First the downfield peaks will be considered. From fitting of simulated spectra, the tilt angles were

estimated as 20°, 2° and 1° for DLPC, DMPC and DPPC respectively. For tilt angles very close to the 0° edge, as in the case of DMPC and DPPC, it is difficult to accurately estimate the tilt angle, but it is clear that the peptide is almost completely parallel to the bilayer normal. The change in tilt angle is likely to arise as a result of the peptide attempting to compensate for the change in bilayer thickness, thereby avoiding hydrophobic mismatch between the protein and bilayer. Changes in the protein tilt angle are a common response to hydrophobic mismatch since it is less energetically demanding than distortion of the lipids to alter the bilayer thickness[48]. A similar trend was observed for increasing thickness in the MD simulations of fukutin TMD monomer in lipid bilayers of DLPC (39±11°), DPPC (30±9°) and POPC (17.6±7°)[62], although the tilt angles in that case were much greater than those determined here from the NMR data. These simulations were only of a single monomer in a bilayer, whilst when a later study probed the impact of dimerisation on the tilt angle in DLPC, a much smaller tilt of 18±10° was determined compared to 39±11° for the monomer[160]. This is very close to the tilt angle of 20° here, and crosslinking experiments reveal the protein predominantly forms dimers in such bilayers[160], indicating that the oligomeric state drives the protein tilt angle, and it therefore seems likely that in the NMR samples here the protein adopted a dimeric state. In the MD studies it is suggested that the interhelix interactions reduce the number of residues which can engage in lipid-protein interactions, thus altering the tilt angle. It is likely that in the DMPC and DPPC the protein reconstituted into the bilayer is also oligomeric, and cross-linking studies indicate that oligomers of increasing size form in bilayers of increasing thickness (Marius and Williamson, paper in preparation).

In all cases these peaks are fairly broad, with FWHM values of 57 ppm, 38.2 ppm, 45.1 ppm for the downfield DLPC, DMPC and DPPC peaks, respectively. Although this provides an indication of the distribution of tilt angles, the proton decoupling power in these experiments was relatively low (27.8 kHz for DLPC, 31.2 kHz for DMPC and DPPC), and less than necessary to fully decouple the spectra. As such observations about the helix tilt distribution should be treated with great care. Due to probe limitations and concerns regarding sample heating it was not possible to use a greater decoupling field.

In addition to the downfield peaks indicating a transmembrane orientation of the peptide, there are also significant components at the 0° edge of the spectra in DMPC and DPPC with increasing intensity. This suggests a secondary contribution to the spectra arising from either a disordered ensemble of peptides, or peptides in the surface bound state. In the case of DPPC this component has much greater intensity than the perpendicular oriented

component at the 0° edge. Peak integration indicates that in the case of DMPC the ratio of downfield to upfield peaks is ~1.5 for DMPC and ~0.5 for DPPC. This contribution may be explained in three ways. Firstly, it represents a peptide associated with the surface of the membrane, oriented perpendicular to the bilayer normal. This seems physiochemically unlikely considering the highly hydrophobic nature of the protein, with approximately 48 % of its residues being hydrophobic. Secondly, it is an oriented peptide in a disordered part of the sample (e.g. vesicles). Thirdly, it is an aggregate or large oligomer of the peptide, in which the amide groups are oriented randomly. To attempt to separate the last two possibilities, ^{15}N spectra were simulated using a powder component which was determined from the ^{31}P spectra using a similar approach to that of Muhle-Goll et al.[212]. Simulated spectra were processed with 800 Hz exponential line broadening to account for the broad lines. For example, the DMPC ^{15}N spectra were calculated assuming a powder contribution of 36 % (from the ^{31}P spectra of DMPC with fukutin TMD). This simulated spectrum overlays the experimental data in Figure 2.8 D. The powder component in the spectra has a similar intensity to the experimental data, suggesting that oriented fukutin TMD in disordered lipid bilayers may give rise to this peak. Improvement of the signal to noise, and of sample preparation may allow more robust analysis. In contrast, when the same approach is applied to the DPPC ^{15}N spectra (with 25 % powder contribution from ^{31}P) there is a large discrepancy between simulated and experimental spectra, indicating that the powder contribution of the fukutin TMD exceeds the powder component of the bilayers. Whilst it is possible that there may be a surface associated state of the protein, due to its hydrophobicity we instead suggest that the monomers form extra-membranous oligomers or aggregates as a result of being unable to alter their tilt further to compensate for hydrophobic mismatch with the thicker lipid bilayer. This is illustrated in Figure 2.10. Similar findings have been observed for the E5 oncoprotein, a monotopic helix with an unusually long hydrophobic segment, although in this case the protein aggregates in thinner bilayers rather than thicker bilayers. On addition of its heterodimeric partner the platelet derived growth receptor (PDGFR), the dimer is able to better manage the hydrophobic mismatch and it no longer forms aggregates[61]. Since it is known that fukutin interacts with the glycosyltransferase POMGnT1[176], which is speculated to recruit other glycosyltransferases[213], it is possible that similar stabilisation of the protein in the bilayer occurs in cellular membranes.

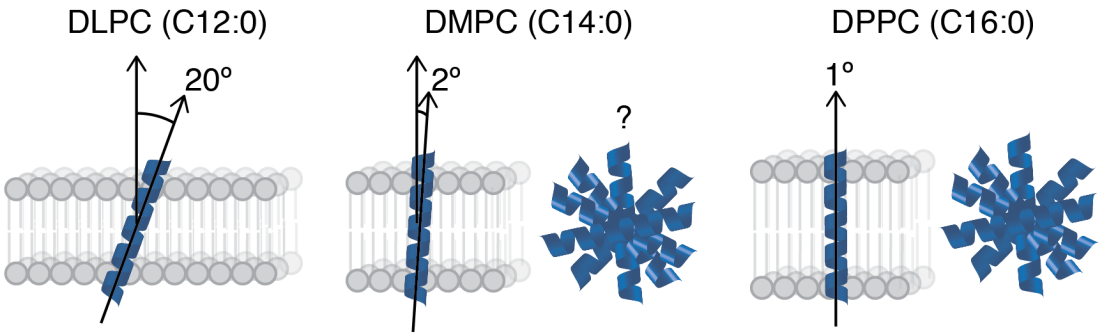

Figure 2.10: ***Schematic of fukutin TMD orientation in lipid bilayers of increasing thickness.*** *To compensate for changes in the bilayer thickness the tilt angle is reduced and aggregates form as a consequence of hydrophobic mismatch. Monomers are shown in the membrane for clarity but it is likely that the TMD forms oligomers in such environments.*

Further evidence for the fukutin TMD oligomerisation is provided by cross-linking studies in different lipids (Marius and Williamson, paper in preparation). As the acyl chain length is increased, increasingly large oligomers are found. In the case of DLPC only dimers are observed, whilst in DMPC and DPPC much larger high molecular weight oligomers were present. It is not possible from the data here to determine whether the disordered TMD component is located within or outside of the membrane. However, if it were present in the bilayer then there may have some form of order with respect to the bilayer normal. It also seems likely that should the aggregate be present within the membrane that it would perturb the membrane and result in greater disorder in the ^{31}P spectra. This is not the case in the fukutin TMD-DPPC spectra despite a large disordered protein component in the ^{15}N spectra. Another interesting observation is that Marius et al.[160] found that increasing the L/P ratio from 100 to 1000 has no effect on the oligomerisation of the peptide in DLPC, suggesting the protein-to-lipid ratio may not be a significant driving factor for oligomerisation. Taken together these results provide mechanistic implications for the retention of fukutin in the Golgi apparatus. In the thick DPPC membranes here, it appears that the protein forms aggregate since it is unable to span the membranes.

To summarise, it appears that fukutin TMD responds in two ways to the change in the lipid bilayer thickness. First it alters its tilt angle to compensate for the difference in hydrophobic thickness of the bilayer. Secondly it appears to aggregate, or possibly form large disordered oligomers. These findings provide a potential model for the retention of fukutin in the Golgi apparatus. Presumably it is unable to partition into the thicker, cholesterol-rich domains of the Golgi membrane which are destined for the plasma

membrane. Within the model membranes there are no thinner regions for the protein to partition into, therefore resulting in its aggregation due to hydrophobic mismatch.

2.4.4. Optimisation of samples for oriented circular dichroism measurements

The NMR studies above were highly useful to provide a reference for the OCD measurements. Like NMR, in order to measure OCD spectra there is a requirement for well oriented, high quality samples, but in addition the OCD samples must have good optical properties to avoid the effects of artefacts. As such, we set about optimising a number of parameters through a combination of NMR to determine sample alignment (^{31}P and ^{2}H NMR) and by measuring the OCD spectra.

First, however, the secondary structure of fukutin TMD in vesicles formed from different lipid vesicles was determined. In order to characterise the secondary structure of fukutin TMD in lipids of various hydrophobic thickness, the peptide was reconstituted into small unilamellar vesicles (SUVs) of DHPC, DDPC, DLPC and DMPC and SRCD spectra measured (Figure 2.11). The spectral shape indicates fukutin TMD adopts a primarily α-helical structure in all of the lipids selected. Namely, in all spectra there is a band with maximal positive intensity at 192±1 nm and negative bands with maximal negative intensity at 210±1 nm and 222±1 nm. In all spectra except DHPC the 210 nm band has greater negative intensity than the 222 nm band. These qualitative observations are verified by secondary structure deconvolution which reveals 77 % helical content in DHPC (C6:0), increasing to 79 % for DDPC (C10:0) and DLPC (C12:0) and 87 % for DMPC (C14:0). Secondary structure prediction using the JPred server[214] indicates that 75 % of residues in the peptide have helical confirmation. Similarly, previous studies by molecular dynamics and circular dichroism also indicate a high helical content greater than 90 %[62]. The distinction between DHPC and the remaining lipids is unsurprising since DHPC has a very short acyl chain and has a tendency to form micellar structures rather than bilayers, in part due to its conical molecular shape. It is conceivable that in the thicker membranes of DMPC more of the peptide is immersed in the bilayer, which induces helical structure in regions that may otherwise have a different conformation. Indeed, in MD studies with thinner bilayers there is a slight loss of helicity (~3 residues) at the N and C terminal ends of the peptide during the course of the simulation[62, 160].

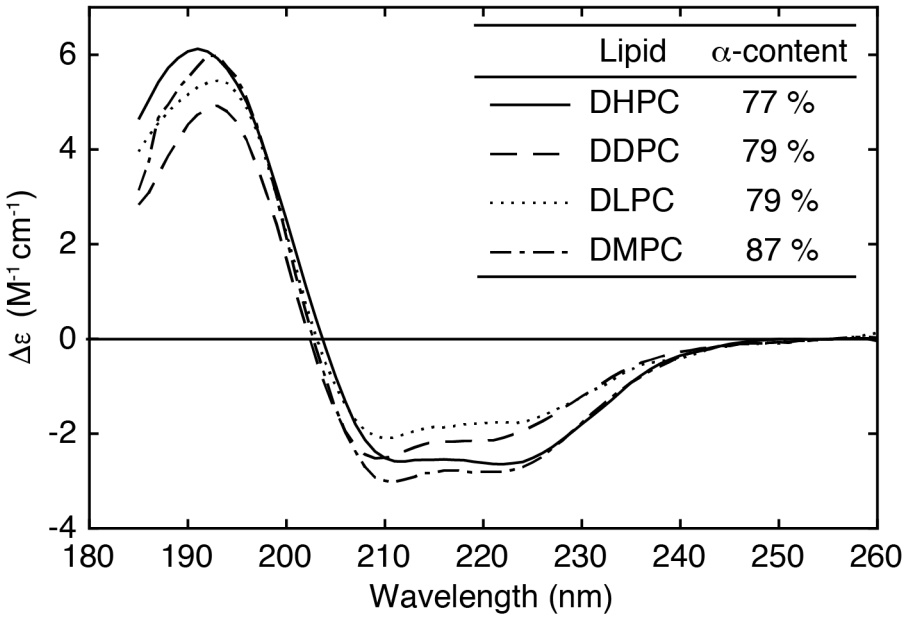

Figure 2.11: ***SRCD spectra of fukutin TMD in SUVs formed of lipids (or surfactant) with varying acyl chain length.*** *Spectra of fukutin TMD in DHPC (solid line), DDPC (dashed line), DLPC (dotted line) and DMPC (dash-dot line) were recorded with L/P ratio of 200 throughout. Spectra were acquired at 25 °C except for DMPC which was recorded at 40 °C to ensure lipids were in the liquid crystalline phase. At least four scans were averaged for each sample and lipid-protein SUVs were baseline corrected against pure lipid SUVs. Inset table: percentage of helical content as determined by secondary structure deconvolution using CONTIN/LL algorithm and basis set 10.*

2.4.4.1. Effect of substrate material on sample quality

To prepare oriented SRCD (OSRCD) samples we initially replicated the method used for oriented NMR samples, but using a reduced quantity of lipid. For initial measurements and to become accustomed with the technique the lipid 1-palmitoyl-2-oleoyl-*sn*-glycero-3-phosphocholine (POPC) was selected for a number of reasons. Namely, it undergoes gel to liquid crystal phase transition well below room temperature, from our preliminary work could be well aligned with relative ease, and from MD simulations gives the smallest tilt angle, which would simplify interpretation of the OSRCD spectra.

A particular advantage of using the B23 beamline for this work is the focused microbeam, which has two principle benefits. Firstly it is possible to use smaller samples and thus reduce the quantity of expensive lipid and peptide required in sample preparation. Secondly, and most significantly, is that the focussed beam allows specific regions of the sample to be investigated. In the case of oriented samples this is useful because any uneven

or defective regions, often the edges of samples, can be avoided, rather than averaged as part of the spectra as is the case of larger beam sizes.

To ensure our initial preparation method yielded well oriented samples ^{2}H NMR was used. Using POPC-d31 samples were prepared with either 0.1 or 0.4 mg lipid per 4x25 mm coverslip (lipid per area of 1.0 or 4.0 μg mm^{-2}) and measured with the coverslip normal both parallel (0°) and perpendicular (90°) to the magnetic field (Figure 2.12). These samples were hydrated directly by the application of a small quantity of water on the surface and incubation for ~1 hour. The quadrupolar splittings of doublets in the deuterium spectra can be used to estimate the bilayer orientation since they are orientationally dependant. The splitting is also dependant on the motion of the group, with the most mobile groups producing the innermost peaks and the most immobilised groups in the outmost peaks in the plateau region. Peaks in the plateau region are those with the smallest motion and therefore greatest S_{CD}. In the spectra for both quantities of lipid there are well resolved pairs of resonances for CD groups in the acyl chain, although there is possibly a small underlying powder component in the 0.4 mg spectra, in contrast to the 0.1 mg spectra where there is no intensity between the resonances. In general it is clear there is a high degree of alignment. The splitting of the powder spectrum 0° edge is 24.6 kHz, and for 0.1 mg of lipid the 0° edge is similarly 26 kHz. For 0.4 mg lipid the splitting is 19.4 kHz, which although representing a significant reduction is likely to be due to misalignment of the sample in the coil. This is reinforced by the splitting between the 90° edges, which is 52.6 kHz for 0.1 mg and 49.6 kHz 0.4 mg, both approximately twice the 0° edge splitting of the powder spectrum.

Initially we tested two substrates for the preparation of oriented samples, UV-grade fused silica and calcium fluoride. Fused silica is the most commonly used material for CD cuvettes and substrates due to its robust nature and excellent transmittance in the UV region. Calcium fluoride has been used previously in SRCD due to its excellent transmittance in the vacuum UV region[197] but it is a relatively soft material that cannot be exposed to harsh conditions such as acids which are normally used to clean cuvettes. The two substrates have different properties, particularly of interest here is the wettability of the surface, i.e. the tendency of a liquid to spread across the surface, which may affect the distribution of lipid on the surface[215].

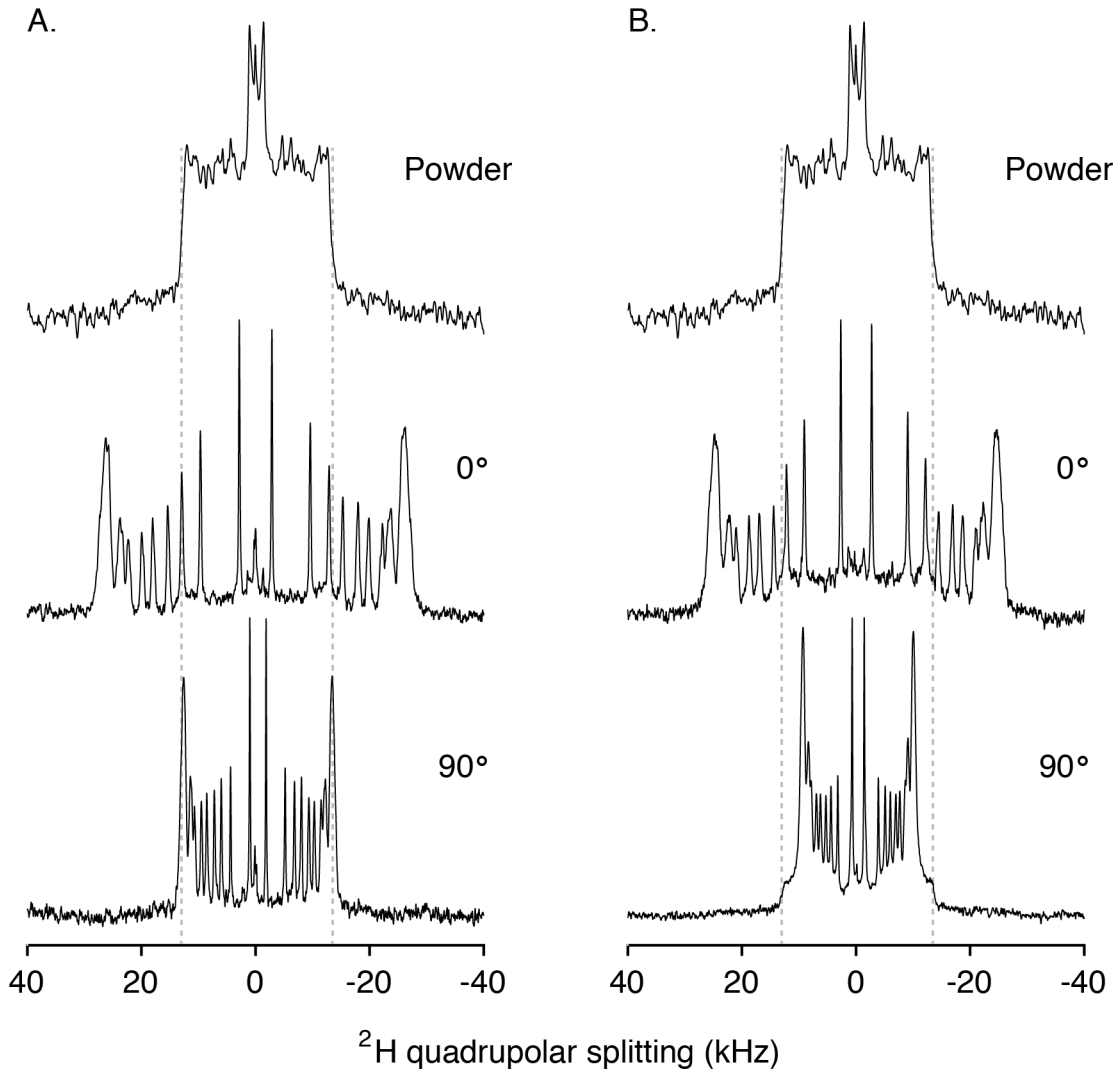

Figure 2.12: ***^{2}H spectra of oriented samples of POPC-d31 on 4x25 mm glass coverslips****. A powder spectrum of POPG-d31/POPC vesicles (30 % w/v; note PG rather than PC deuterated lipid) is given for reference. Oriented spectra at 0° and 90° were prepared with either. 0.1 mg (A.) or 0.4 mg (B.) POPC-d31. Samples were hydrated by direct application of ddH_2O to the surface of the coverslips and spectra were acquired at 25 °C with between 16000 and 131000 scans. Dashed grey lines indicate 90° edges of the powder pattern.*

First samples on CaF window were prepared by deposition of POPC in methanol with and without fukutin TMD at a L/P of 50 (Figure 2.13). Increasing masses of POPC were used, from 0.1 mg to 1 mg to estimate the quantity of lipid required to provide a sufficient protein signal without causing problems due to absorption or artefacts. The CaF windows used were part of a demountable cell, comprising a circular flat window and a second window with a polished recess of 5 mm diameter which was used to contain the sample. Samples were hydrated by the application of a small amount of 5 mM potassium phosphate buffer, pH 7.4, to the surface of the dry film and closed with the flat window to prevent

dehydration. Polarised light micrographs of the samples are shown in the figure to illustrate the challenges associated with the preparation of good quality samples. Interestingly here the samples prepared with fukutin TMD appeared to be much more homogeneous than the pure lipid samples. The pure lipid samples have a much more crusted and inhomogeneous appearance than the fukutin TMD samples at 0.5 and 1 mg POPC. Whilst the signals of these samples are relatively modest in intensity they are inconsistent and clearly the samples do not have suitable optical properties for CD measurements. In the case of 0.1 mg POPC with fukutin TMD there is a similar inhomogeneous distribution. In preparation of samples with very small masses of lipid this is often the case. It appears that the lipid concentrates into a small spot of solvent which is difficult to spread across the surface. The spectra of fukutin TMD in 0.5 and 1 mg of POPC have a helical appearance, with an intense minima at 212 nm, suggesting that the protein is oriented perpendicular to the bilayer normal. This is unexpected, considering the NMR data, MD data and the hydrophobic amino acid composition of the protein. A cautionary note here is that due to the quality of the pure lipid samples, the baseline correction used a clean coverslip rather than the equivalent pure lipid sample, and we have observed that POPC has a relatively strong absorbance band around 200 nm, which may distort the spectra. We were also concerned that although in some cases good quality oriented samples were achieved, a greater number of poor quality samples were prepared. To address this an alternative substrate, fused silica quartz, was tested. Fused silica has been used extensively in the literature as a substrate for OCD samples[60, 133, 138, 145, 216].

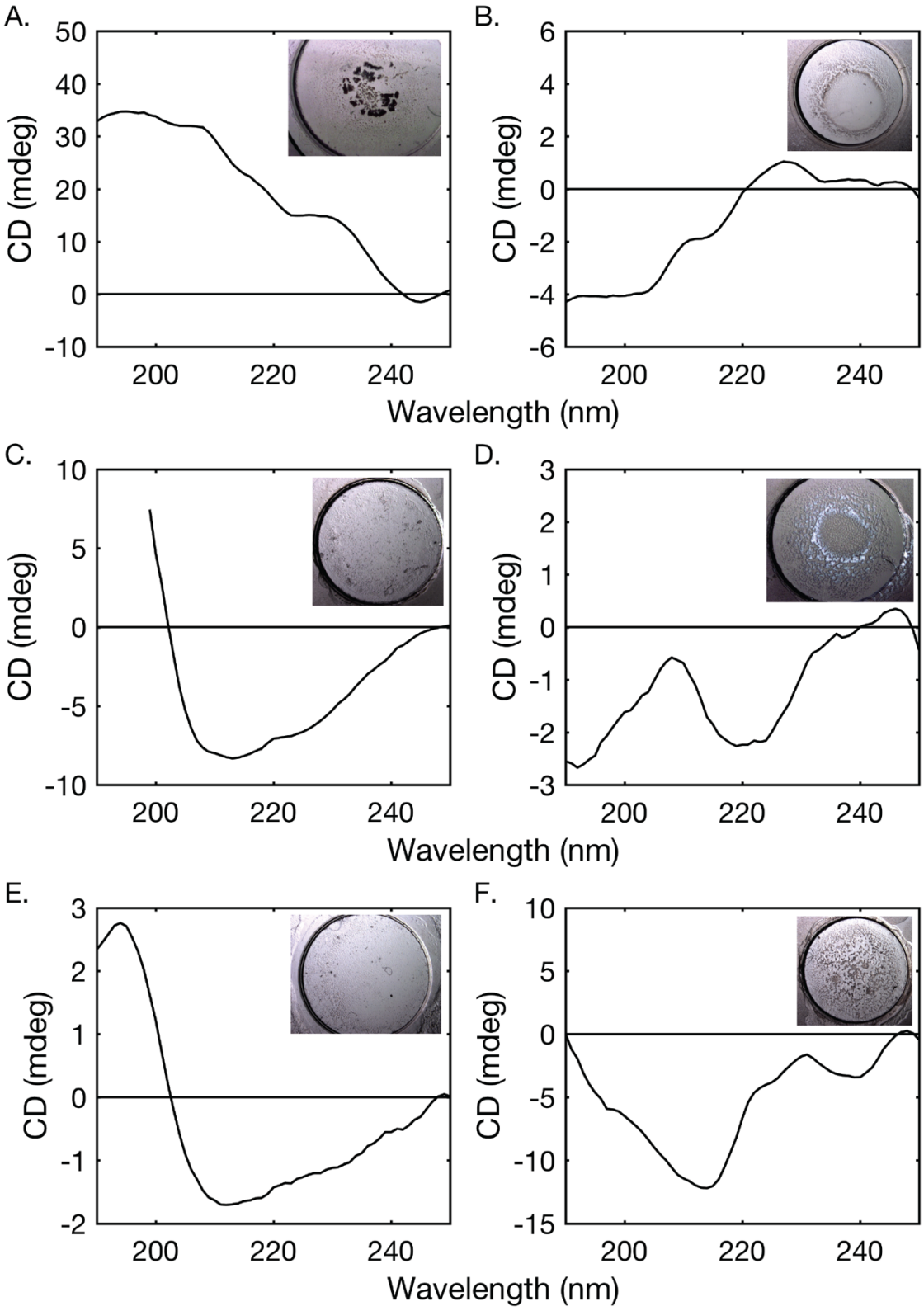

Figure 2.13: ***OSRCD spectra of POPC on calcium fluoride substrate either with (left) or without (right) fukutin TMD at L/P of 50.*** *Inset: micrograph show sample prior to measurement. The sample surface area was approximately 20 mm^2 and different quantities of lipid were applied, either 0.1 mg (A. and B.), 0.5 mg (C. and D.) or 1 mg (E. and F.). Spectra were acquired at 20 °C and baseline corrected against a clean calcium fluoride window. Note the change in scale of the y axis.*

As a comparison, samples were prepared on fused silica demountable cells using methanol deposition. Similar to the CaF this meant that the samples could be hydrated by direct application of buffer and sealed to prevent dehydration. Based on the CaF spectra and a trial and improvement approach approximately 1 mg of lipid was deposited onto each 35x10 mm flat fused silica window (the lipid did not cover the entire surface but lipid per area was estimated as approximately 3 $\mu g\ mm^{-2}$). In addition to POPC, DMPC was also used since it has a different hydrophobic thickness. For both lipids, the samples were notably more homogeneous than those prepared on CaF (Figure 2.14), although it was important to probe the centre of these samples since there were regions of inhomogeneity at the edges (Figure 2.14 E.). In both cases the pure lipid samples produce similar line shapes, with a low intensity broad band centred around 215 nm, similar to those published[136] (in supplementary information). Both of the fukutin TMD spectra (Figure 2.14 A. and C.) have features consistent with a helical protein. However, it appears that these spectra are shifted. For example, the usual minima at 222 nm appears closer to 233 nm in these spectra, even though this peak should be relatively unaffected by orientation. The fukutin TMD in POPC spectra, if taken at face value, also directly contradicts the previous spectra on CaF. It is likely in these spectra that artefactual contributions, although the precise nature of these artefacts is unclear.

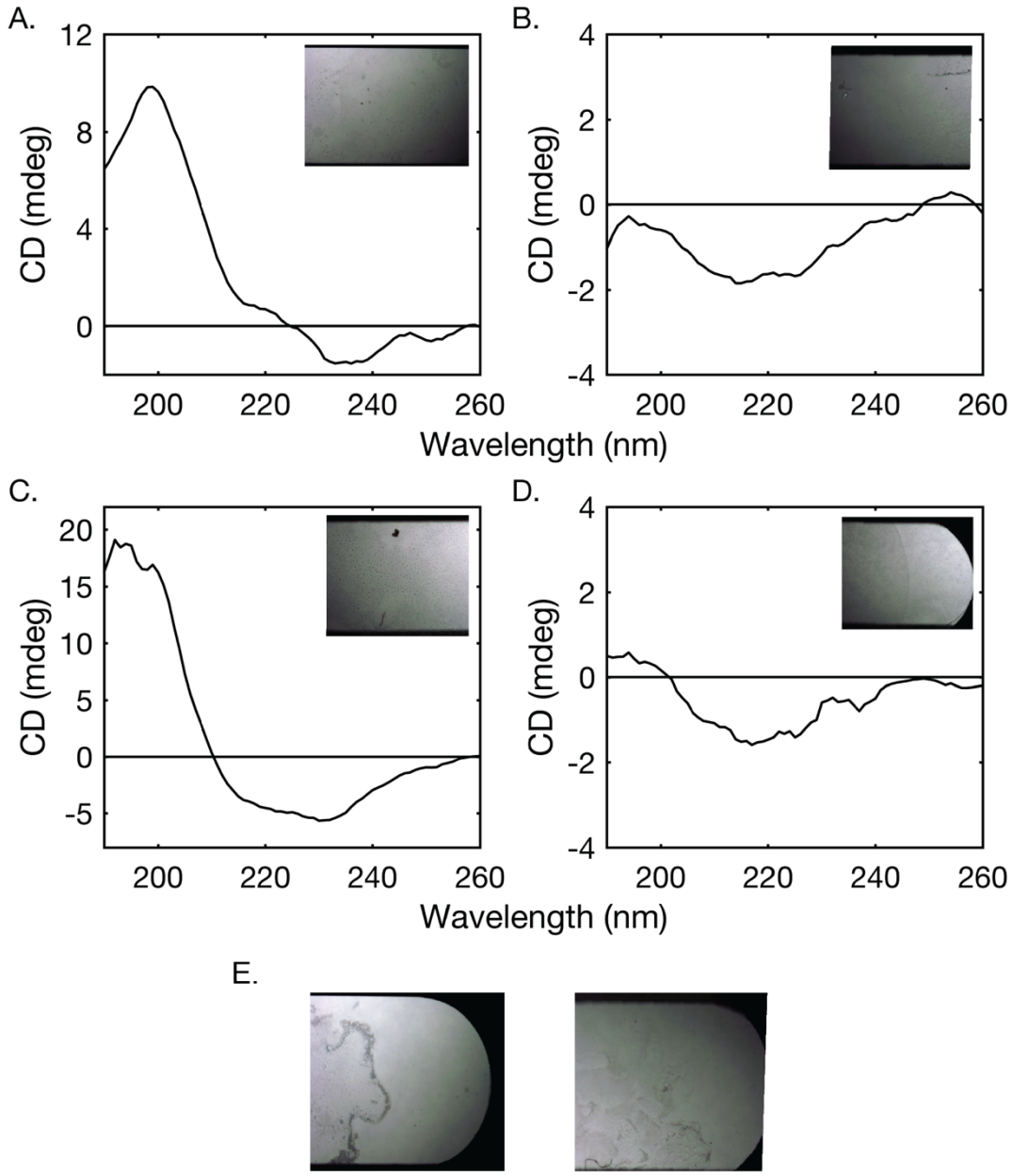

Figure 2.14: ***OSRCD spectra of DMPC (top) and POPC (bottom) oriented samples prepared on fused silica substrate with (left) or without (right) fukutin TMD.*** *E. shows examples of sample edges. The lipid per area was ~3 µg mm^{-2} and samples were hydrated directly with 5 mM potassium phosphate buffer pH 7.4. Spectra were baseline corrected against equivalent pure lipid spectra. Note the change in scale of the y axis.*

Visual inspection of the samples, and CD data, suggest the samples prepared on fused silica possess more suitable optical properties than those prepared on calcium fluoride substrate. As we had already demonstrated using ^{31}P that DMPC could be successfully aligned in the first half of this chapter, we then wanted to confirm that POPC could also be well aligned. Using 2 µg mm^{-2} lipid, samples were prepared on 25 x 10 mm fused silica coverslips. Note that these samples were first partially hydrated then additional water

added prior to sealing in a length of NMR tube. The ^{31}P NMR spectra of these oriented samples (Figure 2.15) are dominated by the presence of a single peak at 33.2 ppm (0°) or -17.1 ppm (90°), matching the 0° and 90° edges of the powder spectrum and demonstrating an excellent degree of macroscopic alignment. Considering the 0° and 90° edges, the CSA of the oriented sample is -50.3 ppm, approximately 4 ppm greater than the CSA of the powder sample. This can be explained by a scaling of the CSA in the powder sample due to the increased hydration. These values are similar to those we have measured for POPC on glass (data not shown) and values given in the literature for POPC oriented on glass substrates[217]. Although generally it is apparent that the samples are well ordered, an important point of contrast here is that whilst the NMR signal is averaged over the entire sample, the OSRCD spectra probe a very small area, so any localised changes in degree of alignment will be reported. Since it appeared that fused silica was preferable to calcium fluoride for sample preparation it was used for the remaining experiments.

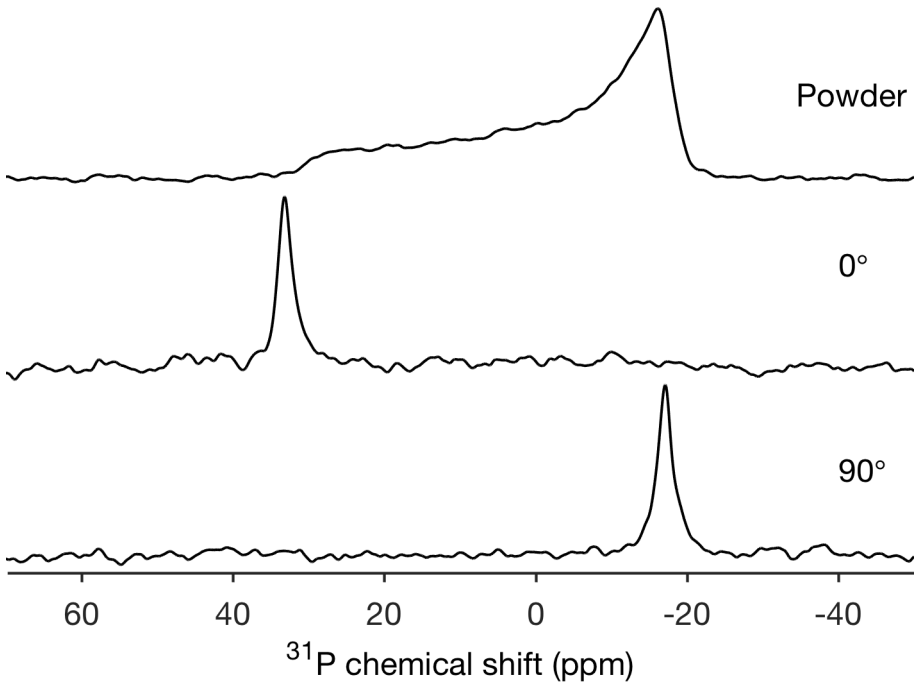

Figure 2.15: ***^{31}P NMR spectra of POPC bilayers on fused silica coverslips.*** *Top: powder spectrum of POPC multilamellar vesicles (30 % w/v). Middle and bottom: oriented POPC samples on fused silica coverslips (0.2 mg per 25x4 mm; lipid per area 2 μg mm^{-2}) aligned with coverslip normal at 0° or 90° to the magnetic field. Spectra were acquired at 25 °C, with 256 scans for the powder sample and 8192 for oriented samples. Oriented samples were hydrated for 16 hours at 97 % humidity then a few μL additional ddH_2O added to the sample directly. All spectra were processed with 200 Hz exponential line broadening.*

2.4.4.2. Demonstrating sample uniformity

To ascertain the uniformity of the sample, OSRCD spectra of fukutin TMD in POPC were acquired whilst scanning across the surface of the demountable cuvette with three positions separated by approximately 1 mm intervals (Figure 2.16). As a comparison the spectra of fukutin TMD in POPC SUVs was also acquired (Figure 2.17). The SUV spectra reveal, as expected, a primarily helical structure indicated by minima at 211 and 222 nm and a maximum at 194 nm. The ratio of intensities of the two minima is 0.9.

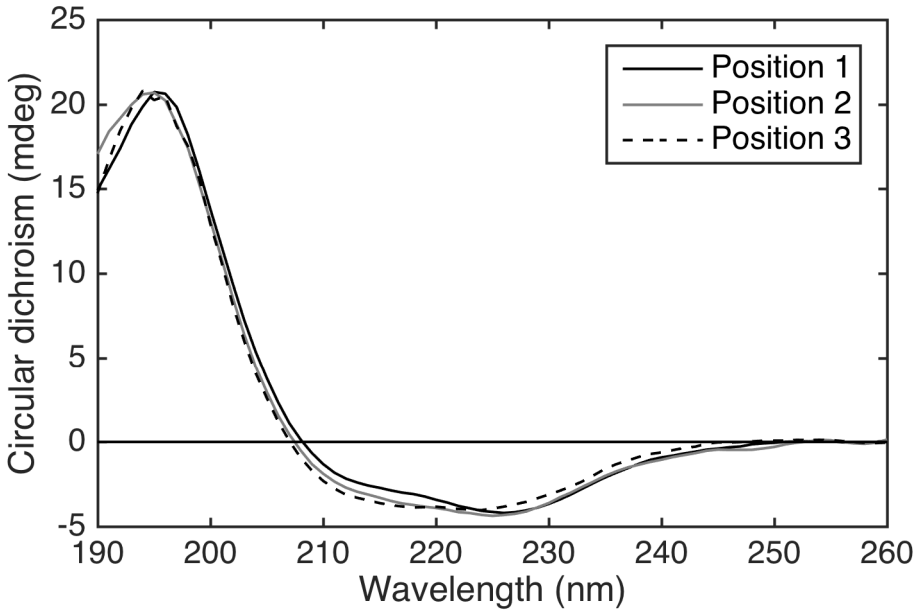

Figure 2.16: ***OSRCD spectra of fukutin in POPC bilayers on fused silica demountable cuvette at L/P of 50.*** *Spectra were acquired at three positions at the centre of the sample seperated by approximately 1 mm. The spectra were baseline corrected against an average of three positions measured on a pure POPC sample.*

The oriented spectra (Figure 2.16) indicate a helical structure, with peaks around 225, 214 and 194 nm. Whilst the three spectra are similar they are not identical. The changes in the spectral intensity do not appear to result from changes in localised protein concentration, as it is not possible to produce identical spectra by scaling the intensity for concentration. According to the theoretical basis of OCD, a completely parallel oriented helix would give no intensity at ~208 nm due to the collinearity of the $\pi - \pi^*_{//}$ transition with the electric field vector of the light. In all three spectra here the 214 nm band has relatively low intensity compared to the 225 nm band, yielding a 214/225 nm ratio of 0.73 for the average of the three spectra. This compares to the 0.9 ratio for the SUV sample, indicating that the relative intensity of the 211 nm band is reduced, and suggesting that whilst the peptide

adopts a transmembrane orientation it is not completely upright since the band is still present. This is broadly consistent with the MD simulations which give a tilt angle of 17.6 ± 7° for fukutin TMD monomers in POPC.

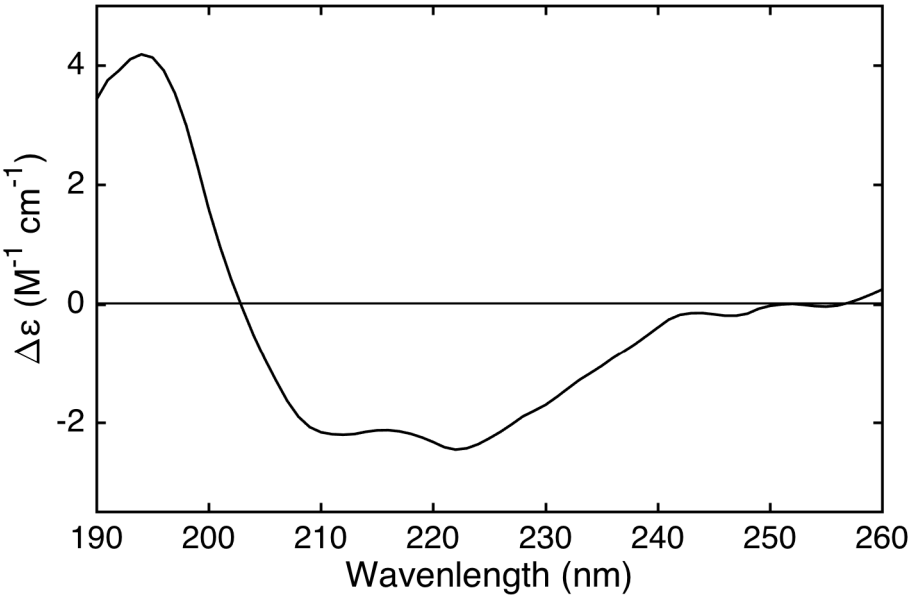

Figure 2.17: ***SRCD spectra of fukutin TMD in POPC SUVs at 20 °C with L/P of 200.*** *The spectrum represents an average of 12 scans baseline corrected against a pure POPC sample. Smoothing was performed using a Savitsky-Golay filter with a polynomial order of 3 and 10 point average*[218].

2.4.4.3. Effect of hydration on OSRCD samples

In order to measure the effect of hydration on the spectra observed we undertook measurements using the module A instrument, which allows for horizontal mounting of the samples. This meant that samples could be directly hydrated and then allowed to dry without moving. (For "fully hydrated" measurements the samples were rehydrated with a small drop of ddH_2O if they appeared to be beginning to dry.)

In Figure 2.18 three spectra are presented which show a sample measured three times at the same position, firstly where it was hydrated just before measurement, a following measurement when the sample began to dry and then a final measurement where the sample had air dried. In these spectra the absorption above 200 nm was such that the data could not be interpreted reliably. Note that these spectra were baseline corrected against a clean coverslip since it was not possible to choose accurately a baseline with identical hydration. It is clear that there is a significant effect, and it appears that the protein becomes more upright in the bilayer as water is removed. de Jongh et al.[135] made a similar observation in oriented bacteriorhodopsin samples at low hydration, where they assigned

the apparent loss of intensity to absorption flattening. Presumably in low hydration conditions the peptide begins to aggregate and produces these flattening effects. It also must be noted that reduced hydration samples appear more 'frosted' than hydrated ones, which may result in other artefacts such as scattering distorting the spectra. In any case, it is clear that hydration is an important consideration for these measurements, which was previously demonstrated by Wu et al. who showed the changing orientation of alamethicin in environments with decreasing humidity[133].

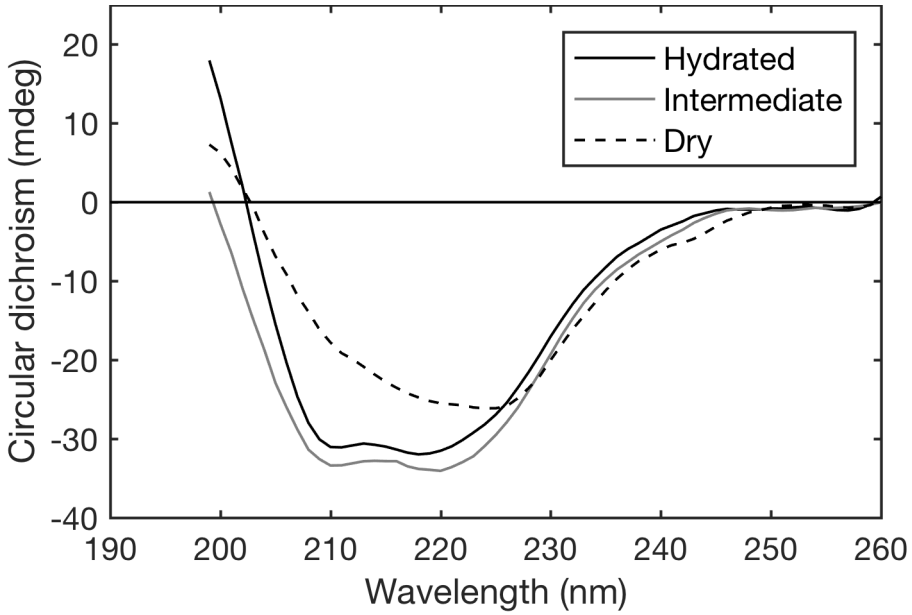

Figure 2.18: ***OSRCD spectra of fukutin TMD in DLPC bilayers as the sample goes from hydrated to low hydration (dry).*** *Sample was prepared on fused silica coverslip with fukutin TMD with a L/P of 50 and 2.5 µg mm^{-2} DLPC. Spectra were baseline corrected against spectra of a clean coverslip.*

2.4.4.4. OSRCD measurements

Having established methods for preparation of samples, and understanding the importance of the substrate material and hydration, we set about performing measurements in the same lipids as the earlier NMR measurements. DLPC and DMPC were selected since fukutin TMD appears to change its tilt angle in response to their bilayer thickness. Although it was desirable to study DPPC it was very challenging to prepare transparent samples, and the relatively high transition temperature would be difficult to maintain evenly across the sample surface. It would also be challenging to interpret spectra in context of the large secondary component observed in the NMR spectra.

The OSRCD spectra of fukutin TMD in DMPC and DLPC bilayers presented in Figure 2.19 (A. and B. respectively), in which the samples were fully hydrated. In Figure 2.19A. the DMPC spectra were acquired at three different positions on the sample. Unlike the POPC sample measured in three positions, these spectra have almost identical lineshapes, with only the intensity changing. This indicates that the intensities of the bands are scalable for concentration, and presumably represents the measurement of thicker regions of the bilayer containing a greater number of proteins. To assess whether these two lipids produce a different tilt angle, the intensity of the 208 nm can be compared. The ratio of the 208/222 nm peaks is 0.73 for DMPC (position 2) whilst the ratio for DLPC is 0.83, indicating that the 208 nm band is less intense in DMPC than DLPC. This suggests that DMPC has a smaller tilt angle than DLPC, which is in agreement with the ^{15}N NMR data, and presumably is a result of hydrophobic mismatch. What is striking, however, is that the ^{15}N data in DMPC indicates that the protein is almost completely parallel to the bilayer normal, which in OSRCD spectra would result in a near complete loss of the 208 nm intensity. There are a number of possible reasons for observation of some intensity at 208 nm in this spectra. Firstly, if there was disordered aggregate in the sample which retained helical structure one would expect to see an increase in the intensity of the 208 nm band in the DMPC spectra. This would give rise to a two component CD spectra (i.e. oriented and powder), which cannot be readily deconvoluted, as unlike in the NMR spectra the disordered component is not spectrally resolved. Secondly, aggregation of the peptide may result in differential flattening artefacts, where the intensity is reduced in a wavelength specific manner due to the uneven distribution of chromophores in the sample. Thirdly, if a proportion of the protein forms unstructured aggregate (or loses some helical structure), this would reduce the overall intensity of the helical spectra. Since is it not possible to precisely correct for the protein concentration in oriented samples it is not possible to perform accurate secondary structure deconvolution. It is difficult to adequately delineate these possibilities, although from the NMR data in DMPC any disordered component is small relative to the oriented peptide, allowing us to tentatively interpret the peptide orientation from the OSRCD spectra.

We were satisfied that these measurements were unaffected by LD and LB artefacts. Care was taken during measurements to ensure that the fused silica substrates were aligned such that the bilayer normal was parallel to the light beam. Further, samples were visually inspected to ensure that the surface was smooth and even, since artefacts in the literature were reported to arise due to sample inhomogeneity[133, 136]. During this work spectra were

acquired of a number of samples afflicted by such artefacts, like those in Figure 2.13, so samples must be judiciously selected and extreme care taken during measurements.

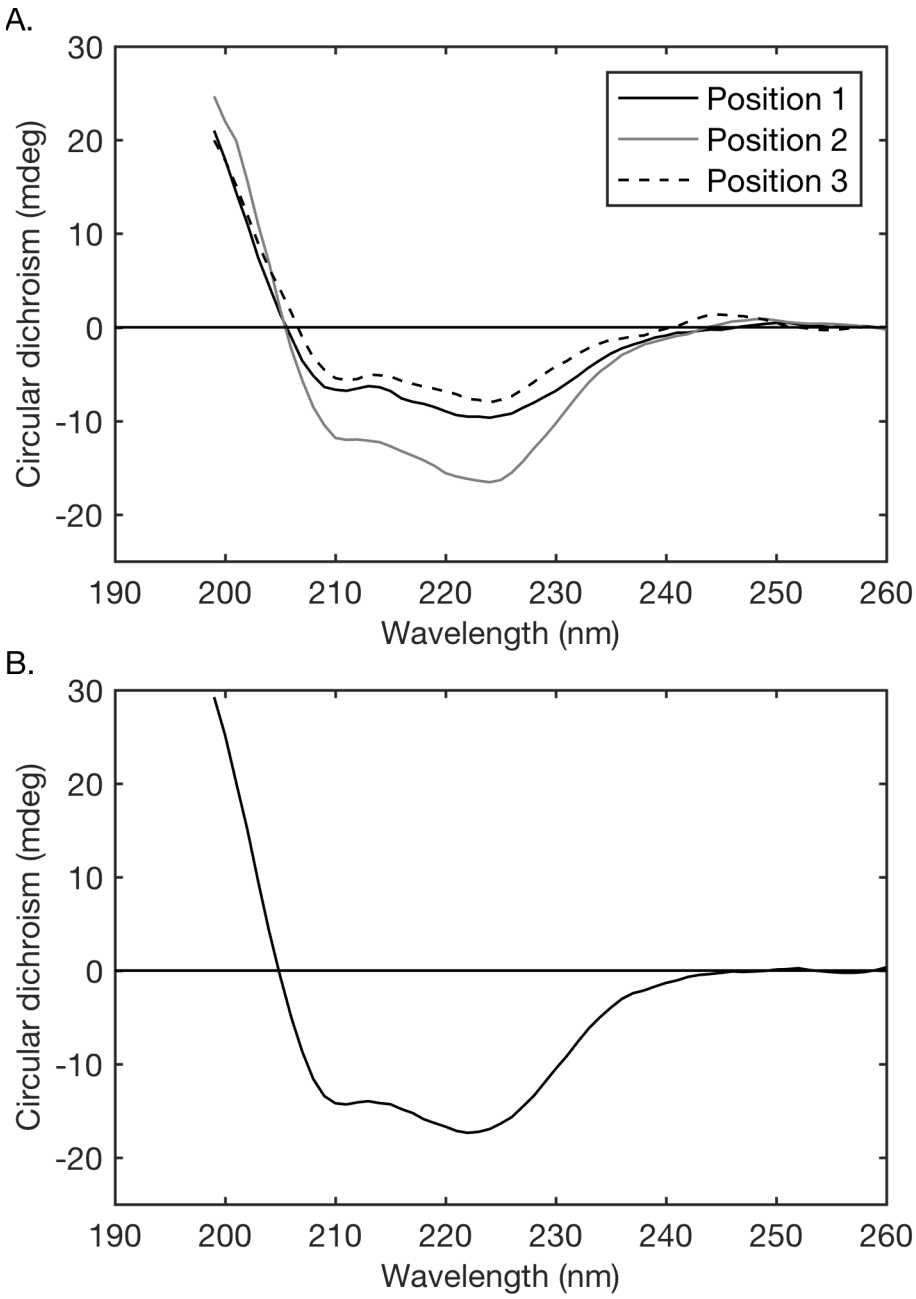

Figure 2.19: ***OSRCD spectra of fukutin TMD in DMPC (A.) and DLPC (B.). Spectra were baseline corrected against pure lipid samples.*** *A L/P ratio of 50 was used throughout. Samples were prepared on fused silica coverslips with 2.5 µg mm^{-2} lipid and baseline corrected against equivalent pure lipid spectra.*

It is apparent from the work here that the fukutin TMD undergoes orientational changes to compensate for hydrophobic mismatch with the lipid bilayer. This provides an insight into potential driving forces for the retention of glycosyltransferases such as fukutin in the correct cellular membranes. Whilst the OSRCD and NMR results correlate there are some experimental variations between the techniques which need to be considered. In the NMR samples partial hydration was used, and although additional water was added prior to measurement this is not identical to SRCD. Possibly more important is that the NMR samples used multiple coverslips which were stacked, providing a degree of pressure which could help to ameliorate sample defects[219], although in the samples here we have no reason to believe they contained a large disordered contribution.

2.5. Summary discussion and conclusions

Using a combination of solid-state NMR and OSRCD spectroscopies we have characterised the response of the TMD of the putative glycosyltransferase fukutin to changes in PC lipid bilayer thickness. Both approaches have revealed that one of the mechanisms fukutin uses to adapt to increasing bilayer thickness is to reorient in the bilayer. The NMR data also implies that the protein aggregates or oligomerises in response to thickening bilayers. Cross-linking and FRET data (Marius and Williamson, paper in preparation) also indicate that thicker bilayers promote the formation of large oligomers of fukutin TMD. Presumably these effects prevent the energetically unfavourable exposure of hydrophobic residues. There is much precedent for these responses to hydrophobic mismatch, such as the HIV-1 derived Vpu peptide, a channel forming protein with one membrane spanning helix, which changes its tilt angle substantially in response to bilayer thickness (i.e. from 18° in C18:1 to 51° in C10:0 bilayers)[220], and the synthetic peptides synthesised by Sparr et al.[221] which form aggregates by engaging in helix-helix interactions to limit lipid-protein interactions in bilayers of differing thickness. Like most Golgi resident proteins the hydrophobic span of fukutin TMD is smaller than proteins of the plasma membrane (an 18 residue stretch of the sequence has positive hydrophobicity based on the Kyte-Doolittle scale[222] (calculated using ExPASy ProtScale[199])), which provides a further driving force for retention within the thin Golgi membranes, as has similarly been demonstrated by Munro in the Golgi resident protein sialyltransferase[223]. It appears here that the fukutin is unable to span the thicker membranes of DPPC completely, and so instead forms aggregates or large oligomers. It is likely in a more complex, biological membrane that fukutin TMD is excluded from thicker regions of the membrane and instead resides in thinner parts of the membrane, which do not form trafficking vesicles to the plasma membrane. Further changes in the protein to adapt to hydrophobic thickness are

possible, including bending or flexing of the protein to span the bilayer[224], which have not been studied but may well have roles here.

Both OSRCD and solid-state NMR provide a means to investigate the tilt angle of fukutin TMD in a lipid bilayer. Whilst the OSRCD provides an estimate of the tilt angle in bilayer, the NMR provides greater resolution and allows determination of the helical tilt angle. The difference in the tilt angle in DMPC by both techniques is likely to be explained by the combination of a powder contribution to the OSRCD spectra and possibly the different timescales of the two methods. This highlights the need to use complementary techniques to fully interpret the data observed. Now we have established a reliable protocol for the production of good quality oriented fukutin TMD samples it should be possible to readily acquire OSRCD spectra of fukutin TMD in various lipid bilayers, which could then possibly be used to select the conditions which require further characterisation by oriented NMR. Further studies in more complex model membranes on the fukutin TMD tilt angle would be particularly interesting, especially the role of charged lipids. Arginine and lysine residues have been implicated in its lipid-protein interactions so it would be unsurprising that charge has an effect on the hydrophobic response, and MD studies indicate that this is the case[62].

An interesting observation from the OSRCD spectra here is that the ability to probe specific areas of a sample can provide advantages in terms of excluding regions of the sample which may produce spectral artefacts, particularly sample edges. This has not been previously reported for OSRCD measurements which generally average a large area. Since beamline access is time limited, if optimising sample preparation using benchtop instruments it would be important to either mask the sample or ensure the sample surface in the light beam is sufficiently uniform. Beamline developments presently ongoing include the introduction of a 'CD imaging' system[225] and new instrumentation to allow simultaneous measurement of CD, circular birefringence, LD and LB. Combined, these have the potential to provide complete reassurance regarding the origin of signals observed in the OSRCD spectra and to eventually automate the collection of OSRCD data.

It is worth noting that although samples for oriented CD require a small amount of material, the optimisation required takes a considerable length of time and material in itself. It often appears that the quality of the sample is driven by luck rather than any empirical efforts, although the attempts here have begun to standardise the preparation methods. Whilst there is a growing body of work demonstrating the value of OCD as a biophysical technique to qualitatively (in most cases) understand the orientation of small

helical peptides such as antimicrobial peptides aligned at extremes of either parallel or perpendicular to the bilayer normal, it is being increasing applied to more challenging proteins. The work here attempts to capitalise on these successful studies and explore a slightly more complex protein which appears to have an intermediate tilt angle and undergoes relatively subtle changes in response to the bilayer composition, where the results are less clear.

If attempts to extend OCD studies to larger, more complex membrane proteins are successful it has the potential to become a powerful technique to understand the structural implications of ligand binding events and other physiological processes. However, this would require the development of new, sensitive algorithms for deconvolution of multiple helices, and methods for the preparation of such samples.

Chapter 3. Developing a novel method for oriented circular dichroism using magnetically-aligned lipid bilayers

3.1. Introduction

As shown in the previous chapter, OCD is a useful technique to study the structure and orientation of membrane proteins in an environment which mimics cellular membranes. However, a number of challenges associated with the preparation and measurement of the conventional mechanically oriented samples make these experiments far from straightforward. In Chapter 3 the aim is to develop a novel strategy for OCD using magnetically aligned lipid bilayers. These have the potential to overcome a number of challenges associated with mechanically aligned samples. Bicelle solutions are transparent and can be aligned by the application of a magnetic field. To obtain bicelles which align in the low field of a magnetic CD (MCD) instrument we have optimised the lipid composition using NMR and electron paramagnetic resonance (EPR) spectroscopy, prior to measurement using a MCD spectrometer. By correlating CD, EPR and NMR data we have characterised a system in which fukutin TMD can be oriented in magnetically aligned bilayers and drawn comparisons with the conventional mechanically aligned approach outlined in Chapter 2. Although the method requires further development before acquisition of magnetic OCD spectra is possible, this method could be applied to larger, more complex proteins which have proven difficult to incorporate into mechanically oriented samples. Protocols for the reconstitution of structurally diverse membrane proteins including KcsA[226], G protein coupled receptors[227-229] and tOmpA[230] into bicelles have already been established.

3.1.1. Magnetically-aligned lipid phases

It has been known for many years that liposomes have a tendency to deform and align in magnetic fields[231-234]. This concept has been exploited for magnetic resonance studies, where bilayered micelles, or bicelles, have been widely used since their first identification around 1990[235-237] due to their propensity to align in a magnetic field. Bicellar phases arise in mixtures of a long chain phospholipid (classically DMPC) and a surfactant (DHPC) (Figure 3.1 A. and B.).

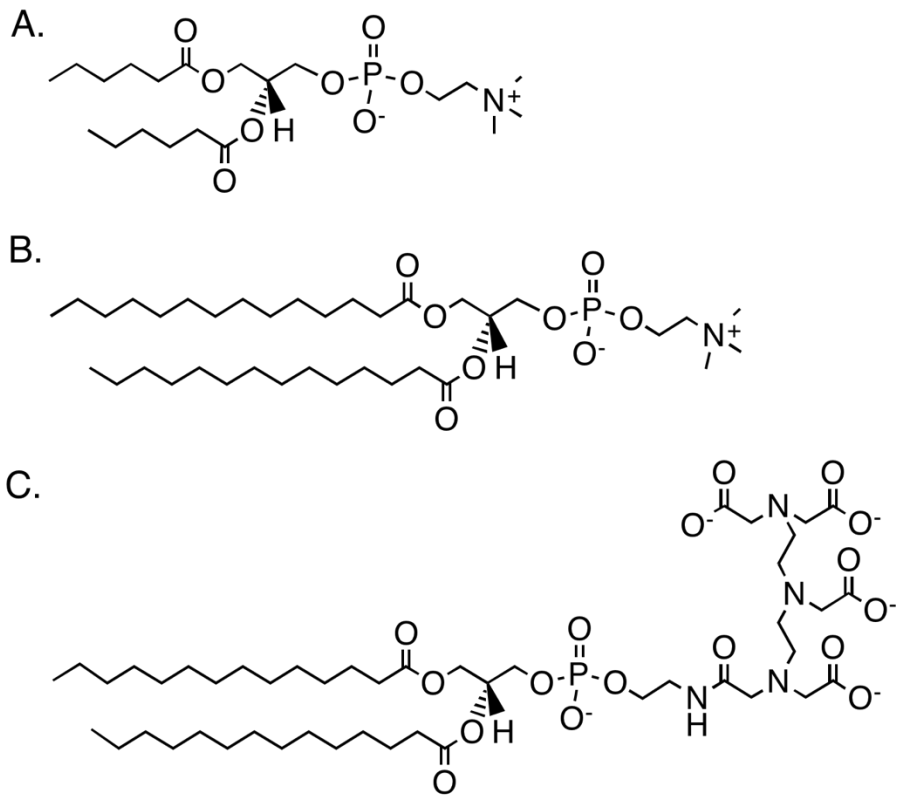

Figure 3.1: ***Molecular structure of DHPC (A.), DMPC (B.) and DMPE-DTPA (C.) lipids.***

The molar ratio of the lipid and surfactant (*q* ratio) is one of a small number of factors which determine the phase behaviour of the system, in addition to the temperature and hydration state. At *q* ratios lower than 2.3 the bicelles are fast tumbling and isotropic[238] and as such have been used commonly in liquid-state NMR studies of membrane proteins. At *q* ratios greater than 2.3 bicelles are anisotropic and orient in the presence of a magnetic field.

However, even with a *q* ratio above 2.3 the correct temperature regime is needed to produce the bicellar phase which is amenable to alignment. A number of temperature induced phase transitions occur, which are independent of an external magnetic field. At low temperatures, below the T_m, the lipids and surfactants form mixed micelle type structures. Above the T_m, the surfactant and lipid begin to partition into a bicellar phase, with the lipids forming a bilayer which is capped at the edges by the surfactant. This is illustrated in Figure 3.2 according to the classical discoidal model[239], although it should be noted that the precise morphology is somewhat controversial[240]. There is a further phase transition at higher temperatures, the critical temperature T_v, upon which the formation of perforated vesicles has been proposed[241], leading to a relatively narrow window (T_m to T_v) in which alignment can be attained.

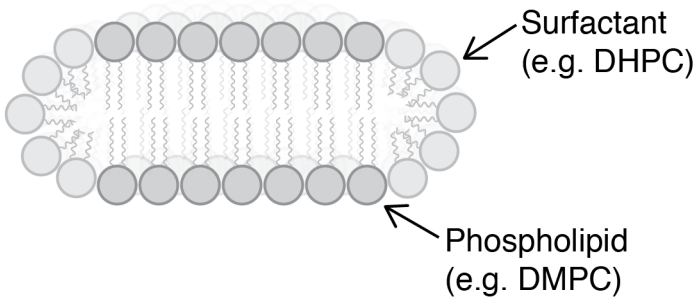

Figure 3.2: ***Classical model of DMPC/DHPC (q > 2.3) bicelle composed of DMPC/DHPC.***

The orientation of bicelles in magnetic fields occurs due to the magnetic anisotropy susceptibility ($\Delta\chi$) of the lipid acyl chains, meaning the molecular magnetic moment has an orientational preference. For an individual molecule, the degree of orientation (β) in a magnetic field is given by[234]:

$$\beta = \Delta\chi B_0^2/kT \qquad (3.1)$$

where B_0 is the magnetic field vector, k is Boltzmann constant and T is the absolute temperature. In a liquid crystalline lipid phase where the acyl chains are aligned parallel, the degree of orientation is summative over the number of lipids N:

$$\beta = N\Delta\chi B_0^2/kT \qquad (3.2)$$

In the case of bicellar phases, N is sufficiently large that the orientation energy can overcome the thermal energy, kT, resulting in orientation of the bicelles in the field. It is also the clear that the degree of orientation is dependent on the magnetic field strength. Although bicelles demonstrably align in magnetic fields below 1.0 T[242, 243] these smaller fields provide a weaker driving force for alignment, especially compared to the larger fields used for NMR studies (typically > 7.0 T). This has been confirmed experimentally for bicellar mixtures (albeit with an alternative lipid composition) using birefringence measurements, where the order parameter gradually increases to a maximum at around 20 T[239].

As $\Delta\chi$ is usually negative for lipids, bicelles composed of DMPC and DHPC align with their normal perpendicular to the magnetic field, resulting in a cylindrical distribution around the field director (Figure 3.3A). In order to modulate the alignment of bicelles, molecules with large $\Delta\chi$ can be added to the samples which interact with the bicelle surface. This has been achieved by the addition of trivalent lanthanide ions which bind to

the phosphate headgroup[244]. Whilst some trivalent lanthanides have $\Delta\chi < 0$ (e.g. Ce^{3+}, Pr^{3+}, Nd^{3+}, Sm^{3+}, Tb^{3+}, Dy^{3+}, Ho^{3+}), some have $\Delta\chi > 0$ (e.g. Eu^{3+}, Er^{3+}, Tm^{3+} and Yb^{3+}) of a sufficient strength to 'flip' bicelles such that the bilayer normal is oriented parallel to the magnetic field (Figure 3.3). Calculated and experimentally determined values for $\Delta\chi$ of a number of lanthanides, measured in metallomesogenic phases, are given in Table 3.1. Discrepancies between calculated and experimental values are explained by incomplete alignment of the lanthanides in the measurements, with maximal $\Delta\chi$ only achieved in fully oriented samples, but the trends between calculated and experimental are consistent.

Table 3.1: ***Calculated and experimental magnetic anisotropy values for various lanthanides in [Ln(LH)$_3$(NO)$_3$] (from Mironov et al[245]) or [Ln(LH)$_3$(DOS)$_3$] (from Binnemans[246]) mesophase****. '–' represents data unavailable.*

Lanthanide	$\Delta\chi$ (10^{-6} cm^3 mol^{-1})		
	[Ln(LH)$_3$(NO)$_3$]		[Ln(LH)$_3$(DOS)$_3$]
	Calculated	Experimental	Experimental
Dy	-20731	-7794	-11820
Tb	-15284	-5550	-3540
Ho	-9098	-4759	-4980
Pr	-2243	-930	-
Ce	-1066	-	-
Nd	-964	-810	-
Sm	-319	-	-
Eu	+1018	-	-
Yb	+5435	-	+615
Er	+7657	1610	+952
Tm	+12103	-	+2535

For the lanthanide with the greatest positive $\Delta\chi$, thulium, a ratio as low as 155:1 DMPC:thulium is sufficient to 'flip' bicelles with certain lipid compositions in a 0.6 T magnetic field[244]. The ability to flip bicelles is particularly advantageous for NMR studies as it results in resonances being distributed across a range of chemical shifts twice as broad than those oriented perpendicular to the field and does not give rise to a cylindrical distribution of helices, therefore improving spectral resolution[247].

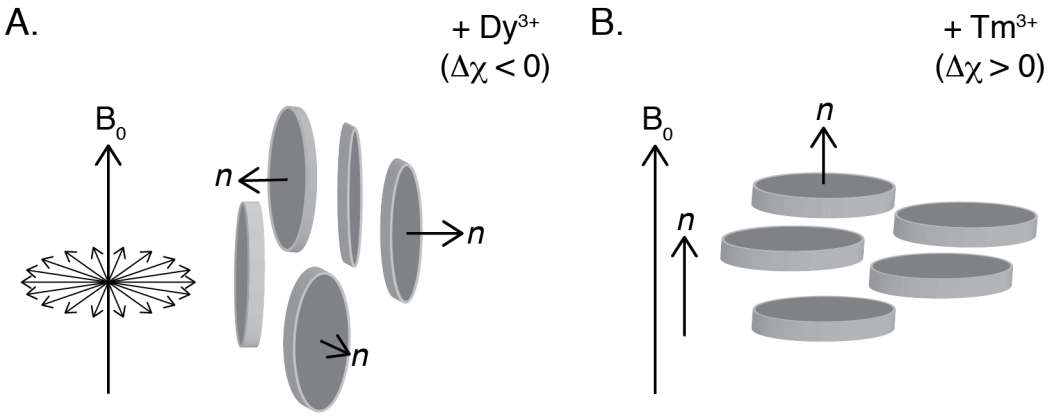

Figure 3.3: ***Orientation of bicelles in magnetic field with lanthanides dysprosium (A) and thulium (B).*** *On addition of dysprosium, with negative diamagnetic anisotropy susceptibility, the bilayer normal (*n*) is oriented perpendicular to the field whilst thulium induces parallel alignment of the field and bilayer normal due to its positive Δχ. Figure redrawn from Prosser et al.*[248].

Whilst lanthanides with positive Δχ provide advantages in terms of resolution, they can also provide challenges for NMR studies which much be addressed. The electronic distribution which gives rise to their magnetic anisotropy also means they act as paramagnetic shift reagents and can thus perturb resonances. The unpaired electrons enhance both T_1 and T_2 relaxation, which can result in broadened spectral lines. Lanthanides are able to exert their paramagnetic effects on nuclear spins as distant as 40 Å[249]. Further, they can interact with negatively charged amino acids with a similar affinity to phosphate groups[250, 251], potentially affecting the protein structure.

One strategy to avoid these deleterious effects is the use of lipids which have headgroups modified with a metal ion chelating group, allowing the lanthanide to be physically bound to the bicelle structure but preventing it from interacting with the protein and the main lipid constituents directly. The lipid headgroups themselves have much lower affinity for the lanthanide than the chelator, so without the chelator there is free lanthanide in solution which is in fast exchange with the lipid headgroups. When the chelator is used the absolute concentration of lanthanide can be reduced since it held with high affinity close to the bicelles surface. This approach has been successfully implemented using the lipid 1,2-dimyristoyl-sn-glycero-3-phosphoethanolamine-N-diethylenetriaminepentaacetic acid (DMPE-DTPA; Figure 3.1C)[252]. DTPA is a strong chelating agent which has been used extensively in magnetic resonance imaging studies with lanthanides. Alternative methods to flip bicelles include cholesterol-DTPA to ‘anchor’ the lanthanide close to the

membranes similarly to DMPE-DTPA[253], formation of bicelles with long chain phospholipids containing biphenyl rings, which have positive $\Delta\chi$ [247, 254] and reconstituting high concentrations of peptides into the membranes[255].

3.1.2. ^{31}P NMR as a tool to probe phase behaviour

The orientation and to some degree the morphology of bicellar lipid mixtures can be readily probed using ^{31}P NMR, analogously to the mechanically oriented samples in Chapter 2. The chemical shift of the DMPC bilayer component, ν, can be expressed as[256]:

$$\nu\,[\text{ppm}] = \delta_{iso} + \delta \left(\frac{3\cos^2\theta - 1}{2} \right) S_{bicelle} \qquad (3.3)$$

where δ_{iso} is the isotropic chemical shift of DMPC, δ is the DMPC CSA (δ_{zz} - δ_{iso}) and $S_{bicelle}$ the bicelle order parameter, a scalar from 0 to 1, given as[257]:

$$S_{bicelle} = \left\langle \frac{3\cos^2\theta - 1}{2} \right\rangle \qquad (3.4)$$

which indicates the relative distribution of bicelle orientations around their director over a time average. Experimentally this can be calculated relative to unoriented multilamellar vesicles (MLV) according to[258]:

$$S_{bicelle} = \frac{\delta_{obs} - \delta_{iso}}{\delta_{\perp} - \delta_{iso}} \qquad (3.5)$$

where δ_{obs} is the position of the DMPC peak and $\delta_{\perp}$ is the 90° edge of the MLV powder pattern. When the membrane normal is aligned perpendicular to the magnetic field (Figure 3.4A) there is a dominant peak centred around -14 ppm from the DMPC in oriented bilayers, and a smaller peak around -4 ppm from the highly curved monolayer of DHPC which caps the edges of the DMPC bilayer (Figure 3.4). On addition of lanthanide to align the bicelles parallel to the field, the DMPC resonance is centred somewhere close to the 0° edge of the DMPC powder pattern, around 28 ppm, and the DHPC resonance at 10 ppm. ^{31}P NMR is thus a useful tool to understand the effect of variables such as temperature, *q* ratio and the addition of protein of the alignment of bicelles.

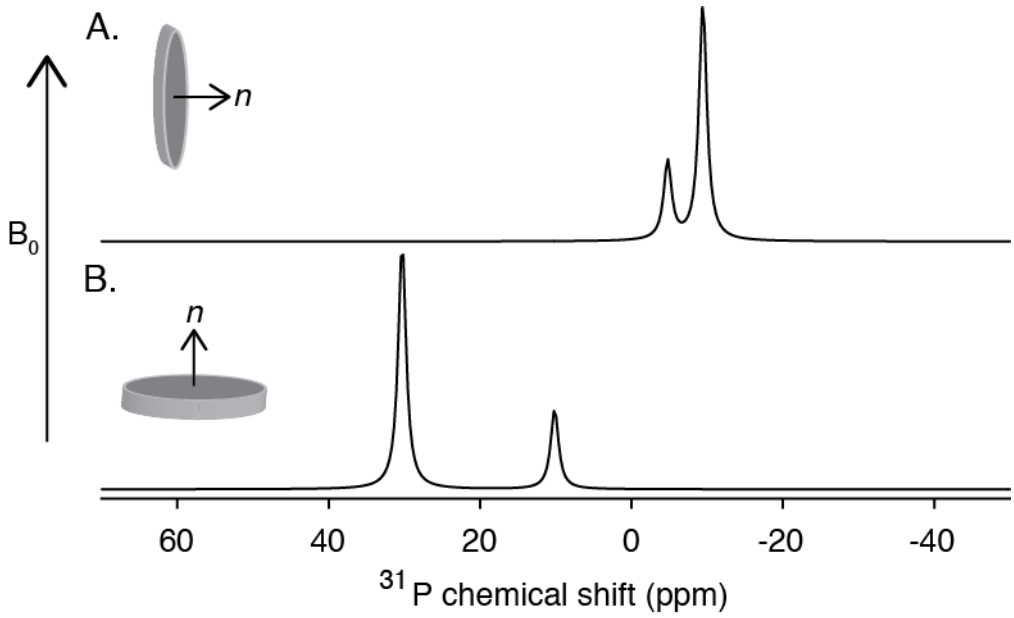

Figure 3.4. ***Simulated ^{31}P NMR spectra of bicelles oriented with the bilayer normal perpendicular (A) or parallel (B) to the magnetic field.*** *Inset shows schematic representation of aligned bicelle with membrane normal director* n*. Note that the line widths are illustrative and not representative of experimental spectra.*

3.1.3. Magnetic circular dichroism

In this chapter we will outline a novel approach to orient membrane proteins for OCD studies using magnetically aligned phases. To achieve this alignment, a magnetic CD (MCD) instrument with a removable 1.4 T static magnet is used. Conventionally, MCD spectroscopy has been used as a technique sensitive to the electronic structure of magnetically active chromophores, usually aromatic amino acids and haem groups in biological systems, which can give site specific resolution. Tryptophan in particular has been probed using MCD, with applications including the quantification of the number of tryptophans in a protein[259] and the characterisation of interactions, for example the hydrogen bonding between W37 and the heam group in human haemoglobin, essential for stabilisation of the relaxed and tense states of the protein[260].

MCD relies on the induction of optical activity due to the presence of a magnetic field (the Faraday effect). The occurrence of MCD signals can be attributed to three effects of the magnetic field on the electronic transitions – types A, B and C[261]. Type A effects arise as a result of the Zeeman interaction, where there is a loss of degeneracy in excited states, resulting in the presence of two optically active transitions. Type B effects occur due to mixing of perpendicular transitions which results in a non-linear displacement of charge in the transition and therefore optical activity. The type C effects occur due a fluorescence

effect known as magnetic circularly polarised emission (MCE). (Sutherland and Holmquist[262] give an eloquent description of these MCD effects.) The MCD signal is dependent on the orientations of the magnetic field, such that spectra acquired with the field N-S with respect to the beam should be of equal intensity but opposite sign to spectra acquired with the field S-N. Conventionally therefore MCD spectra are presented as the difference of the spectra acquired with each field orientation. Unlike typical MCD experiments, in the bicelle measurements here the magnetic field is used purely to align the lipidic phase, and as the measurements are in the far-UV region (< 260 nm) there should be no MCD contributions to the spectra. (Transitions measured in MCD spectra are usually the near-UV to near-infrared region (~ 260 – 800 nm).)

There are a number of experimental parameters that should be taken into account. The magnetic field in MCD instruments is aligned such that the field lines run collinear with the direction of light beam propagation. In bicelles with negative diamagnetic anisotropy this would align bicelles with their normal perpendicular to the light beam, resulting in a cylindrical distribution of the bicelle around the beam director. With positive diamagnetic anisotropy they become oriented such that the bilayer normal is aligned parallel to the beam director with uniaxial distribution, which is desirable to simplify interpretation of the spectra. Fortunately this is relatively easy to achieve through the use of lanthanides with a strong positive diamagnetic anisotropy. A further consideration is that experiments must be performed in a way which ensures there are no MCD contributions to the CD spectra, although it was not expected that any MCD signals should be present in the far-UV region. This can be readily confirmed by acquiring spectra with the magnetic field parallel to the light beam in both N-S and S-N configurations. Any MCD signals will switch sign but have equal magnitude, so these contributions can be eliminated by summing the two spectra.

3.1.4. Continuous wave electron paramagnetic resonance (EPR) spectroscopy

The 1.4 T magnetic field of the MCD instrument is much smaller than the fields used in NMR to induce bicelle alignment, making it necessary to establish conditions for alignment of bicelles in a lower field. In order to determine whether bicelles can be successfully aligned in such a low field X-band EPR can be used, which operates at a maximum instrumental field of 0.6 T. This is a useful approach as it means that the bicelles can be exposed to the magnetic field and then the resultant change in orientation measured directly.

EPR is a spectroscopic technique which is analogous to NMR and measures the spin of unpaired electrons. A free electron has spin-1/2 which means it has a magnetic moment (μ_e) with two allowed orientations. As with nuclei, the Zeeman effect means that in the presence of a magnetic field there are two populations of electrons with spin states either $m_s = -½$ or $m_s = ½$, corresponding to lower and higher energy levels. In contrast to NMR, where the magnetic field is constant, in continuous wave EPR, the magnetic field is modulated whilst continuous microwave irradiation is applied. When the energy separation between the two states is equal to the microwave frequency there is an absorption of energy and transition between spin states. The most common type of EPR spectrometers operate at X band frequencies (~9.8 GHz), with a B_0 field of ~0.35 T for nitroxide spin labels, which have been used extensively in studies of lipid bilayers.

Neglecting the Zeeman interaction the spin Hamiltonian, *H*, for a free electron in the principle axis system is given as[263]:

$$H = \beta_e B_0 \cdot g \cdot \boldsymbol{S} + \boldsymbol{I} \cdot A \cdot \boldsymbol{S} \qquad (3.6)$$

where *g* and *A* are tensors for g-factor and hyperfine coupling respectively, B_0 is the external magnetic field vector, β_e is the Bohr magneton, $\boldsymbol{S}$ is the electron spin operator and $\boldsymbol{I}$ is the nuclear spin operator. Both *g* and *A* are anisotropic parameters expressed as a 3x3 interaction matrix which perturb the Zeeman interaction. The *g*-factor describes the electron's local magnetic field and gives the resonance position at the centre of the spectrum, and is related to the electron spin precession frequency ω[261]:

$$\omega = 2\pi\upsilon = \gamma_e B_0 \qquad (3.7)$$

where γ_e is the electronic gyromagnetic ratio, equal to $g\,\beta_e/\hbar$. For the nitroxide radical usually studied in biological EPR, the *g* value is typically around 2.0. The hyperfine interaction *A* arises from dipolar interactions between the magnetic moments of the spin-1 ^{14}N nucleus and the electron. These interactions determine the number of lines in the spectra according to 2MI+1 where M is the number of equivalent nuclei.

Both *g* and *A* interactions are anisotropic and can be expressed according to their principle values[263]:

$$g = (l_x^2 g_x^2 + l_y^2 g_y^2 + l_z^2 g_z^2)^{\frac{1}{2}} \qquad (3.8)$$

$$A = (l_x^2 A_x^2 + l_y^2 A_y^2 + l_z^2 A_z^2)^{\frac{1}{2}} \qquad (3.9)$$

where l_x, l_y and l_z are the direction cosines between the magnetic field vector B_0 and the molecular axes, given as[263]:

$$\begin{aligned} l_x &= (\cos\gamma\cos\beta\cos\alpha - \sin\gamma\sin\alpha)\sin\theta + \sin\beta\cos\alpha\cos\theta, \\ l_y &= (\cos\gamma\cos\beta\sin\alpha + \sin\gamma\cos\alpha)\sin\theta + \sin\beta\sin\alpha\cos\theta, \\ l_z &= -\cos\gamma\sin\beta\sin\theta + \cos\beta\cos\theta. \end{aligned} \qquad (3.10)$$

where α, β and γ are the Euler angles for transformation of the molecular axis into the laboratory frame (B_0) and θ is the angle between the B_0 field and the molecular axis. The principle axes of g and A are aligned. As these g and A tensors are anisotropic they are particularly valuable when studying macroscopic orientation of samples.

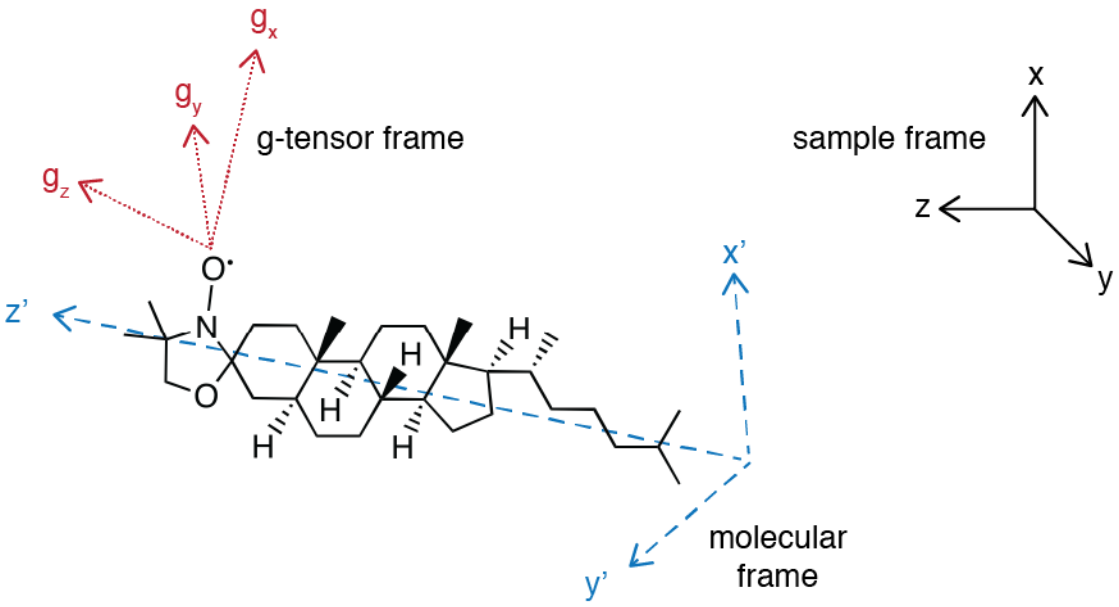

Figure 3.5: ***Reference frames of CSL.*** *Adapted from Hemminga*[263] *and Yankovo*[264].

In EPR studies of biomembranes, spin labelled lipids and other membrane components have been used to probe interactions, as the spectra are highly sensitive to molecular mobility, and the study of membrane orientation. The cholesterol analogue cholestane spin label (CSL; Figure 3.5) has been used as a reporter of orientation in an analogous manner to ^{31}P in solid-state NMR[263]. The free electron is approximately coincident with the π orbital of the N-O bond and not delocalised the cyclic structure. Of the three components of the nitroxide g-tensor (g_z, g_x and g_y), the g_x and g_y components are fully averaged in fluid phase bilayers as there is sufficiently fast motion of the spin label about its long (z)

axis[263], leaving the g_z component which conveniently is nearly parallel to the CSL molecular z axis (Figure 3.5), where the x axis is taken as parallel to the N-O bond.

EPR spectra of CSL are characterised by three lines (Figure 3.6) due to the hyperfine coupling between the ^{14}N nucleus and electron, with the number of lines is given as 2MI+1 in accordance with the selection rules. The splitting of the two outer lines, *a'*, indicates the magnitude of the hyperfine coupling, which is maximal when the long axis of the CSL is oriented parallel with the field and minimal when aligned perpendicular. The change in *a'* ($\Delta a'$) between parallel and perpendicular orientations in cholesterol-free bilayers is typically between 8-20 G[263]. This orientational dependence is clearly demonstrated by the simulated spectra of mechanically oriented samples in Figure 3.6 and as such is relatively straightforward to interpret the alignment of bicelles with respect to the magnetic field.

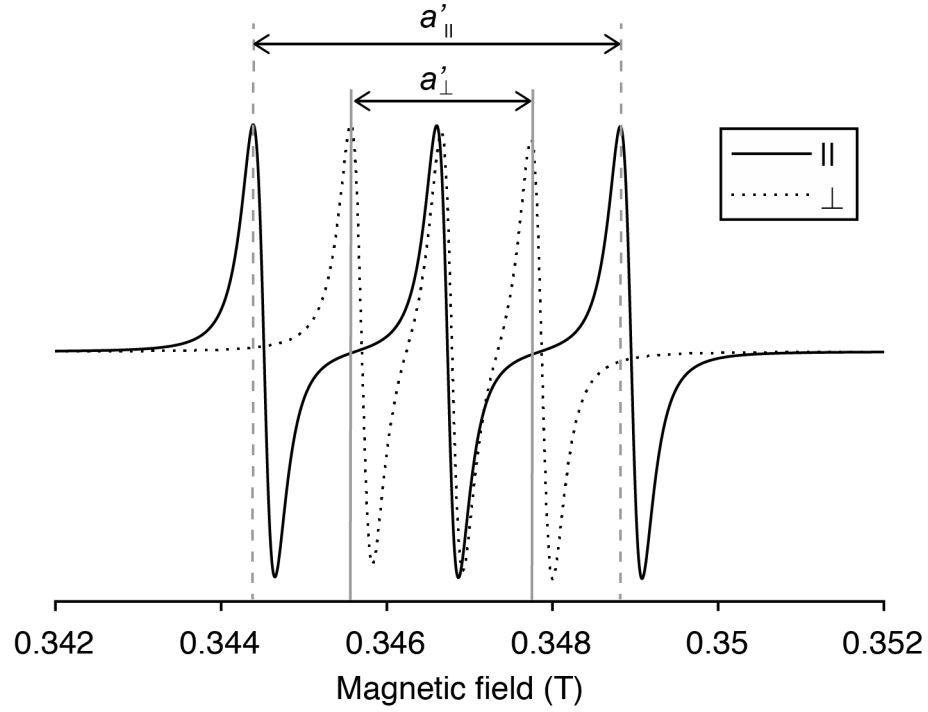

Figure 3.6: ***Simulated EPR spectra of CSL in mechanically oriented rigid lipid bilayers with the bilayer normal parallel (solid line) and perpendicular (dotted line) to the B_0 field.*** *When the bilayer normal is oriented parallel to the field the spectral splitting is at a maximum ($a'_{||}$), and when perpendicular at a minimum ($a'_{\perp}$). Spectra were simulated in Spinach[265].*

3.2. Methods and materials

3.2.1. Materials

For details of materials refer to section 2.2.1. CSL was purchased from Sigma-Aldrich (Gillingham, UK) and was dissolved in chloroform and stored at -20 °C. Lanthanides as chloride hexahydrate salts were purchased from Alfa Aesar (UK) (thulium and dysprosium) or Sigma-Aldrich (ytterbrium) at 99.9 % purity.

3.2.2. Methods

3.2.2.1. Preparation of bicelles

Stocks of lipids and fukutin TMD were prepared in methanol. Appropriate aliquots of lipids and fukutin TMD were mixed in glass vials and dried under a stream of nitrogen gas before being dried under high vacuum for at least four hours to remove any residual solvent. ddH_2O was added to the film to achieve the desired hydration, then subject six cycles of freezing in liquid nitrogen, thawing at 35 °C and vortexing for 30 seconds to ensure full hydration. Generally, samples were prepared and used within 24 hours, otherwise were stored at -20 °C until needed. Samples for CD were degassed to prevent cavitation during measurement in a 600 mmHg vacuum at 5 °C for 30 minutes.

After observations that bicelles with lanthanide added failed to align after storage at -20 °C for ~2 weeks, samples were prepared at first without lanthanide and then lanthanide was added, followed by additional rounds of freeze/thawing, immediately prior to measurement. Above the T_m samples are extremely viscous so to enable transfer to cuvettes or rotors they were cooled on ice and pipetted using chilled tips.

3.2.2.2. SRCD (MCD) measurements

SRCD measurements were recorded at B23, Diamond Light Source, UK, with access provided through beamtime allocations including SM12844, SM14084 and SM16501. Measurements were recorded using the module B equipped with a highly modified DSM 20 spectropolarimeter (Olis Inc, Georgia, USA)[190] with a removable 1.4 T permanent magnet. The field lines of the magnet run collinear to the direction of light propagation. All measurements were recorded without magnetic field and with the field oriented both S-N (‘forward’) and N-S (‘reverse’) with respect to the light beam director. Far-UV measurements from 260 – 185 nm were carried out using slit width of 1 nm, 1 nm step increment and 1 s integration time unless otherwise stated. A 0.1 mm demountable fused

silica cuvette (Hellma, Essex, UK) was used throughout. As in section 2.2.2.6, calibration was confirmed using the camphor sulphonic acid method.

To enable temperature control of samples in the magnetic sample holder, a stream of nitrogen gas was directed onto the face of the sample cuvette. The temperature of the nitrogen gas was regulated using a variable temperature controller (FTS Systems and Kinetics Air-Jet) and the temperature of the sample measured using a fine tipped thermocouple (RS Components, UK) attached to the reverse of the cuvette.

SRCD data was processed with CDApps[192] and MATLAB (MathWorks, Inc.) using custom written scripts. To yield the MCD or CD signal from the data acquired with the magnet in both forward and reverse orientations, spectra were calculated according to:

$$\begin{aligned} MCD &= (CD_{N\text{-}S} - CD_{S\text{-}N}) / 2 \\ CD &= (CD_{N\text{-}S} + CD_{S\text{-}N}) / 2 \end{aligned} \qquad (3.11)$$

To yield the OCD spectra and eliminate any MCD contributions, the spectra for forward and reverse magnet positions are summed and divided by two. Data was converted from machine units (millidegrees, θ) to $\Delta\varepsilon$ as described in Chapter 2, where appropriate. Pure lipid spectra, for example, or protein spectra with large artefactual content are left as millidegrees (mdeg).

3.2.2.3. Benchtop CD measurements

Conventional CD spectra were acquired on a nitrogen-flushed Chirascan Plus spectropolarimeter (Applied Photophysics, Leatherhead, UK). Far-UV spectra were obtained from 260 - 185 nm. A bandwidth of 1 nm, increment of 1 nm and integration time of 1 s were used throughout. As standard a minimum of four spectra were recorded and averaged for each sample and appropriate baseline subtracted (details given in figure legends). The instrument was equipped with a Peltier cell holder (Quantum Northwest, Washington, USA) allowing regulation of sample temperature. For temperature ramp experiments on bicelles the start and end temperatures were 5 and 40 °C, with measurements at 5 °C intervals. The temperature was raised using a stepped ramp with a minimum 10 minute incubation at each point once the temperature had stabilised. All measurements were recorded using 0.1 mm pathlength fused silica fused silica demountable cell (Hellma, Essex, UK) unless otherwise indicated.

3.2.2.4. EPR spectroscopy

Bicelles for EPR studies were doped with 0.5 mol % CSL (with respect to DMPC) as a reporter for orientation which was added to the lipids in solvent before drying. At this low concentration it is unlikely that the CSL has any influence on the bicelle morphology or phase, and in the literature similar concentrations of cholesterol and CSL do not impact the phase transition of PC lipids[266]. 20 μL samples were drawn into 1 mm diameter fused silica capillary tube and heat sealed.

EPR experiments were conducted using an EMXmicro X-band continuous wave spectrometer (Bruker) with temperature control of the sample cavity using a flow of heated nitrogen gas. The microwave frequency was set to 9.85 GHz. The temperature was monitored using a thermocouple placed inside the capillary tube before measurement. To align the bicelles, the magnetic field was set at 0.58 T whilst the temperature was raised gradually from 25 to 45 °C over 15 minutes, and then incubated for an additional 20 minutes with the 0.58 T field. Presented spectra are the average of five scans recorded from 0.34 – 0.36 G with a 30 s scan length.

3.2.2.5. Solid-state NMR measurements

All measurements were acquired using an Agilent DD2 600 MHz spectrometer equipped with a 3.2 mm magic angle spinning probe. For ^{31}P spectra samples were measured without spinning using a Hahn echo pulse sequence[156] at a frequency of 263 MHz with high power proton decoupling, typically with a 90° pulse lengths of 4 μs, echo delay of 50 μs, acquisition time of 50 ms and 2.5 s recycle delay. For temperature ramp experiments there was a 5 minute delay between temperatures to allow the sample temperature to equilibrate. The temperature was checked intermittently using ethylene glycol according to the method outlined in[267]. Data was processed by shifting to the top of fid, zero filling to 8192 points and applying 100 Hz exponential line broadening before Fourier transform.

For ^{15}N measurements spectra were acquired using a variable-amplitude cross polarization (^{1}H to ^{15}N) echo pulse program[156] at a ^{15}N frequency of 60.8 MHz. Typical parameters for acquisition included 6 μs 90° pulse, 1 ms contact time, 20 μs dwell time, 50 μs echo delay, 1024 points and 2.5 s recycle delay. Proton decoupling (71 kHz) was applied throughout acquisition. The number of scans is given in figure legends. Spectra were referenced externally to ^{15}N glycine at 33 ppm[189]. Data was processed in matNMR[188], where the fid

was left-shifted to the top of the echo and exponential line broadening of 300 Hz applied prior to Fourier transformation.

3.3. Results and discussion

3.3.1. Refinement of bicelle composition using nuclear magnetic resonance and electron paramagnetic resonance

There are a small number of examples in the literature suggesting that anisotropic bicelles (i.e. $q \geq 2.3$) can used for CD measurements[211, 268]. These rely on dilute bicelle solutions which are unlikely to align in the low field of an MCD instrument (1.4 T). Although these could be used as a starting point, and indicate the applicability of bicelles to general CD studies, there is a need to fully characterise the phase behaviour, alignment and optical properties of bicellar mixtures such that OCD measurements can be performed successfully. These are outlined below.

3.3.1.1. Preliminary CD studies

A series of preliminary measurements were performed to ascertain the validity of the application of bicelles to CD studies. A temperature ramp experiment was performed using bicelles at 5 % w/v and reveals the expected α-helical structure of fukutin TMD, with a maximum around 195 nm and minima at 214 and 227 nm (Figure 3.7). There are changes in the spectral shape with the temperature, which is unsurprising considering the well characterised temperature dependent phase behaviour of bicellar mixtures. At 50 °C the sample is above the critical temperature T_v and often becomes translucent, which explains the distortion of the 50 °C spectra. As a preliminary experiment this demonstrates the applicability of bicelles for CD studies, although clearly the temperature and optical properties need be to be carefully monitored.

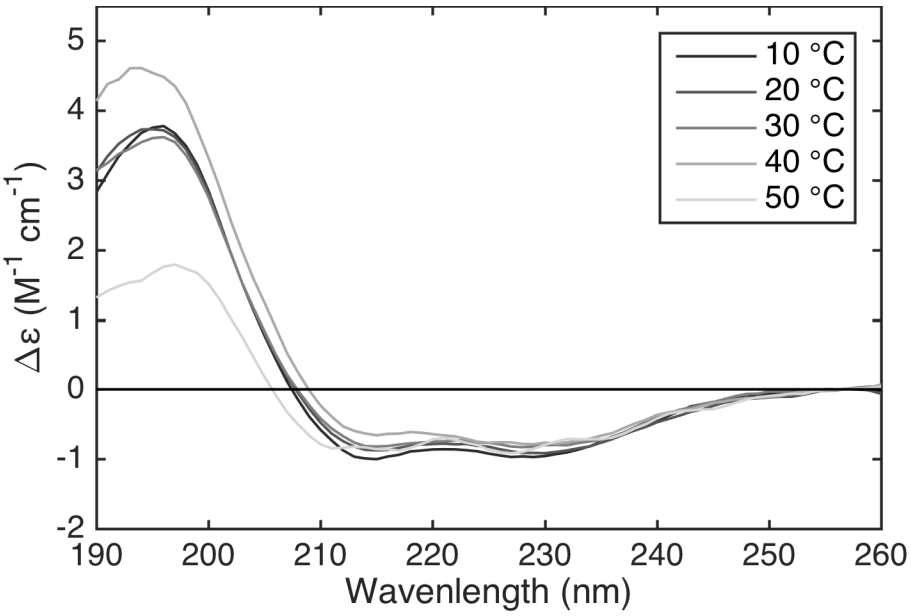

Figure 3.7: ***SRCD spectra of fukutin TMD in DMPC/DHPC (q 3, 5 % w/v) bicelles at 200:1 L/P.*** *Spectra were acquired with three scans per temperature point in 5 °C steps from 5 to 50 °C with a 5 minute incubation at each temperature. Sample was measured in a 0.2 mm fused silica cuvette with 1 s integration time and 1 mm slit width using the DSM20 instrument of B23 module B. Spectra were baseline corrected against pure lipid bicelles measured at 20 °C.*

As bicelles exhibit temperature dependent phases we wanted to quickly gauge the thermostability of fukutin TMD. To do this a thermal denaturation CD experiment was performed from 5 to 90 °C in DHPC micelles (Figure 3.8). The protein adopts the expected helical structure at all temperatures, indicated by the maxima at 192 nm and minima at 209 and 220 nm, but there is a significant loss in spectral intensity with increasing temperature, indicating a loss of structure. This thermal denaturation experiment, although not performed in bicelles, demonstrates the need to avoid any excessive sample heating where possible.

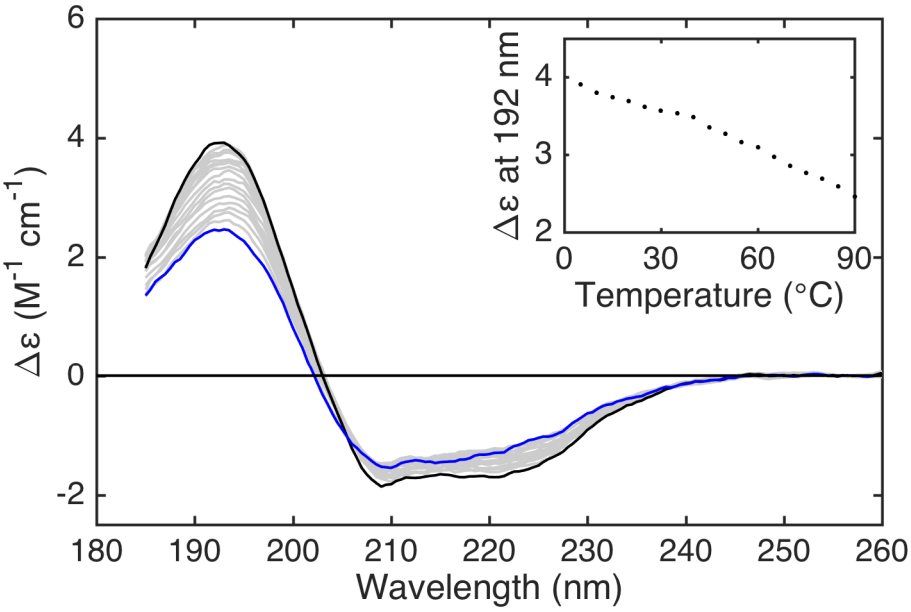

Figure 3.8: ***Conventional CD spectra of fukutin TMD in 20 mM DHPC micelles, 10 mM potassium phosphate pH 7.4 from 5 to 90 °C in 5 °C steps.*** *Spectra in black and blue are 5 and 90 °C measurements respectively. Inset: signal intensity at 192 nm as a function of temperature. One spectra was acquired at each temperature using a 0.2 mm pathlength fused silica cuvette, 1 nm bandwidth and 2 s integration time. Spectra were baseline corrected again 20 mM DHPC in 10 mM potassium phosphate pH 7.4. Data was smoothed using a Savitzky-Golay filter.*

3.3.1.2. Investigation of phase behaviour using ^{31}P NMR

To probe the temperature and its role in bicelle phase behaviour we employed ^{31}P NMR. Initially, the optimum *q* ratio was determined by acquiring spectra from 0 to 60 °C at 2 °C intervals. The *q* ratios investigated were 2.5, 3 and 3.5, which were selected since it has been reported that above *q* of 4 samples begin to become translucent[241] and much below 2.5 yields isotropic bicelles. The aim of these experiments was to determine which *q* ratio gave the highest degree of alignment, and the broadest temperature window of alignment to both avoid unnecessary sample heating and to give maximum flexibility during further measurements. The ^{31}P spectra for bicelles at these three *q* ratios at 30 % w/v are shown in Figure 3.9, and the DMPC resonance positions from were extracted and plotted as a function of temperature (Figure 3.10), determined as either the most upfield peak or peak with most intensity. In both figures the temperature dependence of the samples is clearly visible, with an initial isotropic phase characterised by a single resonance followed by the aligned bicellar phase dominated by two resonances for DMPC and DHPC respectively, and then the fluid bilayer/mixed micelle phase at higher temperatures. At all *q* ratios the isotropic chemical shift below the T_m is ~ –1 ppm, occurring due to a rapidly tumbling

micellar phase. When handling the samples at these temperatures they were found to be fully transparent and highly fluid. The full width at half maximum (FWHM) of the isotropic peaks subtly increases from 2.1 up to 2.3 and 2.4 ppm (at 0 °C) for *q* 2.5 to 3.5, reflecting the slower motions of the mixed micelles with additional DMPC.

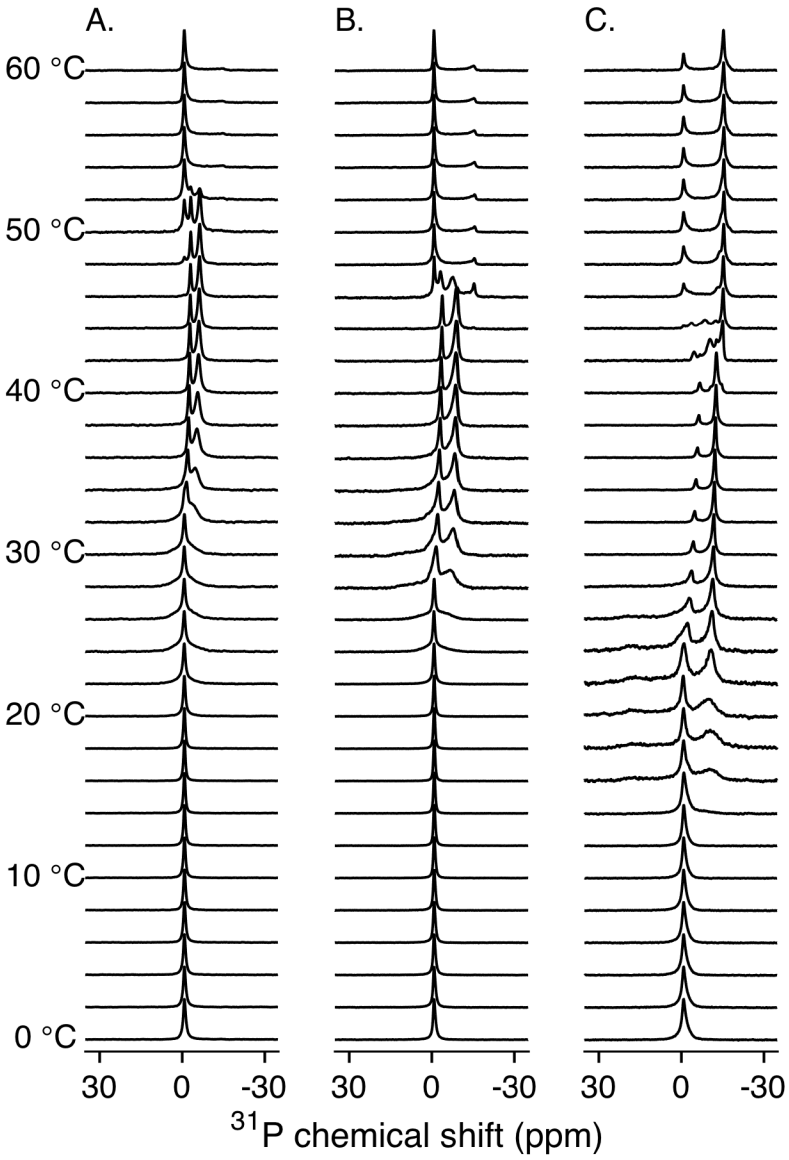

Figure 3.9: ***^{31}P NMR spectra of DMPC/DHPC bicelles at 30 % w/v at* q *ratios 2.5 (A.), 3.0 (B.) and 3.5 (C.) from 0 to 60 °C in 2 °C steps.*** *Samples were incubated for five minutes at each temperature before measurement.*

Above the T_m, at 32, 28 and 16 °C for q = 2.5, 3.0 and 3.5 respectively, there is a transition to the bicellar phase which rapidly orients perpendicularly to the magnetic field, indicated by the upfield resonances around -5.8, -8.8 and -12.7 ppm for *q* 2.5, 3 and 3.5. The position of the peak is indicative of the orientation and the degree of order in the bilayer, which is

characterised with respect to DMPC multilayers by the parameter $S_{bicelle}$ (equation 3.5). The slightly downfield peak of reduced intensity is assigned to the DHPC which forms the rim of the bicelles. The peak position varies slightly with *q* ratio and temperature from ~3 ppm to ~7 ppm, similar to findings in the literature[241]. There is a large difference in the temperature range of orientation and the position of the 90° edge between the three *q* ratios, with the *q* of 3.5 fully aligning at the lowest temperature, around 24 °C, and having the most upfield DMPC resonance, indicating the smallest distribution around the bilayer director. This is confirmed by $S_{bicelle}$ values at 36 °C of 0.31, 0.51 and 0.76 for *q* of 2.5, 3.0 and 3.5 respectively. These values were calculated with a DMPC 90° edge of -16.3 ppm, taken from the powder spectrum in Figure 3.11.

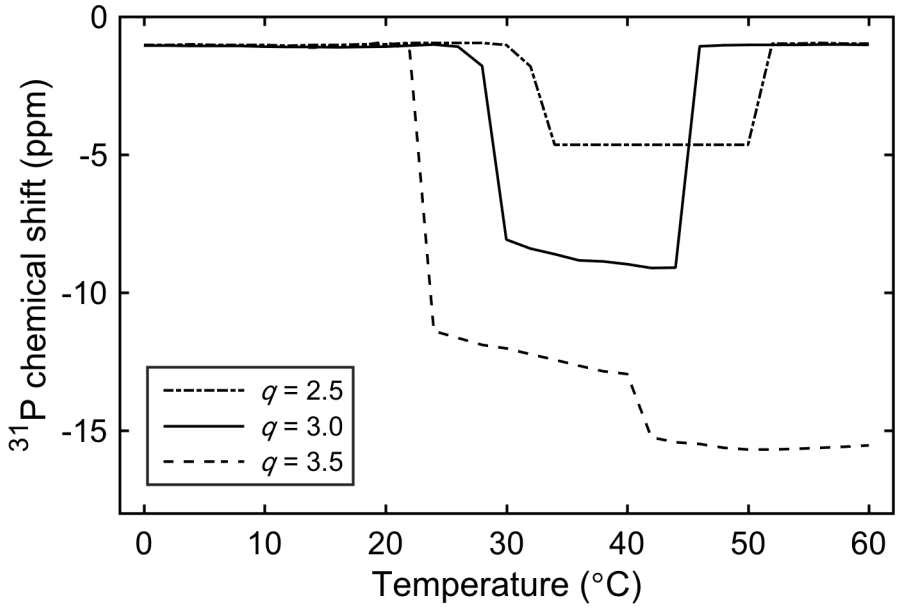

Figure 3.10: ***^{31}P chemical shifts of DMPC resonance for DMPC/DHPC bicelles at 30 % w/v with* q *ratios 2.5 (dash dot line), 3.0 (solid line) and 3.5 (dashed line) from 0 to 60 °C.***

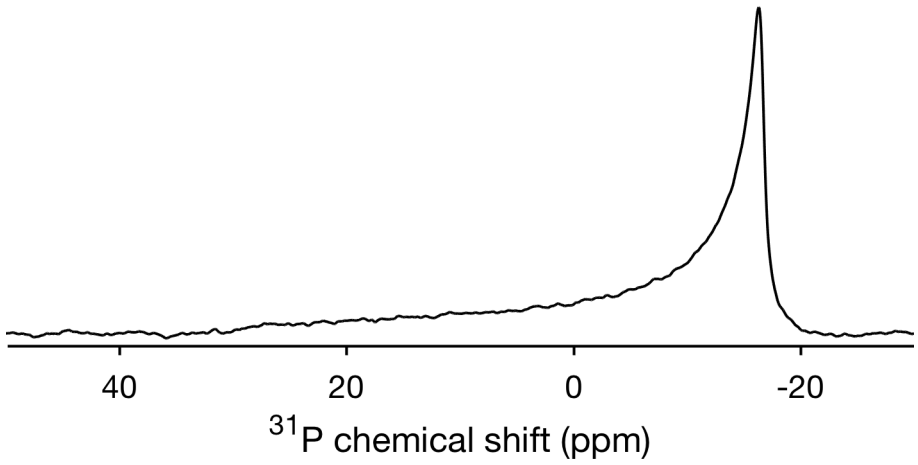

Figure 3.11: ***^{31}P NMR spectrum of DMPC multilamellar vesicles at 35 °C.*** *Vesicles were prepared at 30 % w/v in ddH_2O. 1024 scans were acquired and processed with 50 Hz exponential line broadening prior to Fourier transform.*

In the bicellar phase, samples become much more viscous for all of the *q* ratios tested here and they retain transparency. Above the critical temperature T_v, which been assigned to morphologies of mixed micelles and fluid DMPC bilayers with incorporated DHPC molecules[241], there is a re-emergence of the isotropic peak in addition to an upfield peak close to the DMPC 90° edge. The T_v for the *q* ratios 2.5, 3 and 3.5 are 48, 44 and 40 °C. At *q* 2.5 and 3.0 there is a clear predominace of isotropic peak, whereas at 3.5 the most intense peak at -15.3 ppm originates from a fluid bilayer phase, indicated by the $S_{bicelle}$ of 0.96.

From this point samples with $q = 3.5$ were utilised since they have the highest degree of order and alignment, are visually transparent in the bicellar phase, and importantly have the lowest T_m, which prevents unnecessary heating and potential thermal denaturation of proteins embedded in the bicelles. Having selected the *q* ratio of 3.5 we then aimed to optimise the weight percent of lipid. It is desirable for optical studies to reduce the quantity of lipid as much as possible since the lipid carbonyl groups absorb in the far-UV region, although it would also be optimal to ensure the L/P ratio is large to prevent flattening effects. Conversely, for NMR studies, which are relatively insensitive, it is desirable to maximise the protein content of the sample and therefore also maximise the lipid content. In solid-state NMR measurements 20-30 % w/v are the most commonly used weight percents, with ~50 % w/v the maximum which still aligns[258]. These percents have sufficient viscosity to allow and retain bicelle alignment, which is presumably stabilised by steric effects. Greater weight percents have high viscosity which reduces bicelle motion and prevents orientation[258], but when the weight percent is too low the viscosity is such

that the bicelles cannot stably align[255]. For these experiments samples of DMPC/DHPC with a *q* of 3.5 were prepared at 5, 10, 20 and 30 % w/v and measured using ^{31}P NMR over 0 to 60 °C (Figure 3.12).

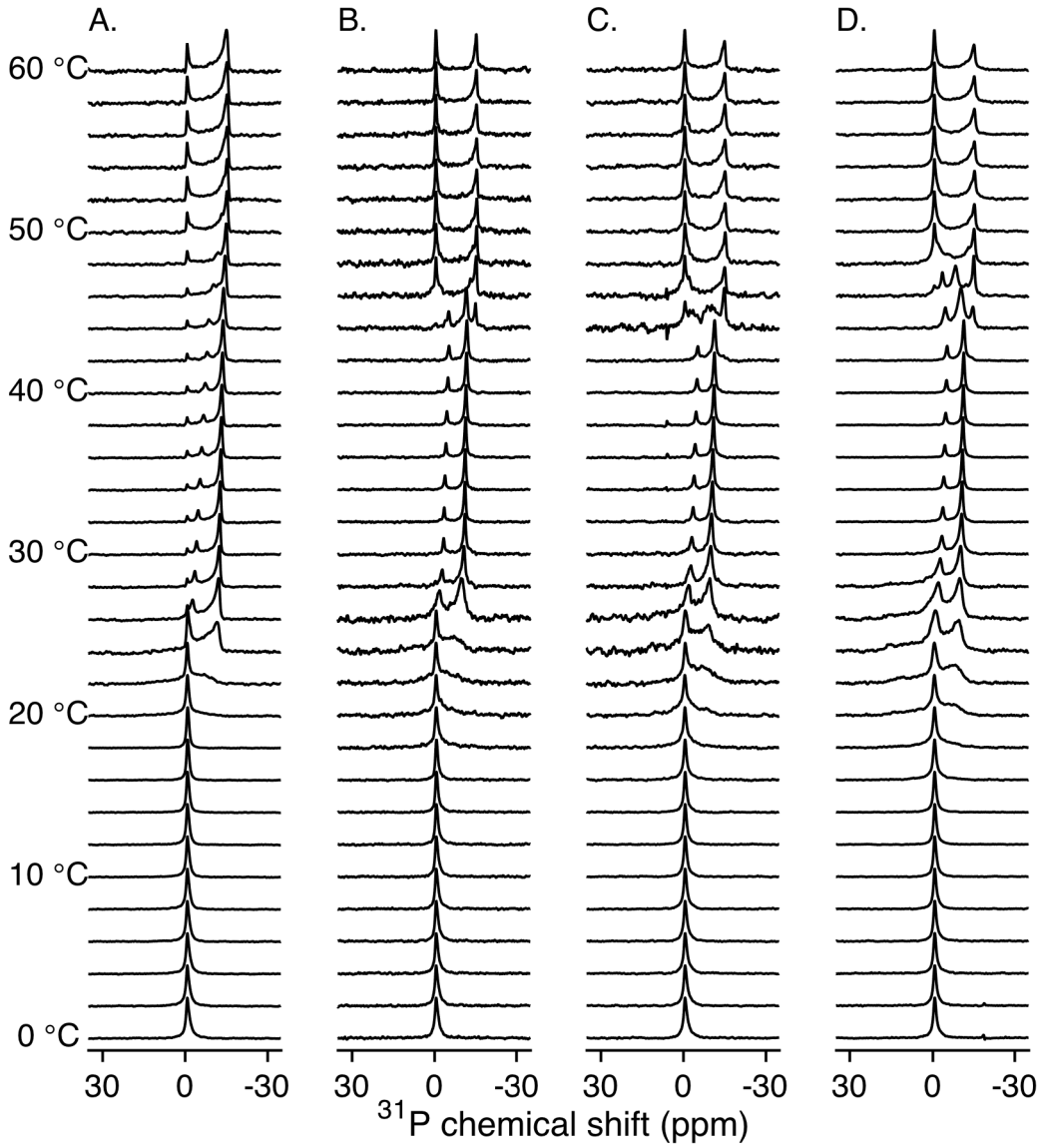

Figure 3.12: ***^{31}P NMR spectra of DMPC/DHPC bicelles at 5 (A.), 10 (B.), 20 (C.) and 30 (D.) % w/v from 0 to 60 °C in 2 °C steps.*** *Spectra were acquired with 128 (20 and 30 % w/v) or 512 (5 and 10 % w/v) scans at each temperature.*

It appears that at 5 % w/v there is an aligned component above ~26 °C, as well as free micellar component indicated by the isotropic peak at all temperatures. The DMPC peak in the 5 % w/v sample is approximately 2 ppm upfield of the equivalent peaks for 10, 20 and 30 % w/v (-13.2 ppm compared to ~ -11.4 ppm). It is likely that there is a combination of bicellar and lamellar phases contributing to the spectra here, indicated by the broadened DMPC peak relative to the higher weight percents (FWHM at 40 °C is 1.15 ppm for

5 % w/v and 0.9 ppm for 10 % w/v). It is possible that in this case that the peak occurs as a result of a combination of the 90° edge of a DMPC powder pattern and the downfield peak from the less ordered DMPC in bicellar phase. More dilute samples are known to be less amenable to alignment, with samples having *q* of 3 at less than 3 % w/v failing to align[269] and SANS studies indicate the presence of multilamellar vesicles rather than a bicelles at 5 % w/v[270]. At 10, 20 and 30 % w/v there is a good degree of alignment from 28 to 42 °C. The $S_{bicelle}$ parameter for 10, 20 and 30 % at 34 °C were 0.69, 0.68 and 0.68 respectively, indicating that although there is a greater degree of motion in the bicelles than multilamellar vesicles there is little difference in phase between the weight percentages. In contrast, the $S_{bicelle}$ of the 5 % w/v samples is 0.8, indicating a greater degree of rigidity, similarly to a lamellar phase sample.

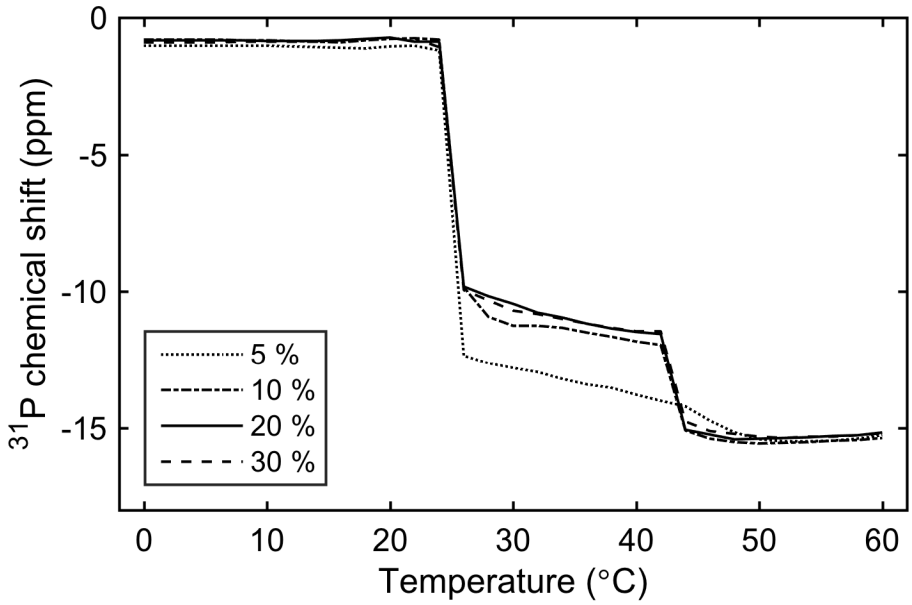

Figure 3.13: ***^{31}P chemical shifts of DMPC in DMPC/DHPC bicelles at 5 (dotted line), 10 (dash-dot line), 20 (solid line) and 30 (dashed line) % w/v as a factor of temperature.***

Despite the insignificant difference in degree of alignment between 10–30 % w/v, as we were using a lower magnetic field for the MCD studies (1.4 T), we opted to use 20 % w/v to ensure a good degree of alignment in the reduced field. With higher concentrations of lipid and *q* ratios the sample viscosity increases[271, 272], which aids alignment and retention of the aligned phase[255]. However, even at 20 % w/v the standard DMPC/DHPC bicelles fail to align at low fields[273]. It was therefore necessary to determine whether the lipid composition could be refined such that alignment is achievable at reduced field strength. Since it is not readily possible to measure the degree of alignment of lipid bilayers using CD, we opted to use EPR spectroscopy to measure bicelle alignment. X-band EPR

spectrometers operate with a maximum field of ~0.6 T and so it is likely that if bicelles can be aligned in these conditions, they could also be aligned in the MCD instrument.

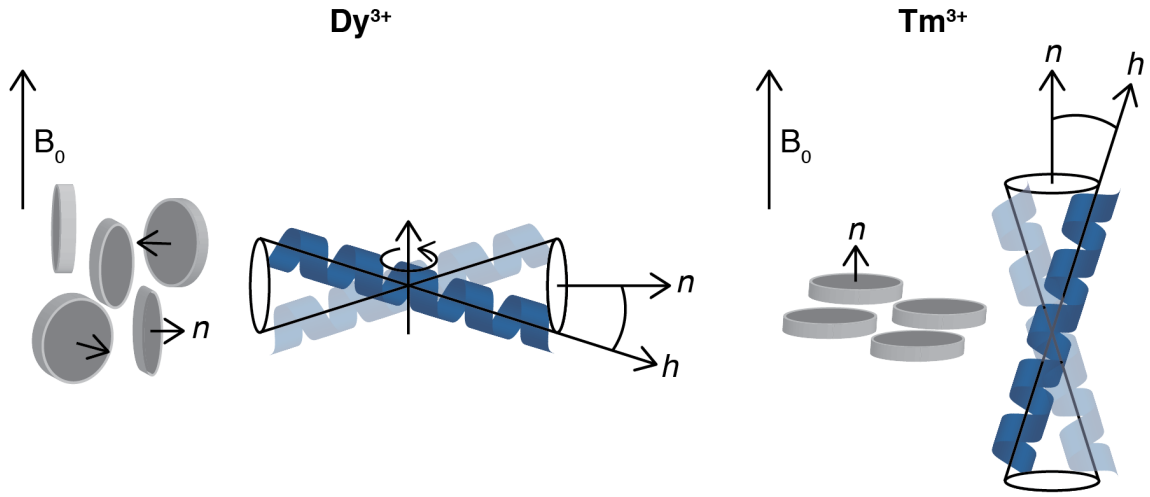

Figure 3.14: ***Representation of helix distribution in bicelles oriented either perpendicular (dysprosium) or parallel (thulium) for a protein inserted in the bicelle with long axis h.*** *In MCD experiments the director of light propagation is collinear with the field director.*

Lorigan and coworkers have extensively studied the alignment of bicelles using X-band EPR, and have developed lipid compositions and protocols for alignment of bicelles in the 0.6 T field[242, 273-277]. To achieve alignment at these low fields, it is necessary to gradually increase the sample temperature from the isotropic phase into the bicellar phase, and then to allow a further period of stabilisation[275, 277]. Additionally, a number of modifications to the basic DMPC/DHPC mixture are required: the introduction of lanthanide ions to alter the natural $\Delta\chi$ of the lipid bilayer and allow control of the direction of alignment; the addition of PEGylated lipids to improve stability; and cholesterol to promote ordering. However, this mixture requires the use of 10 mol % (with respect to DMPC) lanthanide chloride salt. This is problematic in the work here for reasons threefold; firstly the use of chloride salts at this concentration is prohibitive for CD measurements, even using SRCD, secondly one of the aims of this work was to allow direct comparison between CD and NMR, and lanthanides at such high concentrations are likely to have deleterious effects on the NMR spectra, and finally lanthanides can bind to proteins (especially acidic residues) and distort their structure[252]. We opted to try to mediate these challenges using an alternative lipid mixture, based on a method established by Prosser et al.[252] to 'flip' bicelles for NMR studies through the use of DMPE-DPTA to chelate the lanthanide and effectively anchor it to the membrane surface. It is added at 1:150 with DMPC, and a 1:1

ratio between the chelator and lanthanide, which is 15 times less than used by the Lorigan method and sequesters the lanthanide away from proteins and phosphate groups since it has a much greater affinity. The lanthanides selected were dysprosium and thulium. Dysprosium results in one degree of ordering such that the bilayers are aligned perpendicular to magnetic field, and are able to rotate to produce a cylindrical distribution. With thulium however, there is an additional degree of ordering, such that the normal is aligned parallel with the field, essentially creating the same configuration as in a mechanically oriented sample. Similar to NMR, for interpretation of OCD data, the bicelles aligned parallel with the field are preferable. A visual representation is given in Figure 3.14, where *n* is the bilayer normal and *h* is the helical long axis. In these studies both dysprosium and thulium have been used to provide a comparison between parallel and perpendicular alignment.

The alignment of DMPC/DHPC/DMPE-DTPA bicelles with lanthanides at low field was studied using EPR at 25 and 45 °C (Figure 3.15). In the measurements here the temperature was set to 25 °C then raised at approximately 1 °C/minute to 45 °C, followed by a 15 minute incubation at 45 °C, all while the spectrometer field was set at 0.58 T. It has been demonstrated that the initial temperature, 25 °C in this case, cannot be above the T_m to enable complete alignment[277]. The field was then reduced to allow acquisition of spectra.

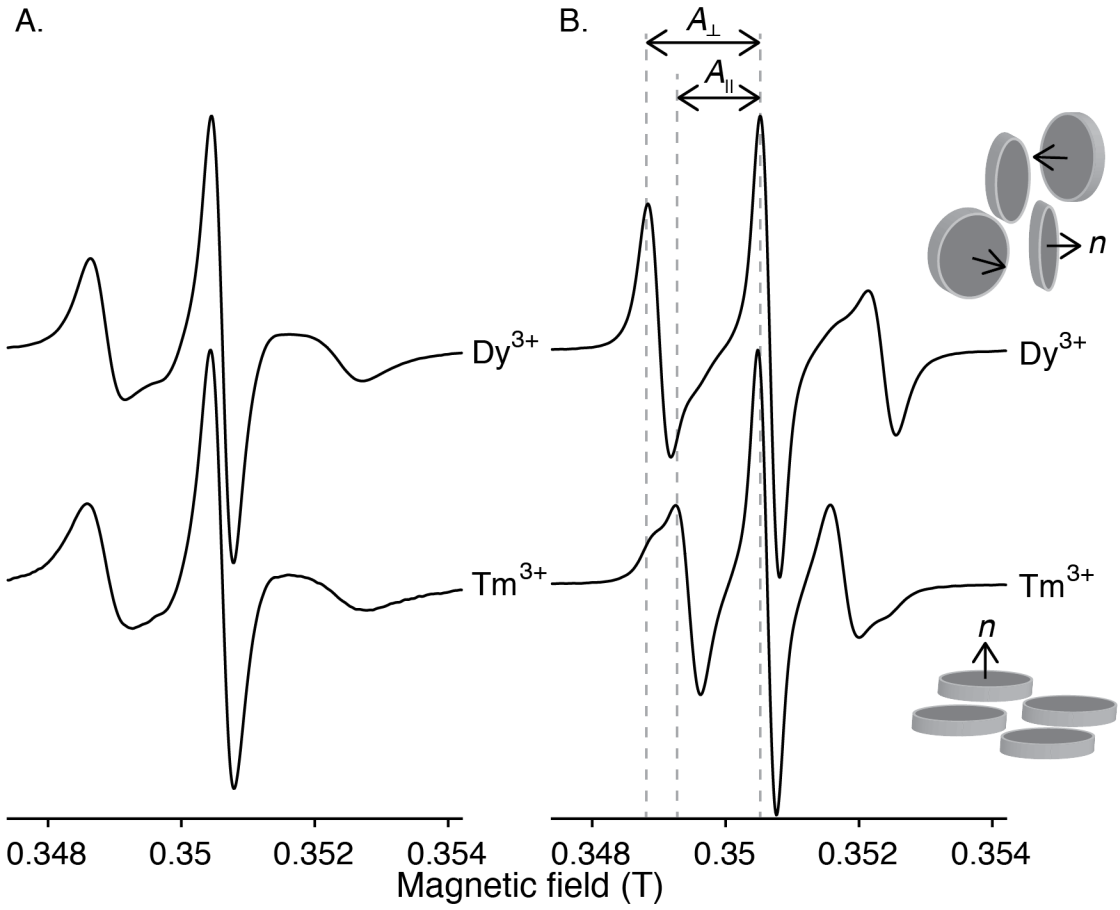

Figure 3.15: ***EPR spectra of CSL in DMPC/DHPC/DMPE-DTPA (3.5/1/0.023) bicelles at 20 % w/v with either dysprosium (top) or thulium (bottom).*** *Spectra were acquired at 25 °C (A) or 45 °C (B) following temperature equilibration (as described in main text). Dashed lines indicate splitting for CSL aligned parallel to the field and dotted the for perpendicular. Spectra were acquired with a centre field of 0.3505 T, sweep width of 0.01 T, sweep time 30 s and frequency of 9.85 GHz. Temperature was confirmed using a fine thermocouple inserted in the sample.*

The EPR spectra acquired at 25 °C show the typical CSL powder spectrum in which the A_{xx} and A_{yy} tensors are averaged due to rapid rotation about the CSL long axis[263], with no significant differences with the two lanthanides. For the spectra at 45 °C there is a clear difference, the splitting changing significantly, with the narrower thulium spectra indicating parallel alignment of the bicelles to the field and boarder spectra with dysprosium indicating perpendicular alignment. The hyperfine splitting (measured between m = +1 and m = 0 peaks) for dysprosium is 17 G whilst for thulium is 12 G. These are slightly different to those in the literature (17.5-19 G and 8-10 G for dysprosium and thulium respectively[273], where 19 G and 6 G are the rigid limit[278]), indicating slightly poorer alignment of the samples here with thulium. One consideration is that the values

quoted in the literature are for CSL in cholesterol-rich bilayers which is likely to alter the values slightly due to changes in the bilayer phase and therefore the spin label order. It is also clear from the thulium spectra that there is an underlying secondary component, a powder contribution, indicated by the shoulders at outer side of the +1 and -1 lines. Although there may be a small disordered component in the sample, since the degree of alignment is dependent on the square of the field strength it is foreseeable that there will be an increase in the orientation in the MCD field. There does not appear to be a powder signal in the dysprosium spectra, presumably since the dysprosium serves to enhance the natural $\Delta\chi$ rather than oppose it, and has a greater absolute $\Delta\chi$, although it is also worth noting that the powder spectrum has similar splittings and so powder contributions may be less obvious than in the thulium spectra. Whilst it was tempting to increase the concentration of thulium to enhance the degree of alignment, this was avoided due to concerns regarding the amount of chloride present in the samples for CD. (Alternative salts of thulium were obtained but were found to be mostly insoluble.) Although in the literature cholesterol has been used to improve the degree of alignment, we were reluctant to use it here since the relatively high concentrations (10 – 20 mol %) may add a further complication to the optical studies[279], although in future confirmatory studies may be useful to further refine the lipid composition. At this point, however, we were satisfied that we would be able to achieve sufficient alignment in the MCD field.

To further characterise the phase behaviour of the bicelles supplemented with DMPE-DTPA, lanthanides, and fukutin TMD we again used ^{31}P NMR (Figure 3.16). For comparisons with EPR, we used thulium and dysprosium, but due to concerns of line broadening effects from the lanthanides we also prepared samples with ytterbium which has a less positive $\Delta\chi$ than thulium but is a weaker relaxation agent[244]. Similar to other ^{31}P NMR temperature arrays the DMPC peak positions have been plotted against temperature, for pure lipid bicelles in (Figure 3.17 A.) and for bicelles with fukutin TMD (Figure 3.17 B.).

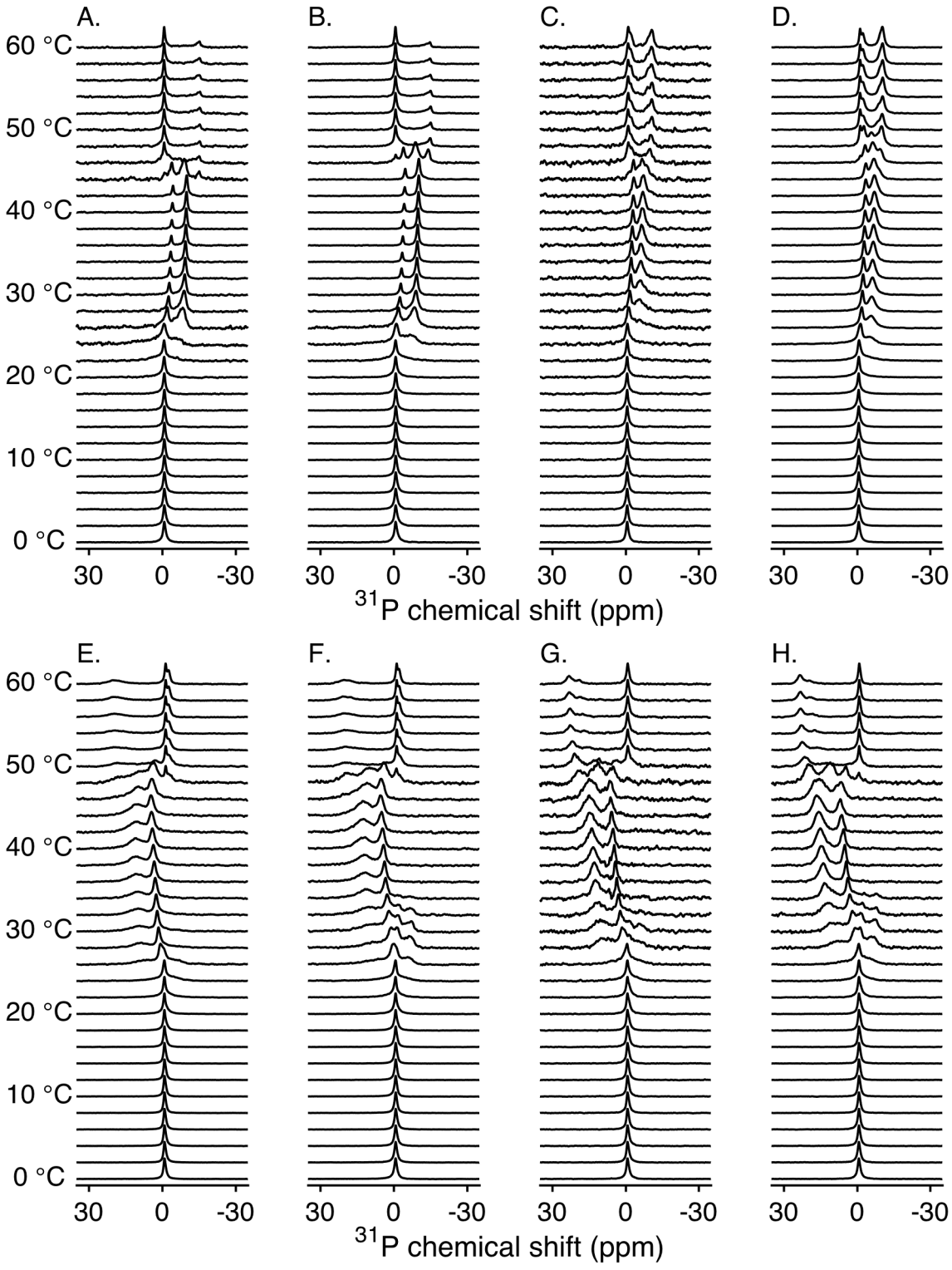

Figure 3.16: ***^{31}P NMR spectra of DMPC/DHPC/DMPE-DTPA bicelles (3.5/1/0.023) at 20 % w/v from 0 to 60 °C with and without fukutin TMD and lanthanide salts.*** *Samples contained no lanthanides (A. and B.), dysprosium (C. and D.), thulium (E. and F.) or ytterbium (G. and H.) at 1:1 DMPE-DTPA:lanthanide. A., C., E. and G. were pure lipid, whilst fukutin TMD was present in B., D., F. and H. at 848 molar L/P. Either 256 or 512 scans were acquired for samples without or with lanthanides respectively.*

When considering the samples without fukutin TMD, the use of dysprosium does not affect orientation of the bicelles, indicated by the continued presence of the DMPC peak around 7 ppm. There is a small increase in alignment temperature from 26 to 28 °C when dysprosium is added. Supplementing the bicellar solutions with positive $\Delta\chi$ lanthanides results in their alignment parallel to the field as would be expected (Figure 3.16 E.-H.). This is clear from the resonance downfield from the isotropic peak for DMPC at around 11.5 ppm for thulium and 14.0 ppm for ytterbium in the aligned phase. Although there is a small difference in the peak position between the two lanthanides it is clear that the bicelles are aligned parallel to the field from their downfield shifts, as has been observed in the literature. It is possible that these changes in peak position occur due to pseudocontact shifts as has been reported previously[244], but since the isotropic peak remains unaffected this seems unlikely. Whilst the aligned phase with thulium remains over a broad range from 28 to 46 °C, the ytterbium phase is smaller, from 32 to 44 °C; presumably since the $\Delta\chi$ of ytterbium is less positive than thulium more thermal energy is required to 'flip' the bicelles. Lanthanides are powerful paramagnetic relaxation agents, explaining the significant line broadening observed, which is greatest in the thulium sample whilst the effects of ytterbium are relatively modest, corresponding with reports in the literature[244]. It was expected that these effects would have been mediated by the use of chelating lipid which should sequester the lanthanide away from the phosphates. Since the interactions giving rise to the relaxation effects are dipolar in nature they have a distance dependence, which may explain the observations here. Lanthanides are able to exert their effect up to 40 Å away[249], which assuming the classical bicelle model results in approximately half of the lipids being within 40 Å of a DMPE-DTPA lipid (calculations given in appendix B). It is unsurprising therefore that such relaxation effects are observed. It is also worth pointing out that in contrast to the ^{31}P spectra here with the chelator, the use of thulium without a chelator results in complete broadening of the DMPC and DHPC peaks such that they can no longer be separated[252].

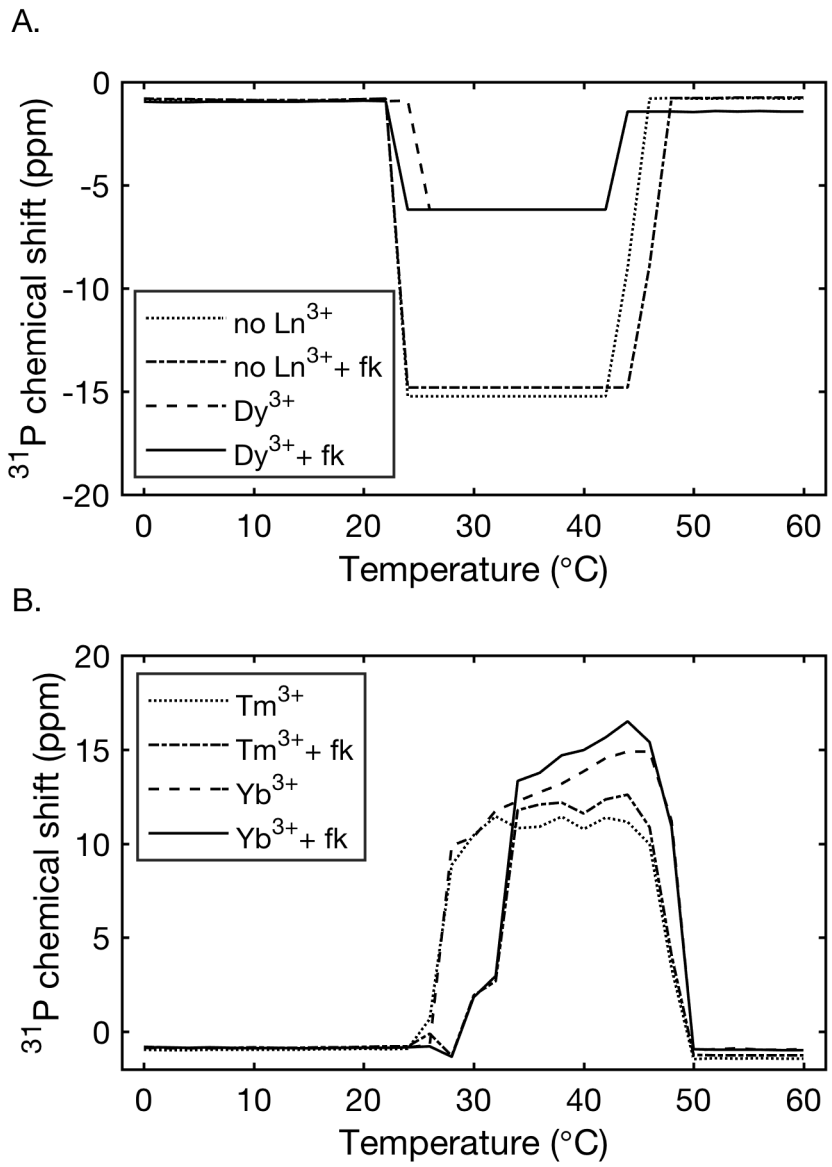

Figure 3.17: ***^{31}P chemical shifts of DMPC in DMPC/DHPC/DMPE-DTPA (3.5/1.0/0.023) bicelles with lanthanides thulium, dysprosium or ytterbium and with or without fukutin TMD (fk).*** *A. Bicelles oriented perpendicular to the field prepared without lanthanide and without fukutin TMD (dotted line) and with fukutin TMD (dot-dash line), or with dysprosium without fukutin TMD (dashed line) and with fukutin TMD (solid line). B. Bicelles oriented parallel to the field prepared with thulium either without fukutin TMD (dotted line) or with fukutin TMD (dot-dash line); or with ytterbium either without fukutin TMD (dashed line) or with fukutin TMD (solid lines).*

It is also important to consider the effect of fukutin TMD on the alignment of bicelles. Helical proteins have weak positive $\Delta\chi$ so in sufficient concentrations can reorient the bilayers. This has been demonstrated for the peptide gramacidin in bicelles with $q = 2.7$ where a 10:1 L/P ratio is calculated to yield a positive $\Delta\chi$ which is twice that of the bicelle

assembly, and was confirmed experimentally to result in perpendicular orientation[255]. Since the L/P ratio of fukutin TMD here is 878 it is unlikely to affect these measurements to any substantial degree. This ratio was selected as it is equivalent to 1.2 mg mL^{-1} which is the target for CD experiments in the 0.1 mm pathlength. In the fukutin TMD sample without lanthanides the bicellar phase is extended by 2 °C to 44 °C relative to the pure lipid sample, and the position of the DMPC peak is unchanged. In the samples with dysprosium, the samples align 2 °C lower at 36 °C that those without fukutin TMD. There is a more significant change in alignment temperature in thulium aligning at 28 °C without and 34 °C with fukutin TMD, whilst for ytterbium there is no change. The reason for these changes is not immediately apparent. It seems that the introduction of fukutin TMD results in a slight increase in the bilayer order, presumably this is due to interactions of the peptide with the lipid headgroups, and whilst 2 °C changes are relatively modest, the 6 °C change in the thulium case is quite dramatic, particularly considering the quantity the small number of fukutin TMD molecules in in the samples (equating to just six fukutin TMD monomers per bicelle using the calculations outlined previously).

Additional confirmation of sample alignment was provided by deuterium NMR on pure lipid samples prepared with acyl chain deuterated DMPC (d54-DMPC) (Figure 3.18). There are no deleterious effects on these spectra due to paramagnetic relaxation effects since the scale of the interaction is much smaller (typically on the order of Hz) than the quadrupolar coupling for a CD group (~125 kHz). Samples were measured at 45 °C, which allows the bilayer alignment to be observed by measurement of quadrupolar splitting, similarly to the deuterium NMR spectra of mechanically oriented samples in Chapter 2. Here the splitting of the spectra with thulium is 40.2 kHz compared to approximately half that value, 20.7 kHz, for dysprosium, indicating parallel and perpendicular alignment of the bicelles normal with the magnetic field respectively. The resolution of individual peaks arising from each CD_2 group and the lack of an isotropic peak indicates there is little or no underlying disordered contribution to the spectra.

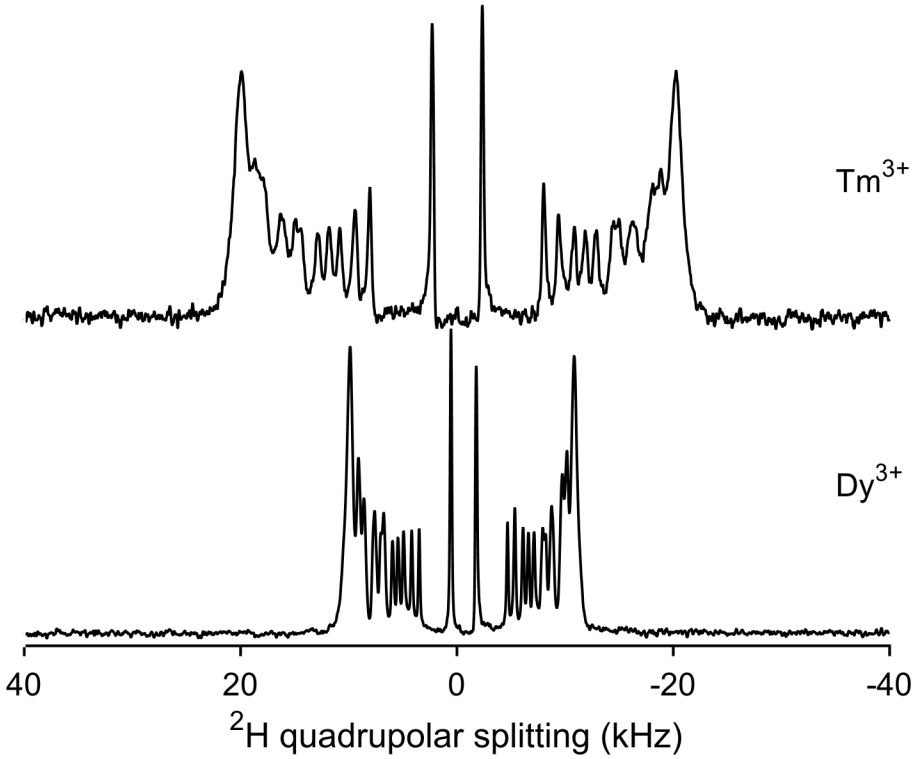

Figure 3.18: ***Deuterium NMR spectra of d54-DMPC in DMPC/DHPC/DMPE-DTPA (3.5/1/0.023) bicelles at 20 % w/v acquired at 45 °C****. Either thulium chloride or dysprosium chloride was added to samples at 1:1 molar ratio with DMPE-DTPA. Spectra were acquired using a quadrupolar echo pulse sequence with 1024 scans, and processed by shifting to the top of the fid, zero filling to 16384 points and applying 100 Hz exponential line broadening before Fourier transform.*

3.3.2. Fukutin TMD tilt angle in bicelles

Validation of this potential new method for OCD required confirmation of the protein tilt angle by an alternative means, and ^{15}N NMR is ideal for this purpose. Spectra of $^{15}N_{leu}$ fukutin TMD were acquired in bicelles of identical lipid composition to those studied by EPR, and ^{31}P and deuterium NMR (DMPC/DHPC/DMPE-DTPA). The L/P ratio was 50. The weight percent was increased to 30 % w/v in order to maximise the quantity of material in the sample. We were not concerned that this would significantly alter the bicelle phase or alignment since earlier in the chapter we established that there was little difference between 20 and 30 % w/v (Figure 3.12).

To acquire ^{15}N NMR spectra with the bicelles oriented perpendicular and parallel to the field, the first sample contained no lanthanide and ytterbium was added to the second. Although thulium has a greater $\Delta\chi$ than ytterbium it also has greater relaxation effects and we have demonstrated that ytterbium is sufficient to flip the bicelles. To confirm the

desired alignment of the bicelles ^{31}P and deuterium NMR were again used (Figure 3.19). A full temperature array was not performed to ensure that the sample did not deteriorate during these initial characterisation measurements, and for both orientations a temperature of 40 °C produced the optimum orientation. The bicelles oriented perpendicular to the bilayer produce a DMPC peak at -11 ppm, as expected, but there is also a shoulder at -0.5 ppm from what may be an isotropic component, although interestingly there is no similar isotropic peak in the deuterium spectra (Figure 3.19A. and B.). Whilst it is not desirable to have an isotropic component in the sample, since for ^{15}N measurements a cross polarisation pulse sequence is used, any fukutin TMD in isotropic mixed micelles will not be observed in the spectra. The deuterium spectrum has a splitting of ~16.8 kHz which is slightly lower than the 20.7 kHz found for the bicelles without fukutin TMD. The lack of defined resonances is unsurprising since most acyl chains will be in contact with the protein which may influence their motion. In the bicelles flipped with ytterbium there is a broad, shallow downfield contribution in the ^{31}P spectra, as well as a peak around -1.1 ppm which may result from an isotropic mixed micellar solution but equally is fairly broad at 1.7 ppm, possibly indicating that the peak also represents the highly curved DHPC region of the bicelles (Figure 3.19D.). It should also be noted that additional ytterbium was titrated into the sample to flip the bicelles completely, with a final ratio of ytterbium:DMPE-DTPA of approximately 1.5:1. It is highly likely therefore that some of the ytterbium is bound to the lipid phosphates. It has been noted previously that bicelles with protein often require additional lanthanides to orient[252]. In the deuterium spectra of samples with ytterbium the splitting between the two edges is ~43.6 kHz, indicative of parallel alignment, but there is also what appears to be an isotropic component at the centre of the spectrum (Figure 3.19E.). As in the perpendicular spectra there is poor resolution between the peaks for individual CD_2 groups, but considering the quantity of protein it is likely that the majority of the acyl chains are interacting with the fukutin TMD.

Although it is difficult to calculate the order parameter from the ^{31}P spectra since with ytterbium the peak is very shallow and broad, an order parameter can be estimated using the splitting of the plateau region in the deuterium spectra. The bicelle order parameter S_{nN} describes the motion of the bicelle director n around the net bicelle normal N and can be estimated simply as $\Delta\upsilon_Q^{bicelle} / \Delta\upsilon_Q^{MLV}$ where $\Delta\upsilon_Q^{bicelle}$ is the bicelle quadrupolar splitting from the outer plateau region and $\Delta\upsilon_Q^{MLV}$ is the splitting of DMPC-d54 MLVs[280]. Taking the $\Delta\upsilon_Q^{MLV}$ as 26 kHz[281] this gives a S_{nN} for the perpendicular aligned sample of 0.61. To approximate S_{nN} for the parallel aligned sample the $\Delta\upsilon_Q^{MLV}$ was multiplied by two to

estimate the 0° splitting of the MLVs, which gives an increased order parameter of 0.83. Considering the addition of lanthanide, and the protein having positive $\Delta\chi$ this increase in order is unsurprising.

The ^{15}N spectra of $^{15}N_{leu}$ fukutin TMD in bicelles reveals a dominant peak centred around 114 ppm for perpendicular and 156 ppm for parallel aligned bicelles (Figure 3.19C. and F. respectively). These positions indicate a tilted transmembrane orientation. The leucines are positioned at different rotations around the helix so their amide planes are not aligned, meaning each gives rise to an individual resonance which is dependent on both the tilt angle and rotation. In this case however we do not have resolution of peaks for different residues since the signal to noise was such that the spectra was processed with a large amount of line broadening. What can be observed is that the peak in the spectra from perpendicular aligned bicelles is much broader than in the parallel aligned bicelles, which is surprising since the distribution of peaks close to the 0° edge should be around twice as broad as the 90° edge. We suggest that this is due to overlapping peaks from oriented peptide as well as an underlying, broad powder component in the perpendicular spectra, which can be seen more clearly in the parallel aligned sample around 60 ppm. This correlates with the mechanically aligned DMPC and DPPC samples, where a powder contribution is also observed, presumably again indicating that the peptide is not readily able to span the bilayer but instead forms a large oligomer or aggregate.

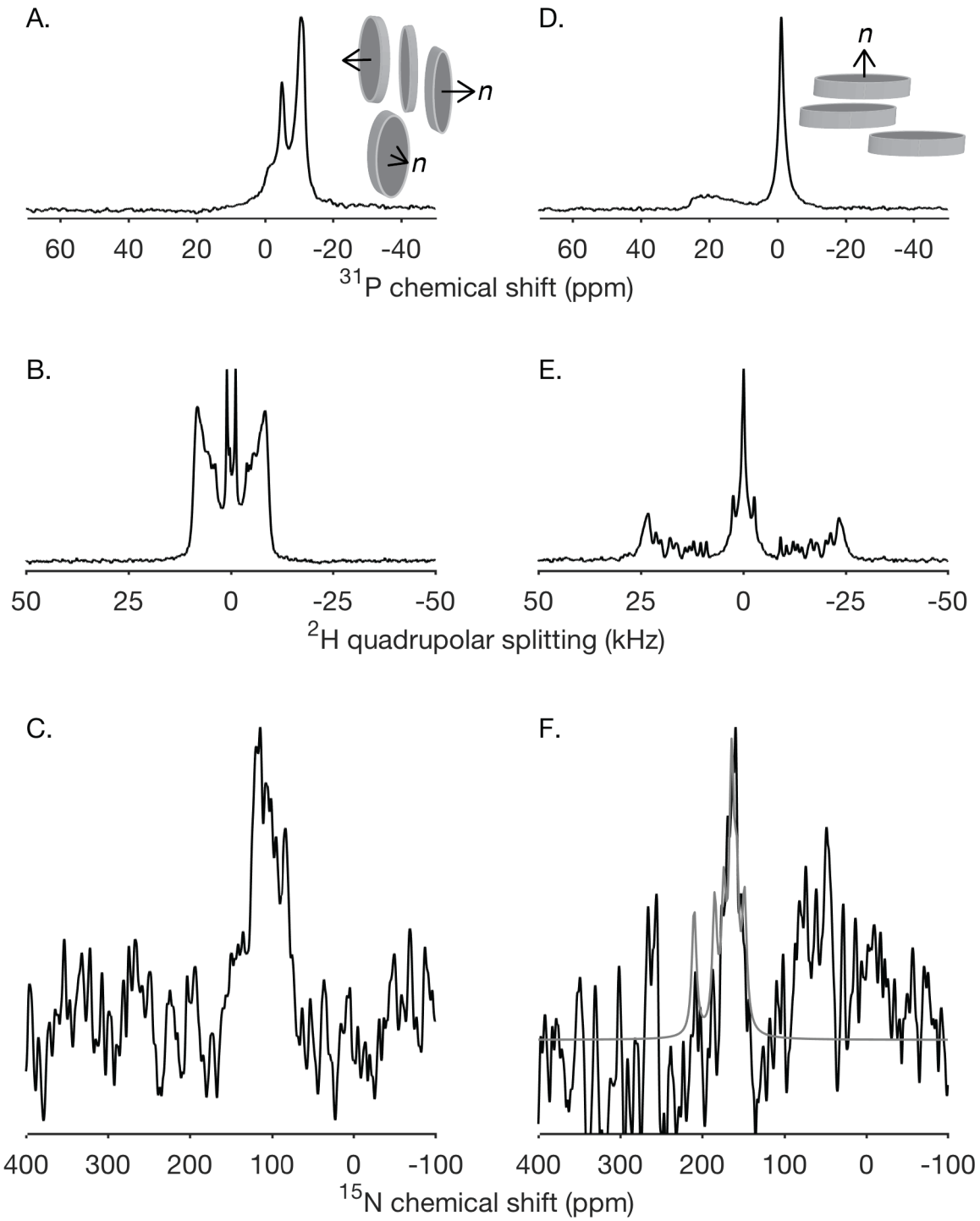

Figure 3.19: ***Spectra of bicelles containing $^{15}N_{leu}$ fukutin TMD aligned either perpendicular (left) or parallel (right) to the magnetic field (14.1 T) at 40 °C.*** *The lipid composition was DMPC/DHPC/DMPE-DTPA (3.5/1/0.023) at 30 % w/v with an L/P ratio of 50 in both samples. 20 mol % DMPC was exchanged for DMPC-d54. For samples aligned perpendicular to B_0 no lanthanide was added, and to align bicelles parallel ytterbium was added at approximately 1.5:1 with DMPE-DTPA. To check alignment samples were measured using both ^{31}P (A. and D.) and deuterium (B. and E.) NMR. The protein orientation was measured using ^{15}N NMR (C. and F.), with 40000 and 12000 scans respectively. F. was fitted with a simulated ^{15}N spectra (grey line).*

By fitting simulated spectra for peptides tilted from 0 to 90° we have been able to estimate the tilt angle of the protein in the bilayer. This was only done for the parallel aligned sample, since for perpendicular there is an additional degree of rotation of the protein around the magnetic field director. The parallel sample has a tilt angle of 30°, which is much greater than the mechanically aligned samples that give a tilt angle of 2° in DMPC. However, these simulations assume an order parameter of 1 which is not the case in bicelles. The reduction in order parameter will scale the chemical shift with respect to the isotropic chemical shift[282]. If we assume an approximate S_{nN} of 0.8, as has been calculated from the deuterium spectrum, and reported in the literature[283], the initial peak position would be ~174 ppm (from $\delta_{iso} + (1/0.8 * \delta_{iso} - \delta_{obs})$). This value correlates to a tilt of approximately 26°, which is still quite distant from the tilt angle in mechanically aligned bilayers. The reasons for this change are not immediately apparent; the bilayer thickness of the DMPC in bicelles and mechanical samples should not be dramatically different. We cannot completely rule out an order parameter lower than 0.8, possibly explaining the apparent disparity in tilt. Reconstitution of protein into bicelles at relatively high L/P ratios, such as the 50 used here, is likely to have implications for the morphology of the bicelles. It is however clear from the deuterium spectra here that the DMPC bilayer is aligned either perpendicular (without lanthanide) or parallel (with ytterbium) to the magnetic field as would be expected, allowing comparison with the mechanically aligned samples in Chapter 2. Indeed, ^{15}N studies on the HIV-1 Vpu peptide by Park et al.[284] comparing magnetic and mechanically aligned samples demonstrates the equivalence of the two approaches. Further studies using lower concentrations of peptide may be useful to attempt to improve the quality of the spectra recorded here, and it may be informative to measure the phase behaviour as a result of changing the L/P ratio. An interesting comparison would to be prepare bicelles with thinner and thicker bilayers, identically to the mechanically aligned samples to see whether similar tilt angles and powder contributions are also seen there. It may also be useful to perform fukutin TMD cross-linking experiments in bicelles to attempt to quantify the size of the aggregates and relative proportions to monomeric in the different environments.

3.3.3. Circular dichroism experiments

3.3.3.1. Conventional CD measurements of the conditions refined using magnetic resonance

Having demonstrated that CD on bicelles is feasible, characterised their phase behaviour and optimised conditions for alignment in a low magnetic field, the next step was to undertake CD measurements. These were initially performed using a conventional CD instrument without a magnetic field to understand the optical properties of the samples. Following the conditions used for EPR and NMR, the same DMPC/DHPC/DMPE-DTPA composition was used here. A 0.1 mm pathlength was selected to minimise the concentration of lipid and therefore its absorbance. An initial observation was a signal with large positive intensity at < 190 nm, which appeared to continue to increase in intensity with each scan (Figure 3.20) and occurred when samples were heated from below the T_m to above it (i.e. 25 to 38 °C). We found that following 40 minutes the signal began to stabilise, so in future measurements there was a 45 minute incubation when raising the temperature in such large steps. Incidentally this also is approximately the length of time required to align the samples in the EPR instrument. This intense peak is likely to originate from linear birefringence since there is no titled surface or uneven film, indicating linear dichroism is not the cause of the signal. This presumably reflects the gradual organisation of the lipids into bicellar morphology with time. The broad positive peak centred around 216 nm can be assigned to the lipid carbonyl absorbance, which is altered to a small degree by the change in intensity of the 185 nm band.

CD spectra of DMPC/DHPC/DMPE-DTPA were acquired with and without fukutin TMD in the presence of no lanthanide, thulium or dysprosium (Figure 3.21). The fukutin TMD spectra were baseline corrected against the equivalent pure lipid bicelles, and pure lipid bicelles baseline corrected against H_2O. For the pure lipid samples, from 5 to 25 °C the spectra are relatively similar, with a broad peak around 216 nm corresponding to carbonyl absorption. The large intensity of the baseline spectra is non-ideal (in mdeg the absolute intensity > 200 nm is approximately equal to that of the fukutin TMD spectra) but the protein spectra are consistent with the expected structure, and the lipid concentration in the two samples is identical so there should be no change in the absorption. Above 25 °C there appears to be correlation between the occurrence of the intense birefringence peak at 185 nm and the phase transitions identified by ^{31}P NMR. It should be noted that in preliminary studies we observed that both the intensity and position of this band was variable, even when measurements were performed on identical samples. This is illustrated when comparing the fukutin TMD spectra with dysprosium against those with thulium or

without lanthanide at all (Figure 3.21), where there is a clear difference in this signal with and without protein, with no obvious explanation. It would be valuable in future experiments to perform specific birefringence measurements to better characterise this aspect of the system. For these reasons we suggest that data at wavelengths shorter than 200 nm cannot be interpreted accurately, even when the apparently appropriate baseline correction is applied. Although this limits secondary structural deconvolution, for oriented studies it is less problematic since the band at ~208 nm is the prime indicator of helix alignment. It is also worth noting that in a study of unoriented bicelles using CD by Loudet et al.[268] there is a similar increase in intensity at the 190 nm region of the spectrum which has not impeded the author's analysis.

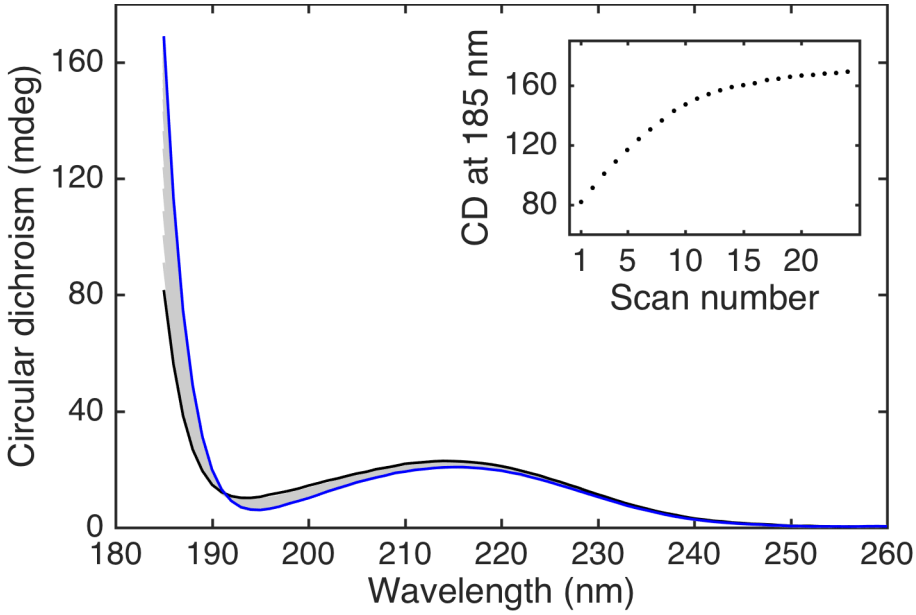

Figure 3.20: ***Conventional CD spectra of DMPC/DHPC/DMPE-DTPA (3.5/1/0.023, 20 % w/v at 38 °C.*** *A five minute incubation was allowed after the temperature was raised from 25 °C to 38 °C, and each scan was approximately two minutes. Consecutive scans were acquired until the spectral intensity began to stabilise. First scan is coloured black and the last blue. Inset: plot of CD signal at 185 nm against number of scans. Spectra presented are baseline corrected against water. Samples were measured in a demountable 0.1 mm pathlength fused silica cuvette with 1 s integration time and 1 mm slit width.*

The spectra of fukutin TMD in the bicelles are characteristic of an α-helical protein, with minima at 210 and 223 nm. In the micellar phase (5 °C) there are subtle differences in the spectral shape between samples with and without lanthanide but nothing to indicate a loss of secondary structure. Further, the corrected spectra here are characteristic of fukutin TMD in lipid environments, with a ratio of 223:211 nm equal to 0.9 ± 0.02 for bicelles

without lanthanide and DMPC SUVs (from Chapter 2). With thulium there is an increase in negative intensity of the signal at 210 and 223 nm as the temperature is increased, suggesting that there is an increase in helical content. It is possible that there is additional structure in the bilayer environment of the bicelles, rather than the micellar environment at lower temperatures, although this would presumably also be observed in the samples without thulium.

At this point since we had established that bicelles composed of DMPC/DHPC/DMPE-DTPA could be aligned in a low magnetic field, had mapped out their phase transition temperatures and demonstrated that with prudent interpretation could be studied by CD, we decided to begin measurements using the magnetic CD instrument on the B23 beamline. Unfortunately the magnet does not have appropriate dimensions to fit into the benchtop instrument, so optimisation with the magnet was time limited by beamtime allocations.

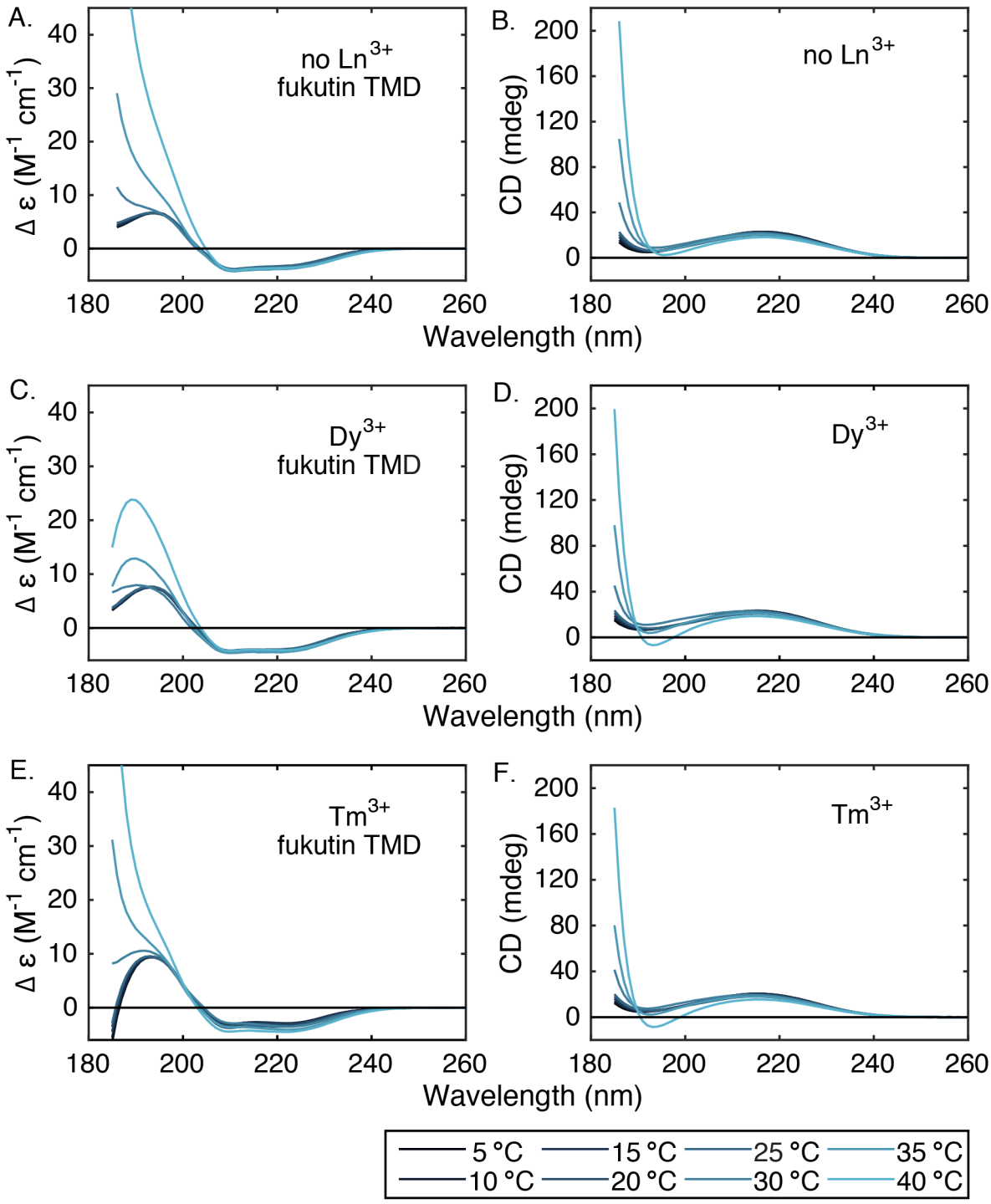

Figure 3.21: ***Conventional CD spectra of pure lipid bicelles (DMPC/DHPC/DMPE-DTPA, q 3.5, 20 % w/v) from 5 to 40 °C in 5 °C steps.*** *Left hand column contain fukutin TMD whilst the right column are the equivalent pure lipid spectra. A. and B. are without lanthanide; each spectrum is an average of four scans. C. and D. are with dysprosium at 1:1 ratio with DMPE-DTPA; each spectrum is an average of two scans. E. and F. are with thulium at 1:1 ratio with DMPA-DTPA; each spectrum is an average of four scans. A 15 minute incubation was allowed at each temperature steps. All spectra were baseline corrected against H_2O and acquired with 1 s integration time and 1 mm slit width in a 0.1 mm pathlength fused silica demountable cuvette.*

3.3.3.2. Magnetic SRCD studies

Although a set of conditions for CD had been established, a technical complication arose in that the magnetic sample holder to be used in these experiments has only sufficient space for a cuvette, and is not provided with temperature control capacity (Figure 3.22 C.). Although it appeared necessary to minimise the pathlength due to lipid absorption, we initially conducted a preliminary test using a water jacketed 10 mm cuvette to provide temperature control. In light of this we reduced the weight percent to 5 to reduce the mass of lipid in the light path. Even still the quantity of lipid generated a variety of unusual spectral shapes. Example spectra are given in Figure 3.23 which were acquired in the absence of a magnetic field using the module B beamline, although a selection of further peculiar line shapes were also observed in the absence and presence of the field. These demonstrate that there are artefactual features in the spectra which are unacceptable and cannot be supressed experimentally without a reduction in pathlength. We assign these features of varying intensity and position to linear birefringence due to the large intensity of the signal. Linear dichroism can be excluded since it arises due to uneven surfaces and defects in the crystalline phase, neither of which are present here.

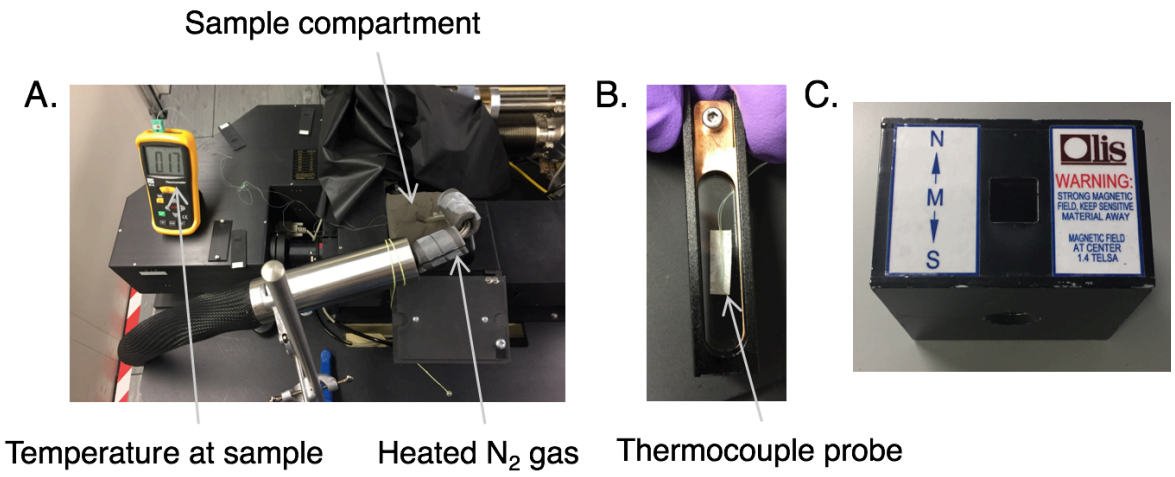

Figure 3.22: ***Set up of magnetic CD instrument temperature control.*** *A. Sample compartment was supplied with heated nitrogen from a variable temperature controller (FTS Systems). The tube was passed through a foam support and rested between the magnet and reverse of the cuvette. B. A fine probed thermocouple was taped to the reverse of the cuvette to measure temperature on an external thermometer. C. 1.4 T magnetic sample holder used for magnetic CD studies. The magnetic field runs parallel to the light director. The magnet is removable and reversible to allow 'forward' and 'reverse' field directions.*

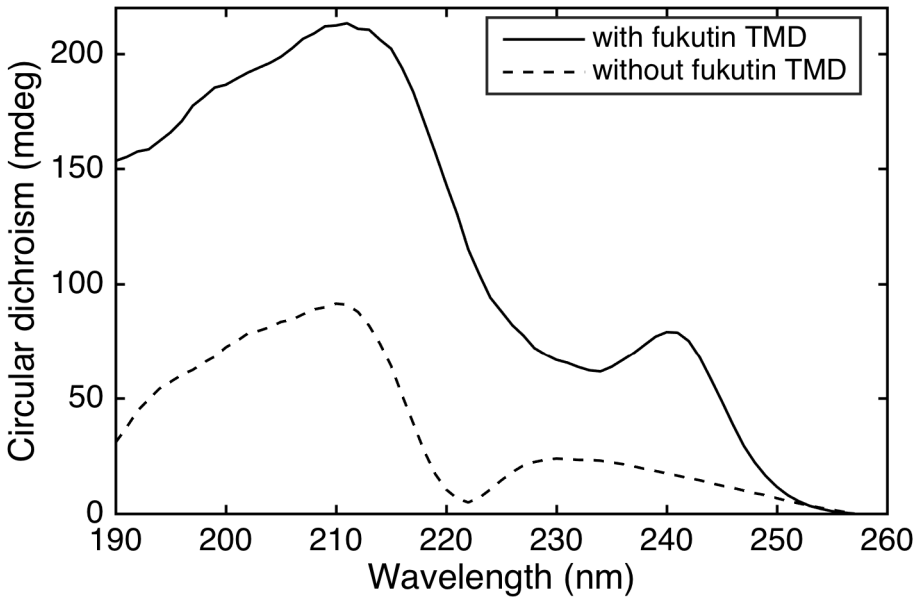

Figure 3.23: ***SRCD spectra of DMPC/DHPC (*q *= 3.5, 5 % w/v) with (solid line) and without (dashed) fukutin TMD at 200 L/P.*** *Spectra were acquired using a fused silica cuvette with 10 mm pathlength at 35 °C. Four spectra were averaged, and the presented spectra are corrected against H_2O. The slit width was 0.5 mm and integration time 0.2 s.*

We sought to address these issues by returning to the thinner pathlength cuvette used for the conventional CD measurements to reduce the quantity of the lipid. This presents a problem in that it is not possible to temperature control the cell, and water jacketed cuvettes were not available at lower pathlengths so an alternative method for temperature control was necessary. The approach implemented involves using a variable temperature controller to supply a stream of heated nitrogen gas which was directed onto the sample cuvette with 0.1 mm pathlength (Figure 3.22). The temperature could be assessed using a fine tipped thermocouple in contact with the cuvette surface, and proved to be efficient for temperatures from 0 to approximately 50 °C.

3.3.3.3. Measurements of bicelles in magnet with temperature control

Following implementation of a temperature control system we were able to begin measuring CD spectra of the bicelles. Spectra of DMPC/DHPC/DMPE-DTPA bicelles with and without fukutin were acquired in the presence of lanthanide ions (Figure 3.24). Pure lipid bicelles were used as a baseline. Although there are no tryptophan residues in fukutin TMD and tyrosine has a relatively weak MCD signal, initially a spectrum was acquired from 300-185 nm with the magnet present, which was completely flat in the 300-250 nm region, indicating there is no MCD contribution from the protein itself. To increase the rate of acquisition future spectra were acquired from 260-185 nm.

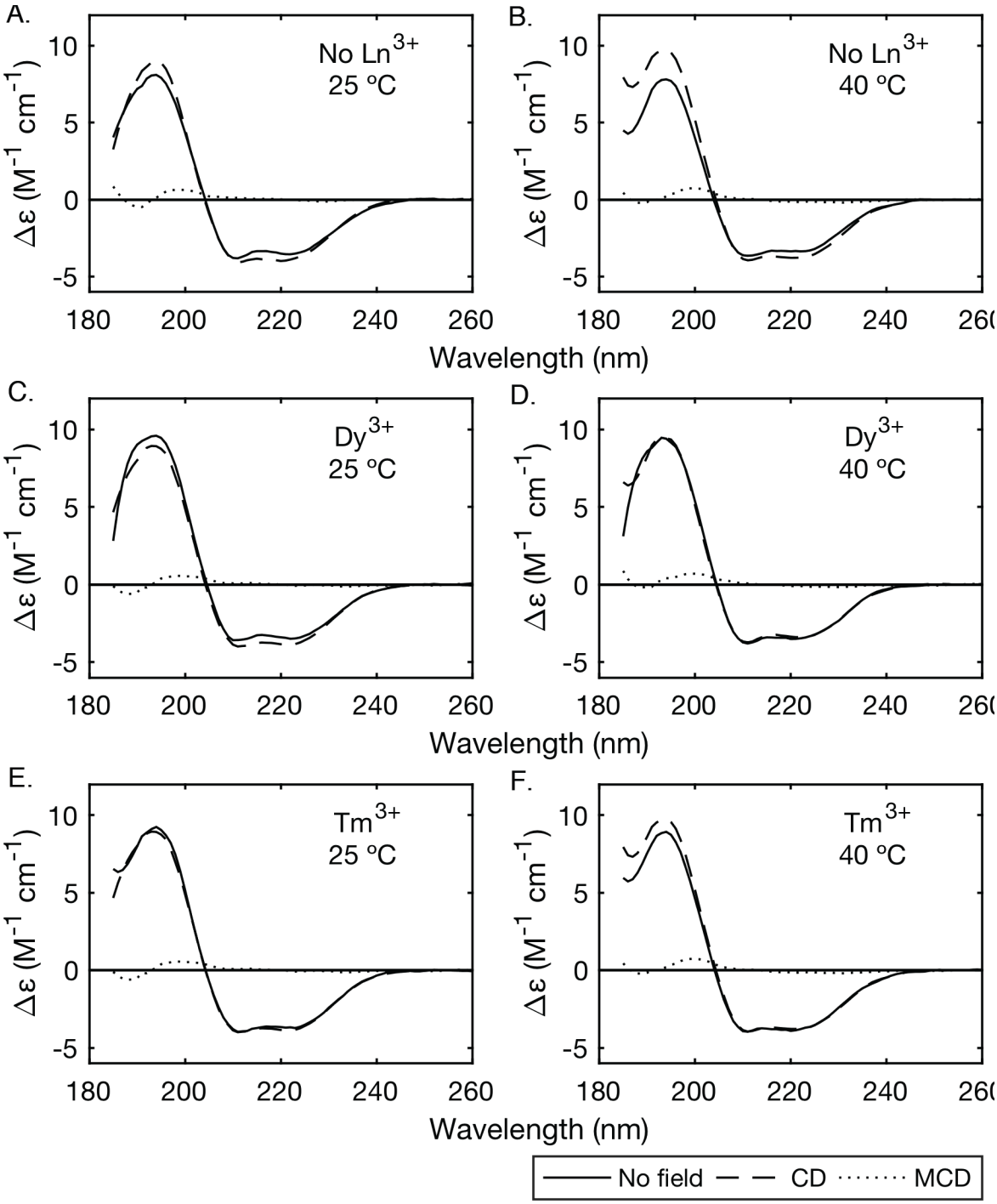

Figure 3.24: ***SRCD spectra of fukutin TMD in DMPC/DHPC/DMPE-DTPA (3.5/1/0.023, 20 % w/v) in the presence and absence of a magnetic field.*** *Samples were prepared either without lanthanide (A. and B.), with dysprosium (C. and D.) or thulium (E. or F.) at 1:1 molar ratio with DMPE-DTPA. A., C. and E. were at 25 °C whilst B., D. and F. were at 40 °C. Spectra were acquired without magnetic field (solid line) or with the 1.4 T field, and are presented as either CD (dashed line) or MCD (dotted line; see processing details in methods). The pathlength of the fused silica demountable cell was 0.1 mm, the slit width 0.5 mm and the integration time 1 s.*

Although in all cases the spectra are consistent with helical structure, there is no significant change between those measured in any condition, either with or without lanthanide or in the presence of the magnetic field, suggesting there is no alignment under these conditions. The corresponding spectra from Figure 3.24 have been overlaid in Figure 3.25. There is a change in intensity of the 190 nm band but as explained earlier with the large artefactual contributions in this region it is difficult to interpret this data. The change in intensity of the thulium sample may be due to experimental error and a slightly higher protein concentration in that sample.

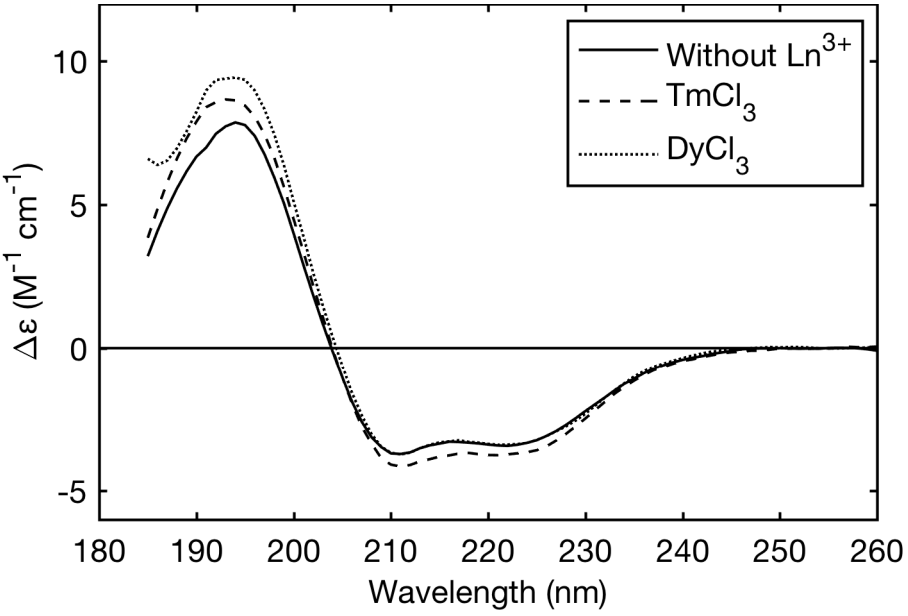

Figure 3.25: ***SRCD spectra of fukutin TMD in DMPC/DHPC/DMPE-DTPA (3.5/1/0.023) at 20 % w/v in the presence of a magnetic field at 40 °C.*** *Spectra are overlaid from Figure 3.24.*

This was a frustrating result, but we believe it can be explained in a number of ways. Firstly, in the EPR spectra for the parallel aligned bicelles we observe an underlying powder component, presumably from unaligned bicelles, which if present in the SRCD sample could dominate the spectra and produce a line shape consistent with a powder distribution of fukutin TMD. Secondly the manifestation of distributions around the bicelle director will be different between NMR/EPR and CD since they are sensitive to different timescales. The timescales of NMR and EPR (~10^{-3} and 10^{-7} s respectively) are much slower than the timescale of CD (~10^{-15} s). In NMR/EPR fluctuations around the membrane director can be described as either static or dynamic mosaic spread[285]. Static mosaic spread results in a distribution of resonances. In contrast the dynamic mosaic spread, characterising the fast (< μs) fluctuations around the bicelle director, leads to a

scaling of the observed CSA (or hyperfine splitting) and can be interpreted as an order parameter ($S_{bicelle}$). On the CD timescale both types of fluctuations around the bicelle director appear as a static mosaic spread, as both are significantly slower than the CD timescale. The resulting CD spectra will therefore be the summation of the CD spectra of all the sampled orientations.

We can estimate the effect of this distribution in the CD spectra using the order parameter from EPR, which has a closer field to the MCD instrument than NMR. Using the splitting from the EPR spectra in Figure 3.15 the order parameter S_{mol} can be calculated according to[274]:

$$S_{mol} = S_{33} [(3 \cos^2 \theta - 1) / 2]^{-1}$$
$$S_{33} = ((A_{\parallel} - A_{\perp}) / (A_{zz} - A_{xx})) (a_N / a'_N)) \quad (3.12)$$

where S_{33} defines the motion of the CLS long axis with respect to bilayer normal, a_N is the isotropic hyperfine splitting (1/3 ($A_{xx} + A_{yy} + A_{zz}$)) and a'_N is the solvent polarity correction factor (1/3 ($A_{\parallel} + 2 A_{\perp}$)), with the principle hyperfine tensors of CSL taken as 6, 6 and 32 G for A_{xx}, A_{yy} and A_{zz} respectively[274]. Since the angle between the bilayer normal and the CSL long axis (θ) is ~0°, $S_{33} \approx S_{mol}$. For the samples here we found $S_{mol} = 0.38$, which indicates there is significant deviation of the bilayer from the magnetic field director, giving a maximum θ of approximately 40°. Coupled with the cone opening angle of fukutin TMD in the bicelles, which the NMR data indicates could be ~30° it is easy to see that a wide distribution of orientations is possible. Although the field of the MCD instrument is greater than the EPR, even in Q band EPR (~1.2 T) an order parameter for a similar lipid mixture has been calculated as 0.56[278].

If it were possible to improve the degree of alignment, and improve the order parameter, the OCD measurements using this approach may become more feasible. Since the alignment energy of the bicelles is determined by the square of the magnetic field strength, the most logical option would be to employ a stronger field. Superconducting MCD instruments are available operating at fields up to ~8 T, which is approaching the field used in NMR[286]. A measurement of bicelles using a superconducting magnet would provide absolute confirmation as to whether the system is feasible for OCD studies, and the ability to alter the field strength in such instruments could also help to ascertain whether there is a minimum field required for such experiments.

An obvious limitation to these measurements is that we remain unable to confirm whether the bicelles are sufficiently oriented on the optical timescale. In linear dichroism

measurements retinoid compounds which partition into bilayers have been used as reporters of bilayer orientation in shear aligned vesicles since the chromophores align with respect to the bilayer normal in an analogous manner to CSL in EPR[287]. The ability to have a similar compound for OCD would be extremely useful for these measurements, and also measurements of mechanically oriented samples, although presently no such reporters have been described. An upcoming development to the B23 beamline aims to introduce a new polarimeter to the beamline which allows the measurement of the full Mueller matrix[288], a 16 element matrix describing the complete optical properties of a system, including the phenomena of CD, circular birefringence, LD and LB. This would allow assessment of sample orientation using one of the probes used in LD, and also would potentially enable characterisation of the LB bands observed in the spectra here. Alternatively, other techniques such as small angle neutron scattering, could be used to measure the degree of alignment, which has a timescale not dissimilar to CD.

3.4. Conclusions

In this chapter the aim was to develop a system to produce oriented samples for OCD using magnetically aligned lipid phases. To achieve this aim ^{31}P NMR was used extensively to characterise the phase behaviour of bicellar samples prepared with various lipid compositions in order to obtain maximal alignment within acceptable temperature ranges. The effect of lanthanide ions as agents to modulate the bicelle alignment was also investigated. To validate that this approach could be feasible using a 1.4 T MCD instrument, X-band EPR was used to demonstrate bicelle alignment at a lower magnetic field. The optical properties of bicelles for CD were characterised, which although giving some limitations due to linear birefringence effects, do not appear to effect the 208 nm band which acts as a marker for helix orientation. Unfortunately we were unable to measure oriented spectra of fukutin TMD in lipid bicelles, which we speculate is due to the poor degree of alignment in these samples and their motions around the magnetic field. We were however able to estimate the fukutin TMD tilt angle in bicelles using ^{15}N NMR, which will provide a basis for any future OSRCD interpretation.

Alternative strategies may be needed such as the use of higher magnetic fields available with superconducting magnets, and if further developed this approach has promise to address some of the challenges posed by mechanically oriented samples. However, the method may still have some limitations over mechanically aligned samples. Even if bicelles can be sufficiently aligned using superconducting magnets, these are not widely

available and are very expensive to operate. Relatively few large proteins have been reconstituted into anisotropic bicelles, which may require further optimisation. A further concern is that a depending upon their mechanism of action antimicrobial peptides may perturb the bicellar structure, as is the case with metillin[289], although bicelles have been used successfully in with antimicrobial peptides such as alamethicin[290] and a series of Australian tree frog derived peptides[291], indicating that they cannot be routinely applied to the study of antimicrobial peptides. Whilst they are amenable to the introduction of various other lipid components such as anionic lipids[292] and cholesterol[289] a greater diversity is possible using mechanically aligned samples. A potential further drawback is the requirement for careful control of the temperature, although as we have demonstrated here it is possible to readily align bicelles below physiological temperatures. Indeed, the use of very short chain lipids[256], unsaturated lipids[293] and increasing concentrations of cholesterol (and cholesterol analogues)[294] can reduce the T_m further.

To summarise, whilst bicelles have the potential to simplify the preparation of oriented samples for CD, and provide consistency which is not possible with mechanically oriented samples, there are a number of further steps of optimisation required before they can be used in OCD.

Chapter 4. Expression and purification of the human *KCNH2* potassium channel (human *Ether-à-go-go*-related gene) for biophysical studies

4.1. Introduction

Whilst the majority of OCD studies have involved relatively simple helical peptides, the ultimate aspiration of this project was to begin to develop methods for the measurement of membrane proteins of greater structural complexity. One of the advantages of OCD is the requirement for small quantities of protein, which is particularly useful in cases of membrane proteins where expression and purification of sufficient yields for high resolution techniques presents a challenge. OCD would allow the investigation of changes in the overall orientation of the protein. One can envisage its use to probe the types of conformational changes occurring as a result of events such as ligand binding in membranes mimicking the physiological environment, and the effect of different types of lipids on gating processes in channels. This could be particularly powerful in collaboration with functional data. In view of this goal attempts were initiated to express and purify the human potassium channel expressed by the *Ether-à-go-go* related gene hERG. (From this point the protein will be referred 'hERG'.) A wide variety of structurally diverse pharmaceuticals are known to block the channel, potentially resulting in cardiac arrhythmia, but the mechanism of such binding events is yet to be elucidated. The ability to probe the conformational changes of the protein in response to binding of known blockers would therefore be highly valuable to begin to understand the underlying molecular mechanism.

There are a great number of potassium channels in addition to hERG, all sharing a common functionality: the passage of potassium ions out of cells in response to some form of stimuli. They are found in cell membranes of almost all organisms and regulate the electrical gradients across cellular membranes. This is especially important in excitable cells, such as neurons, where they regulate resting and action potentials, and cardiac muscle cells, where they regulate ventricular contraction.

Potassium channels are grouped into three classes by their mode of regulation. Namely, the voltage-gated (K_v), inward rectifying (K_{ir}) and tandem pore domain (K2P) channels[295]. Additionally there are ligand gated channels which respond to a variety of stimuli. These families all share a common pore domain, whilst the variation in regulatory mechanism is conferred by additional domains. In the case of K_v channels for example, there is an

additional four helical voltage-sensing domain, yielding total of six transmembrane domains. The number of transmembrane domains varies such that generally K_{ir} channels have two, K2P have four and ligand-gated channels have two or six.

There are structures available for a number of potassium channels which reveal conserved structural features[295]. All potassium channels are homotetrameric complexes, centred around the pore[37]. Each monomer has a two helical pore forming domain consisting of one helix which forms the pore itself, and a second which is fully exposed to the bilayer. At the top of the pore a short re-entrant helix (the 'pore helix') has its N terminus inserted into the central cavity of the protein. The region of the pore which coordinates potassium ions and facilitates their passage out of the channel (at near diffusion rates) is the selectivity filter, which has a common five residue motif (TVGYG) and lines the top of the pore[295]. It is this selectivity filter which gives rise to the high specificity of these channels for potassium over other monovalent cations[37]. Whilst these features appear to be conserved, there are significant variations between members of the potassium channel family, and understanding of how each member is regulated and gated requires structural information[295].

Although there are now a number of potassium channel structures available, at the time of commencing this work there was no structure for the hERG channel. This channel has a number of differences to other K_v channels, and it has a significant physiological role. It is expressed in a range of tissue, particularly neuronal cells and ventricular cardiomyocytes, where it is responsible for the determining the length of the action potential plateau phase[296].

4.1.1. Human *Ether-à-go-go* related gene (hERG)/KCNH2 channel

Numerous ion channels are involved in the regulation of cellular membrane potential, including hERG. The polarisation events in individual cardiomyocytes produce the overall electrical signal of the heart, which can be recorded in an electrocardiogram (ECG) (Figure 4.1 B.). This begins with the P wave which results from atrial depolarisation, followed by the QRS complex which signifies ventricular depolarisation, and finally the T wave which indicates ventricular repolarisation.

In context of the action potential (AP), the role of the hERG channel in cardiomyocytes is as follows[297] (the corresponding changes in membrane potential are outlined in Figure 4.1 A.). During phase 4 (resting) the sodium and calcium voltage-gated channels are closed, whilst K_{ir} potassium channels maintain a membrane potential of -90 mV. This is proceeded

by a rapid influx of sodium through voltage-gated sodium channels, resulting in membrane depolarisation to around 5 mV (phase 0). In phase 1 voltage-gated potassium channels are activated and begin to efflux potassium ions, resulting in a slight repolarisation to 0 mV. The potential is then maintained at 0 mV by the action of L-type calcium channels in phase 2, which causes a slow influx of calcium ions. The calcium channels are gradually inactivated and the efflux of potassium through voltage-gated channels including hERG results in repolarisation back to the resting state (phase 3). The voltage gated potassium channels then inactivate when the resting potential is reached. The length of the plateau (phase 2) is particularly important, because it is the influx of calcium which ultimately stimulates muscle contraction through calcium-induced calcium release from the sarcoplasmic reticulum. The unusual gating kinetics of hERG make it well suited for maintenance of the plateau phase. Unlike homologous channels, such as the Shaker channels from *Drosophila*, hERG exhibits slow activation and fast deactivation, as well as fast voltage-dependent inactivation, meaning it is able to quickly stop effluxing potassium when the appropriate membrane potential is reached.

In an ECG the QT interval accounts for both ventricular depolarisation and repolarisation, providing an estimate of the ventricular action potential length. Extension of this interval gives rise to a condition called long-QT syndrome (LQTS). This is a serious condition which results in an irregular heartbeat, and can ultimately result in ventricular arrhythmia and sudden death. One of the most common types of LQTS, type 2, is closely associated with hERG due to its role in membrane repolarisation, and is caused by channel mutations[298], in which expression of the channel is reduced. hERG is also implicated in drug induced LQTS (diLQTS)[299], which occurs due to channel blockage by drug binding and therefore delayed and heterogenous repolarisation. This is a significant challenge for the pharmaceutical industry, with around 10 % of drug discontinuations attributed to diLQTS[300]. Additionally, hERG has also been associated with cancer[301] and a range of other diseases[302].

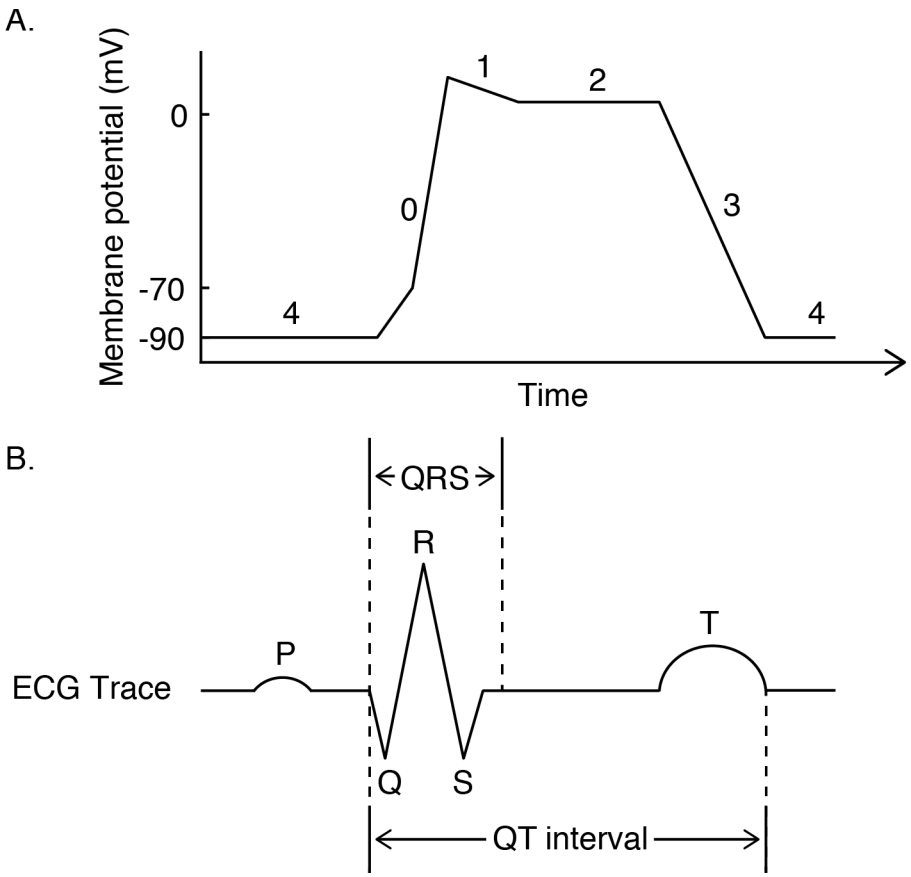

Figure 4.1: ***Schematic diagrams of membrane potential in a cardiomyocyte (A.) and electrocardiogram (ECG) trace (B.) during an action potential.***

In particular the proclivity of hERG for non-specific drug binding and the subsequent effect on the AP has made it an important target for structural studies. It is known to bind a wide range of different pharmaceuticals, including drugs from families including antiarrthymics (e.g. quinidine), antidepressants (e.g. fluoxetine), antihistamines (e.g. astemizole) and antibiotics (e.g. erythromycin)[303]. The extent of its pharmacological promiscuity is such that United States drug regulators indicate that new drugs should undergo preclinical testing to determine whether they block hERG[304]. It was previously suggested that there is a larger cavity in the pore of the channel than other potassium channels, which provides additional space for drug binding[299]. It has also been noted that the drugs which block hERG have conventionally been thought of as having a nitrogen centre flanked with either hydrophobic or aromatic groups, which were viewed to interact with a binding site via hydrophobic or cation-π interactions with specific residues[305, 306], particularly in the pore forming S6 helix. More recently, drugs without these features have also been found to block the channel[307], indicating that there is a broad range of drugs which block the pore. Very recently a cryo-EM structure of the transmembrane domain has been published by Wang and MacKinnon at ~4 Å resolution[308] (Figure 4.2) which

identifies hydrophobic pockets leading off the central pore cavity, which are speculated by the authors to permit part of the drug to bind rather than the complete molecule. They suggest in the case of astemizole, an antihistamine withdrawn from sale due to its potent hERG blocking action, one of its aromatic rings fits well into this hydrophobic pocket. Whilst we are beginning to understand the features of hERG which contribute to its penchant for drug binding, the mechanistic effects of drug binding and resulting conformational changes of the channel remains unknown.

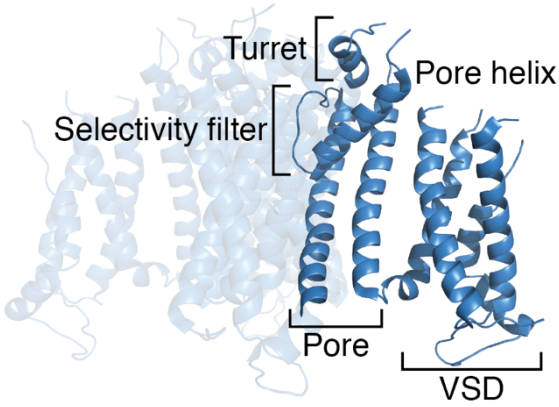

Figure 4.2: ***Structure of hERG TMD****. The S1-S4 helices form the voltage sensing domain (VSD) whilst S5-S6 form the pore. Cytosolic domains have been removed for clarity. Figure drawn from pdb accession number 5va1 from Wang and MacKinnon*[308].

The structure of the TMD comprises six helices (S1-S6) which can be split into two domains, the voltage sensing domain (S1-S4) and the pore forming domain (S5-S6) (Figure 4.2). Within the voltage sensing domain, which gates the channel, the S4 helix is regularly interspersed with positively charged residues which are thought to alter the confirmation of the protein in response to voltage gradients[296]. The pore forming region is somewhat similar to KcsA, with a pore helix and selectivity filter between the two helices. There are subtle changes in the structure of selectivity filter compared with other potassium channels which are apparently responsible for the rapid inactivation observed exclusively in hERG, and seem to result at least partially from sequence of the filter, which in hERG is SVGFG compared to the TVGYG found in a majority of other potassium channels[308]. The change of the F to Y is particularly significant, and has been linked to the rapid inactivation observed in hERG channels. It has been demonstrated in the *Drospohila melanogaster* Shaker potassium channel that mutation of its the GFG sequence to GYG results in accelerated inactivation[309]. A further notable structural dissimilarity between other K_v channels and hERG is the presence of an extended loop region between S5 and

the pore helix, the 'turret', which is approximately 40 residues long in contrast to the typical 15 residues[296]. Isolated fragments of this region have been structurally characterised using solution-state NMR[310] which indicates it forms an amphipathic helix in SDS micelles. It is also suggested that this domain is a determinant of gating, since the addition of exogenous peptide results in disruption of the channel gating[310] and mutation of charged residues in the S5P region of the *Ether-à-go-go* family appears to demonstrate the importance of the interaction of the helix with the rest of the channel to regulate inactivation[311]. The turret has also been demonstrated to have roles in ion selectivity of the channel[310], and can act as a 'pre-filter' to limit which cations are able to reach the selectivity filter[312]. The protein has large cytosolic domains at both the N and C termini. At the N terminus is a Per-Arnt-Sim (PAS) domain[313], whilst the C terminus contains a cyclic nucleotide binding domain[314], both of which are implicated in channel gating.

The work here aims to express, purify and reconstitute in lipids sufficient quantities of hERG to allow study of the response of the pore domain to drug binding events by NMR and OCD. Both techniques would readily allow assessment of the changes in helix orientation when drugs are bound. In order to do this, a construct of the hERG pore was produced encoding the S5-S6 helices complete with extended loop region between, yielding a KcsA-like construct. Using protocols for KcsA expression and purification as a starting point we attempted to optimise expression of hERG pore in *E. coli* and its purification.

4.1.2. *Streptomyces lividans* potassium channel KcsA

Although this chapter aimed to optimise purification and expression of hERG for further studies, the eukaryotic potassium channel KcsA has been studied extensively as a model potassium channel, and as such is used here to develop a basis for hERG expression.

The structure of KcsA was solved in 1998 by the group of Roderick MacKinnon[315], and was the first structure of any potassium channel (Figure 4.3). Since then it has been extensively characterised and has contributed greatly to our understanding of potassium channel structure and function. The protein contains just two transmembrane domains per monomer which form the pore domain (M1 and M2 helices). The selectivity filter is located at the extracellular side of the pore, near to the turret, and has the highly conserved TVGYG amino acid sequence which is present across almost all potassium channels. In the tetrameric complex the selectivity filter forms at least four K^+ binding sites (S1-S4), which are produced from by the positioning of carbonyl oxygens of the selectivity filter. These

act to mimic the hydrating water for K^+ ions in the channel. Only two sites are occupied by K^+ ions at any time, in pairs of S1-S3 or S2-S4, with the remaining sites containing a water molecule[315]. When an ion enters the filter there is a concerted movement of ions through the binding sites, resulting in the ejection of an ion from the opposite side. The channel is regulated via pH. At low pH protonation induces motion of the cytosolic ends of the M2 helices which essentially blocks the channel, and further conformational changes in the selectivity filter to alter its affinity for K^+[316]. Channel gating is also influenced by voltage across the membrane, and appears to be mediated through interactions between E71 and D80 in the selectivity filter, which are disrupted during depolarisation, leading to the filter's collapse[317].

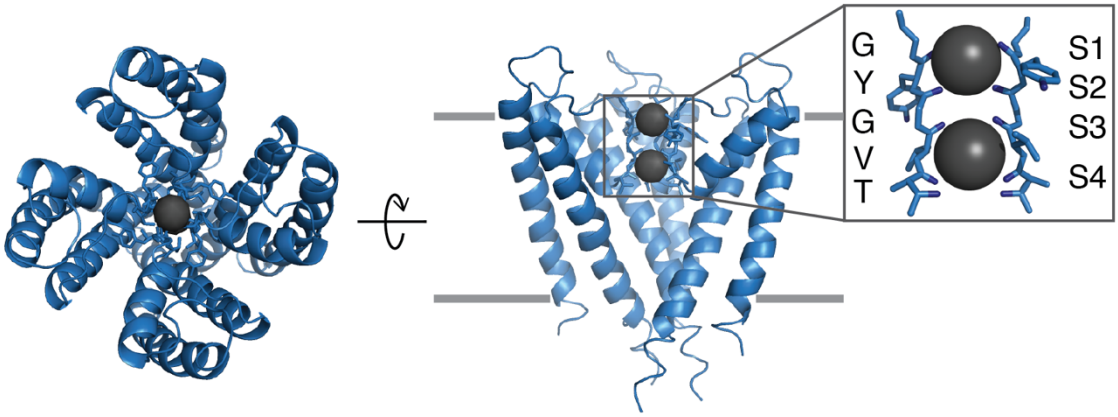

Figure 4.3: ***Structure of the model potassium channel KcsA.*** *One helix from each of four subunits form the pore itself, with a smaller pore helix forming the top of the cone shaped pore. The selectivity filter (inset) at the top of the pore coordinates K^+ binding (shown as grey spheres); only filters from two of the four monomers are shown for clarity. Figure generated using pdb accession number 1bl8.*

4.2. Methods and materials

4.2.1. Materials

Please refer to materials in Chapter 2. OG was sol-grade (≥98 %) and sourced from Anatrace. Sarkosyl solution (30 % w/v) at 99 % purity was purchased from Sigma-Aldrich. Disuccinimidyl suberate (DSS) was purchased from Sigma-Aldrich. Ampicillin was used at 100 mg mL^{-1} concentration in all agar and media.

4.2.2. Methods

4.2.2.1. Molecular cloning

Restriction endonuclease digestions

Restriction digests were performed on 1 μg DNA in a total reaction volume of 20 μL. Each BamHI (Promega, UK) digestion was performed using 5 U of restriction endonuclease, in accordance with the supplied instructions. CpoI digests were prepared with 1 μL of FastDigest CpoI (Thermo Scientific) again in accordance with manufacturer's instructions. Following digestion, the reaction was terminated and DNA purified from the mixture using using phenol-chloroform extraction.

Phenol-chloroform extraction

Phenol-chloroform extraction was employed in order to terminate enzymatic reactions and isolate DNA from reaction mixtures. To one volume of DNA solution, one volume of phenol:chloroform:isoamyl alcohol (25:24:1, pH 8.0) was added. The solution was mixed by vortex and centrifuged at 13 000 *g* for 5 minutes. The upper aqueous phase was aspirated and DNA precipitated using ethanol precipitation: one-tenth volume of 3 M sodium acetate pH 5.4 with two volumes of ice cold absolute ethanol was added to the aqueous phase and the mixture was vortexed and centrifuged again. The supernatant was removed and the resulting DNA pellet washed with 70 % ethanol. The DNA pellet was then dried at 37 °C for 30 minutes before resuspension in an appropriate volume of ddH_2O.

Agarose gel electrophoresis and gel extraction

Plasmid digests were analysed by agarose gel electrophoresis. Gels were prepared with 1.5 % (w/v) agarose and 0.4 μg mL^{-1} ethidium bromide in TAE buffer (40 mM Tris, 20 mM acetic acid, 1 mM EDTA) and run at 120 V. Samples were prepared by addition of 6x orange G dye to yield 1x final concentration. DNA bands were visualised under UV.

To purify the digested DNA from the agarose gels the appropriate bands were excised. The gel slice was then dissolved and DNA purified by anion exchange columns according to the standard protocol provided in the Wizard SV Gel and PCR Clean-up Kit (Promega). The extracted DNA was eluted in 50 μL ddH_2O.

Dephosphorylation reactions

To prevent self-ligation of the vector during ligation, the 5' phosphate was removed using thermosensitive alkaline phosphatase (ThermoScientific FastAP). Typically 0.5 μg of digested plasmid was used per reaction with 0.5 U of enzyme. Reactions were incubated for 10 minutes at 37 °C and then heat inactivated at 75 °C for 5 minutes. Dephosphorylated plasmid from the inactivated reaction was used for ligation without further purification.

Ligation reactions

Ligation reactions were prepared with a total volume of 10 μL and 50 ng digested vector. The amount of insert was varied to achieve molar ratios of 1:1, 3:1 and 10:1 for insert:vector. 1 U of T4 DNA ligase (Promega) was used per reaction in 1x ligase buffer and incubated at 4 °C overnight.

Plasmid isolation and minipreparation

Following ligation, 2 μL of ligation product was diluted to 25 μL in ddH2O and transformed into competent DH5α cells (Invitrogen) using the manufacture's protocol. Following the 1 mL outgrowth stage, 200 μL of culture was spread onto LB-agar plates with ampicillin and incubated at 37 °C overnight. To prepare cultures for plasmid isolation one colony was picked and used to inoculate 5 mL of LB media supplemented with ampicillin. These cultures were incubated at 37 °C, shaking, for 16 – 18 hours. After incubation cells were pelleted at 2000 *g* for 10 minutes at 4 °C and then resuspended, lysed and the plasmids isolated using a Wizard SV Miniprep Kit (Promega) according to manufacture's protocol. The final isolated plasmid was used for sequencing without further purification. Concentrations of DNA were measured at 260 nm and the 260/280 nm ratio was monitored to ensure sample purity.

DNA sequencing

Plasmids were submitted to Eurofins Genomics for Sanger sequencing using the pTrcHis-rev primer (5'-CTTCTGCGTTCTGATTTAATCTG-3') which binds following the C

terminus of the hERG pore gene on the reverse strand. Resulting chromatographs were analysed using 4Peaks software (www.nucleobytes.com/4peaks).

4.2.2.2. KcsA expression

A construct encoding the nucleotide sequence for full-length KcsA with a N-terminal 6x histidine tag was cloned into a pQE32 vector previously by Dr Phedra Marius, yielding a protein with the following amino acid sequence:

```
MRGSHHHHHHGIRMPPMLSGLLARLVKLLLGRHGSALHWRAAGAATVLLV      (50)
IVLLAGSYLAVLAERGAPGAQLITYPRALWWSVETATTVGYGDLYPVTLW     (100)
GRLVAVVVMVAGITSFGLVTAALATWFVGREQERRGHFVRHSEKAAEEAY     (150)
TRTTRALHERFDRLERMLDDNRR                                 (173)
```

The construct was transformed into chemically competent BL21 pLysS *E. coli* (New England Biolabs, UK) according to manufacturer's instructions and used to inoculate 100 mL LB media with ampicillin which was incubated shaking at 37 °C overnight for 16 hours. 10 mL of this culture was used to inoculate 1 L of LB media which was cultured at 37 °C until the OD600 reached 0.8. At this point expression was induced by addition of IPTG to a final concentration of 1 mM, and the cells cultured for an additional 4 hours. Cells were harvested by centrifugation at 4 000 *g* for 20 minutes at 4 °C. If not used immediately cell pellets were stored at -20 °C.

4.2.2.3. KcsA purification

The cell pellet from 2 L culture was resuspended in 80 mL buffer A (50 mM Tris-Cl pH 7.4, 150 mM KCl, 150 mM NaCl) with 1 mM phenylmethane sulfonyl fluoride (PMSF) and lysed by sonication on ice using a programme of 10 s on, 30 s off for 5 minutes total process time at power level 7 (Misonix XL sonicator with stud probe). Cell membranes were fractionated by ultracentrifugation at 142 000 *g* for 40 minutes at 4 °C. The membrane pellet was then homogenised in 40 mL solubilisation buffer (buffer A, 10 mM DDM, 40 mM imidazole) and stirred slowly at room temperature for 90 minutes. Insoluble material was pelleted by centrifugation at 20 000 *g* for 30 minutes at 4 °C. The resulting clarified solubilised membrane fraction was filtered through a 0.45 μm filter. The solubilised membrane fraction was then applied at 0.2 mL/minute to a 1 mL HisTrap column prequilibrated with wash buffer (buffer A, 1 mM DDM, 40 mM imidazole). 1 mL fractions were eluted with elution buffer (buffer A, 1 mM DDM, 400 mM imidazole).

To purify KcsA in sarkosyl the protocol was identical but the DDM was exchanged for sarkosyl at the following concentrations: 0.9 % w/v for solubilisation buffer and 0.15 % w/v for wash and elution buffers.

4.2.2.4. hERG pore expression

A construct for the hERG pore domain was previously produced by Dr Maïwenn Beaugrand (from a full length hERG construct produced by Prof Alvin Shrier, McGill University, Canada), encoding D540-Y673 (UniProt accession number Q12809) in a pPROEX HTa backbone vector. The amino acid sequence of this construct is:

```
MSYYHHHHHHDYDIPTTENLYFQGAMDPDRYSEYGAAVLFLLMCTFALIA      (50)
HWLACIWYAIGNMEQPHMDSRIGWLHNLGDQIGKPYNSSGLGGPSIKDKY     (100)
VTALYFTFSSLTSVGFGNVSPNTNSEKIFSICVMLIGSLMYASIFGNVSA     (150)
IIQRLYSGTARY                                            (162)
```

For recombinant protein expression, the construct was transformed into chemically competent BL21 *E. coli* by diluting 50 ng of plasmid in 25 µL sterile H_2O and adding to 50 µL competent cells. After 30 minutes incubation on ice, the cells were heat shocked at 42 °C for 45 s then incubated on ice for an additional two minutes. 925 µL LB was then added and the mixture incubated at 37 °C, shaking, for one hour. Subsequently it was added to 100 mL LB media with ampicillin. The culture was grown at 37 °C, shaking, for 16 hours overnight and 5 mL was then used to inoculate 500 mL of 2xYT media with ampicillin. The culture was incubated at 37 °C, shaking at 180 rpm, until an OD_{600} of 1.0 was reached. Protein expression was then induced through the addition of IPTG to 1 mM final concentration, and to counter the toxic effects of the pore 10 mM final concentration of tetraethylammonium bromide (TEAB) was also added at this point. After a further 16 hours incubation at 18 °C the cells were harvested at 4 °C by centrifugation at 5000 *g* for 20 minutes.

4.2.2.5. hERG pore purification

Initially hERG pore was purified according to the following protocol with modification and optimisation as described in the results section. Purification buffers were based on phosphate buffered saline (PBS) with composition 137 mM NaCl, 2.7 mM KCl, 10 mM Na_2HPO_4 and 1.8 mM KH_2PO_4, pH 7.4.

The harvested cell pellet was resuspended in 40 mL lysis buffer (PBS pH 7.4, 0.2 mg mL^{-1} lysozyme, 1 mM EDTA) per 1 L culture and incubated for 30 minutes at room temperature. Cells were then lysed by sonication on ice using a programme of 10 s on, 30 s off for 6 minutes total process time at power level 7 (Misonix XL sonicator with stud probe). Cell debris was pelleted by centrifugation at 16 000 *g* for 30 minutes at 4 °C. The cell membranes in the supernatant were then collected by ultracentrifugation at 100 000 *g* for 50 minutes at 4 °C. The membrane pellet was homogenised in 50 mL solubilisation

buffer (PBS pH 7.4, 3 % w/v sarkosyl, 20 mM imidazole) and mixed slowly at 4 °C for 16 hours. The resulting solubilised membrane fraction was passed through a 0.45 μm filter and 1 mL Ni^{2+} Sepharose Fast Flow resin (GE Healthcare, UK) added. After 2 hours incubation at 4 °C the resin was applied to a gravity flow column and the flow through collected. The resin was then washed with 60 mL wash buffer (PBS pH 7.4, 0.5 % w/v sarkosyl, 20 mM imidazole) and 6x 1 mL fractions eluted with elution buffer (PBS pH 7.4, 0.5 % w/v sarkosyl, 600 mM imidazole).

Later in the chapter an inclusion body purification protocol is described, in which the cells are lysed as above and then subjected to centrifugation at 16 000 *g* for 30 minutes at 4 °C. The resulting pellets of cell debris and inclusion bodies were then resuspended in 40 mL/L culture of appropriate solubilisation buffer (PBS pH 7.4, 20 mM imidazole with denaturant as described in results section) using a homogeniser then left to solubilise for at least 16 hours. The centrifuge step was repeated to pellet any remaining insoluble material, and 1 mL Ni^{2+} resin was added to the supernatant. After allowing to bind at 4 °C for 2 hours the resin was washed and protein eluted using PBS with either 20 mM and 600 mM imidazole respectively, with the same concentration of denaturant as solubilisation buffer.

4.2.2.6. Determination of protein concentration

The protein concentration following purification was determined using either absorbance at 280 nm (A_{280}) readings or bicinchoninic acid (BCA) assay. A_{280} reading were measured using 2 μL samples blanked against elution buffer using a NanoDrop 2000C spectrophotometer (Thermo Scientific). BCA assays were performed in 96 well plates using a kit (Pierce protein assay kit) with bovine serum albumin (BSA) standards from 0.25 mg mL^{-1} to 1.5 mg mL^{-1}. The manufacture's microplate protocol was followed, which briefly involves mixing 10 μL of sample or standard with 200 μL kit reagent, incubating at 37 °C for 30 minutes then measuring the absorption at 580 nm. The BSA standard curve was then used to estimate protein concentration.

4.2.2.7. Membrane protein reconstitution

KcsA and hERG were reconstituted in model membranes using the detergent adsorption method. The following protocol was used for approximately 1 mg purified protein and then scaled as appropriate. Lipids from methanol stocks were aliquoted and dried overnight under high vacuum. The resulting film was then resuspended in 10 mL hydration buffer (10 mM Tris-Cl pH 7.4, 1 mM EDTA, 40 mM OG) by gentle pipetting. The lipid suspension was subsequently sonicated at room temperature in an ultrasonic bath for

30 minutes or until the solution had clarified, indicating the formation of SUVs. Protein in elution buffer was then added to the vesicles and gently mixed. Detergent was removed by the addition of 4.4 g Bio-Beads SM2 resin (Bio-Rad, UK) in two batches, with each addition followed by a one hour incubation with slow stirring. The resin was then removed from the solution and the vesicles collected by ultracentrifugation at 133 000 *g* for 30 minutes at 4 °C.

4.2.2.8. Sucrose density gradient

Separation of precipitated protein from proteoliposomes was achieved using a sucrose density gradient with layers of 35, 39 and 50 % w/v sucrose. Each layer was formed of 3 mL sucrose solution at the appropriate concentration and approximately 3 mL sample was applied to the top. The gradients were ultracentrifuged in a swingout rotor (Beckmann-Coulter SW41) at 100 000 *g* for 4 hours at 4 °C. A slow deceleration profile was selected to prevent disruption of the gradient. A fine tube attached to a peristaltic pump was then used to remove the visible band of liposomes, which were analysed by SDS-PAGE.

4.2.2.9. Chemical cross-linking

The stability of the hERG pore tetramer was probed using chemical cross-linking in lipid vesicles. The cross-linker DSS was used, which has a two functional groups which react with primary amines and are separated by an eight carbon spacer. A DSS stock of 90 μg mL^{-1} in dimethylsulphoxide (DMSO) was prepared. To set up cross-linking reactions, 500 μg hERG pore was reconstituted into POPC/POPG (50:50) at approximately 200 L/P ratio. The sample was split into two and either sonicated for 20 minutes (to yield SUVs) or resuspended (for MLVs). Each SUV or MLV sample was then split again and 2 μL of either DSS in DMSO or DMSO added. Samples were incubated at room temperature for 1 hour, then the reaction was terminated by the addition of gel loading buffer.

4.2.2.10. SDS-PAGE and western blot

Success of protein purification and degree of purity was determined using Coomassie stained 10 % polyacrylamide gels and western blotting against the polyhistidine tag. SDS gels were prepared and run according to section 2.2.2.1. Typically 10 μL samples were used without concentration normalisation. Purity of the elution fractions was estimated using densitometry analysis with ImageJ software[318].

For blotting, the unstained gel was wet transferred to 0.2 µm nitrocellulose membrane in transfer buffer (25 mM Tris, 190 mM glycine, 20 % methanol) at 100 V for one hour. Blotting was performed using the Li-Cor Quick Western Blotting kit (Li-Cor, Cambridge, UK). Membranes were blocked for 1 hour at room temperature in 5 % w/v BSA in PBS. Membranes were probed in using anti-polyhistidine antibody (Sigma-Aldrich, UK) at 1:3000 dilution in detection reagent according to manufacturer's instruction. After washing in PBS-Tween-20 (0.5 % v/v), blots were imaged using the 700 nm channel of an Odyssey Classic imager (Li-Cor).

4.2.2.11. Electrospray mass spectrometry

Methanol-chloroform extraction and mass spectrometry were performed as described in section 2.2.2.1.

4.2.2.12. Circular dichroism measurements

CD measurements were recorded using a nitrogen flushed Jasco J720 spectropolarimeter. KcsA was buffer exchanged using a PD-10 desalting column (GE Healthcare, UK) into 10 mM potassium phosphate buffer pH 7.4, 1 mM DDM at 0.1 mg mL^{-1} concentration. Spectra were measured at room temperature using a 2 mm pathlength cuvette with 1 nm step resolution, 2 nm bandwidth and 1 s response time. The presented spectra represent the average of no fewer than eight scans baseline corrected against the sample buffer. Units were converted as described in 2.2.2.1.

4.3. Results

4.3.1. KcsA

Initially to demonstrate the expression and purification of a potassium channel as a basis for hERG pore, the KcsA potassium channel was expressed and purified was based on the method used by Marius et al.[66] and modified within the laboratory. The sequence of the KcsA protein, annotated with key features is given in Figure 4.4.

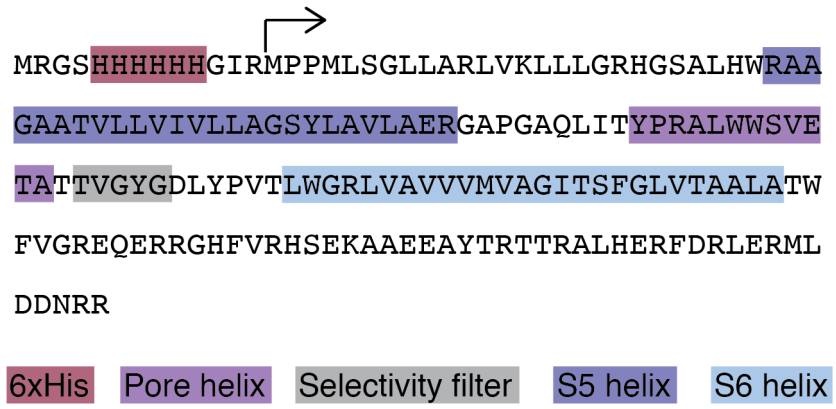

Figure 4.4: ***Annotated sequence of KcsA.*** *The key features of the sequences are indicated, including a 6x histidine tag for affinity chromatography, and selectivity filter, transmembrane helices and the pore helix. Arrow indicates the start of the KcsA sequence (from M1). Sequence from UniProt, accession number P0A334.*

The protocol involves heterologous expression of the protein in *E. coli*, solubilisation in detergent and purification using nickel affinity chromatography. Initially the detergents DDM and sarkosyl were selected, DDM because of its previous use in purification of KcsA and sarkosyl because initial detergent screening by previous members of the group had identified it as an efficient solubiliser of hERG pore. Coomassie stained acrylamide gels of purified KcsA in both detergents (Figure 4.5) have a predominant band at around 55 kDa which is assigned to the tetrameric KcsA complex, despite the predicted molecular weight of a tetramer totalling 77.2 kDa. (The predicted molecular weight of the monomer was determined to be 19.3 kDa by ProtParam[199].) Note that in this gel, as the proceeding gels, the samples were not adjusted for concentration. The shifted band position is a common observation for membrane proteins, and is likely to result from either only partial denaturation of the protein or the change in micelle size due to the solubilising detergent[200]. It is also unsurprising to observe a tetramer in a denaturing environment, since it has been previously reported that the KcsA tetramer is highly stable under the denaturing conditions of SDS-PAGE[319].

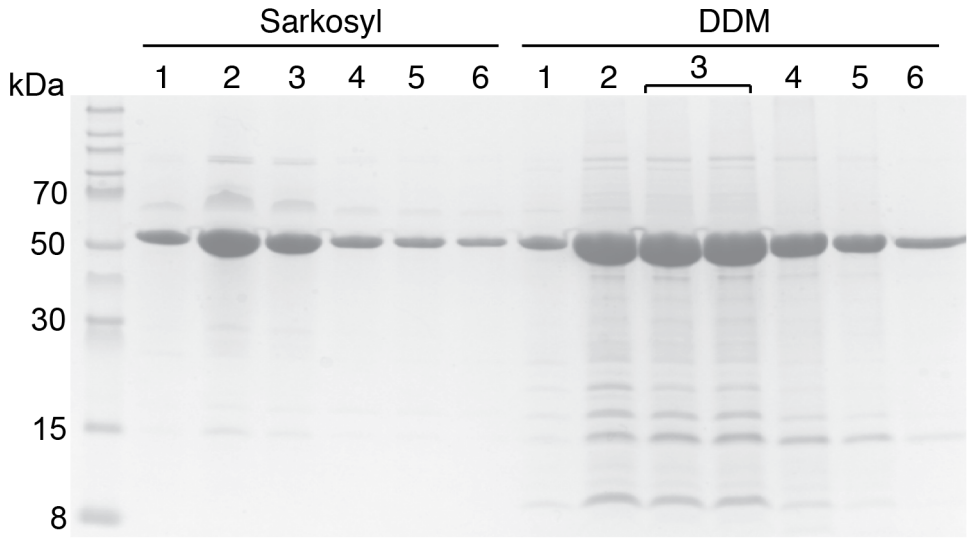

Figure 4.5: ***Coomassie stained SDS gel of KcsA elution fractions following solubilisation in either sarkosyl or DDM.***

There is a notable improvement in purity of the eluate between the KcsA solubilised in DDM and the protein solubilised in sarkosyl. Manufacture's literature for nickel affinity resin generally advices against the use of anionic detergents in purification due to their tendency to limit protein binding, suggesting that affinity for both the contaminating proteins and the KcsA is reduced. Indeed, the total yields (by A_{280}) were 6.38 mg/L culture for sarkosyl and 8.36 mg/L culture for DDM.

Although the yield of sarkosyl solubilised KcsA is lower than DDM, the purity appears to be slightly better. Assessment of the purity was carried out using densitometry analysis. As the lanes were somewhat overloaded the fifth fraction was analysed to ensure the results are accurate. High purity was achieved in both cases, with 93.1 % for sarkosyl, and a slight reduction to 91.4 % for DDM. This purity of the protein was such that further chromatography steps were unnecessary prior to reconstitution in liposomes. The protein was exchanged into 10 mM potassium phosphate, 1 mM DDM from the elution buffer and CD spectra acquired (Figure 4.6) which show features consistent with a predominantly helical structure, with the characteristic positive peak at 190 nm and two negative peaks around 208 and 222 nm. KcsA solubilised in sarkosyl could not be studied by CD due its high absorbance in the far-UV region[320].

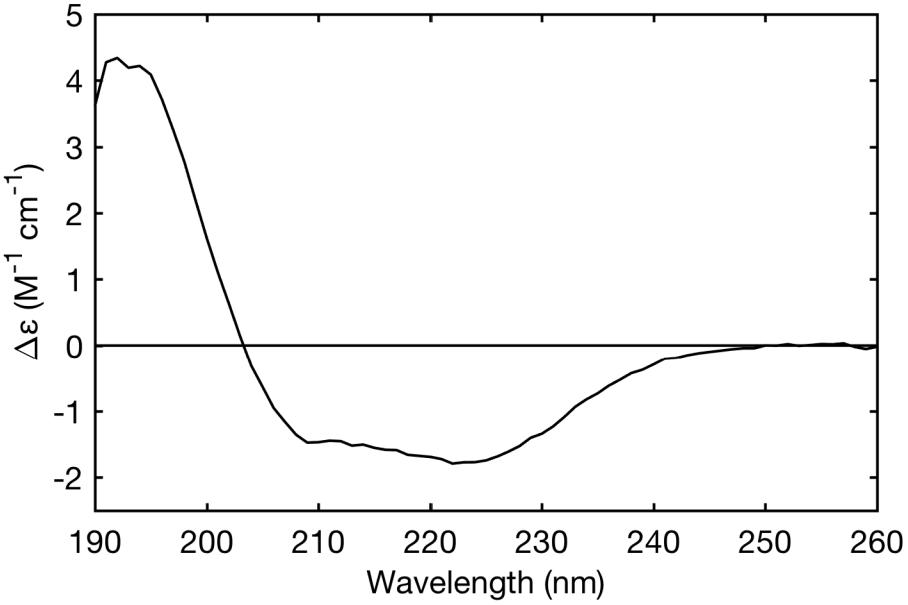

Figure 4.6: ***Conventional CD spectrum of purified KcsA in 1 mM DDM, 10 mM potassium phosphate pH 7.4.*** *Protein concentration was 0.1 mg mL^{-1} and pathlength 2 mm. Spectra were acquired at room temperature with 1 nm step resolution, 2 nm bandwidth and 1 s response time.*

To prepare oriented samples for OCD and NMR studies it is essential to be able to reconstitute the protein of interest into lipid vesicles. We were able to reconstitute KcsA successfully into POPC vesicles using the detergent adsorption method with polystene Bio-Beads resin. POPC was selected as it is a commonly used membrane mimetic with a low phase transition temperature. Following reconstitution, the proteoliposomes were collected and isolated using a sucrose density gradient to ensure that any precipitated protein was removed. Subsequent SDS-PAGE analysis revealed the presence of both monomeric and tetrameric KcsA in both sarkosyl and DDM solubilised protein, although in different ratios. The sarkosyl solubilised KcsA has a predominant monomer band whereas for DDM it is mostly tetrameric, despite a clear predominance of the tetramer in both DDM and sarkosyl eluate fraction. This was somewhat unexpected since the KcsA tetramer is known to be highly stable, resistant to both SDS and thermal induced destabilisation[321]. It is possible in this case that during the reconstitution some of the KcsA in sarkosyl denatures rather than becomes incorporated in the lipid vesicles, resulting in the presence of the monomeric band.

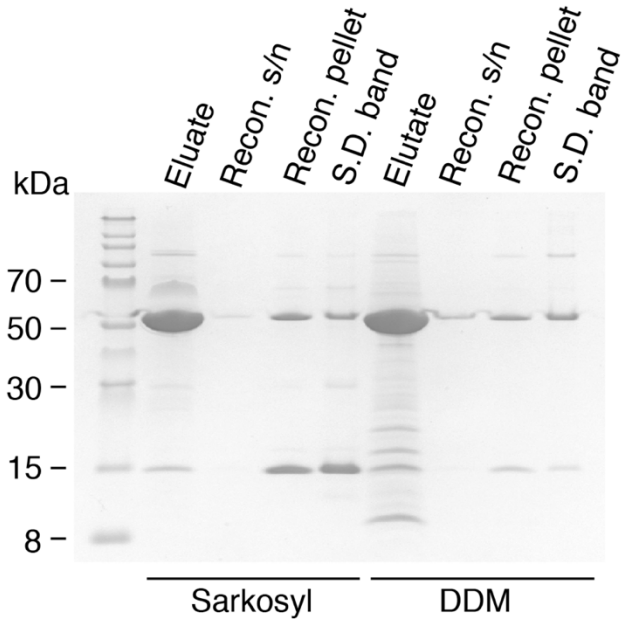

Figure 4.7: ***Coomassie stained SDS gel of purified KcsA in either DDM or sarkosyl reconstituted into POPC vesicles using Bio-Bead adsorption method.*** *Recon s/n is the supernatant following harvesting of proteoliposomes after reconstitution, recon. pellet is the harvested proteoliposomes and the S.D. band is the proteoliposome band collected from the sucrose density gradient.*

Ultimately the results here duplicate the previous successful attempts to express, purify and reconstitute recombinant KcsA in DDM[65], and demonstrate that sarkosyl results in a higher degree of purity than DDM but may present a problem for downstream reconstitution. As a result of the ability to purify mg quantities of KcsA with relative ease, it has been widely studied and investigated as a model potassium channel, but as it is bacterial prokaryotic protein it cannot be fully representative of eukaryotic homologues. It is significantly different to hERG, particularly the extended loop region between S5 and S6. However, the successful expression and purification protocols available for KcsA makes an excellent starting point for the expression and purification of the human potassium channel hERG.

4.3.2. hERG

There are two major structural distinction between the KcsA and hERG transmembrane domains. hERG has a much larger loop region between the two helices of the pore forming domain (S5 and S6 helices) than KcsA, and significantly a four helical voltage sensing domain at the N-terminal transmembranous region. To improve the chances of successful expression and purification of the hERG pore domain in *E. coli*, the sequence encoding a voltage-sensing domain was removed from the construct and a hexahistidine tag and linker

added at the N-terminal end (Figure 4.8), to produce a construct homologous to KcsA. (The cytosolic domains are not present in this construct.)

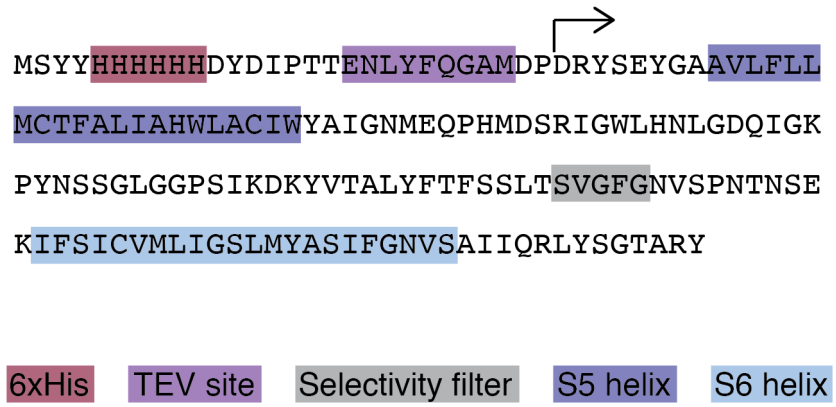

Figure 4.8: ***Annotated amino acid sequence of hERG pore domain from D540 to Y673 construct encoded within phERGPore plasmid.*** *Key features of the sequence are indicated including a 6x histidine-tag (his-tag) to allow affinity chromatography and a tobacco etch virus (TEV) protease cleavage site for removal of the his-tag following purification. Arrow indicates start of hERG pore sequence (from D540). Sequence from UniProt accession number 12809.*

4.3.2.1. Expression and purification of hERG pore with a 6x histidine tag

Extensive previous work within the group (by Dr Maiwenn Beaugrand and Mr Rafael G.B. Gomes) had identified optimal conditions for expression of the hERG pore construct. The plasmid was transformed into *E. coli* BL21 (DE3) and cultured using ampicillin selection. hERG pore expression was induced using 1 mM IPTG for 18 hours at 18 °C. The previous work had determined that the expression of the channel appeared to have toxic effects on the *E. coli*, indicating that the pore has activity in the *E. coli* membrane. To mediate these effects, a potassium channel blocker, TEAB, was found to improve cell viability after induction. TEAB has been used extensively in electrophysiological studies of potassium channels as a blocking agent and is known to block hERG[322], and has been shown to have two distinct binding sites in voltage-gated potassium channels located at both the external mouth and the intraellular side of the channel[323, 324]. As such the concentration required was optimised and found to be 10 mM, which is added at the point of induction.

To initially ensure that this protocol resulted in protein expression the plasmid was transformed into both BL21 (DE3) and BL21 (DE3) pLysS cells and cultured. The pLysS cells contain an additional plasmid that results in reduced basal protein expression prior to

IPTG induction, which may be helpful since there was a suggestion that hERG pore is toxic to *E. coli* and 'leaky' expression may result in cell death. The expression was confirmed by western blot probed for his-tag (Figure 4.9). A single band is observed in each case, corresponding to the hERG pore monomer at approximately 15 kDa which is slightly lower than the predicated molecular weight of 18237.7 Da, not dissimilar to the shift observed for KcsA. There is no difference in band intensity between the two *E. coli* strains, indicating that if toxicity is an issue then it is not addressed by the pLysS. From this point standard BL21 (DE3) cell were used.

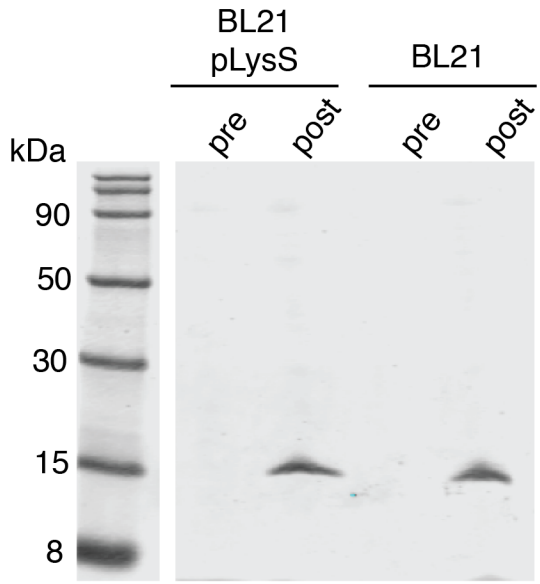

Figure 4.9: ***Western blot of phERGPore-transformed E. coli taken pre- and post-induction of protein expression, in BL21 (DE3) and BL21 (DE3) pLysS strains.*** *Membrane was probed for his-tag using an anti-hexahistidine primary antibody to identify hERG pore. The marker and samples were run on the same gel but lanes for other proteins were cropped for clarity.*

To purify the expressed protein, the previously developed protocol was initially used (*cf.* section 4.2.2.5). This involved binding the protein to a prepacked Ni^{2+} column (2x 1 mL HisTrap Crude (GE Healthcare) columns), washing with 20 mM imidazole (15 column volumes) and eluting in 8x 1mL fractions using 600 mM imidazole. The protocol was applied to cells harvested from 12 L of culture, and yielded a surprisingly low intensity band of hERG pore (Figure 4.10). There also are additional bands of higher molecular weight impurities present in these lanes. Although these bands are broadly in the molecular weight region of dimeric and tetrameric species of hERG pore, and elute in the same fraction as the monomer, previous western blot analysis has not identified these bands as

oligomers. Instead it is likely that these are a number of *E. coli* proteins that have affinity for nickel resin, of which there are a number of suitably sized candidates[325]. The purity of the eluate was low, just 23.6 % for fraction 3. The post-purification yield was approximately 0.5 mg/L culture (by A_{280}), around 13-fold less than for KcsA.

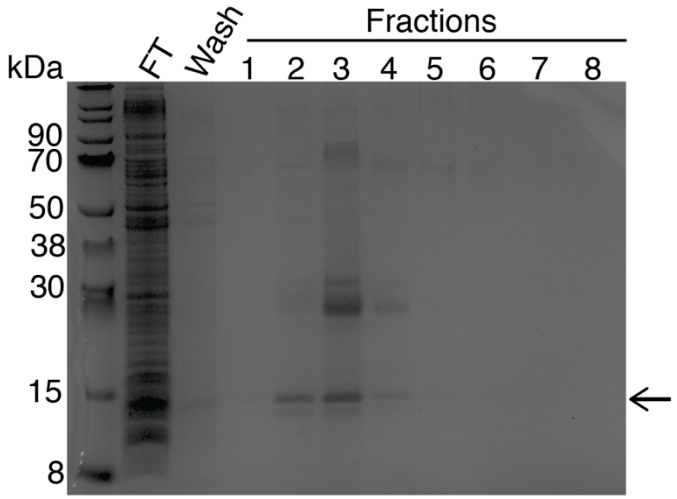

Figure 4.10: ***SDS-PAGE of purification of hERG pore from 12 L E. coli culture using Ni^{2+} Sepharose High Performance resin by batch method.*** *Column flow through (FT), washing and fractions were analysed.*

As the protein fractions were impure, we decided to elute the protein using a gradient of imidazole with the aim of eluting the contaminants and hERG in different fractions. The expression was scaled down to 6 L culture. An FPLC system was used to generate this gradient on a 1 mL Ni^{2+} HisTrap pre-packed column. In order to ensure sufficient contact time of the protein with the column, it was loaded at a flow rate of 0.5 mL $minute^{-1}$. After column washing, a linear gradient of 25 mL from 20 mM to 1 M imidazole was applied and 1 mL fractions collected. A large peak was identified towards the start of the gradient and subsequently these samples were analysed by SDS-PAGE (Figure 4.11). A small peak around fraction 18 was also sampled. hERG pore was apparent from the first peak and possibly in fraction 15, indicating a very broad elution profile. Gel electrophoresis revealed hERG pore in fractions 2, 3, 5, 6 and 15. In fractions 3 and 5, there are almost no other protein contaminants and a feint band of hERG, although there is a small amount of higher molecular weight proteins in fractions 6 and 15. The total yield, determined by BCA assay, was just 0.18 mg/L culture, which although less than fractions eluted using a single concentration of imidazole has vastly improved purity. The elution at the start of the gradient indicates that the protein binds with low affinity to the Ni^{2+} resin. This is also

indicated by bands for hERG pore in both the flow through and wash fractions on the gel, which are clear even though in both cases there was a reasonably large volume, suggesting hERG pore has a significant concentration in both fractions. It may be that longer binding times are required, potentially allowing a greater quantity of the hERG pore to bind, although the flow rate used here is slower than the rate recommended by the manufacture to attempt to improve binding.

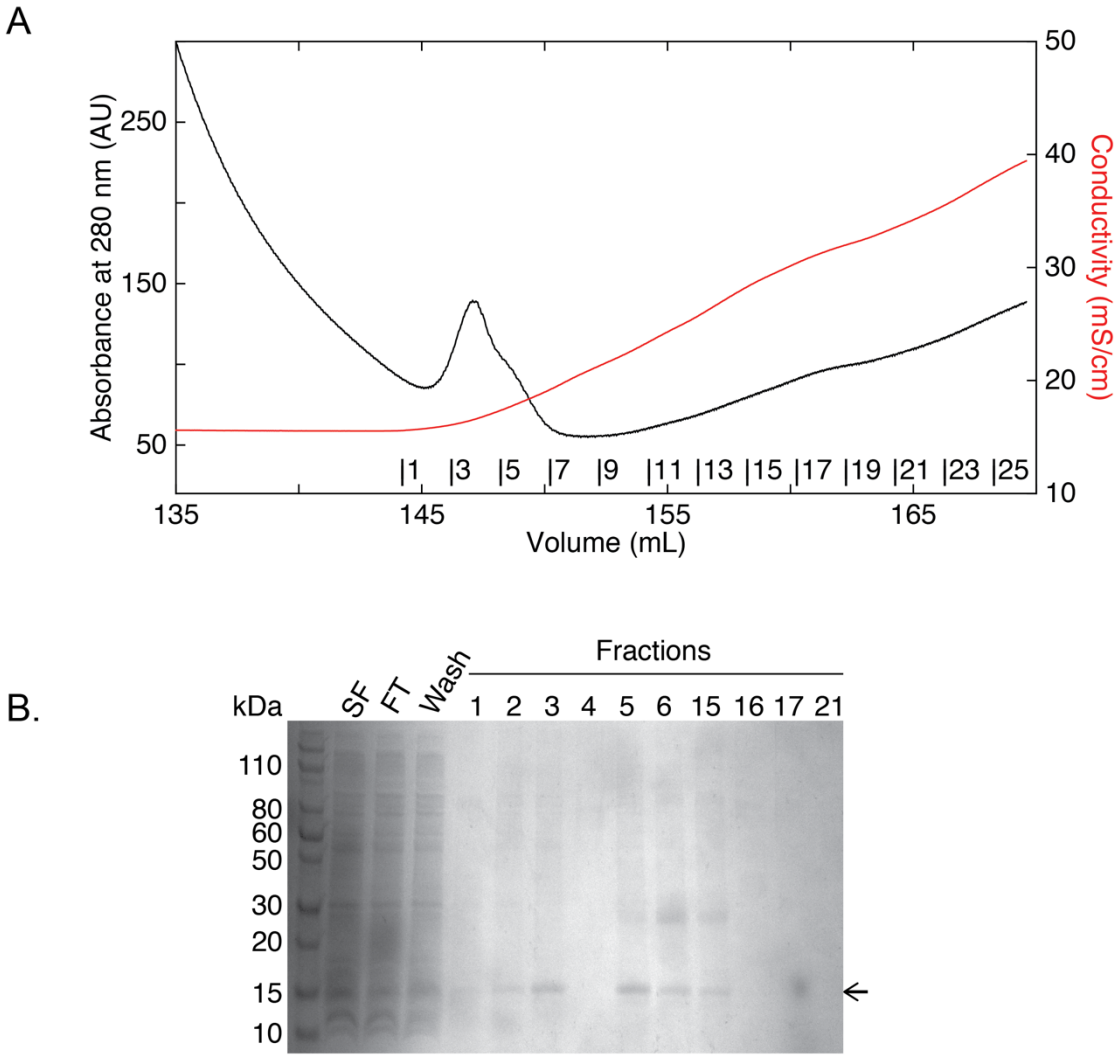

Figure 4.11: ***Purification of hERG pore in sarkosyl from 6 L*** **E. coli** ***culture using pre-packed HisTrap 1 mL Fast Flow (GE) column.*** *A. FLPC chromatograph of absorbance and conductivity. 1 mL fraction numbers are indicated along the x-axis. A 25 mL gradient of 20 mM to 1 M imidazole was initiated at fraction 1. B. SDS-PAGE analysis of stages of purification showing solubilised fraction (SF), column flow through (FT) and column wash. The analysed fractions were selected based on the chromatograph.*

To confirm the identity of the eluted proteins, the elution fractions from the first peak were precipitated using methanol-chloroform (*cf.* section 2.2.2.1) in preparation for mass spectrometry analysis (Figure 4.12). Deconvolution of the m/z spectra revealed a single peak at 18106 Da. This molecular weight corresponds to the calculated molecular weight less the initial methionine residue, which indicates the protein undergoes N-terminal methionine excision cleavage *in vivo*. Many recombinant proteins undergo such cleavage in *E. coli*, and a small group of residues in position two, such as the serine in hERG pore, vastly increase its likelihood[326]. Note that a second envelop is present in the lower end of the m/z spectra which was not included in the deconvolution. We attribute this band to a smaller molecular weight protein which 'flies' more readily from the sample cone, particularly since such a molecular weight band is not observed by SDS-PAGE.

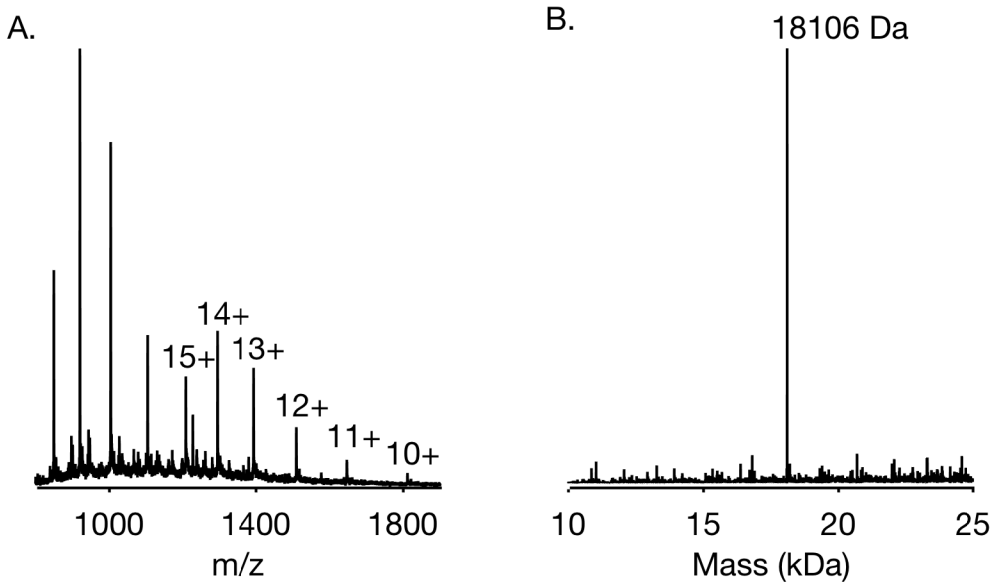

Figure 4.12: ***ESI-ToF spectra of hERG pore.*** *The envelope in the m/z spectra (A.) associated with the peak in the mass spectrum (B.) is annotated with the multiply charged states. The MaxEnt deconvolution was performed using the m/z values 1161 – 1841.*

The poor yield is potentially due to the low affinity binding of the protein with the resin, which may be due to the use of sarkosyl. The solubilised membrane fraction was applied to the column in 0.9 % w/v sarkosyl, and it is possible that this relatively high detergent concentration inhibits some of the protein binding. Manufacture's data sheets indicate that concentrations up to 0.2-0.3 % w/v are compatible in some circumstances but use of sarkosyl (and indeed all anionic detergents) with Ni^{2+} resin is generally discouraged. In light of this, an alternative detergent, DDM, was selected based on its successful use with a number of diverse membrane proteins, particularly KcsA. The purification process was

otherwise the same as for sarkosyl; membrane fractions were solubilised in 10 mM DDM and subsequent wash and elution buffers contained 1 mM, all in excess of the critical micelle concentration (CMC) of 0.2 mM.

The protein was again purified using a pre-packed Ni^{2+} column, with a longer imidazole gradient (50 mL) with a view to increased separation of contaminants and hERG pore (Figure 4.13A). Multiple peaks were identified immediately following the start of the gradient at fraction 27 over the broad range 28 – 38, contrasting with the elution profile observed for the previous purification using sarkosyl, but similarly indicating poor binding to the column, since the protein begins to elute almost immediately following the increase in imidazole concentration. Analysis of these fractions by SDS-PAGE (Figure 4.13B) shows a number of proteins across a broad range of molecular weights, including a band corresponding with those observed for hERG pore previously. This band is also visible in the solubilised membranes fraction, and to a lesser extent the flow through and wash steps. It is not clear whether this is specifically hERG or another *E. coli* protein. Overall there is a clear decrease in the purity of the eluate, and no tangible improvement in binding compared to sarkosyl. Presumably in the purification with sarkosyl it prevents binding of all proteins to the column, which results in the purer eluate. It is possible that with DDM the column is saturated with *E. coli* proteins so that hERG pore is eventually unable to bind, although assuming the his-tag is completely accessible the affinity of hERG pore should be greater than the majority of the native proteins.

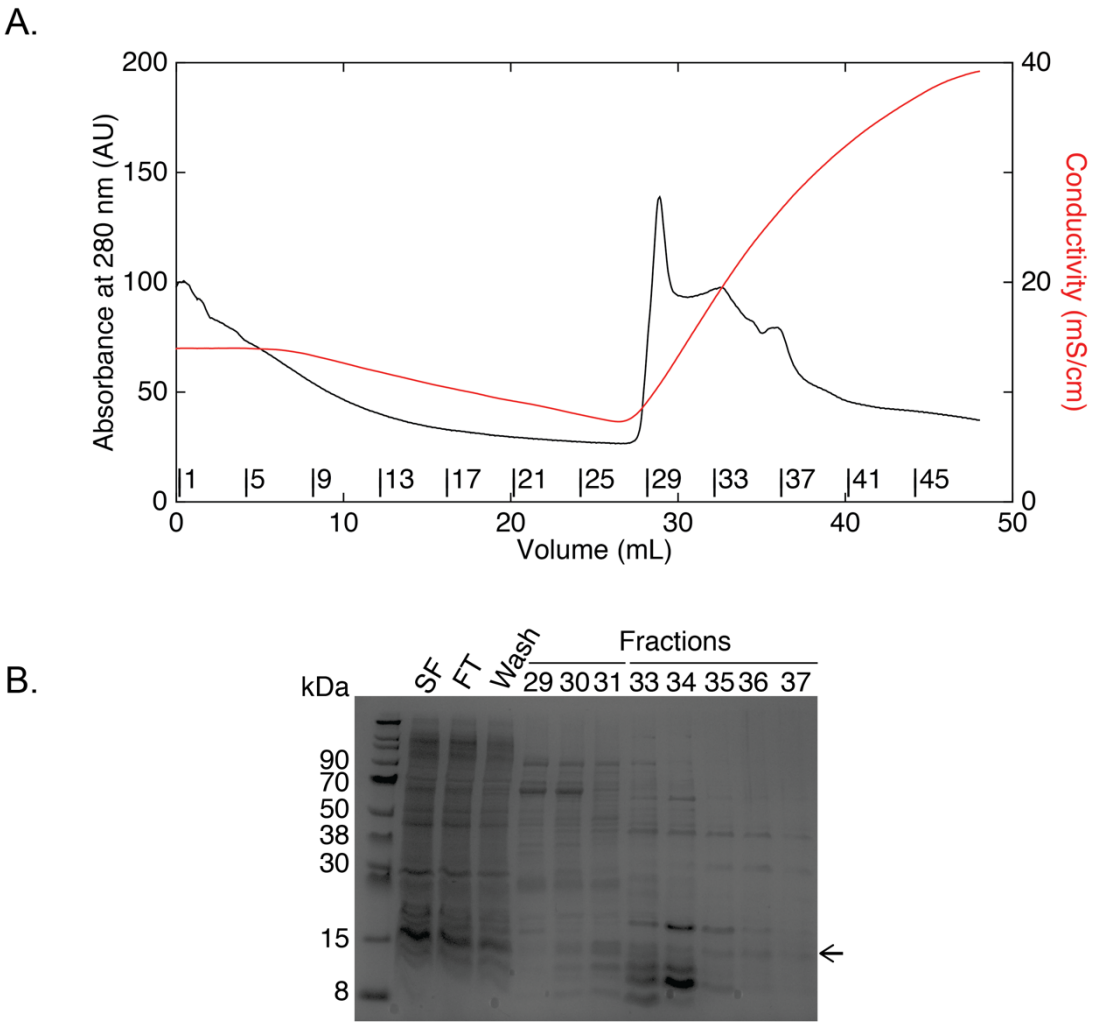

Figure 4.13: ***Purification of hERG pore in DDM from 6 L of E. coli culture using pre-packed HisTrap 1 mL Fast Flow (GE) column.*** *A. FLPC chromatograph of absorbance and conductivity. Number of 1 mL fractions are indicated along the x-axis. A 50 mL gradient of 20 mM to 1 M imidazole was initiated at fraction 1. B. SDS-PAGE analysis of stages of purification showing solubilised fraction (SF), column flow through (FT) and column wash. The analysed fractions were selected based on the chromatograph.*

It is possible that some of the contaminating proteins were interacting with the Ni^{2+} resin non-specifically through ionic interactions of negatively charged residues, both reducing the column binding capacity for hERG pore and also resulting in impure eluate. To limit the chances of such electrostatic interactions an alternative buffer with a greater salt concentration was used. In place of the usual PBS (containing 137 mM NaCl) a 50 mM Tris-HCl (pH 7.4) buffer was used, supplemented with 150 mM NaCl and 150 mM KCl, since this had previously been used successfully for fukutin TMD purification (*cf.* Chapter 2). The elution profile was very similar to that in standard PBS, with elution almost immediately following the start of the imidazole gradient at fraction 24. Western

blot analysis was performed on samples of this purification to identify whether hERG was present in the flow through and wash fractions (Figure 4.14). This analysis did confirm the presence of a modest amount of hERG pore in the elution fractions but also identified large intensity bands in the column flow through and wash, indicating that the protein either binds the column with low affinity or fails to bind at all. These bands are smeared due to the overloading of the gel and presence of DNA in the samples. Overall there is no clear improvement in purity between the low and high salt regimes when purifying in DDM.

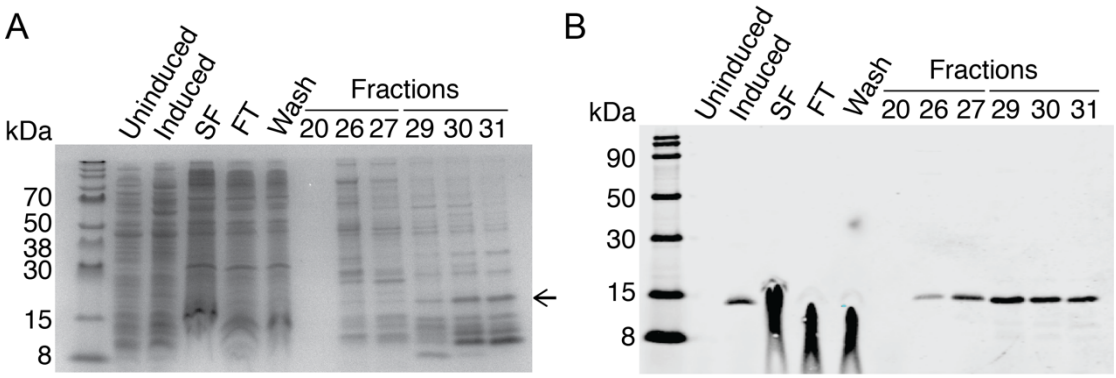

Figure 4.14: ***Purification of hERG pore in DDM from 6 L of E. coli culture using pre-packed HisTrap 1 mL Fast Flow column with increased salt concentration.*** *A gradient of 20 mM to 1 M over 40 mL was applied and 1 mL fractions were collected. A. and B. SDS-PAGE and western blot analysis of the detergent solubilised membrane (SF), the column flow through (FT) and column wash. The analysed fractions were selected based on the chromatograph which gave a similar elution profile to the previous purification.*

It is possible with hERG pore that lower affinity binding may be due to the detergent micelle around the protein, or protein structural features, making the his-tag less accessible. It has been established that extension of the his-tag in recombinant membrane proteins unsurprisingly results in an increased affinity of the tagged membrane protein to Ni^{2+} resin[327]. His-tags of up 14 residues have been used but 10 residues appear to be sufficient to enhance binding without increasing the affinity such that the protein cannot be easily eluted. We thus decided to increase the length of the his-tag on the hERG pore construct to 10, designated hERG Pore 10H.

4.3.2.2. Production of a 10x histidine tagged hERG pore plasmid

Conveniently two restriction sites, BamHI and CpoI, are present in phERGPore on either side of the sequence encoding the 6x his-tag and TEV cleavage site. Thus it could be easily excised and replaced. The cloning strategy applied is outlined in Figure 4.15. A short gene containing the 10x his-tag and TEV site between the same restriction sites was custom

synthesised (Invitrogen GeneArt, LifeTechnologies) and inserted into a vector to generate p10xHis. Both the phERGPore and p10xHis plasmids were digested using BamHI and CpoI seperately, with an ethanol precipitation step between the digestions to remove buffer and salt. The digested plasmid was then run on agarose gels (Figure 4.15) and subsequently purified from excised gel bands. Following the digests linearised plasmid bands are observed, whereas the undigested plasmid is either nicked (phERGPore6H, lane 1) or supercoiled (p10xHis, lane 4). The fragment from the phERGPore plasmid was 5' dephosphorylated to prevent self ligation. The digested phERGPore and 10x his-tag fragment were ligated with insert:vector ratios of 10:1, 3:1 and 1:1 then transformed into *E. Coli* DH5α and plated onto LB-agar plates with ampicillin. After overnight incubation at 37 °C multiple colonies were present on each plate and four from each were used to inoculate separate 5 mL cultures of LB media with ampicillin and grown at 37 °C overnight. The plasmids were then isolated by minipreparation and a number submitted for Sanger sequencing, many of which contained the correct sequence.

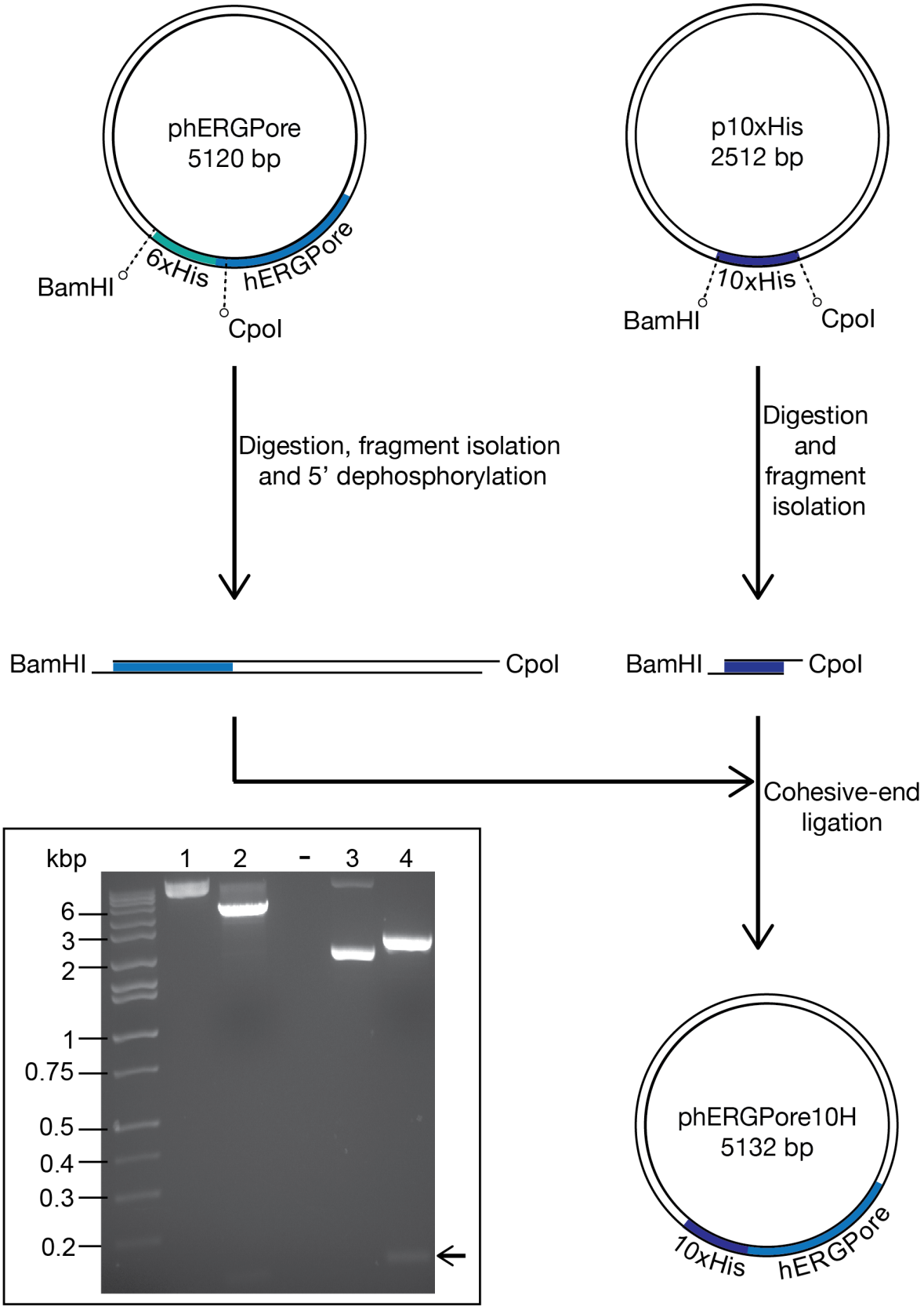

Figure 4.15: ***Cloning strategy for construction of pHERGPore10H****. Inset: Agarose gel of digested plasmids used to assemble phERGPore10H. Lanes 1 and 2 show undigested and digested phERGPore6H respectively, whilst lanes 3 and 4 show undigested and digested p10xHis. The arrow indicates the band of the 10x his-tag gene.*

4.3.2.3. Expression of 10x histidine tagged hERG pore

The phERGPore10H plasmid was transformed into *E. coli* BL21 and cultured identically to phERGPore. The growth of the culture was measured by OD_{600} every 30 minutes prior to induction at 1.0 and then measured once per hour (OD_{600}; Figure 4.16). The post-induction decrease in OD_{600} suggests that there is cell lysis due to toxicity of the expressed protein and that TEAB is not alone able to prevent this toxicity.

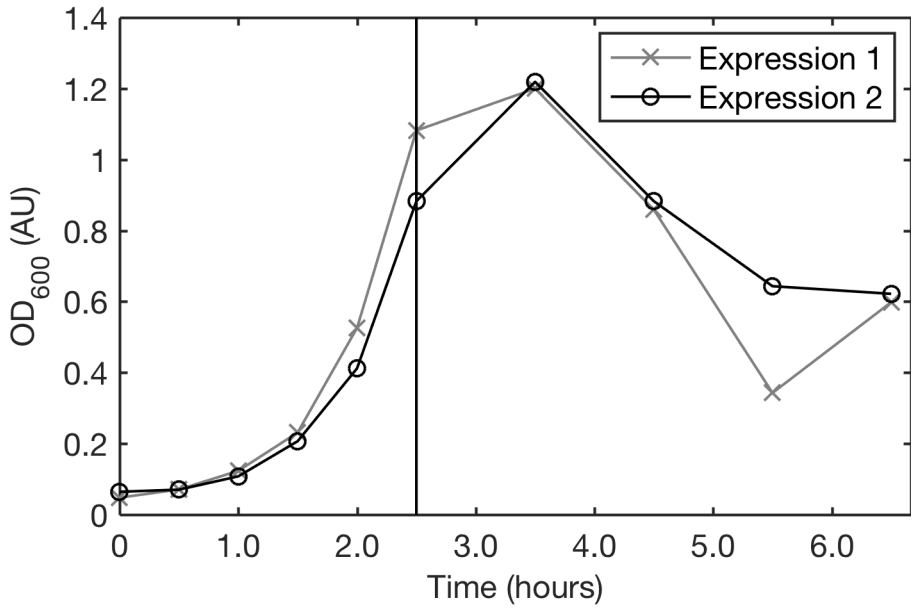

Figure 4.16: ***Growth curve of* E. coli *BL21 (DE3) transformed with phERGPore10H for two expressions.*** *The line at 2.5 hours indicates the point of induction with IPTG and addition of TEAB.*

To estimate the degree of expression over the induction period, samples were taken each hour and analysed by western blot (Figure 4.17). The amount of material loaded was normalised for OD_{600}. Despite the apparent cell death, the blot indicates an increase in expression in each subsequent hour and thus the induction time and expression conditions were not changed.

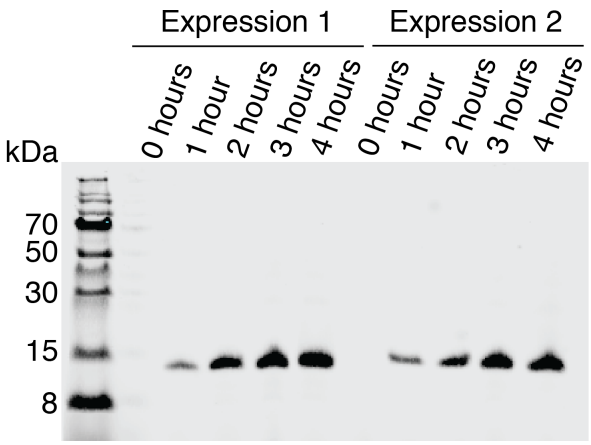

Figure 4.17: ***Western blot showing hERG pore-10H in crude*** **E. coli** ***lysate following induction with 1 mM IPGT and addition of 10 mM TEAB.*** *The 0 hour time point was collected immediately prior to induction and the following samples were taken at 1 hour intervals. For each time point the amount of sample loaded was normalised for cell growth (measured by* OD_{600}*).*

4.3.2.4. Purification of 10x histidine tagged hERG pore from membranes

To test whether the 10x his-tag improved binding affinity to the Ni^{2+} column, the harvested *E. coli* pellets were purified in DDM in the same manner as hERG pore 6H (Figure 4.18). Again, a gradient of imidazole was used to elute the bound protein, but as before the protein is eluted almost immediately at the start of the imidazole gradient, and the elution fractions are highly impure. There may be an improvement in binding affinity, since there is no band on the western blot in the flow through or wash, but it should be noted that these samples are very dilute compare to the eluate, so there may be protein present below the threshold of detection (Figure 4.18C). Ultimately, addition of four extra histidine residues to the his-tag has little is any effect on the purity of the eluted protein.

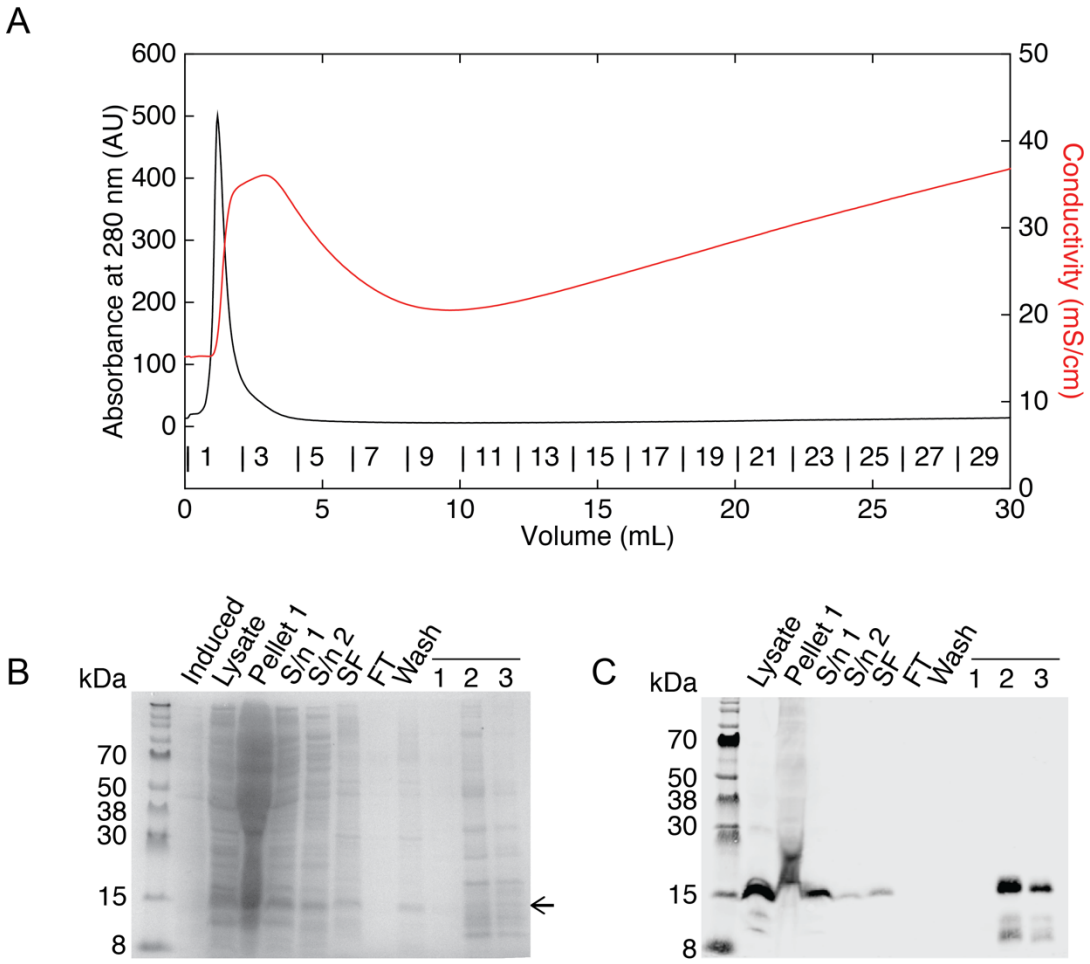

Figure 4.18: ***Purification of hERG pore 10H from 2 L culture in DDM using pre-packed 1 mL HisTrap Fast Flow column.*** *A. FPLC chromatogram showing elution profile of bound protein along a gradient of imidazole from 20 mM to 1 M over 30 1 mL fractions. B. and C. SDS-PAGE and western blot analysis (respectively) of purification process showing induced cell sample, cell lysate, pellet and supernatant from initial lower speed centrifugation step (s/n 1), supernatant from the ultracentrifuge step (s/n 2), the solubilised fraction (SF) and samples of the flow through (FT), column wash and elution fractions 1 to 3.*

Although Ni^{2+} resin is the most commonly used metal affinity resin for purification of his-tagged proteins, alternative divalent cations of transition metals have also been used. Particularly Co^{2+} resin has been proposed to reduce non-specific binding[328]. Co^{2+} TALON resin (Clontech Laboratories Inc.) was thus used to purify hERG pore 10H by batch method (Figure 4.19) as the loose resin already available in the laboratory. The use of batch resin meant that a gradient elution could not be applied, and instead the resin was washed extensively with PBS at 20 mM imidazole and eluted in 600 mM imidazole. Although the eluted fractions appeared to be slightly purer with Co^{2+} resin than Ni^{2+}, there is little noteworthy improvement, to the degree that there is no clear hERG pore 10H band

in the eluate. The most significant observation is from the western blot (Figure 4.19 B.), where a large band of hERG pore 10H is present in the pellet from the initial low speed centrifugation step, compared to the modest band in the subsequent membrane fraction. (Incidentally this is also apparent in Figure 4.18 C., although the band was not initially considered significant since it was greatly smeared.) The mostly likely explanation for this band is that the majority of the expressed protein forms inclusion bodies in the cytoplasm rather than being inserted into the membranes. Inclusion bodies can be harvested readily using low speed centrifugation (~8000 *g*) which explains their presence in this pellet. It is not clear whether this was also the case for the 6H construct. Inclusion bodies are proteinaceous masses of denatured and inactive protein, and often form in *E. coli* expressing recombinant proteins at a high level[329]. There is a small quantity of the protein retained within the membrane fraction, indicating that either not all of the inclusion bodies were collected during the low speed spin or that some of the protein is successfully able to insert into the membrane.

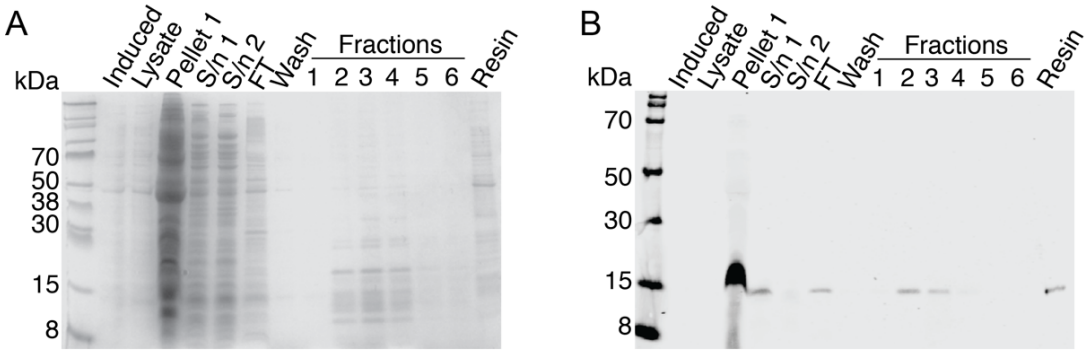

Figure 4.19: ***Purification of hERG pore-10H in DDM using batch Co^{2+} TALON resin.*** *A. and B. SDS-PAGE and western blot analysis respectively. Gels show induced cell sample, cell lysate, pellet and supernatant from initial centrifugation step (s/n 1), supernatant from ultracentrifugation step (s/n 2), flow though (FT), column wash and eluate fractions. A sample of resin was also run to ensure protein was fully eluted.*

4.3.2.5. Purification of 10x histidine tagged hERG pore from inclusion bodies

A small number of membrane proteins have been successfully recovered and refolded from inclusion bodies. This process generally involves the isolation of the inclusion bodies from cell lysates, their solubilisation using a chaotropic agent or harsh detergent, and finally the removal of the denaturant to allow refolding of the protein in the presence of mild detergent. Whilst β-barrel outer membrane proteins appear to be more amenable to

refolding for structural studies[330], success has been made with some helical proteins, including G protein coupled receptors[331].

To determine whether the protein was expressed as inclusion bodies, we applied a crude inclusion body purification protocol to the *E. coli* pellets (*cf.* section 2.2.4). The purification was broadly based on that published by Rogl et al.[332]. Sarkosyl has been used previously to solubilise inclusion bodies[333] in place of the denaturants urea and guanidinium chloride. In combination with the previous knowledge that hERG pore from the membrane is soluble in sarkosyl it was a logical choice for solubilisation of inclusion bodies, and was used at 1.2 % w/v concentration. As a comparison we also solubilised inclusion bodies with 3.2 M urea, and additionally a combination of the two. The cell pellet was resuspended in PBS and lysed by sonication, then the cell debris and inclusion bodies were harvested by a low speed centrifugation. The pellet was divided equally into three then resuspended in solubilisation buffer containing either urea, urea and sarkosyl or sarkosyl, and left to incubate at 4 °C overnight. Following the overnight incubation, there appeared to be precipitant in the urea solubilised sample which was not present in the samples with sarkosyl. The insoluble material was pelleted by repetition of the centrifuge step and the supernatant was incubated with Ni^{2+} resin, then washed and eluted in PBS with the urea or sarkosyl at equal concentration to the solubilisation butter. Figure 4.20 shows the resultant western blot and SDS-PAGE analysis of these purifications. All conditions for purification yielded hERG pore in the eluate, although in urea the fractions were highly impure and contained only a small amount of protein compared to relatively pure fractions in the sarkosyl solubilised samples. Total yields per L culture, determined by A_{280}, indicate that combined urea and sarkosyl (0.82 mg) and sarkosyl (0.76 mg) alone are efficacious relative to urea alone (0.5 mg). Sarkosyl alone also resulted in the purest eluate. It is possible that in the presence of urea the protein is fully unfolded and hydrophobic regions completely exposed, resulting in aggregation of the protein, which may also explain the precipitated material following solubilisation. In contrast in the presence of sarkosyl the protein may be either only partially denatured, and/or the detergent binding prevents exposure of the hydrophobic regions.

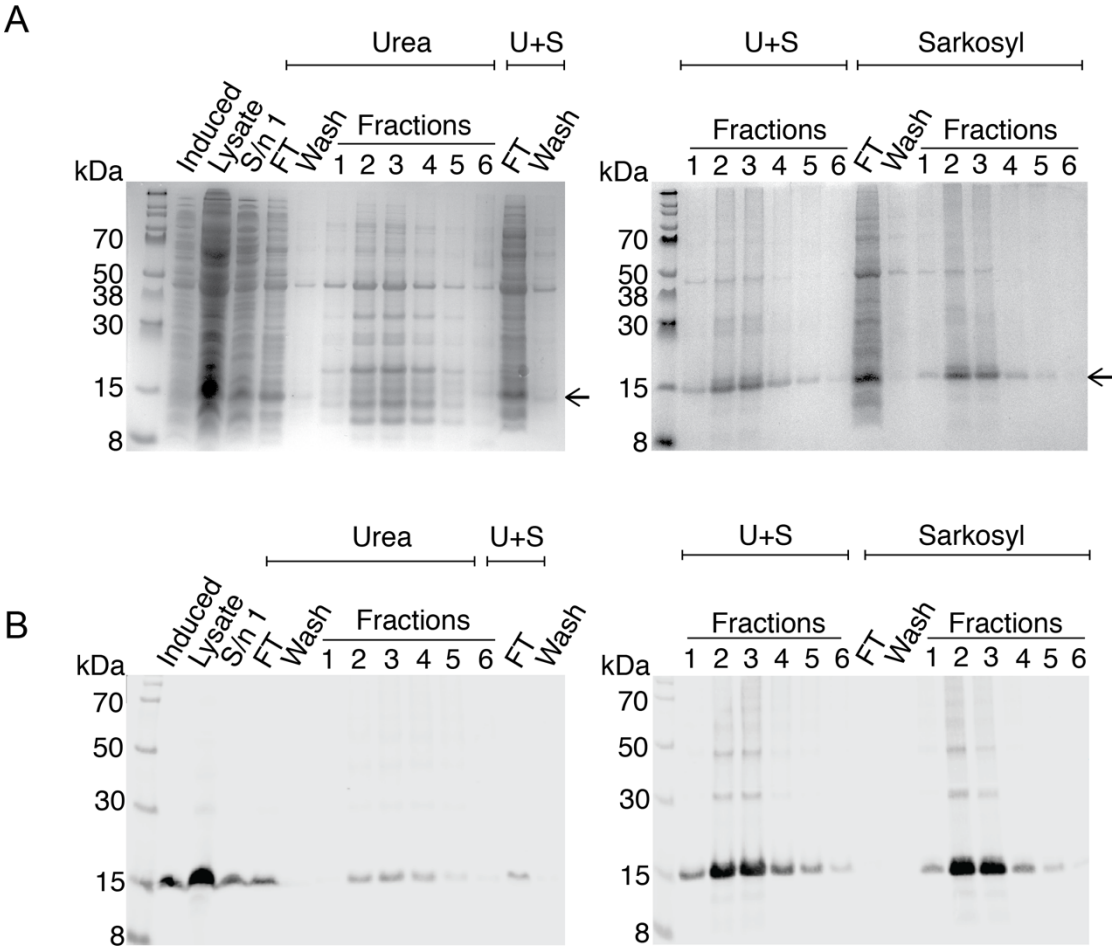

Figure 4.20: ***Purification of hERG pore 10H from 3 L culture using inclusion body extraction scheme and Ni^{2+} resin batch method.*** *A. and B. show SDS-PAGE and western blot analysis respectively. Samples of induced cells, cell lysate and supernatant (s/n 1) from centrifuge step were identical for all preparations. For each purification condition, the flow through (FT), column wash and elution fractions were analysed.*

In contrast to the protein purified from the membrane fraction it is clear that the protein binds with greater affinity from inclusion bodies. It is possible that the protein from inclusion bodies once solubilised by sarkosyl remains unstructured and makes the his-tag assessable to bind the resin, or that the number of contaminants is reduced improving binding of hERG pore to the column. It is however difficult to remove or exchange into either alternative detergents or lipid vesicles for further studies. Sarkosyl also absorbs strongly in the far-UV at approximately 225 nm, which precludes the use of optical techniques for characterisation such as circular dichroism[334]. It may be possible to limit the absorption through the use of concentrated protein and very narrow pathlength cuvettes, but as sarkosyl has such a high binding affinity for proteins it has been shown to 'co-concentrate' with the protein[320]. Since we were concerned about the use of sarkosyl for downstream characterisation and reconstitution, we repeated the purification but this time

solubilising the hERG pore 10H in sarkosyl and then exchanging it into DDM by washing the protein bound to the Ni^{2+} resin with DDM wash buffer. As controls, solubilisation of inclusion bodies was also attempted in either 10 mM DDM or 10 mM DDM and 3.2 M urea. In the wash and elution buffers the DDM concentration was reduced 1 mM.

The SDS-PAGE analysis of the purification (Figure 4.21) indicates that DDM alone does solubilise some of the hERG pore 10H, but the fractions are highly impure as previously observed with DDM. It is unlikely that DDM is able to solubilise inclusion bodies, and instead it may be solubilising hERG pore 10H in membrane fragments or intact cells which were spun down with the inclusion bodies. The combination of DDM and urea resulted in even more impure fractions. Visually, after solubilisation the sarkosyl solution was transparent whereas the DDM samples remained opaque, suggesting the DDM does not adequately disrupt the inclusion bodies. This is not surprising considering DDM is a fairly mild detergent. The use of sarkosyl and DDM resulted in excellent solubilisation and high purity fractions, analogous to the previous inclusion body purification with sarkosyl alone. In all conditions a clear band of hERG pore 10H is visible in the flow through, indicating that despite the 10x his-tag there is poor binding affinity to the resin.

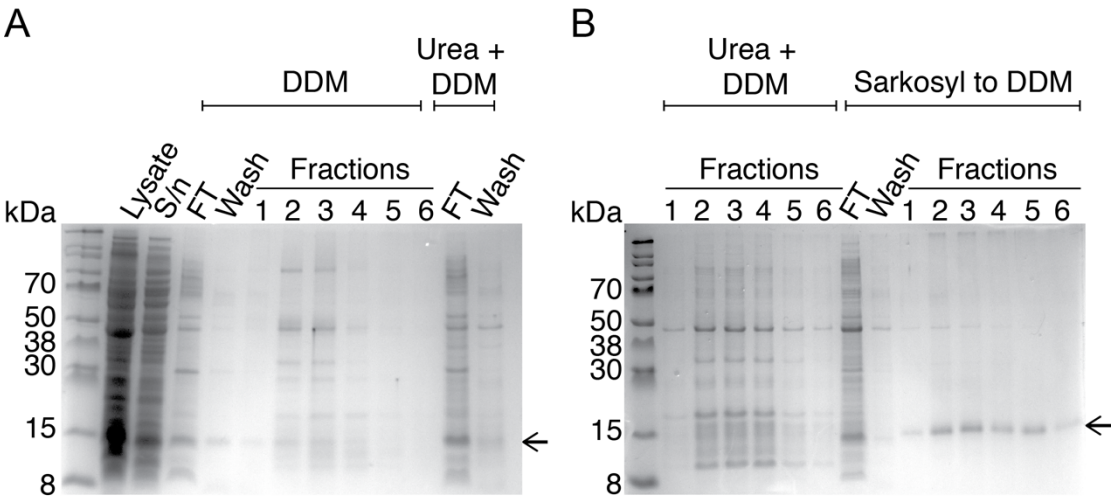

Figure 4.21: ***Purification of hERG pore-10H from 3 L culture using inclusion body extraction scheme with DDM, urea and sarkosyl.*** *A. and B. show SDS-PAGE analysis of the purification process. Samples of cell lysate and supernatant (S/n) from centrifuge step were identical for all preparations. For each purification condition, the flow through (FT), column wash and elution fractions were analysed.*

Since it appeared that sarkosyl was the most successful option for purification of hERG pore 10H from inclusion bodies, it was important to determine whether it could be

removed during reconstitution and if so whether the protein could be refolded by its removal. There has however been difficultly in exchanging and removing sarkosyl due to its high affinity binding to proteins[335]. In order to remove the sarkosyl and attempt to refold the protein it was reconstituted into POPC in a similar manner to KcsA. Indeed, Lange et al.[336] have successfully reconstituted small peptides out of sarkosyl solution for CD studies using Bio-Beads. Since it appeared likely that the sarkosyl would be more challenging to remove than DDM, the reconstitution time was increased from 2 hours to 2 days, following the same protocol otherwise. This was partially based on the observation that for KcsA there is a change in the solution from transparent to translucent as the detergent is removed from the lipid/detergent mixed micelles, which appeared to take much longer for sarkosyl than DDM. Although this is a significant increase, even greater timespans have been used in the literature[337]. Following reconstitution, SDS-PAGE analysis indicates the protein is fully monomeric (Figure 4.22), similarly to the SDS-PAGE gels for the protein in detergent. There is no protein band in the supernatant, suggesting that the majority of the protein is no longer in solution in detergent micelles but instead incorporated in the liposomes, although if the protein was dilute in the supernatant it is unlikely to see observed in by SDS-PAGE.

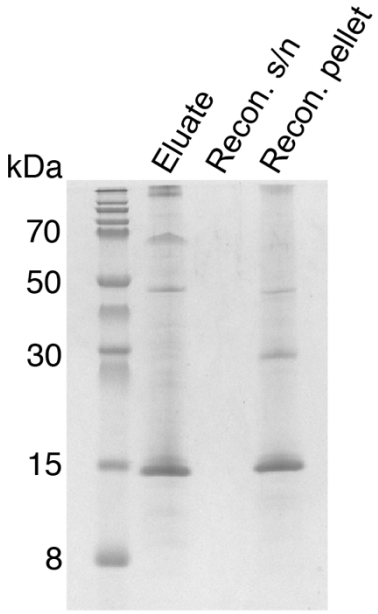

Figure 4.22: ***SDS-PAGE of sarkosyl solubilised hERG pore 10H reconstituted into POPC using detergent absorption method****. The proteoliposomes were harvested by centrifugation and the resulting pellet and supernatant (s/n) analysed on the gel.*

To attempt to determine whether a tetramer of hERG pore 10H does form in the bilayer which then dissociates due to the denaturing conditions of SDS-PAGE, cross-linking

experiments were performed using the chemical cross-linker DSS (Figure 4.23). DSS was selected due to its previous successful application for a number of membrane proteins[160, 338] including ion channels[339]. A number of lysines are present in hERG pore, in the S5-S6 linker and at the N terminus of the S6 helix. In the results here there is no observable oligomer, in either MLVs or SUVs. This may occur for a number of reasons. It is possible that the sarkosyl is still bound to the protein and prevents protein-protein interactions, presumably due to its negative charge repelling other subunits. It is also possible that stability of the tetramer is dependent upon the selectivity filter region, which has been demonstrated for KcsA[319, 340]. Should this region in hERG pore, or indeed other regions, not have its native structure it may result in the failure of oligomerisation. Equally, any particular conclusions cannot be drawn until this experiment with is repeated with cross-linkers of a greater lengths to ensure that the arm length is sufficient to link lysines in different subunits.

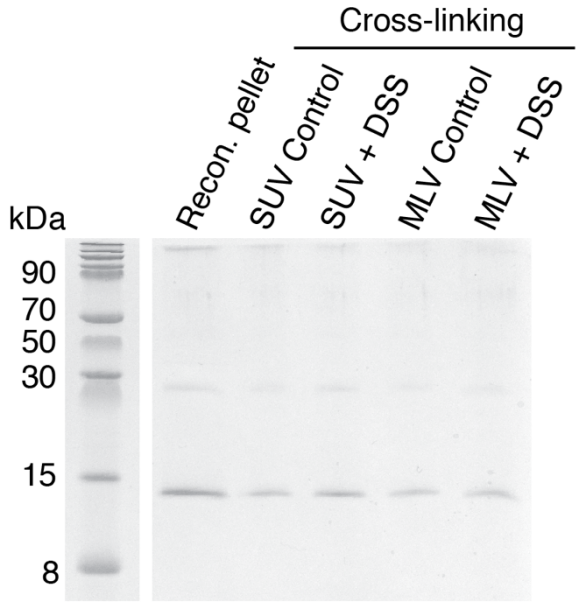

Figure 4.23: ***SDS-PAGE of reconstitution and cross-linking of hERG pore 10H purified from inclusion bodies in sarkosyl.*** *hERG pore 10H was reconstituted into POPC vesicles and subsequently cross-linked with the chemical cross linker DSS in DMSO. For control reactions an equal volume of DMSO without DDS was added.*

4.3.3. Conclusions

Membrane proteins are important but challenging targets for structural biology. In this chapter we have attempted to express the pore domain of the hERG potassium channel with some degree of success, although it is clear that the subsequent extraction of

structurally stable protein is less straightforward. It may be wise to return to optimisation of the expression conditions to attempt to limit the protein from expressing as inclusion bodies. However, expression of eukaryotic membrane proteins in *E. coli* hosts is notoriously challenging and it may be beneficial to use an alternative host. Indeed, for expression of the full length TMD human embryonic kidney (HEK) cells have been used[341], whilst a strategy for purification of the full length channel has also been published using *S. cerevisiae*[342], although it should be noted that unlike the protein produced in HEK cells it has not yet been electrophysiologically and structurally characterised. The availability of these strategies, which were not published when this work was commenced, may also provide hints to allow better purification of the hERG pore. Despite the publication of the cryo-EM structure there is still no established molecular mechanism for drug binding events in the pore domain, so there remains the need to fully characterise these interactions to potentially inform structure based drug design.

Chapter 5. General conclusions and future directions

OSRCD and solid-state NMR are two biophysical techniques which allow the structure and orientation of membrane proteins in lipid bilayers to be investigated. In this project we have enlisted both techniques to study the membrane protein fukutin TMD using either mechanically or magnetically aligned lipid phases.

A protocol was developed for the measurement of mechanically oriented samples using SRCD at the Diamond Light Source B23 beamline, which required optimisation of the quantity of lipid required, support substrate and sample hydration. We have found that optimal samples for OSRCD were prepared on fused silica substrates, with a lipid per area of ~2.5 μg mm^{-2}, with hydration applied by direct application of water to the substrate surface. The use of a horizontally mounted sample was useful to prevent the lipid film "sliding off" the substrate of the coverslip and to allow the surface homogeneity to be investigated. Using ^{31}P and ^{2}H NMR the quality of alignment of samples was measured, indicating that this method produced a high degree of alignment. Having outlined these methods for the preparation of mechanically oriented lipid bilayers with fukutin TMD, we were able to characterise its response to changes in the bilayer thickness. We successfully acquired OSRCD spectra of fukutin TMD in DLPC, DMPC and POPC lipid bilayers. We have also optimised sample preparation methods for oriented solid-state NMR measurements of fukutin TMD, which allow both validation of the OSRCD spectra and also aid in their interpretation. The presence of potentially aggregated material in these samples produces challenges for their analysis, but using this combination of techniques we have been able to speculate on the biological insights provided by this data.

We have established that fukutin TMD is able to span PC bilayers of similar thickness to the Golgi apparatus using DLPC as a model lipid, with a tilt angle of 20°. In thicker membranes its tilt angle is close to 0° (1° and 2° in DMPC and DPPC respectively) as the protein is almost entirely parallel to the bilayer normal. It also appears to form large oligomers, especially in the thickest bilayer measured here, DPPC, as it presumably unable to completely span the bilayer. This may indicate that fukutin is unable to enter the cholesterol-enriched, thicker regions of the Golgi apparatus membrane which bud to form trafficking vesicles destined for the plasma membranes. By its exclusion from such vesicles it may be able to remain resident in the Golgi apparatus, which seems to be essential for its probable function as a glycosyltransferase for α-dystroglycan[173]. Similar aggregation effects have been previously observed in reconstituted proteins, including bovine rhodopsin in bilayers with acyl chains longer than C15[343] as a result of hydrophobic

mismatch. A consideration here which certainly warrants further investigation is whether fukutin TMD is able to span thicker bilayers containing charged lipids, which MD studies suggest interact preferentially with the protein[62], and may therefore stabilise it in the bilayer. It is also possible that the interaction of fukutin with other glycosyltransferases, as has been demonstrated for POMnGT1[176], may stabilise the protein in the bilayer. Similar effects have been observed in the case of the E5 oncoprotein interacting with PDGF receptor[61].

Although we were able to successfully prepare and measure mechanically oriented samples, a significant amount of time and material was required to optimise samples for both sets of measurements, particularly the SRCD, access to which is time limited to beam time sessions. In future, a sensible approach may be to screen a number of lipids using conventional benchtop CD instruments then to perform OSRCD and solid-state NMR measurements on those samples showing promise, in terms of either quality of sample preparation or especially significant effects on the protein orientation. However, now a method for preparation for OSRCD samples using PC lipids is available, it is likely that it could be applied to other hydrophobic peptides in similar lipids. Of course, further refinement may well be necessary for alternative lipid mixtures. It is likely that upcoming beamline developments to allow complete 'mapping' of the sample surface using a CD imaging approach[225] will be invaluable for this sort of measurement. In any case, the ability to examine proteins in oriented lipid bilayers has been essential here to begin to answer questions regarding the role of lipid-protein interactions in the localisation of the putative glycosyltransferase fukutin.

Due to the challenges associated with preparation of mechanically oriented samples we have developed a novel approach for OSRCD using magnetically aligned phases, which have been used extensively in the magnetic resonance community. Magnetically aligned systems can be prepared with greater simplicity, reproducibility and consistency than mechanically aligned bilayers. There are examples in the literature of successful reconstitution of a range of structurally diverse recombinantly expressed proteins into bicelles[227-230], potentially providing a new route to orientation of large, complex proteins for OCD. Whilst a number of studies have been performed using unordered bicelles previously, we believe this is the first time magnetic alignment of lipid phases for OCD has been attempted. Using ^{31}P NMR the phase behaviour of lipid mixtures was investigated, to guide the selection of optimum conditions for bicelles alignment at a reasonably low temperature, with the suitable hydration and q ratio. We were subsequently able to

demonstrate that fukutin TMD has little effect on the phase behaviour of bicelles at a concentration amenable to CD measurements. Since the magnetic field in the MCD instrument was substantially less than the 14.1 T used in NMR measurements, we demonstrated alignment in a lower field using X-band EPR at 1.4 T. Capitalising on the extensive work of Lorgian and coworkers, and through use of lanthanide ions in conjunction with chelating headgroup lipids as described by Prosser[252], bicelles could be aligned both parallel and perpendicular to the 1.4 T field. This was also confirmed using deuterium and ^{31}P NMR. Parallel alignment was particularly desirable to simplify the analysis of both NMR and OSRCD data. Using ^{15}N NMR the alignment of fukutin TMD was found to be ~30°, although there are some caveats on this value, and further studies are certainly warranted. It also appears that there is a powder contribution in the parallel aligned bicelle sample, which may indicate that the powder component observed in the ^{15}N DMPC mechanically aligned samples is also a result of a similar hydrophobic mismatch rather than the lipid disorder. For further measurements, increasing the concentration of chelating lipid may be necessary, and the use of NMR probes with greater sample capacity may allow a reduction in the L/P from the current value of 50.

In addition to magnetic resonance studies, the applicability of this bicellar mixture to CD has been demonstrated without a magnetic field. Although the lipid background has a very strong signal, the resulting baseline corrected spectra give the expected helical line shape. However, an intense, narrow band, which we attribute to linear birefringence, is present around 185 nm, and was inconsistent between spectra. As such it is important to limit data for analysis to ~200 nm. In the case of oriented spectra of helical proteins this does not present a large problem, since the 208 nm band which most clearly reports orientation is unaffected, but if wishing to deconvolute secondary structural features may present more of a challenge. While it has not been possible to perform OSRCD measurements on magnetically aligned phases, we attribute this to a poor degree of order in the samples at the low magnetic field. To address this poor degree of order the natural progression of the technique would be to conduct MCD measurements at a much greater magnetic field, which are accessible using superconducting magnets. An alternative strategy may be to align the samples in an external magnetic field and then transfer the sample to a CD instrument for acquisition, as has been done for SANS measurements with success[344]. This would also remove the need for a dedicated MCD instrument, which are not extensively available, although care would need to be taken to ensure that the bicelles did not relax to an unoriented state. A completely different approach may be to use flow alignment, which has been used previously for linear dichroism measurements[345, 346]. If ultimately successful

a further extension of the method would be to incorporate larger proteins into the bicelles. This would require novel methods to interpret OSRCD data to deconvolute localised changes from global changes in the protein orientation or structure. Indeed, one can envisage that a joint application of solid-state NMR and OSRCD to such large proteins in bicelles would be a powerful approach, examining both the overall changes in architecture and the site specific events leading to such changes. Whilst further optimisation is required before this point is reached, we have demonstrated that bicelles are a useful and complementary tool to conventional mechanically oriented samples, and may provide a new approach to orient membrane proteins for OSRCD.

With the initial goal of reconstituting large membrane proteins in to bicelles, we attempted to express and purify the human potassium channel hERG for oriented studies. The channel has great physiological and pharmacological significance, as it has an unusual proclivity for binding a wide range of drugs, which results in drug induced long-QT syndrome, a potentially fatal condition. At the time of commencing this work there were no published protocols for expression of the protein, and no complete structures, although structures of some components of the channel, and electrophysiological data were available. There are now methods for the expression and purification of the full length protein in both yeast[342] and mammalian cells[308], from which a cryo-EM structure has also been solved. Still, no confirmed structural mechanisms for the drug-hERG interactions leading to drug induced long-QT syndrome have been provided. In our work, to improve the chances of successful expression in *E. coli*, we focused on the pore domain that is implicated in these drug binding events. Previous optimisation of expression meant we were able to begin purification trials under different conditions. Due to the apparent low affinity binding for the Ni^{2+} resin it was difficult to purify the protein solubilised in DDM, even upon extension of the histidine tag. It was most soluble in sarkosyl, which has a number of undesirable properties. Whilst there was hERG present in the *E. coli* membranes, there was also what appeared to be a large quantity of the protein in inclusion bodies. It is common for recombinant proteins expressed in *E. coli* to form inclusion bodies, although attempts to refold helical membrane proteins have not been especially successful. Having tried methods to reconstitute the protein, preliminary cross-linking studies indicate that the protein fails to form its native tetramer, suggesting it may not be correctly structured. Equally, however, it is possible that the other domains of hERG which were removed here are required for tetramerisation of the channel. It appears that the most logical step here would be to return to optimisation of the expression to concentrate the protein in the membranes, from which it may be more readily extracted, as well as altering

the affinity tag, perhaps to a C terminal histidine tag or an alternative such glutathione S-transferase. As a protocol for expression of the full length channel in yeast is now available, which is not overtly more demanding than *E. coli* culture, it may be more useful to capitalise on this existing approach.

Bibliography

1. Singer SJ, Nicolson GL. The fluid mosaic model of the structure of cell membranes. *Science*. 1972;175 (4023):720-31.
2. Adams R, Worth CL, Guenther S, Dunkel M, Lehmann R, Preissner R. Binding sites in membrane proteins--diversity, druggability and prospects. *Eur J Cell Biol*. 2012;91 (4):326-39.
3. Israelachvili JN, Marčelja S, Horn RG. Physical principles of membrane organization. *Q Rev Biophys*. 1980;13 (2):121-200.
4. van Meer G, Voelker DR, Feigenson GW. Membrane lipids: Where they are and how they behave. *Nat Rev Mol Cell Biol*. 2008;9 (2):112-24.
5. Bartke N, Hannun YA. Bioactive sphingolipids: Metabolism and function. *J Lipid Res*. 2009;50:S91-S6.
6. Eze MO. Phase transitions in phospholipid bilayers: Lateral phase separations play vital roles in biomembranes. *Biochem Educ*. 1991;19 (4):204-8.
7. Rawicz W, Olbrich KC, McIntosh T, Needham D, Evans E. Effect of chain length and unsaturation on elasticity of lipid bilayers. *Biophys J*. 2000;79 (1):328-39.
8. Boggs JM. Lipid intermolecular hydrogen bonding: Influence on structural organization and membrane function. *Biochim Biophys Acta*. 1987;906 (3):353-404.
9. Mouritsen OG, Zuckermann MJ. What's so special about cholesterol? *Lipids*. 2004;39 (11):1101-13.
10. Bhattacharya S, Haldar S. Interactions between cholesterol and lipids in bilayer membranes. Role of lipid headgroup and hydrocarbon chain-backbone linkage. *Biochim Biophys Acta*. 2000;1467 (1):39-53.
11. Yeagle PL. The structure of biological membranes, second edition: CRC Press; 2004.
12. Sohlenkamp C, Geiger O. Bacterial membrane lipids: Diversity in structures and pathways. *FEMS Microbiol Rev*. 2016;40 (1):133-59.
13. Welker DR. Lipid assembly into cell membranes. New comprehensive biochemistry. Volume 36: Elsevier; 2002. p. 449-82.
14. Rietschel ET, Kirikae T, Schade FU, Mamat U, Schmidt G, Loppnow H, Ulmer AJ, Zähringer U, Seydel U, Di Padova F. Bacterial endotoxin: Molecular relationships of structure to activity and function. *FASEB J*. 1994;8 (2):217-25.
15. Ikonen E. Cellular cholesterol trafficking and compartmentalization. *Nat Rev Mol Cell Biol* 2008;9 (2):125-38.

16. Mitra K, Ubarretxena-Belandia I, Taguchi T, Warren G, Engelman DM. Modulation of the bilayer thickness of exocytic pathway membranes by membrane proteins rather than cholesterol. *Proc Natl Acad Sci USA*. 2004;101 (12):4083-8.
17. Tu L, Banfield DK. Localization of Golgi-resident glycosyltransferases. *Cell Mol Life Sci*. 2010;67 (1):29-41.
18. van Meer G, de Kroon AI. Lipid map of the mammalian cell. *J Cell Sci*. 2011;124 (Pt 1):5-8.
19. Carvalho K, Ramos L, Roy C, Picart C. Giant unilamellar vesicles containing phosphatidylinositol(4,5)bisphosphate: Characterization and functionality. *Biophys J*. 2008;95 (9):4348-60.
20. Lopez-Marques R, Theorin L, Palmgren M, Pomorski T. P4-ATPases: Lipid flippases in cell membranes. *Pflugers Arch - Eur J Physiol*. 2013:1-14.
21. Williamson P. Phospholipid scramblases. *Lipid Insights*. 2015;8 (Suppl 1):41-4.
22. Simons K, Van Meer G. Lipid sorting in epithelial cells. *Biochemistry*. 1988;27 (17):6197-202.
23. Simons K, Ikonen E. Functional rafts in cell membranes. *Nature*. 1997;387 (6633):569-72.
24. Varma R, Mayor S. GPI-anchored proteins are organized in submicron domains at the cell surface. *Nature*. 1998;394 (6695):798-801.
25. Silvius J. Role of cholesterol in lipid raft formation: Lessons from lipid model systems. *Biochim Biophys Acta*. 2003;1610 (2):174-83.
26. Kahya N, Scherfeld D, Bacia K, Poolman B, Schwille P. Probing lipid mobility of raft-exhibiting model membranes by fluorescence correlation spectroscopy. *J Biol Chem*. 2003;278 (30):28109-15.
27. Lai EC. Lipid rafts make for slippery platforms. *J Cell Biol*. 2003;162 (3):365-70.
28. Casadei Bruna R, Domingues Cleyton C, de Paula E, Riske Karin A. Direct visualization of the action of Triton X-100 on giant vesicles of erythrocyte membrane lipids. *Biophys J*. 2014;106 (11):2417-25.
29. Sodt AJ, Sandar ML, Gawrisch K, Pastor RW, Lyman E. The molecular structure of the liquid-ordered phase of lipid bilayers. *J Am Chem Soc*. 2014;136 (2):725-32.
30. Koukalova A, Amaro M, Aydogan G, Grobner G, Williamson PTF, Mikhalyov I, Hof M, Sachl R. Lipid driven nanodomains in giant lipid vesicles are fluid and disordered. *Sci Rep*. 2017;7 (1):5460.
31. Komura N, Suzuki KG, Ando H, Konishi M, Koikeda M, Imamura A, Chadda R, Fujiwara TK, Tsuboi H, Sheng R, Cho W, Furukawa K, Furukawa K, Yamauchi Y,

Ishida H, Kusumi A, Kiso M. Raft-based interactions of gangliosides with a GPI-anchored receptor. *Nat Chem Biol*. 2016;12 (6):402-10.

32. Dennis EA. Diversity of group types, regulation, and function of phospholipase A_2. *J Biol Chem*. 1994;269 (18):13057-60.
33. Burke JE, Hsu YH, Deems RA, Li S, Woods VL, Jr., Dennis EA. A phospholipid substrate molecule residing in the membrane surface mediates opening of the lid region in group IVA cytosolic phospholipase A_2. *J Biol Chem*. 2008;283 (45):31227-36.
34. Bracey MH, Cravatt BF, Stevens RC. Structural commonalities among integral membrane enzymes. *FEBS Lett*. 2004;567 (2):159-65.
35. Jensen RE, Dunn CD. Protein import into and across the mitochondrial inner membrane: Role of the TIM23 and TIM22 translocons. *Biochim Biophys Acta*. 2002;1592 (1):25-34.
36. Zimmermann R, Eyrisch S, Ahmad M, Helms V. Protein translocation across the ER membrane. *Biochim Biophys Acta*. 2011;1808 (3):912-24.
37. Luckey M. Membrane structural biology: With biochemical and biophysical foundations: Cambridge University Press; 2014.
38. Sato K, Nakano A. Mechanisms of COPII vesicle formation and protein sorting. *FEBS Lett*. 2007;581 (11):2076-82.
39. Rodriguez-Boulan E, Müsch A. Protein sorting in the Golgi complex: Shifting paradigms. *Biochim Biophys Acta - Mol Cell Res*. 2005;1744 (3):455-64.
40. Stockklausner C, Klöcker N. Surface expression of inward rectifier potassium channels is controlled by selective Golgi export. *J Biol Chem*. 2003;278 (19):17000-5.
41. Hofherr A, Fakler B, Klöcker N. Selective Golgi export of Kir2.1 controls the stoichiometry of functional Kir2.X channel heteromers. *J Cell Sci*. 2005;118 (9):1935-43.
42. Ulmschneider MB, Sansom MSP. Amino acid distributions in integral membrane protein structures. *Biochim Biophys Acta*. 2001;1512 (1):1-14.
43. Lemmon MA, Flanagan JM, Treutlein HR, Zhang J, Engelman DM. Sequence specificity in the dimerization of transmembrane alpha-helices. *Biochemistry*. 1992;31 (51):12719-25.
44. Walters RFS, DeGrado WF. Helix-packing motifs in membrane proteins. *Proc Natl Acad Sci USA*. 2006;103 (37):13658-63.

45. von Heijne G. Membrane-protein topology. *Nat Rev Mol Cell Biol*. 2006;7 (12):909-18.
46. Strandberg E, Killian JA. Snorkeling of lysine side chains in transmembrane helices: How easy can it get? *FEBS Lett*. 2003;544 (1):69-73.
47. Guilhelmelli F, Vilela N, Albuquerque P, Derengowski Lda S, Silva-Pereira I, Kyaw CM. Antibiotic development challenges: The various mechanisms of action of antimicrobial peptides and of bacterial resistance. *Front Microbiol*. 2013;4.
48. Lee AG. Lipid-protein interactions. *Biochem Soc Trans*. 2011;39 (3):761-6.
49. East JM, Melville D, Lee AG. Exchange rates and numbers of annular lipids for the calcium and magnesium ion dependent adenosinetriphosphatase. *Biochemistry*. 1985;24 (11):2615-23.
50. Taylor AM, Watts A. Spin-label studies of lipid-protein interactions with reconstituted band 3, the human erythrocyte chloride-bicarbonate exchanger. *Biochem Cell Biol*. 1998;76 (5):815-22.
51. Marsh D. Electron spin resonance in membrane research: Protein-lipid interactions from challenging beginnings to state of the art. *Eur Biophys J*. 2010;39 (4):513-25.
52. Marsh D, Watts A, Pates RD, Uhl R, Knowles PF, Esmann M. ESR spin-label studies of lipid-protein interactions in membranes. *Biophys J*. 1982;37 (1):265-74.
53. Knowles PF, Watts A, Marsh D. Spin-label studies of lipid immobilization in dimyristoylphosphatidylcholine-substituted cytochrome oxidase. *Biochemistry*. 1979;18 (21):4480-7.
54. Lee AG. How lipids affect the activities of integral membrane proteins. *Biochim Biophys Acta*. 2004;1666 (1-2):62-87.
55. Powl AM, East JM, Lee AG. Lipid−protein interactions studied by introduction of a tryptophan residue: The mechanosensitive channel MscL. *Biochemistry*. 2003;42 (48):14306-17.
56. Knight JD, Falke JJ. Single-molecule fluorescence studies of a PH domain: New insights into the membrane docking reaction. *Biophys J*. 2009;96 (2):566-82.
57. Weingarth M, Prokofyev A, van der Cruijsen EA, Nand D, Bonvin AM, Pongs O, Baldus M. Structural determinants of specific lipid binding to potassium channels. *J Am Chem Soc*. 2013;135 (10):3983-8.
58. Yao H, Hong M. Membrane-dependent conformation, dynamics, and lipid interactions of the fusion peptide of the paramyxovirus PIV5 from solid-state NMR. *J Mol Biol*. 2013;425 (3):563-76.

59. Opella SJ, Ma C, Marassi FM. Nuclear magnetic resonance of membrane-associated peptides and proteins. *Methods Enzymol*. 2001;339:285-313.
60. Perrone B, Miles AJ, Salnikov ES, Wallace BA, Bechinger B. Lipid interactions of LAH4, a peptide with antimicrobial and nucleic acid transfection activities. *Eur Biophys J*. 2014.
61. Windisch D, Ziegler C, Grage SL, Bürck J, Zeitler M, Gor'kov PL, Ulrich AS. Hydrophobic mismatch drives the interaction of E5 with the transmembrane segment of PDGF receptor. *Biophys J*. 2015;109 (4):737-49.
62. Holdbrook DA, Leung YM, Piggot TJ, Marius P, Williamson PTF, Khalid S. Stability and membrane orientation of the fukutin transmembrane domain: A combined multiscale molecular dynamics and circular dichroism study. *Biochemistry*. 2010;49 (51):10796-802.
63. Zhou Y, Morais-Cabral JH, Kaufman A, MacKinnon R. Chemistry of ion coordination and hydration revealed by a K^+ channel-Fab complex at 2.0 Å resolution. *Nature*. 2001;414 (6859):43-8.
64. Marius P, de Planque MRR, Williamson PTF. Probing the interaction of lipids with the non-annular binding sites of the potassium channel KcsA by magic-angle spinning NMR. *Biochim Biophys Acta*. 2012;1818 (1):90-6.
65. Marius P, Alvis SJ, East JM, Lee AG. The interfacial lipid binding site on the potassium channel KcsA is specific for anionic phospholipids. *Biophys J*. 2005;89 (6):4081-9.
66. Marius P, Zagnoni M, Sandison ME, East JM, Morgan H, Lee AG. Binding of anionic lipids to at least three nonannular sites on the potassium channel KcsA is required for channel opening. *Biophys J*. 2008;94 (5):1689-98.
67. Laganowsky A, Reading E, Allison TM, Ulmschneider MB, Degiacomi MT, Baldwin AJ, Robinson CV. Membrane proteins bind lipids selectively to modulate their structure and function. *Nature*. 2014;510 (7503):172-5.
68. van den Brink-van der Laan E, Chupin V, Killian JA, de Kruijff B. Stability of KcsA tetramer depends on membrane lateral pressure. *Biochemistry*. 2004;43 (14):4240-50.
69. Curran AR, Templer RH, Booth PJ. Modulation of folding and assembly of the membrane protein bacteriorhodopsin by intermolecular forces within the lipid bilayer. *Biochemistry*. 1999;38 (29):9328-36.
70. Baneyx F, Mujacic M. Recombinant protein folding and misfolding in *Escherichia coli*. *Nat Biotechnol*. 2004;22 (11):1399-408.

71. Schlegel S, Hjelm A, Baumgarten T, Vikstrom D, de Gier JW. Bacterial-based membrane protein production. *Biochim Biophys Acta*. 2014;1843 (8):1739-49.
72. Mitra N, Sinha S, Ramya TN, Surolia A. N-linked oligosaccharides as outfitters for glycoprotein folding, form and function. *Trends Biochem Sci*. 2006;31 (3):156-63.
73. Boer E, Steinborn G, Kunze G, Gellissen G. Yeast expression platforms. *Appl Microbiol Biotechnol*. 2007;77 (3):513-23.
74. Andréll J, Tate CG. Overexpression of membrane proteins in mammalian cells for structural studies. *Mol Membr Biol*. 2013;30 (1-2):52-63.
75. Bill RM, Henderson PJF, Iwata S, Kunji ERS, Michel H, Neutze R, Newstead S, Poolman B, Tate CG, Vogel H. Overcoming barriers to membrane protein structure determination. *Nat Biotechnol*. 2011;29:335-40.
76. Lund S, Orlowski S, de Foresta B, Champeil P, le Maire M, Moller JV. Detergent structure and associated lipid as determinants in the stabilization of solubilized Ca^{2+}-ATPase from sarcoplasmic reticulum. *J Biol Chem*. 1989;264 (9):4907-15.
77. Stangl M, Veerappan A, Kroeger A, Vogel P, Schneider D. Detergent properties influence the stability of the glycophorin A transmembrane helix dimer in lysophosphatidylcholine micelles. *Biophys J*. 2012;103 (12):2455-64.
78. Cross TA, Sharma M, Yi M, Zhou HX. Influence of solubilizing environments on membrane protein structures. *Trends Biochem Sci*. 2011;36 (2):117-25.
79. Popot JL, Althoff T, Bagnard D, Baneres JL, Bazzacco P, Billon-Denis E, Catoire LJ, Champeil P, Charvolin D, Cocco MJ, Cremel G, Dahmane T, de la Maza LM, Ebel C, Gabel F, Giusti F, Gohon Y, Goormaghtigh E, Guittet E, Kleinschmidt JH, Kuhlbrandt W, Le Bon C, Martinez KL, Picard M, Pucci B, Sachs JN, Tribet C, van Heijenoort C, Wien F, Zito F, Zoonens M. Amphipols from A to Z. *Annu Rev Biophys*. 2011;40:379-408.
80. Popot JL. Amphipols, nanodiscs, and fluorinated surfactants: Three nonconventional approaches to studying membrane proteins in aqueous solutions. *Annu Rev Biochem*. 2010;79:737-75.
81. Lee SC, Knowles TJ, Postis VL, Jamshad M, Parslow RA, Lin YP, Goldman A, Sridhar P, Overduin M, Muench SP, Dafforn TR. A method for detergent-free isolation of membrane proteins in their local lipid environment. *Nat Protoc*. 2016;11 (7):1149-62.
82. Orwick-Rydmark M, Lovett JE, Graziadei A, Lindholm L, Hicks MR, Watts A. Detergent-free incorporation of a seven-transmembrane receptor protein into

nanosized bilayer lipodisq particles for functional and biophysical studies. *Nano Lett*. 2012;12 (9):4687-92.

83. Landau EM, Rosenbusch JP. Lipidic cubic phases: A novel concept for the crystallization of membrane proteins. *Proc Natl Acad Sci USA*. 1996;93 (25):14532-5.
84. Ai X, Caffrey M. Membrane protein crystallization in lipidic mesophases: Detergent effects. *Biophys J*. 2000;79 (1):394-405.
85. Kulkarni CV, Wachter W, Iglesias-Salto G, Engelskirchen S, Ahualli S. Monoolein: A magic lipid? *Phys Chem Chem Phys*. 2011;13 (8):3004-21.
86. Moraes I, Evans G, Sanchez-Weatherby J, Newstead S, Stewart PD. Membrane protein structure determination - the next generation. *Biochim Biophys Acta*. 2014;1838 (1 Pt A):78-87.
87. Ujwal R, Bowie JU. Crystallizing membrane proteins using lipidic bicelles. *Methods*. 2011;55 (4):337-41.
88. Newstead S, Ferrandon S, Iwata S. Rationalizing α-helical membrane protein crystallization. *Protein Sci*. 2008;17 (3):466-72.
89. Hunte C, Michel H. Crystallisation of membrane proteins mediated by antibody fragments. *Curr Opin Struct Biol*. 2002;12 (4):503-8.
90. Murakami M, Kouyama T. Crystal structure of squid rhodopsin. *Nature*. 2008;453 (7193):363-7.
91. Deupi X, Dolker N, Lopez-Rodriguez ML, Campillo M, Ballesteros JA, Pardo L. Structural models of class a G protein-coupled receptors as a tool for drug design: Insights on transmembrane bundle plasticity. *Curr Top Med Chem*. 2007;7 (10):991-8.
92. Fujiyoshi Y, Unwin N. Electron crystallography of proteins in membranes. *Curr Opin Struct Biol*. 2008;18 (5):587-92.
93. Ubarretxena-Belandia I, Stokes DL. Present and future of membrane protein structure determination by electron crystallography. *Adv Protein Chem Struct Biol*. 2010;81:33-60.
94. Henderson R, Unwin PNT. Three-dimensional model of purple membrane obtained by electron microscopy. *Nature*. 1975;257 (5521):28-32.
95. Miyazawa A, Fujiyoshi Y, Stowell M, Unwin N. Nicotinic acetylcholine receptor at 4.6 Å resolution: Transverse tunnels in the channel. *J Mol Biol*. 1999;288 (4):765-86.
96. Cao E, Liao M, Cheng Y, Julius D. Trpv1 structures in distinct conformations reveal activation mechanisms. *Nature*. 2013;504 (7478):113-8.

97. Whicher JR, MacKinnon R. Structure of the voltage-gated K^+ channel Eag1 reveals an alternative voltage sensing mechanism. *Science*. 2016;353 (6300):664-9.
98. Park E, Campbell EB, MacKinnon R. Structure of a CLC chloride ion channel by cryo-electron microscopy. *Nature*. 2017;541 (7638):500-5.
99. Kempner ES. Movable lobes and flexible loops in proteins. Structural deformations that control biochemical activity. *FEBS Lett*. 1993;326 (1-3):4-10.
100. Penczek PA, Kimmel M, Spahn CMT. Identifying conformational states of macromolecules by eigen-analysis of resampled cryo-EM images. *Structure*. 2011;19 (11):1582-90.
101. Bai XC, McMullan G, Scheres SH. How cryo-EM is revolutionizing structural biology. *Trends Biochem Sci*. 2015;40 (1):49-57.
102. Liao M, Cao E, Julius D, Cheng Y. Structure of the trpv1 ion channel determined by electron cryo-microscopy. *Nature*. 2013;504 (7478):107-12.
103. Dutta A, Saxena K, Schwalbe H, Klein-Seetharaman J. Isotope labeling in mammalian cells. In: Shekhtman A, Burz DS, editors. Protein NMR techniques. Methods in molecular biology. 831: Humana Press; 2012. p. 55-69.
104. Salom D, Cao P, Yuan Y, Miyagi M, Feng Z, Palczewski K. Isotopic labeling of mammalian G protein-coupled receptors heterologously expressed in *Caenorhabditis elegans*. *Anal Biochem*. 2015;472:30-6.
105. Hauser H. Short-chain phospholipids as detergents. *Biochim Biophys Acta*. 2000;1508 (1–2):164-81.
106. Arora A, Abildgaard F, Bushweller JH, Tamm LK. Structure of outer membrane protein A transmembrane domain by NMR spectroscopy. *Nat Struct Biol*. 2001;8 (4):334-8.
107. Polenova T, Gupta R, Goldbourt A. Magic angle spinning NMR spectroscopy: A versatile technique for structural and dynamic analysis of solid-phase systems. *Anal Chem*. 2015;87 (11):5458-69.
108. Wang S, Munro RA, Shi L, Kawamura I, Okitsu T, Wada A, Kim SY, Jung KH, Brown LS, Ladizhansky V. Solid-state NMR spectroscopy structure determination of a lipid-embedded heptahelical membrane protein. *Nat Methods*. 2013;10 (10):1007-12.
109. Vogeley L, Sineshchekov OA, Trivedi VD, Sasaki J, Spudich JL, Luecke H. Anabaena sensory rhodopsin: A photochromic color sensor at 2.0 Å. *Science*. 2004;306 (5700):1390-3.

110. Wu CH, Ramamoorthy A, Opella SJ. High-resolution heteronuclear dipolar solid-state NMR spectroscopy. *J Magn Reson Ser A*. 1994;109 (2):270-2.
111. Park SH, Prytulla S, Angelis AAD, Brown JM, Kiefer H, Opella SJ. High-resolution NMR spectroscopy of a GPCR in aligned bicelles. *Journal of the American Chemical Society*. 2006;7402 (128):7402-3.
112. Wang J, Denny J, Tian C, Kim S, Mo Y, Kovacs F, Song Z, Nishimura K, Gan Z, Fu R, Quine JR, Cross TA. Imaging membrane protein helical wheels. *J Magn Reson*. 2000;144 (1):162-7.
113. Chekmenev EY, Hu J, Gor'kov PL, Brey WW, Cross TA, Ruuge A, Smirnov AI. ^{15}N and ^{31}P solid-state NMR study of transmembrane domain alignment of M2 protein of influenza A virus in hydrated cylindrical lipid bilayers confined to anodic aluminum oxide nanopores. *J Magn Reson*. 2005;173 (2):322-7.
114. Hu J, Asbury T, Achuthan S, Li C, Bertram R, Quine JR, Fu R, Cross TA. Backbone structure of the amantadine-blocked trans-membrane domain M2 proton channel from influenza A virus. *Biophys J*. 2007;92 (12):4335-43.
115. Sharma M, Yi M, Dong H, Qin H, Peterson E, Busath DD, Zhou H-X, Cross TA. Insight into the mechanism of the influenza A proton channel from a structure in a lipid bilayer. *Science*. 2010;330 (6003):509-12.
116. Sahu ID, Lorigan GA. Biophysical EPR studies applied to membrane proteins. *J Phys Chem Biophys*. 2015;5 (6):188.
117. Ling S, Zhang C, Wang W, Cai X, Yu L, Wu F, Zhang L, Tian C. Combined approaches of EPR and NMR illustrate only one transmembrane helix in the human IFITM3. *Sci Rep*. 2016;6:24029.
118. Li Q, Wanderling S, Sompornpisut P, Perozo E. Structural basis of lipid-driven conformational transitions in the KvAP voltage-sensing domain. *Nat Struct Mol Biol*. 2014;21 (2):160-6.
119. Lees JG, Miles AJ, Wien F, Wallace BA. A reference database for circular dichroism spectroscopy covering fold and secondary structure space. *Bioinformatics*. 2006;22 (16):1955-62.
120. Abdul-Gader A, Miles AJ, Wallace BA. A reference dataset for the analyses of membrane protein secondary structures and transmembrane residues using circular dichroism spectroscopy. *Bioinformatics*. 2011;27 (12):1630-6.
121. Evans P, Bateman OA, Slingsby C, Wallace BA. A reference dataset for circular dichroism spectroscopy tailored for the βγ-crystallin lens proteins. *Exp Eye Res*. 2007;84 (5):1001-8.

122. Tatulian SA. Structural characterization of membrane proteins and peptides by FTIR and ATR-FTIR spectroscopy. In: Kleinschmidt JH, editor. Lipid-protein interactions: Methods and protocols. Totowa, NJ: Humana Press; 2013. p. 177-218.
123. Ding F-X, Xie H, Arshava B, Becker JM, Naider F. ATR-FTIR study of the structure and orientation of transmembrane domains of the Saccharomyces cerevisiae α-mating factor receptor in phospholipids. *Biochemistry*. 2001;40 (30):8945-54.
124. Fasman GD, editor. Circular dichroism and the conformational analysis of biomolecules: Springer US; 1996.
125. Levitt MH. Spin dynamics: Basics of nuclear magnetic resonance: Wiley; 2008.
126. Moffitt W. The optical rotatory dispersion of simple polypeptides. II. *Proc Natl Acad Sci USA*. 1956;42 (10):736-46.
127. Moffitt W, Yang JT. The optical rotatory dispersion of simple polypeptides. I. *Proc Natl Acad Sci USA*. 1956;42 (9):596-603.
128. Bulheller BM, Rodger A, Hirst JD. Circular and linear dichroism of proteins. *Phys Chem Chem Phys*. 2007;9 (17):2020-35.
129. Burkhard P, Ivaninskii S, Lustig A. Improving coiled-coil stability by optimizing ionic interactions. *J Mol Biol*. 2002;318 (3):901-10.
130. Mao D, Wallace BA. Differential light scattering and absorption flattening optical effects are minimal in the circular dichroism spectra of small unilamellar vesicles. *Biochemistry*. 1984;23 (12):2667-73.
131. Loudet C, Khemtemourian L, Aussenac F, Gineste S, Achard MF, Dufourc EJ. Bicelle membranes and their use for hydrophobic peptide studies by circular dichroism and solid state NMR. *Biochim Biophys Acta*. 2005;1724 (3):315-23.
132. Miles AJ, Wallace BA. Circular dichroism spectroscopy of membrane proteins. *Chem Soc Rev*. 2016.
133. Wu Y, Huang HW, Olah GA. Method of oriented circular dichroism. *Biophys J*. 1990;57 (4):797-806.
134. Tinoco I. Circular dichroism and rotatory dispersion curves for helices. *J Am Chem Soc*. 1964;86 (2):297-8.
135. de Jongh HHJ, Goormaghtigh E, Killian JA. Analysis of circular dichroism spectra of oriented protein-lipid complexes: Toward a general application. *Biochemistry*. 1994;33 (48):14521-8.
136. Burck J, Wadhwani P, Fanghanel S, Ulrich AS. Oriented circular dichroism: A method to characterize membrane-active peptides in oriented lipid bilayers. *Acc Chem Res*. 2016;49 (2):184-92.

137. Caracciolo G, Pozzi D, Caminiti R. Hydration effect on the structure of dioleoylphosphatidylcholine bilayers. *Applied Physics Letters*. 2007;90 (18):183901.
138. Dave PC, Billington E, Pan YL, Straus SK. Interaction of alamethicin with ether-linked phospholipid bilayers: Oriented circular dichroism, ^{31}P solid-state NMR, and differential scanning calorimetry studies. *Biophys J*. 2005;89 (4):2434-42.
139. Vogel H. Comparison of the conformation and orientation of alamethicin and melittin in lipid membranes. *Biochemistry*. 1987;26 (14):4562-72.
140. Muccio DD, Cassim JY. Interpretation of the absorption and circular dichroic spectra of oriented purple membrane films. *Biophys J*. 1979;26 (3):427-40.
141. Olah GA, Huang HW. Circular dichroism of oriented α-helices. I. Proof of exciton theory. *J Phys Chem*. 1988;89 (4):2531-8.
142. Olah GA, Huang HW. Circular dichroism of oriented α-helices. II. Electric field oriented polypeptides. *J Chem Phys*. 1988;89 (11):6956-62.
143. Huang HW, Wu Y. Lipid-alamethicin interactions influence alamethicin orientation. *Biophys J*. 1991;60 (5):1079-87.
144. Glaser RW, Sachse C, Dürr UHN, Wadhwani P, Afonin S, Strandberg E, Ulrich AS. Concentration-dependent realignment of the antimicrobial peptide PGLa in lipid membranes observed by solid-state ^{19}F-NMR. *Biophys J*. 2005;88 (5):3392-7.
145. Bürck J, Roth S, Wadhwani P, Afonin S, Kanithasen N, Strandberg E, Ulrich AS. Conformation and membrane orientation of amphiphilic helical peptides by oriented circular dichroism. *Biophys J*. 2008;95 (8):3872-81.
146. Ge M, Budil DE, Freed JH. ESR studies of spin-labeled membranes aligned by isopotential spin-dry ultracentrifugation: Lipid-protein interactions. *Biophys J*. 1994;67 (6):2326-44.
147. Gröbner G, Taylor A, Williamson PTF, Choi G, Glaubitz C, Watts JA, de Grip WJ, Watts A. Macroscopic orientation of natural and model membranes for structural studies. *Anal Biochem*. 1997;254 (1):132-8.
148. Sutherland JC, Desmond EJ, Takacs PZ. Versatile spectrometer for experiments using synchrotron radiation at wave-lengths greater than 100 nm. *Nucl Instr Meth*. 1980;172 (1):195-9.
149. Nesgaard LW, Hoffmann SV, Andersen CB, Malmendal A, Otzen DE. Characterization of dry globular proteins and protein fibrils by synchrotron radiation vacuum UV circular dichroism. *Biopolymers*. 2008;89 (9):779-95.

150. Powl AM, O'Reilly AO, Miles AJ, Wallace BA. Synchrotron radiation circular dichroism spectroscopy-defined structure of the C-terminal domain of NaChBac and its role in channel assembly. *Proc Natl Acad Sci USA*. 2010;107 (32):14064-9.
151. Javorfi T, Hussain R, Myatt D, Siligardi G. Measuring circular dichroism in a capillary cell using the B23 synchrotron radiation CD beamline at diamond light source. *Chirality*. 2010;22 Suppl 1:E149-53.
152. Hussain R, Jávorfi T, Rudd TR, Siligardi G. High-throughput SRCD using multi-well plates and its applications. *Sci Rep*. 2016;6:38028.
153. Miles AJ, Janes RW, Brown A, Clarke DT, Sutherland JC, Tao Y, Wallace BA, Hoffmann SV. Light flux density threshold at which protein denaturation is induced by synchrotron radiation circular dichroism beamlines. *J Synchrotron Rad*. 2008;15:420-2.
154. Longo E, Hussain R, Siligardi G. Application of circular dichroism and magnetic circular dichroism for assessing biopharmaceuticals formulations photo-stability and small ligands binding properties. *Int J Pharm*. 2015;480 (1-2):84-91.
155. Haeberlen U. High resolution NMR in solids: Selective averaging: Academic Press; 1976.
156. Hahn EL. Spin echoes. *Phys Rev*. 1950;80 (4):580-94.
157. Freude D. Quadrupolar nuclei in solid-state nuclear magnetic resonance. Encyclopedia of analytical chemistry: John Wiley & Sons, Ltd; 2006.
158. Pines A, Gibby MG, Waugh JS. Proton-enhanced nuclear induction spectroscopy. A method for high resolution NMR of dilute spins in solids. *J Chem Phys*. 1972;56 (4):1776-7.
159. Marius P, Wright JN, Findlow IS, Williamson PT. Expression and purification of the transmembrane domain of Fukutin-I for biophysical studies. *Protein Expression Purif*. 2010;72 (1):107-12.
160. Marius P, Leung YM, Piggot TJ, Khalid S, Williamson PT. Probing the oligomeric state and interaction surfaces of Fukutin-I in dilauroylphosphatidylcholine bilayers. *Eur Biophys J*. 2012;41 (2):199-207.
161. Watanabe M, Kobayashi K, Jin F, Park KS, Yamada T, Tokunaga K, Toda T. Founder SVA retrotransposal insertion in Fukuyama-type congenital muscular dystrophy and its origin in japanese and northeast Asian populations. *Am J Med Genet A*. 2005;138 (4):344-8.

162. Fukuyama Y, Osawa M, Suzuki H. Congenital progressive muscular dystrophy of the Fukuyama type - clinical, genetic and pathological considerations. *Brain Dev*. 1981;3 (1):1-29.
163. de Graffenried CL, Bertozzi CR. The roles of enzyme localisation and complex formation in glycan assembly within the Golgi apparatus. *Curr Opin Cell Biol*. 2004;16 (4):356-63.
164. Michele DE, Barresi R, Kanagawa M, Saito F, Cohn RD, Satz JS, Dollar J, Nishino I, Kelley RI, Somer H, Straub V, Mathews KD, Moore SA, Campbell KP. Post-translational disruption of dystroglycan-ligand interactions in congenital muscular dystrophies. *Nature*. 2002;418.
165. Hayashi YK, Ogawa M, Tagawa K, Noguchi S, Ishihara T, Nonaka I, Arahata K. Selective deficiency of α-dystroglycan in Fukuyama-type congenital muscular dystrophy. *Neurology*. 2001;57.
166. Matsumoto H, Noguchi S, Sugie K, Ogawa M, Murayama K, Hayashi YK, Nishino I. Subcellular localization of fukutin and fukutin-related protein in muscle cells. *J Biochem*. 2004;135 (6):709-12.
167. Saito F, Matsumura K. Fukuyama-type congenital muscular dystrophy and defective glycosylation of α-dystroglycan. *Skeletal Muscle*. 2011;1 (1):22.
168. Kobayashi K, Nakahori Y, Miyake M, Matsumura K, Kondo-Iida E, Nomura Y, Segawa M, Yoshioka M, Saito K, Osawa M, Hamano K, Sakakihara Y, Nonaka I, Nakagome Y, Kanazawa I, Nakamura Y, Tokunaga K, Toda T. An ancient retrotransposal insertion causes Fukuyama-type congenital muscular dystrophy. *Nature*. 1998;394 (6691):388-92.
169. Kondo-Iida E, Kobayashi K, Watanabe M, Sasaki J, Kumagai T, Koide H, Saito K, Osawa M, Nakamura Y, Toda T. Novel mutations and genotype-phenotype relationships in 107 families with Fukuyama-type congenital muscular dystrophy (FCMD). *Hum Mol Genet*. 1999;8.
170. Ismail S, Schaffer AE, Rosti RO, Gleeson JG, Zaki MS. Novel mutation in the fukutin gene in an egyptian family with Fukuyama congenital muscular dystrophy and microcephaly. *Gene*. 2014;539 (2):279-82.
171. Brockington M, Torelli S, Prandini P, Boito C, Dolatshad NF, Longman C, Brown SC, Muntoni F. Localization and functional analysis of the LARGE family of glycosyltransferases: Significance for muscular dystrophy. *Hum Mol Genet*. 2005;14 (5):657-65.

172. Pereira NA, Pu HX, Goh H, Song Z. Golgi phosphoprotein 3 mediates the Golgi localization and function of protein O-linked mannose β-1,2-N-acetlyglucosaminyltransferase 1. *J Biol Chem*. 2014;289 (21):14762-70.
173. Tachikawa M, Kanagawa M, Yu CC, Kobayashi K, Toda T. Mislocalization of fukutin protein by disease-causing missense mutations can be rescued with treatments directed at folding amelioration. *J Biol Chem*. 2012;287 (11):8398-406.
174. Jackson CL. Mechanisms of transport through the Golgi complex. *J Cell Sci*. 2009;122 (Pt 4):443-52.
175. Colley KJ. Golgi localization of glycosyltransferases: More questions than answers. *Glycobiology*. 1997;7 (1):1-13.
176. Xiong H, Kobayashi K, Tachikawa M, Manya H, Takeda S, Chiyonobu T, Fujikake N, Wang F, Nishimoto A, Morris GE, Nagai Y, Kanagawa M, Endo T, Toda T. Molecular interaction between fukutin and POMGnT1 in the glycosylation pathway of α-dystroglycan. *Biochem Biophys Res Commun*. 2006;350.
177. Gao C, Cai Y, Wang Y, Kang BH, Aniento F, Robinson DG, Jiang L. Retention mechanisms for ER and Golgi membrane proteins. *Trends Plant Sci*. 2014.
178. Adamian L, Liang J. Interhelical hydrogen bonds and spatial motifs in membrane proteins: Polar clamps and serine zippers. *Proteins*. 2002;47 (2):209-18.
179. Lemmon MA, Treutlein HR, Adams PD, Brünger AT, Engelman DM. A dimerization motif for transmembrane α–helices. *Nat Struct Biol*. 1994;1:157.
180. Bocharov EV, Mineev KS, Goncharuk MV, Arseniev AS. Structural and thermodynamic insight into the process of "weak" dimerization of the erbb4 transmembrane domain by solution NMR. *Biochim Biophys Acta*. 2012;1818 (9):2158-70.
181. Alhamidi M, Kjeldsen Buvang E, Fagerheim T, Brox V, Lindal S, Van Ghelue M, Nilssen O. Fukutin-related protein resides in the Golgi cisternae of skeletal muscle fibres and forms disulfide-linked homodimers via an N-terminal interaction. *PLoS One*. 2011;6 (8):e22968.
182. Sasai K, Ikeda Y, Tsuda T, Ihara H, Korekane H, Shiota K, Taniguchi N. The critical role of the stem region as a functional domain responsible for the oligomerization and Golgi localization of N-acetylglucosaminyltransferase v: The involvement of A domain homophilic interaction. *J Biol Chem*. 2001;276 (1):759-65.
183. Seelig J. ^{31}P nuclear magnetic resonance and the head group structure of phospholipids in membranes. *Biochim Biophys Acta*. 1978;515 (2):105-40.

184. Seelig J. Deuterium magnetic resonance: Theory and application to lipid membranes. *Q Rev Biophys*. 1977;10 (3):353-418.
185. Cheng VB, Suzukawa HH, Wolfsberg M. Investigations of a nonrandom numerical method for multidimensional integration. *J Chem Phys*. 1973;59 (8):3992-9.
186. Tristram-Nagle SA. Preparation of oriented, fully hydrated lipid samples for structure determination using X-ray scattering. *Methods Mol Biol*. 2007;400:63-75.
187. Greenspan L. Humidity fixed points of binary saturated aqueous solutions. *J Res Natl Bur Stand A*. 1977;81a (1):89-96.
188. van Beek JD. matNMR: A flexible toolbox for processing, analyzing and visualizing magnetic resonance data in Matlab. *J Magn Reson*. 2007;187 (1):19-26.
189. Bertani P, Raya J, Bechinger B. ^{15}N chemical shift referencing in solid state NMR. *Solid State Nucl Magn Reson*. 2014;61-62:15-8.
190. Hussain R, Javorfi T, Siligardi G. Circular dichroism beamline B23 at the Diamond Light Source. *J Synchrotron Rad*. 2012;19 (Pt 1):132-5.
191. Chen GC, Yang JT. Two-point calibration of circular dichrometer with d-10-camphorsulfonic acid. *Anal Lett*. 1977;10 (14):1195-207.
192. Hussain R, Benning K, Javorfi T, Longo E, Rudd TR, Pulford B, Siligardi G. CDApps: Integrated software for experimental planning and data processing at beamline B23, Diamond Light Source. *J Synchrotron Rad*. 2015;22 (2):465-8.
193. Whitmore L, Wallace BA. Dichroweb, an online server for protein secondary structure analyses from circular dichroism spectroscopic data. *Nucleic Acids Res*. 2004;32 (Web Server issue):W668-73.
194. van Stokkum IH, Spoelder HJ, Bloemendal M, van Grondelle R, Groen FC. Estimation of protein secondary structure and error analysis from circular dichroism spectra. *Anal Biochem*. 1990;191 (1):110-8.
195. Provencher SW, Gloeckner J. Estimation of globular protein secondary structure from circular dichroism. *Biochemistry*. 1981;20 (1):33-7.
196. Miles AJ, Wallace BA. Synchrotron radiation circular dichroism spectroscopy of proteins and applications in structural and functional genomics. *Chem Soc Rev*. 2006;35 (1):39-51.
197. Wien F, Wallace BA. Calcium fluoride micro cells for synchrotron radiation circular dichroism spectroscopy. *Appl Spectrosc*. 2005;59 (9):1109-13.
198. Wallace BA, Lees JG, Orry AJ, Lobley A, Janes RW. Analyses of circular dichroism spectra of membrane proteins. *Protein Sci*. 2003;12 (4):875-84.

199. Gasteiger E, Hoogland C, Gattiker A, Duvaud Se, Wilkins MR, Appel RD, Bairoch A. Protein identification and analysis tools on the expasy server. In: Walker JM, editor. The proteomics protocols handbook. Totowa, NJ: Humana Press; 2005. p. 571-607.
200. Rath A, Glibowicka M, Nadeau VG, Chen G, Deber CM. Detergent binding explains anomalous SDS-PAGE migration of membrane proteins. *Proc Natl Acad Sci USA*. 2009;106 (6):1760-5.
201. Kučerka N, Liu Y, Chu N, Petrache HI, Tristram-Nagle S, Nagle JF. Structure of fully hydrated fluid phase DMPC and DLPC lipid bilayers using X-ray scattering from oriented multilamellar arrays and from unilamellar vesicles. *Biophys J*. 2005;88 (4):2626-37.
202. Nagle JF, Wiener MC. Structure of fully hydrated bilayer dispersions. *Biochim Biophys Acta*. 1988;942 (1):1-10.
203. Ouellet M, Doucet JD, Voyer N, Auger M. Membrane topology of a 14-mer model amphipathic peptide: A solid-state NMR spectroscopy study. *Biochemistry*. 2007;46 (22):6597-606.
204. Lindström F, Williamson PTF, Gröbner G. Molecular insight into the electrostatic membrane surface potential by $^{14}N/^{31}P$ MAS NMR spectroscopy: Nociceptin−lipid association. *J Am Chem Soc*. 2005.
205. Pukala TL, Boland MP, Gehman JD, Kuhn-Nentwig L, Separovic F, Bowie JH. Solution structure and interaction of cupiennin 1a, a spider venom peptide, with phospholipid bilayers. *Biochemistry*. 2007;46 (11):3576-85.
206. Jacobs RE, Oldfield E. NMR of membranes. *Prog Nucl Magn Reson Spectrosc*. 1980;14 (3):113-36.
207. Marassi FM, Crowell KJ. Hydration-optimized oriented phospholipid bilayer samples for solid-state NMR structural studies of membrane proteins. *J Magn Reson*. 2003;161 (1):64-9.
208. Ulrich AS, Watts A. Molecular response of the lipid headgroup to bilayer hydration monitored by ^{2}H-NMR. *Biophys J*. 1994;66 (5):1441-9.
209. Cooper GM. The Cell - A Molecular Approach. 2nd Ed. Sunderland, Massachusetts, USA Sinauer Associates; 2000.
210. Moll F, Cross TA. Optimizing and characterizing alignment of oriented lipid bilayers containing gramicidin D. *Biophys J*. 1990;57 (2):351-62.

211. Williamson PTF, Zandomeneghi G, Barrantes FJ, Watts A, Meier BH. Structural and dynamic studies of the γ-M4 trans-membrane domain of the nicotinic acetylcholine receptor. *Mol Membr Biol*. 2005;22 (6):485-96.
212. Muhle-Goll C, Hoffmann S, Afonin S, Grage SL, Polyansky AA, Windisch D, Zeitler M, Bürck J, Ulrich AS. Hydrophobic matching controls the tilt and stability of the dimeric platelet-derived growth factor receptor (PDGFR) β transmembrane segment. *J Biol Chem*. 2012;287 (31):26178-86.
213. Kuwabara N, Manya H, Yamada T, Tateno H, Kanagawa M, Kobayashi K, Akasaka-Manya K, Hirose Y, Mizuno M, Ikeguchi M, Toda T, Hirabayashi J, Senda T, Endo T, Kato R. Carbohydrate-binding domain of the POMGnT1 stem region modulates O-mannosylation sites of α-dystroglycan. *Proc Natl Acad Sci USA*. 2016;113 (33):9280-5.
214. Drozdetskiy A, Cole C, Procter J, Barton GJ. JPred4: A protein secondary structure prediction server. *Nucleic Acids Res*. 2015;43 (W1):W389-W94.
215. Bartle KD, Wright BW, Lee ML. Characterization of glass, quartz, and fused silica capillary column surfaces from contact-angle measurements. *Chromatographia*. 1981;14 (7):387-97.
216. Sani MA, Whitwell TC, Separovic F. Lipid composition regulates the conformation and insertion of the antimicrobial peptide maculatin 1.1. *Biochim Biophys Acta*. 2012;1818 (2):205-11.
217. Buffy JJ, McCormick MJ, Wi S, Waring A, Lehrer RI, Hong M. Solid-state NMR investigation of the selective perturbation of lipid bilayers by the cyclic antimicrobial peptide RTD-1. *Biochemistry*. 2004;43 (30):9800-12.
218. Greenfield NJ. Using circular dichroism collected as a function of temperature to determine the thermodynamics of protein unfolding and binding interactions. *Nat Protoc*. 2006;1 (6):2527-35.
219. Asher SA, Pershan PS. Alignment and defect structures in oriented phosphatidylcholine multilayers. *Biophys J*. 1979;27 (3):393-421.
220. Park SH, Opella SJ. Tilt angle of a trans-membrane helix is determined by hydrophobic mismatch. *J Mol Biol*. 2005;350 (2):310-8.
221. Sparr E, Ash WL, Nazarov PV, Rijkers DT, Hemminga MA, Tieleman DP, Killian JA. Self-association of transmembrane α-helices in model membranes: Importance of helix orientation and role of hydrophobic mismatch. *J Biol Chem*. 2005;280 (47):39324-31.

222. Kyte J, Doolittle RF. A simple method for displaying the hydropathic character of a protein. *J Mol Biol*. 1982;157 (1):105-32.
223. Munro S. An investigation of the role of transmembrane domains in Golgi protein retention. *EMBO J*. 1995;14 (19):4695-704.
224. Yeagle PL, Bennett M, Lemaitre V, Watts A. Transmembrane helices of membrane proteins may flex to satisfy hydrophobic mismatch. *Biochim Biophys Acta*. 2007;1768 (3):530-7.
225. Zinna F, Resta C, Górecki M, Pescitelli G, Di Bari L, Jávorfi T, Hussain R, Siligardi G. Circular dichroism imaging: Mapping the local supramolecular order in thin films of chiral functional polymers. *Macromolecules*. 2017;50 (5):2054-60.
226. Kim DM, Dikiy I, Upadhyay V, Posson DJ, Eliezer D, Nimigean CM. Conformational heterogeneity in closed and open states of the KcsA potassium channel in lipid bicelles. *J Gen Physiol*. 2016.
227. Duc NM, Du Y, Zhang C, Lee SY, Thorsen TS, Kobilka BK, Chung KY. Effective application of bicelles for conformational analysis of G protein-coupled receptors by hydrogen/deuterium exchange mass spectrometry. *J Am Soc Mass Spectrom*. 2015;26 (5):808-17.
228. Chen Q, Vishnivetskiy SA, Zhuang T, Cho MK, Thaker TM, Sanders CR, Gurevich VV, Iverson TM. The rhodopsin-arrestin-1 interaction in bicelles. *Methods Mol Biol*. 2015;1271:77-95.
229. Park SH, Prytulla S, De Angelis AA, Brown JM, Kiefer H, Opella SJ. High-resolution NMR spectroscopy of a GPCR in aligned bicelles. *J Am Chem Soc*. 2006;128 (23):7402-3.
230. Triba MN, Zoonens M, Popot J-L, Devaux PF, Warschawski DE. Reconstitution and alignment by a magnetic field of a β-barrel membrane protein in bicelles. *Eur Biophys J*. 2006;35 (3):268-75.
231. Pachence J, Knott R, Schoenborn B, Wallace B. Formation of oriented membrane multilayers of Na/K-ATPase. *Ann N Y Acad Sci*. 1984;435 (1):566-9.
232. Boroske E, Helfrich W. Magnetic anisotropy of egg lecithin membranes. *Biophys J*. 1978;24 (3):863-8.
233. Helfrich W. Lipid bilayer spheres: Deformation and birefringence in magnetic fields. *Phys Lett A*. 1973;43 (5):409-10.
234. Speyer JB, Sripada PK, Das Gupta SK, Shipley GG, Griffin RG. Magnetic orientation of sphingomyelin-lecithin bilayers. *Biophys J*. 1987;51 (4):687-91.

235. Sanders CR, Prestegard JH. Magnetically orientable phospholipid bilayers containing small amounts of a bile salt analogue, CHAPSO. *Biophys J*. 1990;58 (2):447-60.
236. Sanders CR, Prosser RS. Bicelles: A model membrane system for all seasons? *Structure*. 1998;6 (10):1227-34.
237. Ram P, Prestegard JH. Magnetic field induced ordering of bile salt/phospholipid micelles: New media for NMR structural investigations. *Biochim Biophys Acta*. 1988;940 (2):289-94.
238. Beaugrand M, Arnold AA, Henin J, Warschawski DE, Williamson PT, Marcotte I. Lipid concentration and molar ratio boundaries for the use of isotropic bicelles. *Langmuir*. 2014;30 (21):6162-70.
239. Liebi M, van Rhee PG, Christianen PC, Kohlbrecher J, Fischer P, Walde P, Windhab EJ. Alignment of bicelles studied with high-field magnetic birefringence and small-angle neutron scattering measurements. *Langmuir*. 2013;29 (10):3467-73.
240. Nieh MP, Raghunathan VA, Glinka CJ, Harroun TA, Pabst G, Katsaras J. Magnetically alignable phase of phospholipid "bicelle" mixtures is a chiral nematic made up of wormlike micelles. *Langmuir*. 2004;20 (19):7893-7.
241. Triba MN, Warschawski DE, Devaux PF. Reinvestigation by phosphorus NMR of lipid distribution in bicelles. *Biophys J*. 2005;88 (3):1887-901.
242. Caporini MA, Padmanabhan A, Cardon TB, Lorigan GA. Investigating magnetically aligned phospholipid bilayers with various lanthanide ions for X-band spin-label EPR studies. *Biochim Biophys Acta*. 2003;1612 (1):52-8.
243. Harroun TA, Desrochers CM, Nieh MP, Watson MJ, Katsaras J. 0.9T static magnetic field and temperature-controlled specimen environment for use with general-purpose optical microscopes. *Rev Sci Instrum*. 2006;77 (1):014102.
244. Prosser RS, Volkov VB, Shiyanovskaya IV. Solid-state NMR studies of magnetically aligned phospholipid membranes: Taming lanthanides for membrane protein studies. *Biochem Cell Biol*. 1998;76 (2-3):443-51.
245. Mironov VS, Galyametdinov YG, Ceulemans A, Binnemans K. On the magnetic anisotropy of lanthanide-containing metallomesogens. *J Chem Phys*. 2000;113 (22):10293-303.
246. Binnemans K. Physical properties of metallomesogens. Molecular materials: John Wiley & Sons, Ltd; 2010. p. 61-141.
247. Park SH, Loudet C, Marassi FM, Dufourc EJ, Opella SJ. Solid-state NMR spectroscopy of a membrane protein in biphenyl phospholipid bicelles with the bilayer normal parallel to the magnetic field. *J Magn Reson*. 2008;193 (1):133-8.

248. Prosser RS, Hwang JS, Vold RR. Magnetically aligned phospholipid bilayers with positive ordering: A new model membrane system. *Biophys J*. 1998;74 (5):2405-18.
249. Otting G. Prospects for lanthanides in structural biology by NMR. *J Biomol NMR*. 2008;42 (1):1-9.
250. Perkins SJ, Wüthrich K. Structural interpretation of lanthanide binding to the basic pancreatic trypsin inhibitor by 1H NMR at 360 MHz. *Biochim Biophys Acta*. 1978;536 (2):406-20.
251. Prosser RS, Bryant H, Bryant RG, Vold RR. Lanthanide chelates as bilayer alignment tools in NMR studies of membrane-associated peptides. *J Magn Reson*. 1999;141 (2):256-60.
252. Prosser RS, Volkov VB, Shiyanovskaya IV. Novel chelate-induced magnetic alignment of biological membranes. *Biophys J*. 1998;75 (5):2163-9.
253. Liebi M, Kuster S, Kohlbrecher J, Ishikawa T, Fischer P, Walde P, Windhab EJ. Cholesterol-diethylenetriaminepentaacetate complexed with thulium ions integrated into bicelles to increase their magnetic alignability. *J Phys Chem B*. 2013;117 (47):14743-8.
254. Tan C, Fung BM, Cho G. Phospholipid bicelles that align with their normals parallel to the magnetic field. *J Am Chem Soc*. 2002;124 (39):11827-32.
255. Marcotte I, Belanger A, Auger M. The orientation effect of gramicidin A on bicelles and Eu^{3+} -doped bicelles as studied by solid-state NMR and FT-IR spectroscopy. *Chem Phys Lipids*. 2006;139 (2):137-49.
256. Yamamoto K, Pearcy P, Lee DK, Yu C, Im SC, Waskell L, Ramamoorthy A. Temperature-resistant bicelles for structural studies by solid-state NMR spectroscopy. *Langmuir*. 2015;31 (4):1496-504.
257. Prosser RS, Hunt SA, DiNatale JA, Vold RR. Magnetically aligned membrane model systems with positive order parameter: Switching the sign of S_{zz} with paramagnetic ions. *J Am Chem Soc*. 1996;118 (1):269-70.
258. Yamamoto K, Soong R, Ramamoorthy A. Comprehensive analysis of lipid dynamics variation with lipid composition and hydration of bicelles using nuclear magnetic resonance (NMR) spectroscopy. *Langmuir*. 2009;25 (12):7010-8.
259. Holmquist B, Vallee BL. Tryptophan quantitation by magnetic circular dichroism in native and modified proteins. *Biochemistry*. 1973;12 (22):4409-17.
260. Vitale DJ, Goldbeck RA, Kim-Shapiro DB, Esquerra RM, Parkhurst LJ, Kliger DS. Near-ultraviolet magnetic circular dichroism spectroscopy of protein conformational

states: Correlation of tryptophan band position and intensity with hemoglobin allostery. *Biochemistry*. 2000;39 (24):7145-52.

261. Campbell I. Biophysical techniques: OUP Oxford; 2012.
262. Sutherland JC, Holmquist B. Magnetic circular dichroism of biological molecules. *Annu Rev Biophys Bioeng*. 1980;9:293-326.
263. Hemminga MA. Analysis of the ESR spectra of the cholestane spin label in oriented multibilayers of lecithin and cholesterol in the gel state. *J Magn Reson (1969)*. 1977;25 (1):25-45.
264. Yankova TS, Bobrovsky AY, Vorobiev AK. Order parameters ⟨p2⟩, ⟨p4⟩, and ⟨p6⟩ of aligned nematic liquid-crystalline polymer as determined by numerical simulation of electron paramagnetic resonance spectra. *J Phys Chem B*. 2012;116 (20):6010-6.
265. Hogben HJ, Krzystyniak M, Charnock GT, Hore PJ, Kuprov I. Spinach--a software library for simulation of spin dynamics in large spin systems. *J Magn Reson*. 2011;208 (2):179-94.
266. Presti FT, Chan SI. Cholesterol-phospholipid interaction in membranes. 1. Cholestane spin-label studies of phase behavior of cholesterol-phospholipid liposomes. *Biochemistry*. 1982;21 (16):3821-30.
267. Ammann C, Meier P, Merbach A. A simple multinuclear NMR thermometer. *J Magn Reson (1969)*. 1982;46 (2):319-21.
268. Loudet C, Khemtémourian L, Aussenac F, Gineste S, Achard M-F, Dufourc EJ. Bicelle membranes and their use for hydrophobic peptide studies by circular dichroism and solid state NMR. *Biochim Biophys Acta*. 2005;1724 (3):315-23.
269. Sanders CR, Schwonek JP. Characterization of magnetically orientable bilayers in mixtures of dihexanoylphosphatidylcholine and dimyristoylphosphatidylcholine by solid-state NMR. *Biochemistry*. 1992.
270. Nieh M-P, Glinka CJ, Krueger S, Prosser RS, Katsaras J. SANS study on the effect of lanthanide ions and charged lipids on the morphology of phospholipid mixtures. Small-angle neutron scattering. *Biophys J*. 2002;82 (5):2487-98.
271. Hwang JS, Oweimreen GA. Anomalous viscosity behavior of a bicelle system with various molar ratios of short-and long-chain phospholipids. *Arab J Sci Eng - Sect B Eng*. 2003;28 (1A):43-9.
272. Struppe J, Vold RR. Dilute bicellar solutions for structural NMR work. *J Magn Reson*. 1998;135 (2):541-6.

273. Cardon TB, Tiburu EK, Padmanabhan A, Howard KP, Lorigan GA. Magnetically aligned phospholipid bilayers at the parallel and perpendicular orientations for X-band spin-label EPR studies. *J Am Chem Soc*. 2001;123 (12):2913-4.
274. Dave PC, Nusair NA, Inbaraj JJ, Lorigan GA. Electron paramagnetic resonance studies of magnetically aligned phospholipid bilayers utilizing a phospholipid spin label: The effect of cholesterol. *Biochim Biophys Acta*. 2005;1714 (2):141-51.
275. Mangels ML, Cardon TB, Harper AC, Howard KP, Lorigan GA. Spectroscopic characterization of spin-labeled magnetically oriented phospholipid bilayers by EPR spectroscopy. *J Am Chem Soc*. 2000;122 (29):7052-8.
276. Garber SM, Lorigan GA, Howard KP. Magnetically oriented phospholipid bilayers for spin label EPR studies. *J Am Chem Soc*. 1999;121 (13):3240-1.
277. Cardon TB, Tiburu EK, Lorigan GA. Magnetically aligned phospholipid bilayers in weak magnetic fields: Optimization, mechanism, and advantages for X-band EPR studies. *J Magn Reson*. 2003;161 (1):77-90.
278. Ghimire H, Inbaraj JJ, Lorigan GA. A comparative study of the effect of cholesterol on bicelle model membranes using X-band and Q-band EPR spectroscopy. *Chem Phys Lipids*. 2009;160 (2):98-104.
279. Miller IR, Chapman D, Drake AF. Circular dichroism spectra of aqueous dispersions of sphingolipids. *Biochim Biophys Acta*. 1986;856 (3):654-60.
280. Whiles JA, Brasseur R, Glover KJ, Melacini G, Komives EA, Vold RR. Orientation and effects of mastoparan X on phospholipid bicelles. *Biophys J*. 2001;80 (1):280-93.
281. Weber DK, Sani MA, Downton MT, Separovic F, Keene FR, Collins JG. Membrane insertion of a dinuclear polypyridylruthenium(II) complex revealed by solid-state NMR and molecular dynamics simulation: Implications for selective antibacterial activity. *J Am Chem Soc*. 2016;138 (46):15267-77.
282. Ramamoorthy A. NMR spectroscopy of biological solids: CRC Press; 2005.
283. Howard KP, Opella SJ. High-resolution solid-state NMR spectra of integral membrane proteins reconstituted into magnetically oriented phospholipid bilayers. *Journal of Magnetic Resonance, Series B*. 1996;112 (1):91-4.
284. Park SH, Das BB, De Angelis AA, Scrima M, Opella SJ. Mechanically, magnetically, and "rotationally aligned" membrane proteins in phospholipid bilayers give equivalent angular constraints for NMR structure determination. *J Phys Chem B*. 2010;114 (44):13995-4003.
285. Beaugrand M, Arnold AA, Juneau A, Gambaro AB, Warschawski DE, Williamson PTF, Marcotte I. Magnetically oriented bicelles with monoalkylphosphocholines:

Versatile membrane mimetics for nuclear magnetic resonance applications. *Langmuir*. 2016;32 (49):13244-51.

286. McMaster J, Oganesyan VS. Magnetic circular dichroism spectroscopy as a probe of the structures of the metal sites in metalloproteins. *Curr Opin Struct Biol*. 2010;20 (5):615-22.
287. Svensson FR, Lincoln P, Norden B, Esbjorner EK. Retinoid chromophores as probes of membrane lipid order. *J Phys Chem B*. 2007;111 (36):10839-48.
288. Shindo Y, Nakagawa M, Ohmi Y. On the problems of CD spectropolarimeters. II: Artifacts in CD spectrometers. *Appl Spectrosc*. 1985;39 (5):860-8.
289. Sasaki H, Fukuzawa S, Kikuchi J, Yokoyama S, Hirota H, Tachibana K. Cholesterol doping induced enhanced stability of bicelles. *Langmuir*. 2003;19 (23):9841-4.
290. Bortolus M, De Zotti M, Formaggio F, Maniero AL. Alamethicin in bicelles: Orientation, aggregation, and bilayer modification as a function of peptide concentration. *Biochim Biophys Acta*. 2013;1828 (11):2620-7.
291. Marcotte I, Wegener KL, Lam Y-H, Chia BCS, de Planque MRR, Bowie JH, Auger M, Separovic F. Interaction of antimicrobial peptides from Australian amphibians with lipid membranes. *Chem Phys Lipids*. 2003;122 (1–2):107-20.
292. Marcotte I, Dufourc EJ, Ouellet M, Auger M. Interaction of the neuropeptide met-enkephalin with zwitterionic and negatively charged bicelles as viewed by ^{31}P and ^{2}H solid-state NMR. *Biophys J*. 2003;85 (1):328-39.
293. McCaffrey JE, James ZM, Thomas DD. Optimization of bicelle lipid composition and temperature for EPR spectroscopy of aligned membranes. *J Magn Reson*. 2015;250:71-5.
294. Shapiro RA, Brindley AJ, Martin RW. Thermal stabilization of DMPC/DHPC bicelles by addition of cholesterol sulfate. *J Am Chem Soc*. 2010;132 (33):11406-7.
295. Kuang Q, Purhonen P, Hebert H. Structure of potassium channels. *Cell Mol Life Sci*. 2015;72 (19):3677-93.
296. Vandenberg JI, Perry MD, Perrin MJ, Mann SA, Ke Y, Hill AP. hERG K^+ channels: Structure, function, and clinical significance. *Physiol Rev*. 2012;92 (3):1393-478.
297. Nerbonne JM, Kass RS. Molecular physiology of cardiac repolarization. *Physiol Rev*. 2005;85 (4):1205.
298. Zhou Z, Gong Q, Epstein ML, January CT. HERG channel dysfunction in human long QT syndrome: Intracellular transport and functional defects. *J Biol Chem*. 1998;273 (33):21061-6.

299. Milnes JT, Crociani O, Arcangeli A, Hancox JC, Witchel HJ. Blockade of HERG potassium currents by fluvoxamine: Incomplete attenuation by S6 mutations at F656 or Y652. *Br J Pharmacol*. 2003;139 (5):887-98.
300. Stummann TC, Beilmann M, Duker G, Dumotier B, Fredriksson JM, Jones RL, Hasiwa M, Kang YJ, Mandenius CF, Meyer T, Minotti G, Valentin YJ, Zunkler BJ, Bremer S. Report and recommendations of the workshop of the european centre for the validation of alternative methods for drug-induced cardiotoxicity. *Cardiovasc Toxicol*. 2009;9 (3):107-25.
301. Jehle J, Schweizer PA, Katus HA, Thomas D. Novel roles for hERG K^+ channels in cell proliferation and apoptosis. *Cell Death Dis*. 2011;2:e193.
302. Babcock JJ, Li M. hERG channel function: Beyond long QT. *Acta Pharmacol Sin*. 2013;34 (3):329-35.
303. Kannankeril P, Roden DM, Darbar D. Drug-induced long QT syndrome. *Pharmacol Rev*. 2010;62 (4):760-81.
304. Administration FaD. Guidance for industry. In: Services USDoHaH, editor. S7B Nonclinical Evaluation of the Potential for Delayed Ventricular Repolarization (QT Interval Prolongation) by Human Pharmaceuticals 2005.
305. Fernandez D, Ghanta A, Kauffman GW, Sanguinetti MC. Physicochemical features of the hERG channel drug binding site. *J Biol Chem*. 2004;279 (11):10120-7.
306. Mitcheson JS, Chen J, Lin M, Culberson C, Sanguinetti MC. A structural basis for drug-induced long QT syndrome. *Proc Natl Acad Sci USA*. 2000;97 (22):12329-33.
307. Aronov AM. Common pharmacophores for uncharged human Ether-a-go-go-related gene (hERG) blockers. *J Med Chem*. 2006;49 (23):6917-21.
308. Wang W, MacKinnon R. Cryo-em structure of the open human *Ether-à-go-go*-related K^+ channel hERG. *Cell*. 2017;169 (3):422-30 e10.
309. Vandenberg JI, Torres AM, Campbell TJ, Kuchel PW. The HERG K^+ channel: Progress in understanding the molecular basis of its unusual gating kinetics. *Eur Biophys J*. 2004;33 (5):468-.
310. Torres AM, Bansal PS, Sunde M, Clarke CE, Bursill JA, Smith DJ, Bauskin A, Breit SN, Campbell TJ, Alewood PF, Kuchel PW, Vandenberg JI. Structure of the HERG K^+ channel S5P extracellular linker: Role of an amphipathic α-helix in C-type inactivation. *J Biol Chem*. 2003;278 (43):42136-48.
311. Clarke CE, Hill AP, Zhao J, Kondo M, Subbiah RN, Campbell TJ, Vandenberg JI. *J Physiol*. 2006;573 (Pt 2):291-304.

312. Stephens RF, Guan W, Zhorov BS, Spafford JD. Selectivity filters and cysteine-rich extracellular loops in voltage-gated sodium, calcium, and NALCN channels. *Front Physiol*. 2015;6:153.
313. Cabral JHM, Lee A, Cohen SL, Chait BT, Li M, Mackinnon R. Crystal structure and functional analysis of the HERG potassium channel N terminus. *Cell*. 1998;95 (5):649-55.
314. Li Y, Ng HQ, Li Q, Kang C. Structure of the cyclic nucleotide-binding homology domain of the hERG channel and its insight into type 2 long QT syndrome. *Sci Rep*. 2016;6:23712.
315. Doyle DA, Morais Cabral J, Pfuetzner RA, Kuo A, Gulbis JM, Cohen SL, Chait BT, MacKinnon R. The structure of the potassium channel: Molecular basis of K^+ conduction and selectivity. *Science*. 1998;280 (5360):69-77.
316. Baker KA, Tzitzilonis C, Kwiatkowski W, Choe S, Riek R. Conformational dynamics of the KcsA potassium channel governs gating properties. *Nat Struct Mol Biol*. 2007;14 (11):1089-95.
317. Cordero-Morales JF, Cuello LG, Zhao Y, Jogini V, Cortes DM, Roux B, Perozo E. Molecular determinants of gating at the potassium-channel selectivity filter. *Nat Struct Mol Biol*. 2006;13 (4):311-8.
318. Schneider CA, Rasband WS, Eliceiri KW. Nih image to ImageJ: 25 years of image analysis. *Nat Methods*. 2012;9 (7):671-5.
319. Heginbotham L, Odessey E, Miller C. Tetrameric stoichiometry of a prokaryotic K^+ channel. *Biochemistry*. 1997;36 (33):10335-42.
320. Chisnall B, Johnson C, Kulaberoglu Y, Chen YW. Insoluble protein purification with sarkosyl: Facts and precautions. *Methods Mol Biol*. 2014;1091:179-86.
321. Molina ML, Encinar JA, Barrera FN, Fernandez-Ballester G, Riquelme G, Gonzalez-Ros JM. Influence of C-terminal protein domains and protein-lipid interactions on tetramerization and stability of the potassium channel KcsA. *Biochemistry*. 2004;43 (47):14924-31.
322. Choi KH, Song C, Shin D, Park S. hERG channel blockade by externally applied quaternary ammonium derivatives. *Biochim Biophys Acta*. 2011;1808 (6):1560-6.
323. Lenaeus MJ, Vamvouka M, Focia PJ, Gross A. Structural basis of TEA blockade in a model potassium channel. *Nat Struct Mol Biol*. 2005;12 (5):454-9.
324. Kavanaugh MP, Varnum MD, Osborne PB, Christie MJ, Busch AE, Adelman JP, North RA. Interaction between tetraethylammonium and amino acid residues in the

pore of cloned voltage-dependent potassium channels. *J Biol Chem*. 1991;266 (12):7583-7.

325. Bolanos-Garcia VM, Davies OR. Structural analysis and classification of native proteins from E. coli commonly co-purified by immobilised metal affinity chromatography. *Biochim Biophys Acta*. 2006;1760 (9):1304-13.
326. Frottin F, Martinez A, Peynot P, Mitra S, Holz RC, Giglione C, Meinnel T. The proteomics of N-terminal methionine cleavage. *Mol Cell Proteomics*. 2006;5 (12):2336-49.
327. Mohanty AK, Wiener MC. Membrane protein expression and production: Effects of polyhistidine tag length and position. *Protein Expression Purif*. 2004;33 (2):311-25.
328. Bornhorst JA, Falke JJ. [16] purification of proteins using polyhistidine affinity tags. *Methods Enzymol*. 2000;326:245-54.
329. Kane JF, Hartley DL. Formation of recombinant protein inclusion bodies in *Escherichia coli*. *Trends Biotechnol*. 1988;6 (5):95-101.
330. Bannwarth M, Schulz GE. The expression of outer membrane proteins for crystallization. *Biochim Biophys Acta*. 2003;1610 (1):37-45.
331. Casagrande F, Maier K, Kiefer H, Opella SJ, Park SH. Expression and purification of G-protein-coupled receptors for nuclear magnetic resonance structural studies. Production of membrane proteins: Wiley-VCH Verlag GmbH & Co. KGaA; 2011. p. 297-316.
332. Rogl H, Kosemund K, Kühlbrandt W, Collinson I. Refolding of *Escherichia coli* produced membrane protein inclusion bodies immobilised by nickel chelating chromatography. *FEBS Lett*. 1998;432 (1–2):21-6.
333. Tao H, Liu W, Simmons BN, Harris HK, Cox TC, Massiah MA. Purifying natively folded proteins from inclusion bodies using sarkosyl, Triton X-100, and CHAPS. *BioTechniques*. 2010;48 (1):61-4.
334. Wei Y, Thyparambil AA, Latour RA. Protein helical structure determination using CD spectroscopy for solutions with strong background absorbance from 190 to 230nm. *Biochim Biophys Acta*. 2014;1844 (12):2331-7.
335. Kiefer H, Maier K, Vogel R. Refolding of G-protein-coupled receptors from inclusion bodies produced in *Escherichia coli*. *Biochem Soc Trans*. 1999;27 (6):908-12.
336. Lange C, Muller SD, Walther TH, Burck J, Ulrich AS. Structure analysis of the protein translocating channel TatA in membranes using a multi-construct approach. *Biochim Biophys Acta*. 2007;1768 (10):2627-34.

337. Wallgren M, Lidman M, Pedersen A, Br‰nnstrˆm K, Karlsson BG, Grˆbner G. Reconstitution of the anti-apoptotic Bcl-2 protein into lipid membranes and biophysical evidence for its detergent-driven association with the pro-apoptotic Bax protein. *PloS One*. 2013;8 (4):e61452.
338. Ashworth Briggs EL, Gomes RG, Elhussein M, Collier W, Findlow IS, Khalid S, McCormick CJ, Williamson PT. Interaction between the NS4B amphipathic helix, AH2, and charged lipid headgroups alters membrane morphology and AH2 oligomeric state--implications for the Hepatitis C virus life cycle. *Biochim Biophys Acta*. 2015;1848 (8):1671-7.
339. Yang H, Hu M, Guo J, Ou X, Cai T, Liu Z. Pore architecture of TRIC channels and insights into their gating mechanism. *Nature*. 2016;538 (7626):537-41.
340. Irizarry SN, Kutluay E, Drews G, Hart SJ, Heginbotham L. Opening the KcsA K^+ channel: Tryptophan scanning and complementation analysis lead to mutants with altered gating. *Biochemistry*. 2002;41 (46):13653-62.
341. Su Z, Brown EC, Wang W, MacKinnon R. Novel cell-free high-throughput screening method for pharmacological tools targeting K^+ channels. *Proc Natl Acad Sci USA*. 2016;113 (20):5748-53.
342. Molbaek K, Scharff-Poulsen P, Helix-Nielsen C, Klaerke DA, Pedersen P. High yield purification of full-length functional hERG K^+ channels produced in *Saccharomyces cerevisiae*. *Microb Cell Fact*. 2015;14 (1):15.
343. Ryba NJP, Marsh D. Protein rotational diffusion and lipid/protein interactions in recombinants of bovine rhodopsin with saturated diacylphosphatidylcholines of different chain lengths studied by conventional and saturation-transfer electron spin resonance. *Biochemistry*. 1992;31 (33):7511-8.
344. Loudet-Courreges C, Nallet F, Dufourc EJ, Oda R. Unprecedented observation of days-long remnant orientation of phospholipid bicelles: A small-angle X-ray scattering and theoretical study. *Langmuir*. 2011;27 (15):9122-30.
345. Kogan M, Norden B, Beke-Somfai T. High anisotropy of flow-aligned bicellar membrane systems. *Chem Phys Lipids*. 2013;175-176:105-15.
346. Kogan M, Beke-Somfai T, Norden B. Flow-alignment of bicellar lipid mixtures: Orientations of probe molecules and membrane-associated biomacromolecules in lipid membranes studied with polarized light. *Chem Commun*. 2011;47 (26):7356-8.
347. Vold RR, Prosser RS. Magnetically oriented phospholipid bilayered micelles for structural studies of polypeptides. Does the ideal bicelle exist? *J Magn Reson Ser B*. 1996;113 (3):267-71.

Appendix A EasySpin script used to generate EPR simulation in Figure 1.10

```
% Nitroxide radical, various correlation times
%-----------------------------------------------------------------------

clear

% Parameters
%-----------------------------------------------------------------------
g = [2.0088,2.0061,2.0027];
A = mt2mhz([5.8,5.8,30.8]/10); % G -> MHz

Sys = struct('g',g,'Nucs','14N','A',A);
Sys.lw = [0 0.1]; % Lorentzian, mT

Exp.mwFreq = 9.85;
Exp.Range = [346 356];

% Simulation - fast motion
%-----------------------------------------------------------------------

Sys.tcorr = 1e-12; % correlation time in s
[B{1},spc{1}] = garlic(Sys,Exp);

% Simulation - slow motion
%-----------------------------------------------------------------------

Sys.tcorr=0.2e-8; % correlation time in s
[B{2},spc{2}] = garlic(Sys,Exp);

% Simulation - powder
%-----------------------------------------------------------------------

Sys.lw=0.5;
[B{3},spc{3}] = pepper(Sys,Exp);

% Plotting
%-----------------------------------------------------------------------

figure(1)

labels={'C.','B.','A.'};

for i=1:3
    B{i}=B{i}/1000; % convert to T
    hold on
    spc{i}=spc{i}./max(spc{i});
    spc{i}=spc{i}+i*2;
    plot(B{i},spc{i},'k');
    text(0.3455,1+i*2,labels(i));
end

ax1=gca
set(ax1,'ytick',[]);
set(ax1,'tickdir','out');
axis([0.346 0.356 0.8 7.2]);
ax1.YRuler.Visible='off';
xlabel('Magnetic field (T)');
```

Appendix B Calculation of idealised bicelle surface area

The bicelle radius *R* was calculated according to[347]:

$$R = \frac{1}{2}\, r\, q\, (\pi + \left(\pi^2 + \frac{8}{q}\right)^{\frac{1}{2}})$$

where *r* is the radius of the DMPC rim region and *q* is the DMPC/DHPC ratio.

The values calculated in the table below assume a lipid headgroup area of 65 Å, $q = 3.5$, 1:150 DMPC:DMPE-DTPA ratio and 40 Å radius for lanthanide dipolar interactions.

Bicelle radius	232 Å
Surface area of one leaflet	169093 $Å^2$
Number of lipids per leaflet	169093/65 = 2601
Number of DMPE-DTPA per leaflet	2601/150 = 17.3
Area affected by lanthanide effect	π x 40^2 = 5026 $Å^2$
Total lanthanide effect area per leaflet	5026 x 17.3 = 87159 $Å^2$
Ratio of lanthide effect/total leaflet area	87159/169093 = 0.52